

HEAT TRANSFER IN CIRCULATING FLUIDIZED BED BOILERS

by

Animesh Dutta

Submitted
in partial fulfillment of the requirements
for the degree of

DOCTOR OF PHILOSOPHY

Major Subject: Mechanical Engineering
at

DALHOUSIE UNIVERSITY

Halifax, Nova Scotia

August, 2002

© Copyright by Animesh Dutta, 2002



National Library
of Canada

Acquisitions and
Bibliographic Services

395 Wellington Street
Ottawa ON K1A 0N4
Canada

Bibliothèque nationale
du Canada

Acquisitions et
services bibliographiques

395, rue Wellington
Ottawa ON K1A 0N4
Canada

Your file Votre référence

Our file Notre référence

The author has granted a non-exclusive licence allowing the National Library of Canada to reproduce, loan, distribute or sell copies of this thesis in microform, paper or electronic formats.

The author retains ownership of the copyright in this thesis. Neither the thesis nor substantial extracts from it may be printed or otherwise reproduced without the author's permission.

L'auteur a accordé une licence non exclusive permettant à la Bibliothèque nationale du Canada de reproduire, prêter, distribuer ou vendre des copies de cette thèse sous la forme de microfiche/film, de reproduction sur papier ou sur format électronique.

L'auteur conserve la propriété du droit d'auteur qui protège cette thèse. Ni la thèse ni des extraits substantiels de celle-ci ne doivent être imprimés ou autrement reproduits sans son autorisation.

0-612-77590-9

Canada

Dalhousie University
Faculty of Engineering

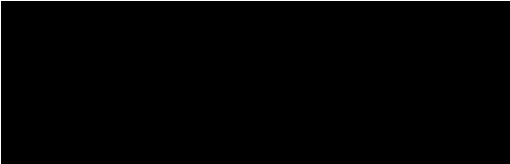
The undersigned hereby certify that they have examined, and recommended to the Faculty of Graduate Studies for acceptance, the thesis entitled "Heat Transfer in Circulating Fluidized Bed Boilers" by Animesh Dutta in partial fulfillment of the requirements for the degree of Doctor of Philosophy.

Dated: Sept 6, 2002

Supervisor:


Dr. Prabir Basu

External Examiner:


Dr. M. A. Bergougnou
University of Western Ontario

Examiners:


Dr. Y.P. Gupta


Dr. J.M. Chuang

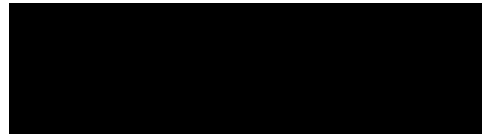


Dalhousie University
Faculty of Engineering

DATE: Sept 09, 2002

AUTHOR: Animesh Dutta
TITLE: Heat Transfer in Circulating Fluidized Bed Boilers
MAJOR SUBJECT: Mechanical Engineering
DEGREE: Doctor of Philosophy
CONVOCATION: October 2002

Permission is herewith granted to Dalhousie University to circulate and to have copied for non-commercial purposes, at its discretion, the above thesis upon the request of individuals or institutions.



Signature of Author

The author reserves other publication rights, and neither the thesis nor extensive extracts from it may be printed or otherwise reproduced without the author's written permission.

The author attests that permission has been obtained for the use of any copyrighted material appearing in this thesis (other than brief excerpts requiring only proper acknowledgements in scholarly writing), and that all such use is clearly acknowledged.

To my parents, Minu Prava Dutta and Satyananda Dutta

TABLE OF CONTENTS

List of Tables	ix
List of Figures	x
List of Abbreviations and Symbols	xiv
Acknowledgements	xviii
Abstract	xix
1 Introduction	1
1.1. Background	1
1.2. Objectives	11
1.3. Scope and limitations	11
1.4. Contribution of this dissertation	13
1.5. Work published from this study	15
1.6. Organization of the study	16
2 Literature Review	19
2.1. Introductory remarks	19
2.2. Hydrodynamics	21
2.3. Heat transfer	22
2.3.1. Effect of operating parameters on heat transfer	24
2.3.1.1. Suspension density	24
2.3.1.2. Bed temperature	27
2.3.1.3. Fluidization velocity	29
2.3.1.4. Particle size	29
2.3.1.5. Vertical length of heat transfer surface	30
2.3.2. Heat transfer to the suspended surfaces	33
2.3.3. Heat transfer in the standpipe	34
2.3.4. Heat transfer data in commercial boiler	36
2.3.5. Mechanistic model of heat transfer	38
2.4. Concluding remarks	40
3 Overall heat transfer to water-walls and wing-walls of commercial CFB boilers	42
3.1. Introductory remarks	42
3.2. Data from commercial unit	43
3.3. Methodology for estimating heat transfer coefficient	49
3.4. Results and discussion	52
3.4.1. Suspension density effect	52
3.4.2. Temperature effect	52
3.5. Empirical correlation of heat transfer coefficient	59
3.6. Comparison of proposed empirical correlation with reported by other researchers	61
3.7. Concluding remarks	64

4	An experimental investigation into the heat transfer on wing walls in a CFB Boiler	65
4.1.	Introductory remarks	65
4.2.	Experiment on pilot plant	66
4.2.1.	Description of pilot plant	66
4.2.2.	Wing wall	68
4.2.3.	Solids flux measuring system	69
4.2.4.	Water wall	69
4.2.5.	Experimental techniques	73
4.2.6.	Bed material	75
4.3.	Results and discussion of data from CFB pilot plant	75
4.3.1.	Hydrodynamics	75
4.3.1.1.	CASE-1 (Top of the riser)	75
4.3.1.2.	CASE-II (1.3 m below the roof)	78
4.3.2.	Heat transfer	80
4.3.2.1.	Axial distribution of heat transfer coefficient	80
4.3.2.2.	Lateral distribution of heat transfer coefficients	85
4.3.3.	Comparison between water wall and wing wall Heat Transfer	90
4.4.	Concluding remarks	92
5	An investigation on heat transfer to the standpipe of a CFB boiler	93
5.1.	Introductory remarks	93
5.2.	Experimental set-up	95
5.3.	Experimental procedure and measurement techniques	98
5.4.	Model for heat transfer in the standpipe	100
5.4.1.	Predictive model for dense section	100
5.4.2.	Predictive model for dilute section	103
5.5.	Results and discussion	107
5.5.1.	Hydrodynamics in the dense section	107
5.5.2.	Hydrodynamics in the dilute section	109
5.5.3.	Heat transfer in the dense section	109
5.5.4.	Heat transfer in the dilute section	115
5.5.5.	Comparison on heat transfer between dense and dilute section	120
5.6.	Concluding remarks	123
6	Heat transfer on cavity-type inertial separators in a CFB boiler	124
6.1.	Introductory remarks	124
6.2.	Experimental unit	126
6.2.1.	Experimental set-up	126
6.2.2.	Solids flux measuring system	130

6.2.2.1.	Axial solids flux measuring probe	130
6.2.2.2	Lateral solids flux probe	130
6.2.3.	Experimental techniques	132
6.2.4.	Bed material	131
6.3.	Results and Discussion	133
6.3.1.	Gas solids suspension flow	133
6.3.1.1.	Suspension densities	133
6.3.1.2.	Lateral solids flux distributions	135
6.3.1.4.	Axial solids flux in the 1 st row of the separator (in the riser)	137
6.3.1.5.	Solids collection in the 2 nd row of the separator (in the primary chamber)	138
6.3.2.	Expected mode of solid separation	140
6.3.2.1.	1 st row of inertial separator (in the riser)	140
6.3.2.2.	2 nd row of the separator (in the primary chamber)	140
6.3.3.	Heat transfer to cavity-type inertial separators	141
6.3.3.1.	Inside the cavity-type inertial separator (1 st row)	141
6.3.3.2.	Outer wall of the cavity-type inertial separator (1 st row)	144
6.3.3.3.	Comparison of heat transfer for both surfaces (1 st row)	148
6.3.3.4.	Inside the cavity-type inertial separator (2 nd row)	150
6.3.3.5.	Comparison of heat transfer for both 1 st and 2 nd row (Inner wall)	152
6.3.3.6.	Comparison of heat transfer with the water walls	152
6.4.	Concluding remarks	154
7	Models for the vertical walls of CFB boilers	155
7.1.	Model for water walls	155
7.1.1.	Background	155
7.1.2.	Model Development	158
7.1.2.1.	Heat transfer mechanism	158
7.2.	Model for wing walls	169
7.2.1.	Background	169
7.2.2.	Model development	169
7.2.2.1.	Dilute convection	171
7.2.2.2.	Radiation	172
7.3.	Models for cavity-type inertial separator	174
7.3.1.	Model development	174
7.3.1.1.	Inside the inertial separator	174
7.3.1.2.	Outside the inertial separator	175
7.4.	Results and discussion	178
7.4.1.	Water wall	178
7.4.2.	Wing wall	180
7.4.3.	Cavity type inertial separator	181

7.5. Concluding remarks	182
8 Overall conclusions and recommendations	183
8.1. Overall conclusion	183
8.2. Closure	185
8.2. Recommendations for future work	188
References	189
Appendices	201
Appendix A: Construction of CFB pilot plant at CFB laboratory	202
Appendix B: Properties of bed material used in the experiment	220
Appendix C: Calibration of instruments used	226
Appendix D: Experiments on wing wall	237
Appendix E: Experiments on standpipe	247
Appendix F: Experiments on cavity-type inertial separator	258

LIST OF TABLES

1.1	Contribution of the proposed study	14
2.1	Summary of empirical correlations of heat transfer in large-scale CFB boilers	25
2.2	Major studies on the measurement of cluster velocity on the wall	31
2.3	Heat transfer studies in moving bed (adopted from Colakyan, 1984)	35
2.4	Dimensions, operating conditions and measured heat transfer coefficients for large-scale CFB boilers (adopted from Basu and Nag, 1996; Golriz, 2002)	37
2.5	Review of mechanistic models of heat transfer in fast beds (adopted from Basu and Nag; 1996)	39
3.1	Measurement on heat transfer on water wall in different commercial units	63
4.1	Location of pressure transducers in the riser	72
6.1	Comparison on height average heat transfer coefficient in the experimental unit	153
7.1	Measurement on heat transfer in different commercial units	157
7.2	Heat transfer data on cavity-type inertial separator in a 0.3 MW _{th} pilot plant	181
8.1	Summary of the results on cold bed pilot plant and their comparison for a given operating condition	186
8.2	Summary of results on commercial boilers and hot bed pilot plant	187

LIST OF FIGURES

1.1	Schematic diagram of a CFB boiler	2
1.2	Location of heat transfer surfaces (research areas) in the CFB loop	3
1.3	Detailed diagram of furnace water wall	4
1.4	Detailed diagram of wing wall	5
1.6	Picture of standpipe with loop seal	6
1.5	Detailed of the proposed cavity-type inertial separator	6
1.6	Summary of the study	18
2.1	Location of heat transfer surfaces in a CFB boiler	20
2.2	Core annulus structure of CFB	21
2.3	Mechanism of heat transfer to walls of a CFB boiler	23
2.4	Effect of bed temperature on heat transfer coefficients	28
3.A (1)	General arrangement drawing of 170 MW _e boiler	45
3.A (2)	A simplified general arrangement side elevation of 170 MW _e boiler	46
3.B (1)	General arrangement drawing of 20 MW _e boiler	47
3.B (2)	A simplified general arrangement side elevation of 20 MW _e boiler	48
3.1a	Water walls heat transfer coefficient with non-dimensional suspension density (170 MW _e boiler)	53
3.1b	Wing walls heat transfer coefficient with non-dimensional suspension density (170 MW _e boiler)	53
3.2a	Water walls heat transfer coefficient with non-dimensional bed temperature (170 MW _e boiler)	54
3.2b	Wing walls heat transfer coefficient with non-dimensional bed temperature (170 MW _e boiler)	54
3.3a	Heat transfer coefficient for water walls of 170 MW _e boiler (Temperature 930-940C)	55
3.3b	Heat transfer coefficient for wing walls of 170 MW _e boiler (Temperature 930-940C)	55
3.4	The percentage reduction of heat transfer coefficient between water walls and wing walls at different operating conditions	56
3.5a	Water walls heat transfer coefficient with non-dimensional suspension density (20 MW _e boiler)	57
3.5b	Water walls heat transfer coefficient with non-dimensional bed temperature (20 MW _e boiler)	58
3.6a	Heat transfer coefficient to the water walls; estimated versus predicted	60
3.6b	Heat transfer coefficient to the wing walls; estimated versus predicted	61
3.7	Experimental versus predicted overall heat transfer coefficient for water walls	62

4.1	Schematic diagram of the experimental unit	67
4.2a	Details of experimental set-up of wing wall when it is placed at 1300 mm below the roof (case-2)	70
4.2b	Details of experimental set-up of wing wall when it is placed at the top of the roof (case-1)	71
4.3	Schematic diagram of solid flux measuring probe	72
4.4	Details of experimental set-up of water wall	73
4.5a	Variation of upward and downward solids mass fluxes with external solids circulation rates for a constant superficial velocity ($V_s = 3.9$ m/s) for wing wall (Case-1).	76
4.5b	Variation of net downward fluxes and ratio of downward and upward fluxes with external solids circulation rates for a constant superficial velocity ($V_s = 3.9$ m/s) for wing wall (Case-1).	77
4.5c	Expected gas solids motion at the top of the riser	77
4.6a	Variation of upward and downward solids mass fluxes with external solids circulation rates at two different superficial velocities ($V_s = 3.9$ m/s, $V_s = 4.4$ m/s) for wing wall (Case-2).	79
4.6b	Variation of net downward fluxes and ratio of upward and downward fluxes with external solids circulation rates at two different superficial velocities ($V_s = 3.9$ m/s, $V_s = 4.4$ m/s) for wing wall (Case-2).	79
4.7	Local heat transfer coefficients measured along the height of the wing wall placed at the top of the roof at different operating conditions (Case-1)	81
4.8a	Local heat transfer coefficients measured along the height of the wing wall placed 1300 mm below the top of the roof at different operating conditions (Case-2)	83
4.8b	The ratio of forced convection with particles and without particles with the ratio of suspension density and gas density for a superficial velocity of 3.9 m/s (Case-2)	84
4.9	Comparison on local heat transfer coefficients along the height of the heating strip between case-1 and case-2 for a specific operating condition.	85
4.10a.	Local heat transfer coefficients along the width of the wing wall for case-1 (a) $V_s = 3.9$ m/s; $G_s = 8$ kg/m ² .s	86
4.10b.	Local heat transfer coefficients along the width of the wing wall for case-1 (b) $V_s = 3.6$ m/s; $G_s = 2$ kg/m ² .s	87
4.10c.	Local heat transfer coefficients along the width of the wing wall for case-2 (c) $V_s = 4.4$ m/s; $G_s = 7.4$ kg/m ² .s	87
4.10d.	Local heat transfer coefficients along the width of the wing wall for case-2(d) $V_s = 4.4$ m/s; $G_s = 3.6$ kg/m ² .s	88
4.10e.	Local heat transfer coefficients along the width of the wing wall for case-2 (e) $V_s = 4.4$ m/s; $G_s = 6$ kg/m ² .s	88

4.10f.	Local heat transfer coefficients along the width of the wing wall for case-2 (f) $V_s=3.9$ m/s; $G_s=6$ kg/m ² .s	89
4.11	Local heat transfer coefficients measured along the height of the water wall at different operating conditions.	90
4.12	Comparison on local heat transfer coefficients along the height of the heating strips for wing wall (Case-1 and Case-2) and water wall at a specific operating condition.	91
5.1	Schematic diagram of the experimental unit	96
5.2	Schematic diagram of the experimental set-up	97
5.3a	Solids volume concentration profile measured along the standpipe ($G_s=18$ kg/m ² .s)	108
5.3b	Suspension density profile measured along the standpipe ($G_s=18$ kg/m ² .s)	108
5.4a	Local heat transfer coefficients measured along the height of the dense section at different solids circulation rates (Particle B)	110
5.4b	Local heat transfer coefficients measured along the height of the dense section at different solids circulation rates (Particle A)	111
5.5	Comparison of local heat transfer for dense and light particles in the dense section. Predicted values are also shown for comparison	112
5.6a	Average heat transfer coefficients versus external solids circulation rates	113
5.6b	Average heat transfer coefficient versus solids velocity	114
5.7	Ratio of measured and predicted heat transfer coefficients versus external solids circulation rates in dense bed	115
5.8a	Local heat transfer coefficients against height of the dilute section (Particle A)	116
5.8b	Local heat transfer coefficients against height of the dilute section (Particle B)	116
5.9	Comparison on local heat transfer coefficients in the dilute section for two types of particles	117
5.10a	Average heat transfer coefficients with average solids concentration at dilute section for both types of particles	118
5.10b	Average heat transfer coefficients with average suspension density at dilute section for both types of particles	118
5.11	Predicted and measured heat transfer coefficients in the dilute section	119
5.12	Comparison of heat transfer between dense and dilute section for both types of particles	120
5.13	Ratio of average heat transfer coefficients in dense and dilute phase plotted against solids circulation rates	121
5.14	Predicted fractional wall coverage versus solids circulation rates	122

6.1	Schematic diagram of the experimental unit	128
6.2	Details of experimental set-up of inertial separators: a) arrangements of the separators, b) position of heating strip along height (Case-1), and c) position of the heating strip along depth (Case-2)	129
6.3	Schematic diagram of the lateral solids flux measuring system	131
6.4	Suspension density profile along the riser column: a) $V_s=3.6$ m/s and $G_s=3$ kg/m ² .s, b) $V_s=4.4$ m/s and $G_s=5.7$ kg/m ² .s,	134
6.5a	Lateral outward solids mass fluxes ($V_s=4.4$ m/s and $G_s=5.7$ kg/m ² .s)	136
6.5b	Comparison of non-dimensional lateral outward solids mass flux for different riser diameter	137
6.6	Downwards solids flux with solids circulation rates on the inner walls of the separator in the 1 st row	138
6.7	Overall efficiency of the inertial separators in the primary chamber with superficial velocity	139
6.8	Local heat transfer coefficients measured along the height (Case-1) of the inner wall of a separator placed at the riser.	143
6.9	Local heat transfer coefficients measured along the depth (Case-2) of the inner wall of a separator placed at the riser	144
6.10a	Local heat transfer coefficients measured along the height (Case-1) of the outer wall of a separator placed at the riser	145
6.10b	Ratio of forced convection with particles and without particles with the ratio of suspension density and gas density for a superficial velocity of 3.9 m/s (Case-2)	146
6.11	Local heat transfer coefficients measured along the depth (Case-2) of the outer wall of a separator placed at the riser	147
6.12	Comparison of local heat transfer coefficient measured along the height for both inner wall and outer wall of the separators placed at the riser	149
6.13	Local heat transfer coefficients measured along the height (Case 2) of the inner wall of a separator placed at the primary chamber	150
6.14	Local heat transfer coefficients measured along the depth (Case-2) of the inner wall of a separator placed at the primary chamber	151
7.1	Heat transfer mechanism	159
7.2	Single cluster at the wall showing deposition locations and contact length	161
7.3	Most common rectangular cross-section of a riser	170
7.4	Proposed heat transfer mechanism inside the separator	175
7.5	Proposed heat transfer mechanism outside the separator	176
7.6	Comparison of estimated versus predicted wall coverage for a number of commercial boilers	178
7.7	Predicted heat transfer coefficients with measured heat transfer coefficients	179
7.8	Experimental versus predicted heat transfer coefficients for wing wall	180
7.9	Experimental versus predicted heat transfer coefficients for cavity type inertial separators	181

LIST OF ABBREVIATION AND SYMBOLS

Abbreviations

CFB	circulating fluidized bed boiler
CO	carbon monoxide
GRI	Greenfield research Inc.
HTC	heat transfer coefficient
N ₂ O	nitrous oxide
NO	nitric oxide
NS	not specified
PC	pulverized coal fired boiler
SAS	statistical analysis software
T/h	ton per hour
Wall	water wall

Symbol

$(h_{cluster})$	cluster heat transfer coefficient (particle), [W/m ² .K]
$(h_{con})_{cluster}$	cluster convective heat transfer coefficient, [W/m ² .K]
$(h_{con})_{dilute}$	dilute convective heat transfer coefficient, [W/m ² .K]
$(h_{rad})_{cluster}$	cluster radiative heat transfer coefficient, [W/m ² .K]
$(h_{rad})_{dilute}$	dilute radiative heat transfer coefficient, [W/m ² .K]
A	projected area [m ²]
$A_{inertial\ separator}$	projected area of cavity-type inertial separator, [m ²]
BHP	break horse power
C_c	specific heat of cluster in the dilute section, [J /kg.K]
C_e	emulsion specific heat in the dense section, [J /kg.K]
C_g	specific heat of gas, [J /kg.K]
C_l	correction factor for length, [-]
C_p	specific heat of particle, [J /kg.K]
c_{sf}	cluster solid fraction, [-]
C_t	correction factor for temperature, [-]
D_{eq}	hydraulic diameter, [m]
$D_{eq\ separator}$	hydraulic diameter of separator, [m]
d_p	diameter of particle, m (by sieve)
d_{pi}	average of adjacent sieve apertures for material retained on i th sieve, [m]
d_t	tube diameter in the wing wall, [m]
E	electric heat input, [W]
e_b	dilute phase emissivity, [-]
e_c	cluster emissivity, [-]
e_d	dilute phase emissivity, [-]

e_g	gas emissivity, [-]
e_p	particle emissivity, [-]
e'_p	effective emissivity of particle cloud, [-]
e_w	wall emissivity, [-]
f	fraction of wall covered by cluster, [-]
G	solid mass flux, [kg/m ² .s]
G_s	external solids circulation rate, [kg/m ² .s]
G/S	gas-solids, [-]
h	heat transfer coefficient, [W/m ² .K]
H	height from the bottom of the heating strip of the wing wall [m]
H	height from the secondary air supply to the top of the combustor in commercial boiler, [m]
h_g	gas convective heat transfer coefficient, [W/m ² .K]
h_i	instantaneous heat transfer coefficient/average heat transfer coefficient inside the inertial separator [W/m ² .K]
h_o	average heat transfer coefficient outside the inertial separator [W/m ² .K]
h_p	particle convective heat transfer coefficient, [W/m ² .K]
h_{tot}	total heat transfer coefficient, [W/m ² .K]
h_w	conduction heat transfer coefficient through gas layer, [W/m ² .K]
k	proportionality constant
k_c	thermal conductivity of cluster in the dilute section, [W/m.K]
k_e	thermal conductivity of emulsion in the dense section, [W/m.K]
k_g	thermal conductivity of gas, gas film, [W/m.K]
k_s	thermal conductivity of particle, [W/m.K]
K	degree kelvin
L	height between measuring points, height of the heat transfer surface, m (Chapter 5)
L_c	characteristic length, [m]
L_e	mean beam length, [m]
L_x	distance along the depth [m]
L_y	distance along the width [m]
L/S	liquid-solids, [-]
N	number of vertical tube in the wing wall, [-]
Nu	Nusselt number, [-]
P	power input [W]
Pr	Prandtl number, [-]
ΔP	differential pressure, [N/m ²]
Q	heat duty [W]
Q_{air}	flow rate of gas in the riser, [m ³ /s]
\dot{Q}	heat flux [W/m ²]
r/R	non-dimensional radial distance, [-]
Re	Reynold number, [-]
RPM	rotation per minute

S_{cal}	thickness of fluid mechanical wall zone, [m]
T	temperature [K]
T_b	bed temperature, [K]
t_c	residence time of cluster with wall, [sec]
T_s	first row of solids temperature (near the heat transfer surface), [K]
T_w	average wall temperature, [K]
T_{w_i}	local surface temperature, [K]
U_{cl}	downwards velocity of cluster, [m/s]
U_g	superficial gas velocity, [m/s]
U_{gc}	velocity at core, [m/s]
u_o	upward superficial velocity of gas, [m/s]
U_s	downwards velocity of solids, [m/s]
$U_{separator}$	velocity at the separator, [m/s]
Δu	relative velocity of gas with respect to solid, [m/s]
V	velocity [m/s]
W	watt
X	width of the riser (m)
Y	solids volume concentration in dispersed phase, [-]
Y'	voidage in the riser interior, [-]

Greek letters

δ	boundary layer thickness on the wall of the combustor, [-]
δ	non-dimensional gas layer thickness between wall and cluster, [-]
ε_{avg}	average voidage in the dilute section, [-]
ε_c	average voidage in the cluster, [-]
ε_i	local radial voidage in the combustor, [-]
ε_s	average voidage in the dense section, [-]
μ_g	viscosity of gas, [kg/ms]
ρ	gas density, [kg/m ³]
ρ_c	cluster density in the dilute section, [kg/m ³]
ρ_{dis}	density of dispersed phase, [kg/m ³]
ρ_e	emulsion density in the dense section, [kg/m ³]
ρ_g	density of gas, [kg/m ³]
ρ_p	density of particle, [kg/m ³]
ρ_s	average suspension density, [kg/m ³]
σ	stefan-boltzmann constant, [W/m ² .K ⁴]
ϕ_s	sphericity of a particle, [-]

Subscript

<i>avg</i>	average
<i>b</i>	bed
<i>ewwall</i>	evaporator wing wall
<i>g</i>	gas
<i>max</i>	maximum operating
<i>p</i>	particle convection
<i>s</i>	superficial
<i>sl</i>	lateral
<i>swwall</i>	superheater wing wall
<i>w</i>	wall
<i>wwall</i>	evaporator water wall
<i>x</i>	local
<i>x_i</i>	weight fraction on <i>i</i> th sieve, [-]

Superscript

'	superheater wing wall
“	evaporator wing wall

ACKNOWLEDGEMENTS

The author wishes to express eternal gratitude and deep appreciation to his thesis supervisor Dr. Prabir Basu, who played a key role at every stage of this study with conceptual discussion. His guidance was crucial and invaluable in bringing this thesis to its fruition.

The author wishes to express his sincere appreciation and gratitude to Dr. Y. P. Gupta and Dr. J. M. Chuang for their constructive comments, valuable suggestions and meaningful discussions in serving as a member of the guiding committee. Special thanks are to Prof. M. A. Bergounou of Western Ontario, who kindly agreed to serve as the external examiner.

The author pays special tribute to Dr. J.H. Greenblatt who passed away on August 11, 2000, for his encouragement, meticulous attention in details project work, report organization and exemplary editing in the early days of the study. The author owes much thanks to Ms. Sara Greenblatt, beloved daughter of Dr. J.H. Greenblatt, for making the manuscript more readable.

The author is grateful to Dr. Murat Koksai for his magnanimous gesture showed in discussions, comments and reference materials, which have influenced the author in carrying out this thesis work.

The author would like to acknowledge the support and help of the following individuals:

Dr. P. Allen, Dr. L. Cheng, Dr. B.V. Reddy, Dr. S. Saha, Ms. S. Baskovic, Mr. N. Winaya, Mr. S. Dhal, Mr. R. Hickey, Ms. E. Fukuda, Mr. A. L. Roa, Mr. S. Kumar, Mr. P. Langile, Mr. M. Horne, Mr. J. Chowdury, Mr. M. Ahmed, Ms. N. Ahmed, Mr. F. Ahmed, Mr. P. Roy, Mr. A. Basu, Mr. L. Miller, Dr. Swaray, Mr. R. Dube, Ms. C. Wood, Ms. D. Devis, Ms. M. McLeod, Ms. S. Jones, Ms. V Stoyles, and Ms. C. Thrault

Three couples deserve most special recognition: Sunny and Dolly, Tapas and Ujjaini, Rupom and Shammi, who played an important role during the author's study life at Dalhousie by sharing diversified ideas and extending constant support.

The author acknowledges financial supports of National Science and Engineering Research Council (NSERC), Canada; Faculty of Graduate studies, Reid scholarship fund, Medjuck scholarship fund, Dalhousie; Greenfield Research Inc. Halifax.

Finally, the authors gratefully acknowledges the continuing patience and encouragement of his beloved parents, only sister and two brothers whose love, supports and tremendous sacrifices have encouraged the author in all his worthwhile pursuits throughout the life.

ABSTRACT

In circulating fluidized bed (CFB) boilers, provision of required amounts of heating surfaces inside the combustor is an important design issue especially when the capacity of the boilers increases. The enclosing wall, which constitutes the principal heat transfer surfaces, needs to be supplemented with additional heat transfer surfaces. Wing wall is the most common additional heat transfer surface used in the CFB-boiler furnace at present. Despite its frequent utilization, there is no reported study available on hydrodynamics and heat transfer mechanism on wing wall in the literature.

The thesis investigates the flow dynamics and heat transfer mechanism on wing wall in both pilot plant and commercial units. It also investigates the potential of using two new heat transfer surfaces; walls of standpipe and cavity-type inertial separators in the CFB loop. In the experimental part of this thesis, measurements on temperature, pressure, axial and lateral solids fluxes were carried out to understand the flow hydrodynamics and heat transfer mechanism on above surfaces. Experiments were performed in a pilot scale CFB riser (1 m \times 0.5 m in cross section and 5 m in height) with sand particles. In the theoretical part of this study, mechanistic models were proposed to predict the heat transfer coefficients on all those surfaces. A correlation on fractional wall coverage by the cluster on the enclosing wall was developed to improve the cluster renewal model to estimate the heat transfer coefficients on the enclosing wall. Two empirical correlations for both enclosing water walls and wing walls were also developed by relating heat transfer coefficients, which are averaged over the entire height of the absorbing walls with suspension density and average bed temperature.

Analysis of data from a 170 MW_e commercial unit showed that heat transfer coefficients on the wing walls were always smaller than that on enclosing water wall. Experiments conducted in the pilot plant revealed that hydrodynamics condition on the wing wall are different from the enclosing water wall. Gas convection dominates the convective heat transfer to the wing wall whereas particle convection dominates on the wall layer. Exploratory research on new heat transfer surfaces i.e., standpipe and cavity-type inertial separators, shows an encouraging result for using these types of surfaces in the CFB loop. Use of in-furnace cavity-type inertial separator increases the overall solids hold up in the riser and hence increase the heat transfer coefficients of the enclosing wall.

Mechanistic models developed for all the surfaces predict the heat transfer coefficients within $\pm 10\%$ error. Empirical correlations developed from the data on commercial units predict heat transfer coefficients within $\pm 15\%$ error which is of the same order as the experimental error.

Chapter 1

Introduction

1.1 Background

In comparison to conventional combustors, the circulating fluidized bed (CFB) has two major advantages as a furnace for combustion of fossil fuels. In the first place, it enables combustion with low emissions of nitric and sulphur oxides without flue gas treatment. In the second instance, the CFB combustor is fuel flexible; and several fuels can be burned in the same furnace. Therefore, in view of the continuing depletion of high grade fuels and the relative abundance of low grade fuels, combined with stringent environmental laws, the opportunity for the application of CFB technology in steam generation is greatly enhanced.

An improved control of bed temperature is required for lower emissions of harmful compounds. A lower bed temperature results in an increase in emissions of carbon monoxide (CO), hydrocarbons and nitrous oxides (N₂O), whereas a higher temperature results in an increase in nitric oxide (NO) emissions and a decrease in sulphur capture efficiency of added limestone. In addition, if the temperature is too high, an agglomeration of the bed material may result, which disturbs fluidization. Therefore, a reliable temperature control is essential in the CFB loop (Fig. 1.2).

Figure 1.1 shows a schematic diagram of an industrial CFB boiler. A simpler schematic of the CFB combustion chamber is shown in Figure 1.2. The average temperature in the combustion chamber is controlled mainly by heat absorption through heat transfer

surfaces located in the CFB loop, which comprises the combustion chamber, gas-particle separator and standpipe. Heat is extracted by a water/steam circuit flowing through each heat transfer surface. After leaving the particle separator, flue gases are further cooled in the convection heat transfer section of the boiler, located downstream. This study is about heat transfer to different parts (wing wall, water wall, cavity type inertial separator and standpipe) of the CFB loop, which is shown in Figure 1.2 with detailed diagram (Fig. 1.3-1.5).

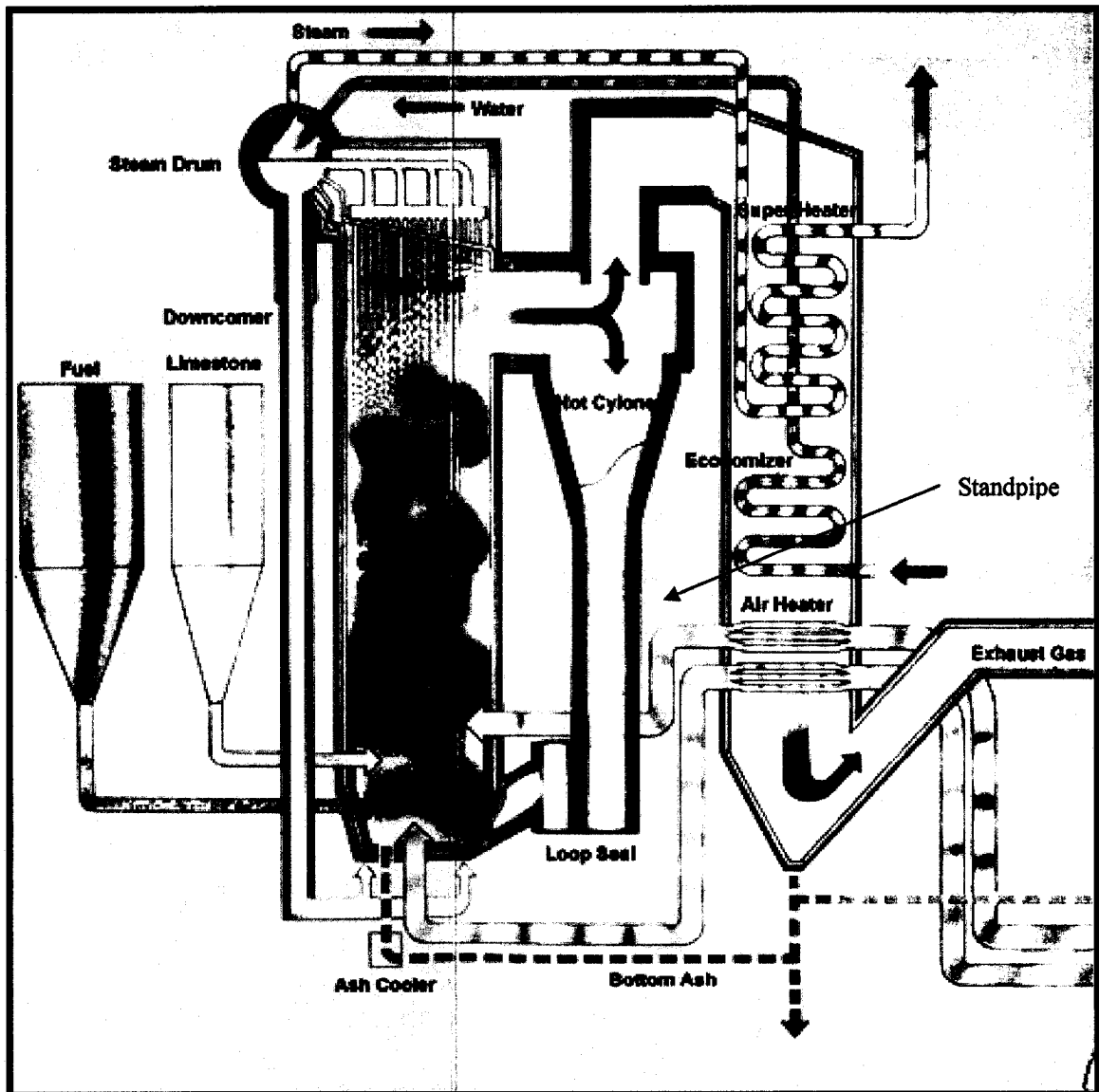


Figure 1.1. Schematic diagram of a CFB boiler

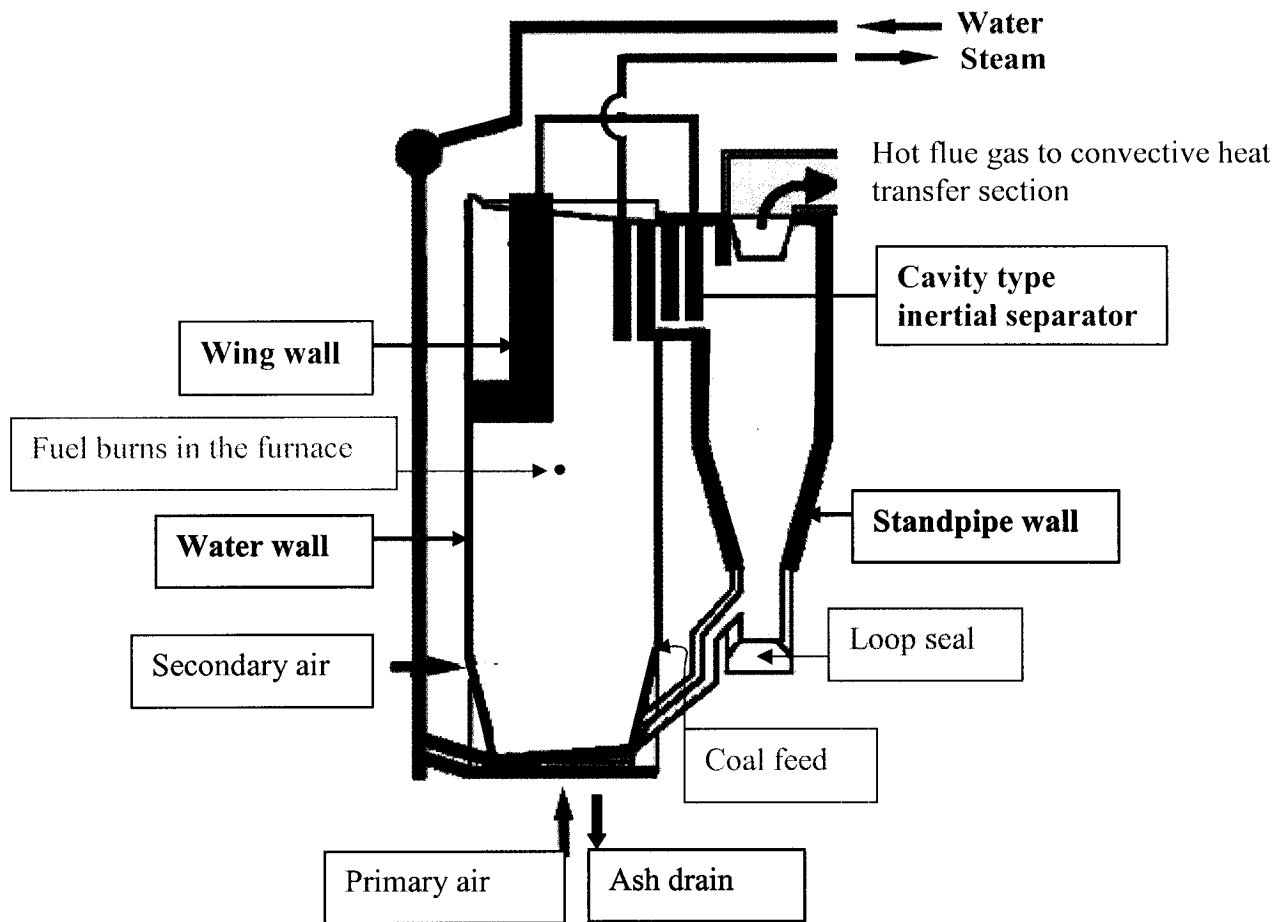


Figure 1.2. Location of heat transfer surfaces (research areas) in the CFB loop

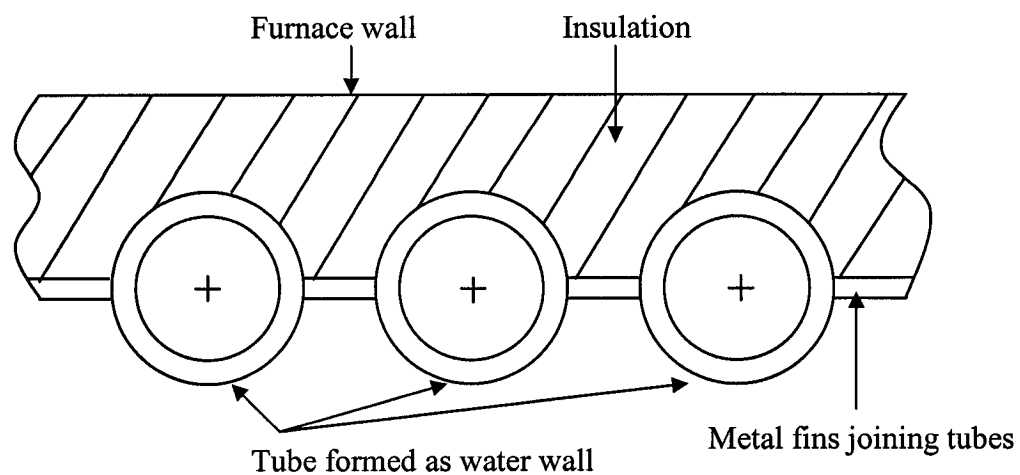
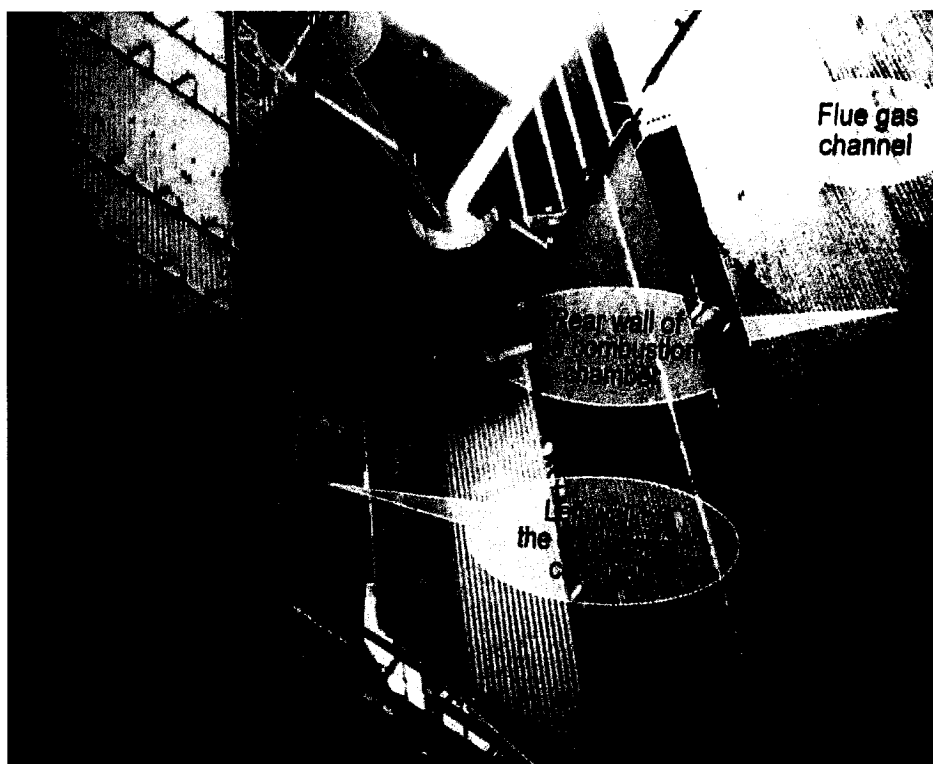


Figure 1.3: Detailed diagram of furnace water wall

Note: The principal heat transfer surface area in the boiler is in the form of enclosing wall of the furnace, which is termed as water wall/membrane tube wall.

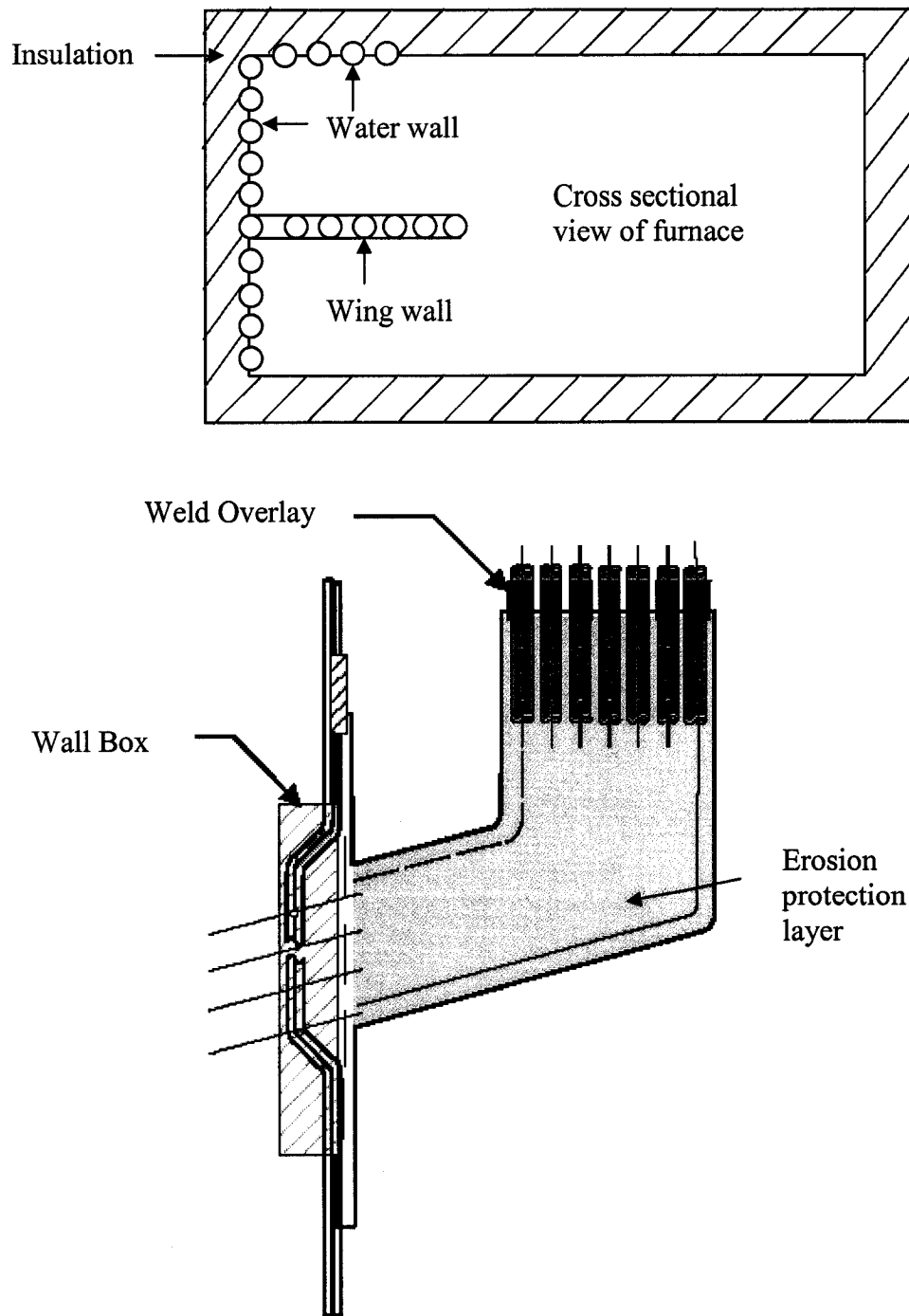


Figure 1.4. Detailed diagram of wing wall

Note: Most commonly used additional heat transfer surface areas in a boiler, which are hung from the roof and extend from the front wall to some distance towards the opposite wall, where the furnace exit located is termed as wing wall.

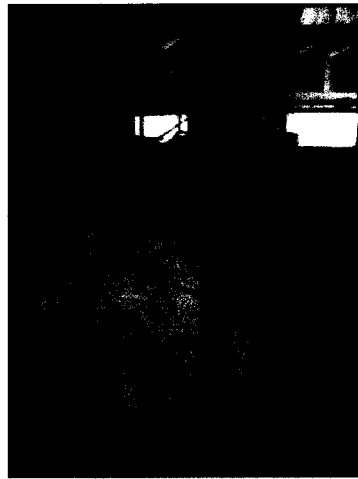


Figure 1.5. Picture of standpipe with loop seal

Note: Standpipes, which transfer solids from the cyclone to the loop seal, are traditionally refractory lined. Standpipes, with their refractory lined walls have high surface heat loss and high maintenance cost. Furthermore, besides adding to the weight of the standpipe assembly, their high thermal inertia severely restricts the fast light up of the boiler.

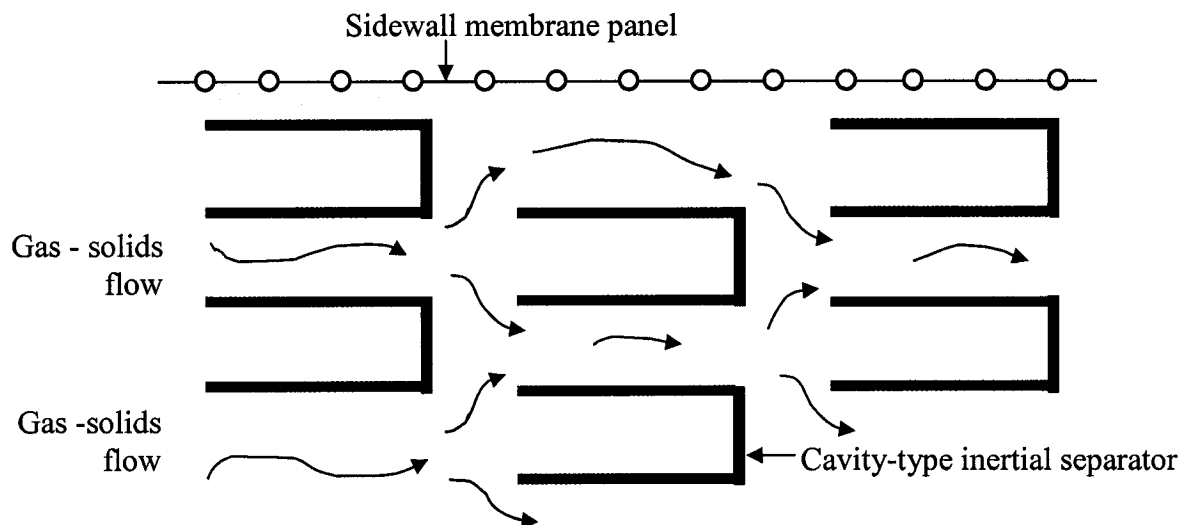


Figure 1.6. Details of the proposed cavity-type inertial separator

Note: A newly developed heat transfer surface area in the form of rectangular deep cavity where separation of solids will be due to the inertial effect rather than impaction of the particles and which will be located at the exit of the furnace is termed as inertial cavity-type separator.

Following are the main features of importance for heat transfer in CFB, which are common to most designs:

- 1) Avoidance of erosion from bed particles
 - i) The heat transfer surfaces are vertical, parallel to the direction of the gas-solids flow. Those surfaces which are not parallel to the direction of particle flow, where particle impingement may occur, are protected by refractory and are, therefore, of only minor importance to heat transfer.
 - ii) Tube walls are located in the bottom part or dense bed of the combustion chamber and are protected by refractory, in order to avoid contact with the dense bed. Because of this refractory, the bottom part of the chamber has little importance in heat transfer.
 - iii) A presence of flow-disturbance elements on the tubes may enhance the heat transfer (Leckner, 1992). At present, the effect of flow-disturbance characteristics on tube surfaces cannot be considered as influencing heat transfer, because the consequent deterioration of the tube metal, caused by these elements, cannot be predicted.
- 2) According to modern boiler design practice, the walls of the combustion chamber consist of heat transfer tubes connected with fins to form a membrane wall. The tubes have a circular cross-section.
- 3) The heat transfer surfaces are usually 10 to 30 meters in length. The height of the combustion chamber is determined by the residence time required for reaction of gases and by the heat transfer surface area (Basu *et al*, 1999).
- 4) The cross-section of a boiler combustion chamber is large, when compared with many other CFB applications. The grate heat release rate is approximately 3-4 MW/m² and the volumetric heat release rate is between 0.10-0.21 MW/m³ (Basu *et al*, 1999)

- 5) The pressure drop over the bed (equal to the amount of bed material in the combustion chamber) is kept as low as possible, subject to the requirement of maintaining an even bed temperature. Depending on the size of the boiler, typical values range from 5 to 15 kPa in the heat transfer part of the combustion chamber. The range of cross sectional average densities could typically be from 1 to 20 kg/m³ (ash and sand or lime) (Leckner, 1991)
- 6) Combustibles constitute less than 1%-3% by weight of all solids in the furnace and the rest of the solids are noncombustible: ash, sand, or sorbents (Baskakov *et al.*, 2001). Due to combustion, there is always a wide size distribution of bed material composed of ash, unburned fuel and added material. The presence of unburned carbon in the fly ash decreases combustion efficiency and lowers the grade of fly ash for recycled uses. The cut size of the particles, which will elutriate from the CFB loop is determined by the fractional separation efficiency of the particle separator(s).
- 7) There is a small range of variation of temperature of the furnace volume. A mean temperature of about 850⁰C is considered to be optimum (from the view point of sulphur capture). Depending on the mode of other factors, it is usually maintained within a range 850-950⁰C. It is mainly due to intense inner and outer circulation of particles, which makes a temperature in the furnace virtually constant (at least under nominal load) over its height and section.
- 8) The vertical suspension density profile in the combustion chamber is influenced by a two step delivery of primary and secondary air (Leckner, 1991). The addition of secondary air usually takes place in the refractory-lined lower part of the combustion chamber. The upper combustion chamber (above the secondary air supply) is of major importance in heat transfer.

The vertical water walls (Fig. 1.3) of the upper combustion chamber are the principal heat transfer surfaces in the CFB loop. CFB boilers become more economically feasible as the capacity increases. As the size of the boiler increases, the ratio of the circumference and the cross section of the furnace decreases. The latter is proportional to the heat release

rate, while the former is proportional to the available heat absorption area. As this change in area ratio with size does not permit a smooth scaling-up of the combustion chamber, it becomes necessary to insert additional heat transfer surfaces in the loop of large CFB boilers. An enhancement of heat transfer is of particular interest, because the walls in large boilers do not provide sufficient surfaces for cooling gas solid suspension and meeting heat duty. At present, additional surface areas, in the form of wing walls (Fig. 1.4) or division wall, are immersed in the furnace and external heat exchanger in the solid return system of the CFB loop.

These additional heat transfer surfaces are expensive and, at the same time, do not contribute to the collection of solids. Recently, revamping/retrofitting of pulverized coal (PC)-fired boilers with CFB firing is also being considered as an effective means of inexpensively rehabilitating old power plants (Basu and Talukder, 1999). Because of higher heat fluxes in the PC fired boiler furnaces, a CFB revamping requires additional heat transfer surfaces in the CFB loop to achieve the same throughput after conversion. It is, therefore, necessary to seek new means for heat absorption in the CFB boiler. The standpipe (Fig. 1.5) and cavity-type inertial separator (Fig. 1.6) provide such options. Moreover, the underlying hydrodynamic and heat transfer mechanisms for commonly used wing walls are still unknown.

Standpipes (Fig. 1.5), which transfer solids from the cyclone to the loop seal, are traditionally refractory lined. They offer an opportunity for additional heat transfer in large capacity CFB boilers. The hydro-dynamics of the standpipe consists of dense and dilute phases. Recently, research has been conducted on heat transfer in the dense section of the standpipe and in the downflow moving bed (Liu, 1999; Colakyan, 1984). However, most of this research has focused on the heat transfer to the vertical tubes passing in the standpipe. Such a configuration may adversely affect the free flow of solids down the standpipe, contrary to what is required in CFB boilers. Thus, it is necessary to understand the heat transfer mechanism between gas-solids flow and the standpipe walls.

Current investigation is utilizing a rectangular shape cooled standpipe, as developed by Greenfield Research Inc. (GRI), for revamping old Pulverized Coal (PC) boilers.

The Cavity type inertial separator (Fig. 1.6) is an alternative design for additional heat transfer surfaces developed by GRI, which is less expensive and, at the same time, captures a significant amount of solids entrained from the CFB furnace. The new system is composed of a set of heat absorbing tube panels, which are arranged so as to form a deep cavity i.e., the depth of the cavity is much greater than its width. Because the cavity affects separation primarily by inertia, it is called the inertial-cavity separator. These vertical cavities are installed near the exit of the furnace, leading to the cyclone. Solids exiting the furnace are trapped and separated in the arrays of cavities. Thus, relatively clean gas flows to the convective section of the boiler and the bulk of solids are recycled back inside the furnace. Besides acting as an efficient heat exchange surface, the inertial cavity-type separator could also contribute to the reduction in the loop seal duty, if part of it is used inside the furnace. It would, therefore, be of greater use to make the design of CFB plants more compact and cost effective than the conventional CFB boiler.

The present research has been conducted to fill the gaps regarding the underlying mechanism of heat transfer in the wing walls and to investigate the possibilities of using two innovative ideas, the standpipe and the cavity-type inertial separators in the CFB loop, for additional heat transfer surfaces. This work uses engineering approximation with meaningful simplification of complex processes. It provides the mechanism, mechanistic model and the correlation to predict the heat transfer in the wing walls and compares that with the water walls of a commercial boiler. This thesis also explains the hydrodynamics and heat transfer mechanism of the proposed cavity-type inertial separator and standpipe and proposes mechanistic models with a view to apply the obtained results in a commercial CFB boiler.

1.2 Objectives

The overall objective of this research is to optimize the design of heat transfer surfaces in a CFB boiler by improving the understanding of the heat transfer mechanisms on different surfaces of the boiler.

The specific objectives are as follows:

1. To investigate the heat transfer mechanism on the wing walls
2. To study the heat transfer mechanism on the standpipe
3. To investigate the heat transfer mechanism on the cavity-type inertial separator and the effect of its presence on the heat transfer to the enclosing walls in the furnace
4. To study the overall heat transfer to the walls and wing walls of commercial boilers
5. To develop a mechanistic model of heat transfer on the vertical walls of commercial boilers.

1.3 Scope and limitations

The research comprises five individual studies, scopes of which are explained below.

Study #1: A circulating fluidized bed of 1m × 0.5m in cross section and 5 m in height was designed and fabricated as a part of the thesis work (Appendix A). Experiments on the wing walls were carried out in this pilot plant, operated at room temperature. A wing wall (918 mm [height] × 500 mm [width]) was hung at two different positions in the riser. Heat transfer rates and axial solids fluxes were measured on the wing walls. Superficial velocity and the external solids circulation rate were varied between 3.1 m/s to 4.4 m/s and 1 kg/m².s to 5.8 kg/m².s, respectively. These data were analyzed to study the heat transfer mechanism.

Study #2: The heat transfer was studied in a standpipe test section, 1.94 m long with a square cross section of 100 mm side. Heat transfer rates and axial pressure drops were measured in both dense and dilute sections of the standpipe. Solids used in this study were Ceramic Microsphere (Type A) and Nova Scotia sand (Type B) with densities of 700 kg/m^3 and 2564 kg/m^3 , and sizes of 0.130 mm and 0.266 mm, respectively (Appendix B). Standpipe superficial velocity and the external solids circulation rate were varied between 0.016 m/s to 0.085 m/s and $G_s=9$ to $47.2 \text{ kg/m}^2\cdot\text{s}$, respectively. Heat transfer mechanism was studied by analysing the measured data.

Study #3: Experiments on the cavity-type inertial separators were carried out in the experimental unit described in study #2. Three rows of cavity-type inertial separators were hung from the roof, with one row inside the riser (simulating the furnace) and two rows in the primary chamber, located between the back-pass and the riser. Heat transfer rates, axial and lateral solids fluxes were measured on both inner and outer walls of the separators. Superficial velocity and the external solids circulation rate were varied between 3.1 m/s to 4.4 m/s and $1 \text{ kg/m}^2\cdot\text{s}$ to $5.8 \text{ kg/m}^2\cdot\text{s}$, respectively. Data obtained from the experiments were analyzed to study the heat transfer mechanism.

Study #4: Commercial secrecy and lack of proper instrumentation made it difficult to get reliable data in commercial CFB boilers. However, some data on heat transfer coefficients were deduced from a set of measured operating parameters in two large commercial CFB boilers. One unit is in the range of 20 MW_e , while the other unit produces more than 170 MW_e power. Like any commercial unit, these boilers were operated under different loads at different times. Data logged at different loads were analyzed to deduce heat transfer coefficients under different conditions. Empirical correlations were developed based on those data.

Study #5: Data deduced in study #4 were used to develop a correlation for the fractional wall coverage of the water walls in commercial boilers. Mechanistic models for the wing walls of commercial boilers, and inertial cavity type separators for a hot bed pilot plant are also proposed based on the heat transfer mechanism observed in studies #1 and 3.

1.4 Contribution of this dissertation

Table 1 shows how the present research contributed to the science of fluidized bed boilers.

Study #1: This work is a new and original piece of research. There exists no previous information within the public domain. The heat transfer on wing wall was entirely unexplored.

Study #2: The work comprises both experimental and theoretical investigations. No information on heat transfer is available in the dilute section of the standpipe. The present investigation fills that gap by providing both experimental and theoretical analysis.

Study #3: The idea of using an inertial cavity type separator as heat exchanger is an invention of P. Basu (1999). The heat transfer mechanism on this separator has never been reported. The present work is the first attempt to explore this potential and provide a reliable body of data.

Study #4: A methodology is developed to deduce heat transfer coefficients on wing walls from the measured overall heat duties of the entire evaporator. Correlations for both water walls and wing walls were developed by relating height-average heat transfer coefficients, with operating parameters i.e., average suspension density and average bed temperature. No information concerning the research/correlation for wing walls is currently available to the scientific community. Though a number of researchers showed that radiation is a

factor dominating the heat transfer in the upper part of the water wall, no correlation is available in the open literature, which includes bed temperature as a dependent variable. The newly developed correlation on the water walls has been tested against heat transfer coefficients, already measured and reported by other researchers.

Table 1.1. Contribution of the present study

Heat Transfer in CFB boiler			
P L A N T	Heat Transfer in standpipe	Heat Transfer in Pilot Plant	Heat Transfer in Commercial Unit
B A C K G R O U N D	Study on dense section of the standpipe is available but study on the dilute section of the standpipe is unavailable	Investigations are limited mostly to circular enclosing walls with high solid circulation rates. Limited study is available on rectangular sections with enclosing walls Studies on wing walls and cavity type separators are not available	Available heat transfer correlations use suspension density as the only variable No study on wing wall surfaces is available
C O N T R I B U T I O N	<i>New data on heat transfer are generated and a mechanistic model proposed</i>	<i>First reported study on heat transfer to wing walls and inertial separators</i>	<i>Improvement of correlations and models for heat transfer in CFB boilers including effects of bed temperature</i>

Study #5: The cluster renewal model, the most accepted model for estimating heat transfer coefficients to the water wall, has been further improved by adding new information on certain parameters of this model, such as: fractional wall coverage, contact time, gas gap etc. A correlation for the fractional wall coverage in commercial boilers was developed including recent findings on other parameters and assuming a thermal boundary layer along the height of the water wall. In addition, mechanistic models on wing walls of commercial boilers and cavity-type inertial separators for hot bed pilot plant are also proposed for the first time in this study.

1.5 Works published from this study

In refereed journals

“An experimental investigation into the heat transfer on wing walls in a circulating fluidized bed boiler”, Animesh Dutta and Prabir Basu, International Journal of Heat and Mass Transfer (Accepted, April 2002)

“Overall heat transfer to water walls and wing walls of commercial circulating fluidized bed boilers”, Animesh Dutta and Prabir Basu, Journal of the Institute of Energy (Accepted, June 11, 2002)

In refereed conferences

“Performance of a Novel Horizontal Gas Solid Separator in a Circulating Fluidized Bed Riser” S. Saha, P. Basu and A. Dutta, proceedings of CFB-VII , Niagara, Canada, 2002.

In non-refereed conferences

“Effect of wing wall on hydrodynamics and wing wall in a circulating fluidized bed boiler furnace”, A. Dutta and P. Basu, 51st Canadian Chemical Engineering conference, Halifax, 2001.

Paper submitted for review

“An Investigation on heat transfer to the standpipe of a circulating fluidized bed boiler”, A. Dutta and P. Basu, Journal of Chemical Engineering research and Design, (Revised, August 2002)

“Experimental Investigation into heat transfer on cavity-type inertial separators-A novel technique for development of subcompact circulating fluidized bed boilers” A. Dutta and P. Basu, Int. J. Heat and Mass Transfer, August 2002.

1.6 Organization of the thesis

The summary of the study, forming the basis of this thesis, is outlined in Figure 1.7. The contents of the individual chapters are as follows:

Chapter 2 presents a review of literature on heat transfer and its dependent parameters in the CFB boiler; especially for commercial units. It also discusses the available mechanistic models for predicting heat transfer coefficients on the surfaces in the CFB loop.

Chapter 3 presents overall heat transfer coefficients on water walls and wing walls and their comparison in a commercial boiler. It also proposes a methodology to deduce heat transfer coefficients on wing walls from the measured overall heat duties of the entire

evaporator. Two correlations on heat transfer into wing walls and water walls are also presented based on estimated data.

In *Chapter 4*, detailed descriptions of experimental investigation on heat transfer into wing walls in a pilot plant at room temperature are presented. It also compares the mechanism of heat transfer both on wing and water walls.

Chapter 5 presents detailed descriptions of experimental investigations on heat transfer into standpipe in a laboratory unit at room temperature. It also presents a theoretical model for predicting heat transfer in the standpipe.

In *Chapter 6*, detailed descriptions of experimental investigations on heat transfer into cavity-type inertial separators in a pilot plant at room temperature are presented. It also presents the enhancement of heat transfer on the riser walls due to its presence in the riser.

Chapter 7 presents mechanistic models on water walls and wing walls of commercial units. It also proposes a mechanistic model to predict the heat transfer coefficients in the cavity-type inertial separator for a hot bed pilot plant.

Chapter 8 lists principal conclusions from this study and some recommendations for further research.

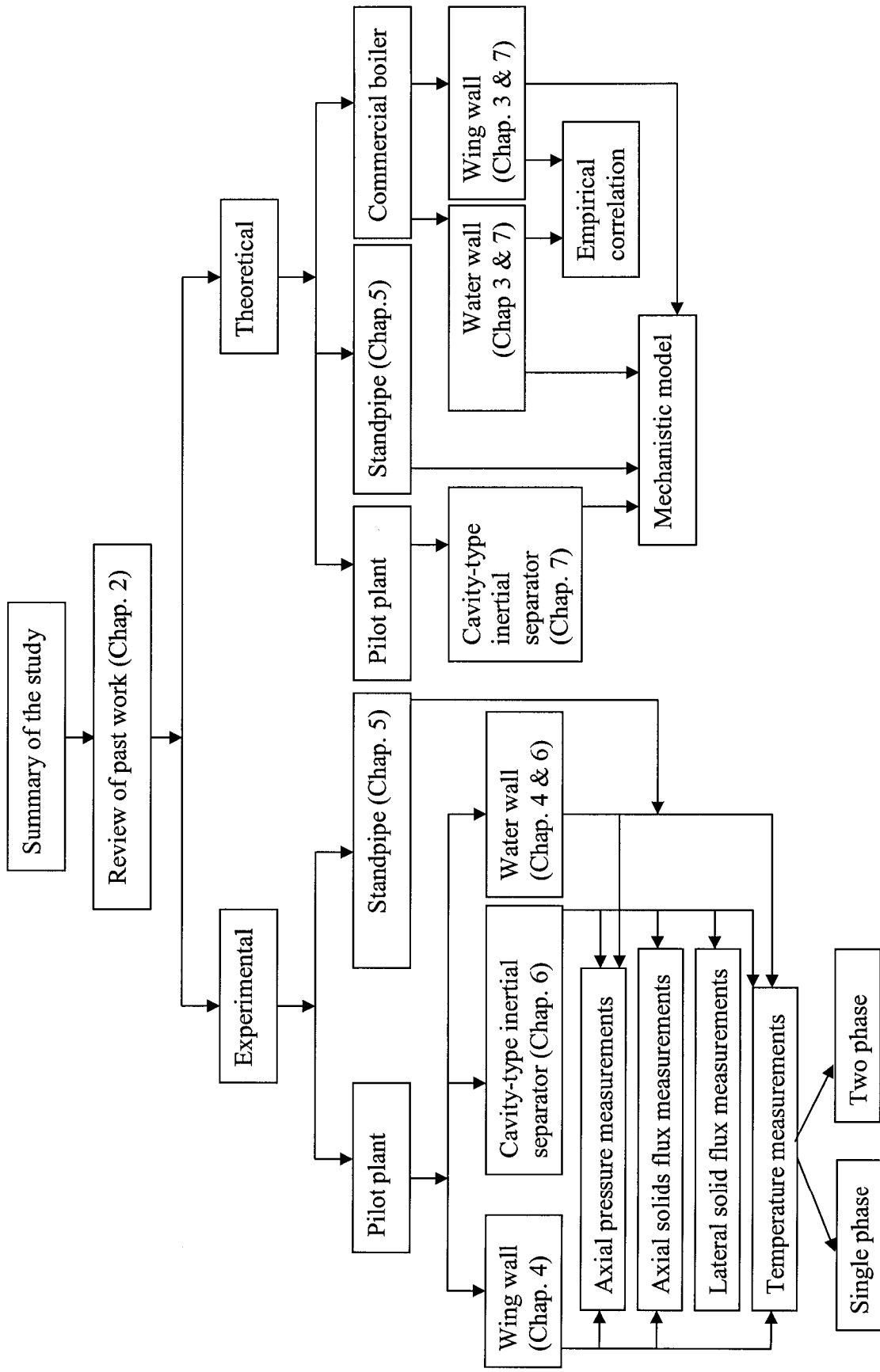


Figure 1.7. Summary of the study

Chapter 2

Literature Review

The purpose of this section is to describe the present level of understanding of the heat transfer processes in the Circulating Fluidized Bed (CFB) loop of CFB boilers with special emphasis on large commercial units. This review focuses on three important areas of heat transfer in CFB boilers, i.e., (1) fast bed to the furnace walls, (2) fast bed to the suspended bodies and (3) moving bed to the wall of standpipe. This study also summarizes the effect of different parameters on the heat transfer.

2.1 Introductory remarks

The heat transfer mechanisms of CFB boilers differ greatly from those in conventional boilers. In a conventional fossil fuel steam generator (boiler), the physical mechanism of heat transfer is restricted to radiation and gas convection. However, the mechanism occurring in CFB boilers, though not yet fully understood is believed to be dominated by particle convection. An accurate understanding of heat transfer to the bed walls, as well as to immersed surfaces is required for proper design, operation and trouble-shooting of CFB boilers. To develop an economic boiler design, one must understand how different design and operating parameters influence the heat transfer coefficient.

In a circulating fluidized-bed boiler, the heat generated from combustion in the furnace is transferred to water and steam in two sections. The primary area for heat absorption is the circulating fluidized bed (CFB) loop around which hot solids circulates, and the secondary area is the back-pass or convective heat transfer section beyond the CFB loop (Fig. 2.1). The CFB loop comprises the furnace, operating in fast and turbulent fluidized-

bed regimes, and the standpipe, which includes cyclones and bubbling fluidized beds. The following modes of heat transfer are involved in the CFB loop (Basu and Nag, 1996):

1. Fast bed to the furnace walls;
2. Fast bed to suspended bodies in the furnace;
3. Bubbling fluidized bed to surfaces in the external heat exchanger;
4. Swirl flow to the wall of the cyclone;
5. Moving bed to the wall of the standpipe;
6. Gas to particle in lower turbulent-bed and bubbling-bed classifier

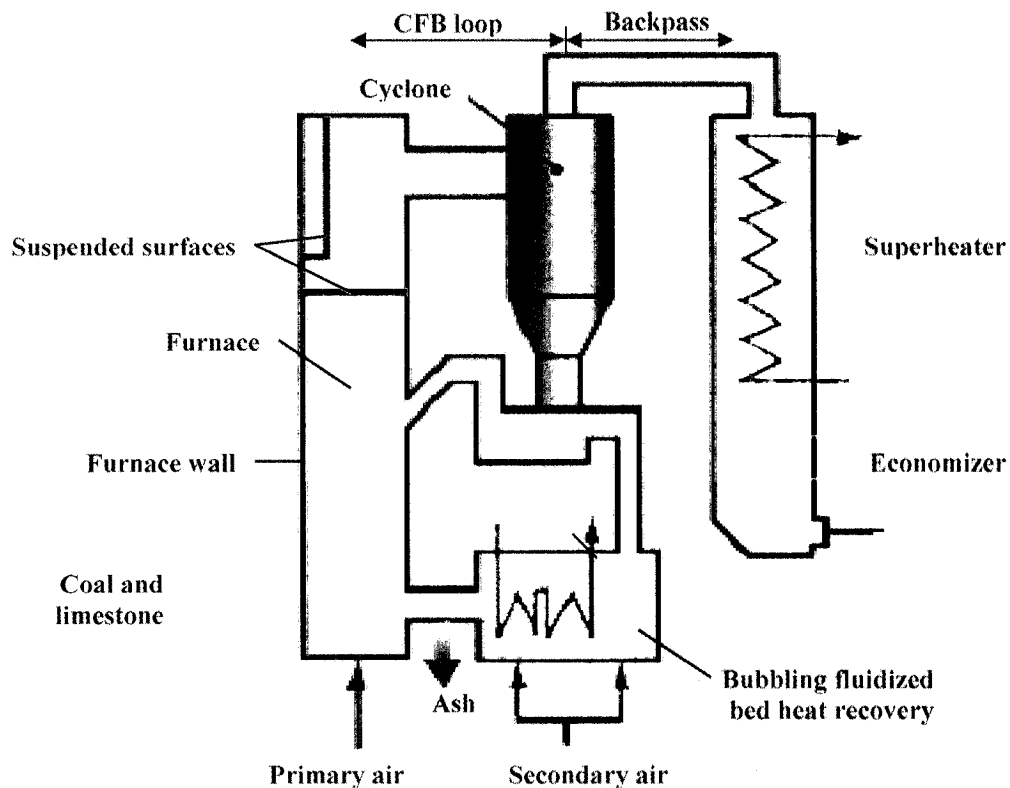


Figure 2.1. Location of heat transfer surfaces in a CFB boiler

The majority of the heat in the primary loop is, however, transferred in the “fast bed”, which is the section of the furnace above the secondary air injection level. The present review will concentrate on three types of heat transfer, i.e., (1) fast bed to the furnace walls, (2) to the suspended bodies and (3) moving bed to the wall of the standpipe.

2.2 Hydrodynamics

The primary focus of this review will be on the heat transfer occurring between the circulating bed and the bed walls. The heat transfer process is controlled by the hydrodynamics of the solids and gas mixture in the vicinity of the wall. Although the wall hydrodynamics are important in heat transfer, comprehensive information on this is still awaited. Some limited information relevant to heat transfer is available (Lim *et al.* 1995; Berruti *et al.* 1995; Horio 1997). As per these works the overall structure of a circulating or fast bed includes a core with clusters of particles and individual particles moving upward in the gas stream (Figure 2.2).

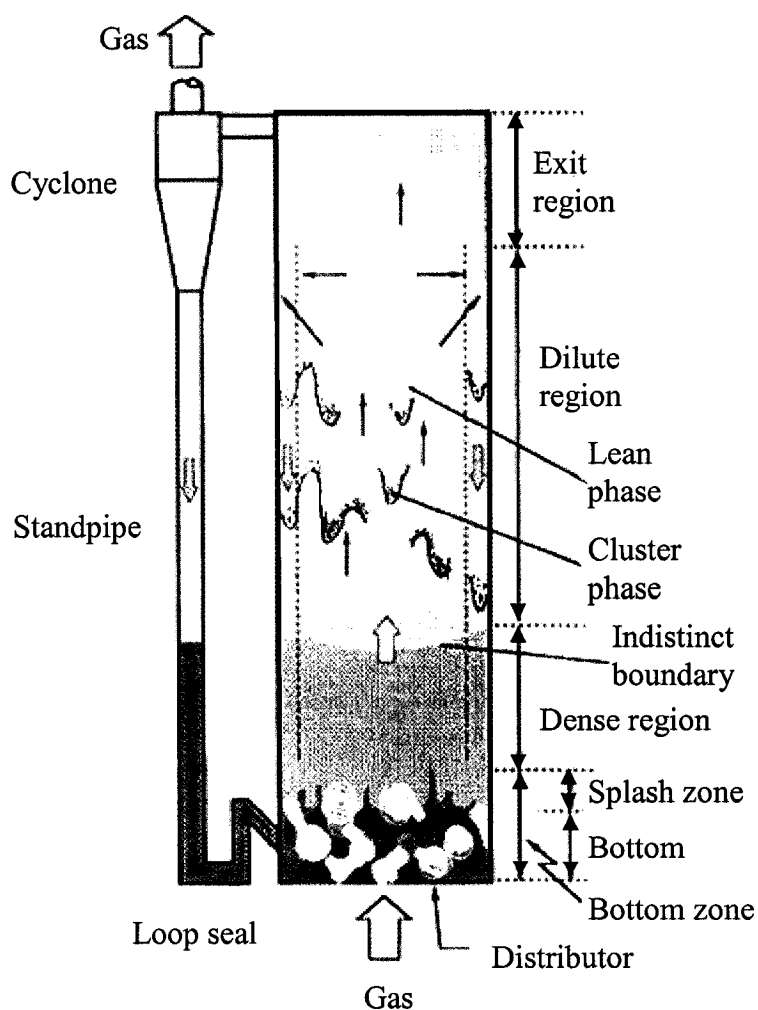


Figure 2.2. Core annulus structure of CFB (adapted from Horio, 1997)

The particles generally move upward in the core, where the temperature is nearly uniform. In the annular region, near the walls, where the gas velocity is low, the particles tend to fall downward. Between these two regions there lies a transition zone where the net solids flux (upward minus downward) is zero. The width of the annular zone makes up only a minor portion of the bed diameter (Glicksman, 1997; Zhang, 1995). Clusters or individual particles enter the annular region from the core at the mean bed temperature. From the core to the annulus, there will be a lateral temperature gradient due to the cooling on the boiler furnace (Golriz, 1995).

The radial transfer of solids from the core to the wall has been linked to the radial deposition process (Bolton and Davidson 1988). Glicksman and Westphalen (1994) argued, that in the upper dilute region of the bed, the radial flux is due primarily to radial motion of dispersed particles, rather than radial motion of concentrated particle-clusters. In the lower portion of the bed, a particle motion to the wall may be largely due to particles ejected with a radial component of velocity from the dense region near the base of the bed.

2.3 Heat transfer

Heat can be transferred from the core of the bed to the wall by several different mechanisms. In a CFB of fine solids (Geldart Group A and B), the particles agglomerate, forming clusters or strands in a continuum of generally up flowing gas containing sparsely dispersed solids. The latter form is called the dispersed phase, while the former form is called the cluster phase. The majority of the bed particles move upwards through the core of the bed, but they flow downwards along the wall in the form of clusters of particles or strands. These agglomerates, termed clusters, are not permanent; they form, dissolve and reform leading to a dynamic flow structure. Thus the heat transfer to the wall occurs through convection from particle clusters, through convection from the dispersed phase, and through radiation from both phases (Figure 2.3).

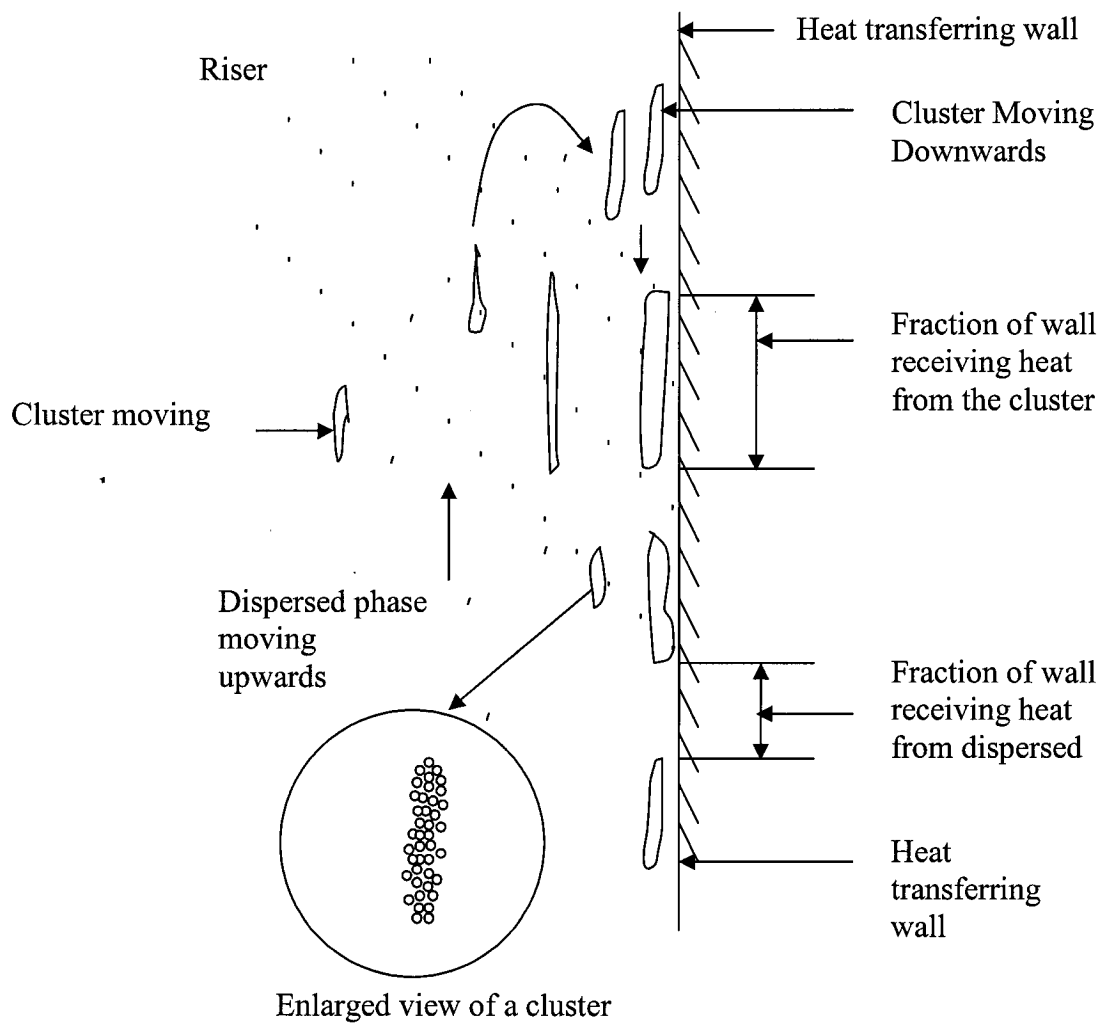


Figure 2.3. Schematic representation of the mechanism of heat transfer to walls of a circulating fluidized bed. (Basu and Fraser, 1991)

Heated particles, at core temperature, move to the wall and transfer their energy, upon contact with the wall. This is termed particle convection. Since the particles seldom touch the wall most of the heat transfer must occur through the gas layer separating the particles and the wall.

The remainder of the wall area, not covered by clusters, is contacted by gas or a very dilute particle-gas mixture. This sparse collection of particles may aid in the heat transfer, but the primary heat transfer is from the gas, at or near bulk temperature, through its contact with the wall. The motion of the gas is the primary means of transferring energy from the core or inner portion of the annulus to the wall. This action is termed as dispersed phase/gas convection.

At an elevated temperature, radiation serves to augment the heat transfer both to the uncovered surface, as well as the surface covered by clusters. To obtain the overall average heat transfer to the wall, some investigators have advocated simple superposition of particle convection, gas convection and radiation, each calculated in the absence of the other two mechanisms.

2.3.1 Effect of Operating Parameters on Heat Transfer

Based on a critical analysis of the experimental results presented in the literature (Table 2.1 -2.5) for both laboratory and industrial scale units, the effects of different operating and design parameters on the measured heat transfer coefficients are summarized as follows:

2.3.1.1. Suspension density

A number of researchers (Kobro and Breton, 1986; Basu, 1990; Wu *et al.* 1989a) found that suspension density is the most dominant operating factor influencing the heat transfer to the wall. Experimental data, gathered both in laboratory units and in commercial units by different investigators, show that heat transfer coefficients increased with the suspension density. This is expected because the thermal capacity of solids is much higher than that of gas. The heat transfer coefficient is found to vary as the square root of the cross-section average suspension density (Glicksman, 1988; Basu, 1991; Ebert *et al.*,

1993). A summary of proposed correlations for overall heat transfer coefficients in large commercial boilers is presented in Table 2.1.

Table 2.1. Summary of empirical correlations of heat transfer in large-scale CFB boilers

Investigators	Correlations (W/m ² .K)	Suspension density ρ_{sus} , (kg/m ³)	Bed temperature T_b , (°C)
Anderson and Leckner (1992b)	$h_{tot} = 30\rho_{sus}^{0.5}$	5-80	750-895
Golriz and Sunden (1994)	$h_{tot} = 88 + 9.45\rho_{sus}^{0.5}$	7-70	800-850
Anderson (1996)	$h_{tot} = 70\rho_{sus}^{0.085}$ $h_{tot} = 58\rho_{sus}^{0.36}$	>2 ≤	637-883
Basu and Nag (1996)	$h_{tot} = 40\rho_{sus}^{0.5}$	$5 < \rho_{sus} < 20$	$750 < T_b < 850$
Breitholtz <i>et al</i> (2000)	$h_{tot} = 110\rho_{sus}^{0.21}$	NS	$750 < T_b < 900$
Baskakov <i>et al</i> (2001)	$h_{tot} = 85\rho_{sus}^{0.3}$	$5 < \rho_{sus} < 10$	800-850

Divilio and Boyd (1994) presented an interesting overview of the effect of solids suspension density on heat transfer in large-scale CFB boilers. In typical CFB boilers the temperature of the combustor or of the bed is a function of the heat transfer between the combustor walls and the circulating bed material. The heat transfer rate is again a function of the suspension density in the combustor and the bed temperature. As the height of the combustor increases, the solid suspension density may decrease, resulting in lower heat transfer coefficients. Using data from cold bench scale beds by a number of researchers (Kiang *et al*, 1976; Basu and Subbarao, 1986; Fraley *et al*, 1983; and Mickley and Trilling, 1949), Divilio and Boyd (1994) obtained the following empirical relationship for the convective heat transfer coefficient:

$$h_c = 23.2\rho_{sus}^{0.55} \quad \text{W/m}^2\cdot\text{K} \quad (2.1)$$

It shows that doubling the suspension density within the CFB will increase the convective heat transfer coefficient by only 46%. However, while analysing the effect of suspension density on heat flux for a large-commercial CFB boiler at Nucla, the same researchers

found a minor effect of suspension density. They correlated the result on heat flux to the furnace wall by the following equation:

$$\text{Heat flux} = 36,700 \rho_{sus}^{0.062} V_s^{0.574} \quad \text{W/m}^2 \quad (2.2)$$

Equation 2.2 shows that doubling the suspension density will result in a mere 4% increase in the heat flux to the combustor walls, which is considerably lower than the expected 46% increase in the heat transfer coefficient predicted by Equation 2.1. For a suspension density of 3 kg/m³, the convective heat transfer coefficient is found to be 42 W/m² K from Equation 2.1. However, the radiative heat transfer coefficient, under CFB operating condition is found to be approximately 135 W/m² K (Divillio and Boyd, 1994). Thus radiation, rather than convection would appear to be the dominating factor in a large-scale CFB's heat transfer mechanism.

Breitholtz *et al* (2000) propose a correlation for the convective heat transfer coefficient for a large commercial unit.

$$h_c = 25 \rho_{sus}^{0.58} \quad \text{W/m}^2 \cdot \text{K} \quad (2.3)$$

For a suspension density of 3 kg/m³, Equation 2.3 gives the convective heat transfer coefficient to be 47 W/m² K. This result agrees well with the result from the Equation 2.1.

Werdermann and Werther (1994) correlated their results for convective heat transfer on vertical walls of CFB boilers in the following way:

$$\text{Nu}_c = 7.46 \times 10^{-4} \text{Re}_t^{0.757} \rho_{sus}^{0.562} \quad (2.4)$$

where Re_t is the Reynolds number based on the bed diameter.

It may, therefore, be concluded that the heat transfer correlations, based on suspension density alone, would not give the appropriate estimation of heat transfer coefficients on the enclosing walls of CFB boilers. The present work, therefore, tried to develop a correlation taking account of other factors like bed temperature.

2.3.1.2 Bed temperature

The heat transfer coefficient increases with bed temperature, due to higher thermal gas conductivity and higher radiation at increased temperatures, as demonstrated in Figure 2.4 (Basu and Nag, 1996) for laboratory units. The large contribution of radiation to the total heat transfer is a good indicator of the role of bed or furnace temperature. For example, in boilers operating with low suspension densities, (less than 20 kg/m^3) (Divilio and Boyd 1994, Lackner and Andersson 1992, Couturier *et al* 1993, Andersson 1996), the radiation dominates the heat transfer in most parts of the combustion chamber (Divilio and Boyd 1994, Andersson and Lackner 1994, Wirth 1994, Baskakov *et al* 2001). Tang and Engstrom (1987) have reported an increase in the contribution of radiation from 60 to 90% of the total heat transfer when the load on the boiler dropped from a full to a minimum load. The suspension density reduces greatly when the fluidization velocity was decreased from 5.2 m/s at full load to 1.8 m/s in low load in a commercially operating CFB boiler. This appears to contradict common observations in laboratory units.

In commercial boilers air is supplied in two stages. The primary air comes through the grid plate while the secondary air is injected from the walls above the refractory lined lower combustor. The bulk of the bed solids resides in the lower bed. At low load, the air velocity is reduced down to bubbling bed regime. Thus solids from the lower bed are not transported to the upper bed where the heat absorbing surfaces are located. Basu and Konuche (1988), who measured the radiative flux and the total heat flux in a CFB pilot plant operating in temperatures in the range of 650 to 900°C , found that when the bulk density decreased from 20 to 6 kg/m^3 , the radiative part of the heat transfer increased

from 74 to 91%. This happened due to the reduction in the convective component of the heat transfer.

Jestin *et al* (1992) measured heat transfer coefficients in the 125 MW_e boiler at Carling, and they correlated their data in the form similar to that used by Basu & Nag (1996).

$$h = k(\Delta p)^\alpha (T_b)^\beta \quad \text{W/m}^2 \cdot \text{K} \quad (2.5)$$

where Δp is the pressure drop across the entire furnace (a measure of the suspension density), T_b is the temperature of the bed and k , α , β are empirical constants. Equation 2.5 appears to be promising, but it is of very little use to the designers as they did not report the values of the empirical constants in their paper.

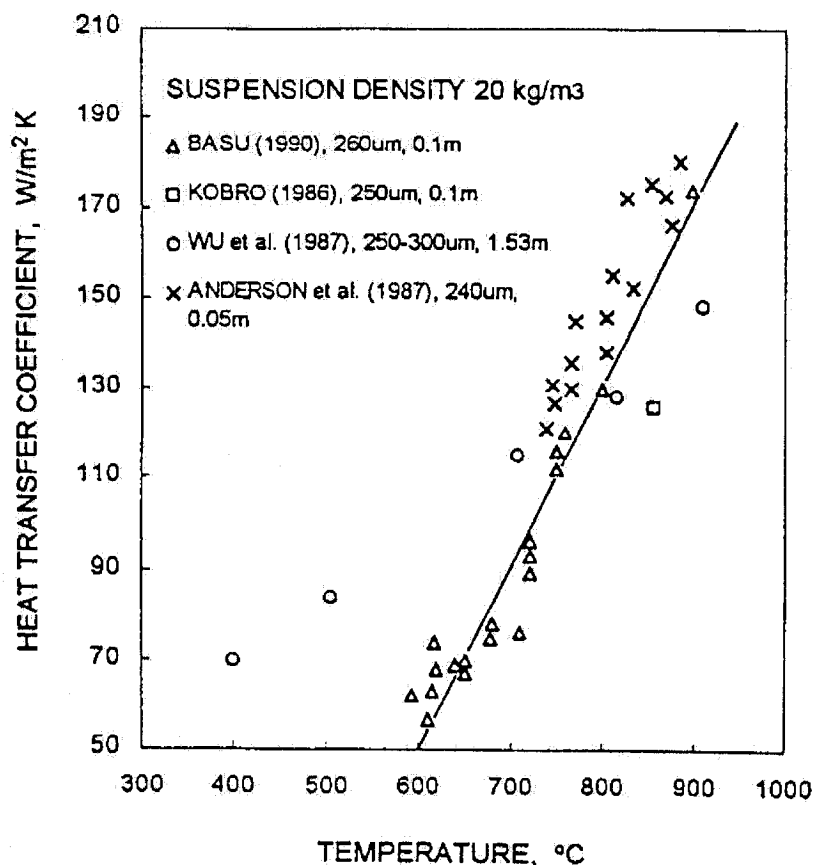


Figure 2.4. Effect of bed temperature on heat transfer coefficients (Basu and Nag, 1996)

2.3.1.3 Fluidization Velocity

Except for a very dilute bed, the superficial velocity does not have any great influence on the heat transfer coefficient (Wu *et al.*, 1987; Furchi *et al.*, 1988; Ebert *et al.*, 1993). In most CFB, heat is carried primarily by particles. So the gas convection plays a minor role in the heat transfer. In a large CFB boiler, where the upper part of the combustion chamber contains a dilute phase, fluidization velocity might have some effect on the heat transfer. Equation 2.2 (Divillio and Boyd, 1994) and Equation 2.4 (Werdermann and Werther, 1994) indicate that superficial velocity has some effect on heat transfer. Contrary data are reported from the Chalmers unit (12 MW_{th}), where the combustion air is added at two levels in the furnace, and a change in the secondary air rate did not have much effect on the heat transfer coefficient in the upper part of the furnace. However, an increase in the primary air velocity raises the heat transfer coefficients, because of an increase in suspension density in that region of the bed (Anderson and Leckner, 1992a, b). This was also explained in the earlier section. In general, in the annular section i.e., on the enclosing wall, one might observe negligible gas velocity and, hence, ignore its contribution to heat transfer. However, in the core, the measured gas velocity is found to be almost twice that of the superficial gas velocity (Moran and Glicksman, 2001) and, therefore, its contribution to heat transferring surfaces exposed to the core must be considered.

2.3.1.4 Particle size

The particle size has an important effect on heat transfer in bubbling fluidized beds (Basu, 1985). For CFB the effect is less clear. Higher heat transfer coefficients for smaller particles were observed in CFB by several investigators including Mickley and Trilling (1949), Basu and Nag (1987), Stromberg (1983) and Fraley *et al.* (1983). However, all these investigators used short heat transfer sections located on adiabatic walls, where the cluster would have only brief residence on the heat-transferring surface. As a result, the

contact resistance of the particles on the wall dominates the heat transfer to the surface. Since the contact resistance is directly proportional to the particle diameter, the above investigators noted lower overall heat transfer coefficients for the larger particles. Measurements with relatively long (>1.5 m) heat transfer surfaces, used with the typical size-range particles common in CFB boilers, did not demonstrate this effect (Wu *et al.*, 1987). Thus, in large-scale CFB boilers with water-wall furnaces, one would not expect a direct effect of the particle size on the heat transfer. This is a significant departure from the bubbling fluidized bed boiler. However, some indirect effect may occur through the effect of particle size on the suspension density.

2.3.1.5 Vertical length of heat transfer surface

The residence time of a cluster on the heat transfer surface depends on its velocity and the length of the surface on the length over which the particle remains on the wall before detaching to it. A number of investigators (Bi *et al.*, 1991; Wu *et al.*, 1990a, b; Nag and Moral, 1990a; Zheng *et al.*, 1991; Kolar and Sundaresan, 2002) observed that the heat transfer coefficient decreases with the length of the heat transferring surface. A number of researchers have measured the velocity of clusters in the wall layer, including Barder *et al.* (1988); Horio *et al.*, (1988); Hartge *et al.* (1988); Wu *et al.* (1989a); Gidaspow *et al.* (1989); Yang *et al.* (1991); Nowak *et al.* (1992); Wirth and Seiter (1991); Rhodes (1990) Lints and Glicksmann (1994); Griffith and Louge (1998); and Noymer and Glicksmann (2000). Most of the data reports cluster velocity, within 0.5 to 3 m/s depending mainly on particle size. Table 2.2 presents a summary of measured cluster velocity on the wall.

Measurements by Noymer and Glicksman, (1998) showed that the contact time (residence time), cannot be correctly estimated by using a constant falling velocity as the particles accelerate to the terminal settling velocity while falling. Based on the above observation, Zevenhoven *et al.* (1999) estimated the cluster velocity as well as the contact time. They conducted experiments on both cold and hot CFB facilities at Foster Wheeler Energia Oy,

at Karhula. Video recordings were made using a multiple exposur technique. Results indicated that in the cold unit, particles return into the main gas stream, when their vertical velocity equals approximately 80% of the terminal settling velocity, after a contact time in the order of 0.5 second. However, in the hot CFB, the particles return into the main gas stream with a velocity equaling approximately 50% of the terminal settling velocity, after a contact time in the order of 0.1 second. The reason for this shorter wall-residence time in hot bed is unknown.

Table 2.2: Major studies on the measurement of cluster velocity on the wall

Authors	Bed Temp K	Bed Material	d_p (μm)	ρ_s (kg/m^3)	U_{cl} (measured)
Rohdes et al (1992)	300	Alum.	75	2460	0.3
Zhou et al (1995)	300	Sand	213	2640	1.5
Harris et al (1994)	300	FCC	60	1700	0.8
Ishii et al (1989)	300	FCC	60	1000	0.5
Bader et al (1988)	300	FCC	76	1710	0.9
Noymer and Glicksmann (1998)	300	Steel	69	6980	1.2
Noymer (1997)	300	Sand	128	2660	1.2
Noymer (1997)	300	Sand	182	2650	1.1
Hartge et al (1988)	300	FCC	85	1500	1.0
Hartge et al (1988)	300	Ash	120	2600	1.0
Zhang et al (1995)	1125	n/a	330	2600	0.9
Yang and Gautam (1995)	300	n/a	250	2250	0.4
Wang et al (1993)	300	Sand	530	2300	2.0
Lints (1992)	300	Sand	80	2660	1.6
Lints (1992)	300	Alum.	600	2750	1.8
Wu et al (1991)	300	Sand	170	2650	1.3
Lim et al (1996)	300	Sand	213	2640	1.0
Zevenhoven et al (1999) a. D_{eq} =0.4 m and b. D_{eq} =0.65m	a. 300 b. 1108	Quartz- like glass	310	1700	a. 1.25 b. 0.71
Caloz et al (1999) a. D_{eq} =0.41 m, b. D_{eq} =0.83 m and c. D_{eq} =12.3 m	a. 313 b. 313 c. 1183	n/a	n/s	n/a	a. 0.7-1.5 b. 2-2.4 c. 5-8
Hartge et al (2002) D_{eq} =12.3 m	n/a	Sand- Ash	150	2600	5-8

n/a-Not available

Zhang (1995) measured the cluster velocity in a 12.7 MW_{th} Chalmers unit and found a downflow velocity ranging from 0.9 m/s to 1.6 m/s. He observed that closer to the wall, the falling velocity is closer to 0.9 m/s.

Hartge *et al.* (2002) and Caloz *et al.* (1999) independently measured the downward velocity at the wall, which was much higher than that previously reported. The values vary between 5 and 8 m/s, in the 600 MW_{th} Gardanne boiler. They also demonstrated that cluster velocity on the wall increases with increasing the size of the riser. The velocity also increases with the distance from the top of the riser to the measuring point. These seem to indicate that in large units solids move in solids agglomerates which is larger in larger units. Hartge *et al.* (2002) observed a dependence of cluster velocity on wall layer thickness and proposed the following correlation by assuming the cluster velocity at the top of the riser as zero:

$$U_{cl} = 20.4S_{cal} \quad (2.6)$$

where S_{cal} can be estimated by the correlation proposed by Werdermann and Werther (1994)

$$\frac{S_{cal}}{D_{eq}} = 0.55 \cdot \text{Re}_t^{-0.22} \cdot \left(\frac{H_t}{D_{eq}} \right)^{0.21} \cdot \left(\frac{H_t - h}{H_t} \right)^{0.73} \quad (2.7)$$

Of late, Noymer and Glicksman (2000) proposed a correlation for cluster velocity which gives better predictions for most of the data reported in Table 2.2.

$$U_{cl} = 0.75 \sqrt{\frac{\rho_p}{\rho_g} g d_p} \quad (2.8)$$

Equation 2.6 is derived by fitting the experimental data on cluster velocity at the wall of some commercial units and by assuming the cluster velocity as zero at the top of the riser.

The exceptionally high cluster velocity predicted by Hartge *et al* (2002) for a larger riser, are yet to be confirmed by other researchers. The Equation 2.8, based on a more simplified model, which was developed on the basis of the drag force acting on a cluster, predicts cluster velocity (Table 2.2) satisfactorily.

It is observed that the heat transfer coefficient decreases with the length of the heat transferring surface (Bi *et al.*, 1991; Wu *et al.*, 1990a, b; Nag and Moral, 1990a; Zheng *et al.*, 1991; Kolar and Sundaresan, 2002). This effect can be explained by the fact that as the solids fall along the wall they get cooled and the thermal driving force decreases which reduces the heat transfer coefficients. Wu *et al* (1989) measured this “characteristic” resident length of particles and found that it could be correlated by

$$L_c = 0.0178\rho_{sus}^{0.596} \quad (2.9)$$

Since, the furnace walls of the commercial boilers are longer than this length, the effect of length is not observed on heat transfer coefficients on most commercial CFB boilers.

2.3.2 Heat transfer to the suspended surfaces

Large capacity commercial boilers use suspended surfaces inside the furnace in the form of wing wall, division wall, omega tubes etc. A number of researchers (Bi *et al.*, 1991; Zheng *et al.*, 1991a) measured the lateral distribution of heat transfer at room temperatures using bench-scale units. They found the heat transfer coefficient to increase towards the wall following the pattern of variation of local suspension densities. Recently, Kolar and Sundaresan (2002) measured average heat transfer coefficients on four vertical tubes of different lengths, located at the axis in a laboratory unit. They observed lower heat transfer coefficients in the core compared to what was measured on the wall. The heat transfer coefficient decreased with increasing tube length. Measurements carried out by Couturier (1989) for a 22 MW_e CFB boiler noted that the lateral profile of heat

transfer coefficient was flat for the suspension densities of 0.5 and 4.6 kg/m³, which somewhat contradicts the measurements made in a laboratory unit (Kolar and Sundaresan, 2002). One possible explanation for this is given below.

In large boilers, radiation becomes the predominant mode of heat transfer. Away from the wall, the particle convective heat transfer is low, but the radiation is high because the view factor is highest at the center of the furnace, decreasing continuously towards the wall. This results in a higher or at best equal heat transfer coefficient in the core of the furnace than that on the wall. Heat transfer coefficients measured on horizontal tube banks in the Duisberg boiler (Werdermann and Werther, 1994) supports the above reasoning. The heat transfer coefficients on tubes located in the middle (Basu, 1990) as well as adjacent to the wall (Wu *et al.*, 1989a) were found to be higher than those on the wall for all temperatures in the range of 400-900 °C. However, most of these studies were carried out on a single tube placed at the center of the core in the furnace of a laboratory unit. On the other hand, the heat transfer mechanism on most commonly used suspended heat transfer surface areas in a boiler, which are hung from the roof and extend from the front wall to some distance towards the opposite wall, where the furnace exit located is yet to be explored. From the reported study it would not be possible to draw a conclusion on the understanding of gas solids flow structure in the riser with suspended bodies and hence study in this direction is required.

2.3.3 Heat transfer in the standpipe

The hydrodynamics of solids flow in the standpipe of a CFB has been studied by some investigators (Knowlton, 1997; Basu and Fraser, 1991; Jones *et al* 1985). A number of studies (Table 2.3) have been carried out on heat transfer in fluidized and moving bed flows, which do not exactly match the conditions of a standpipe, but provide a useful starting point for understanding the heat transfer behaviour in the standpipe. Most of the studies reported in the Table 2.3 were carried out in the moving downflow bed. However,

no study is reported for the dilute section of the standpipe and the only study (Liu, 1999), which is available for the dense section of the stand pipe is also carried on vertical tubes passing inside the standpipe. Such a configuration may affect free flow solids down the standpipe as required in CFB boilers. So, there is a need to understand the heat transfer between the solids and the standpipe walls and hence, investigations required in this direction.

Table 2.3. Heat transfer studies in moving bed (adopted from Colakyan, 1984)

Investigator	Particles (mm)	Materials	Gas	U_s (m/s)	Comments
Kurochkin (1958)	0.4-3	Sand	Air	0.0023 -0.023	Flowing bed, single heated tube; data correlated
Donskov (1958)	0.3-0.7	Sand, wet coal	Air	0.0024 -0.023	Flowing bed, tube arrays, single tube, data correlated
Kurochkin (1966)	0.25-1.77	Sand	Air	NA	Flowing bed, single heated circular, elliptical tube; data correlated
Botterill and Hampshire (1968)	0.17-1.3	Steel, copper shots	Air	NA	Flowing bed, flat heated surface
Botterill and Desai (1972)	0.15-0.625	copper shots	Air	NA	Flowing bed, flat heated surface
Sullivan and Sabersky (1975)	0.2-2.16	Mustard seeds, glass beads, sand	Air	NA	Flowing bed, flat heated surface, data correlated
Denloye and Botterill (1977)	0.16-2.4	Copper shot sand, sand coal, ash soda glass	Air, Fe, He, CO ₂	0.003-0.03	Flowing bed, flat heated surface, maximum value of h correlated
Colakyan and Levenspiel (1984)	0.2-2	Cork, sand, polyethylene, zirconia, copper	Air	0.007-0.36	Flowing bed, single heated tube
Jingyuan Liu et al (1999)	0.19-0.68	Resin, sand	Air	0.012-.05	Dense section of standpipe, single heated tube

NA= Not available

2.3.4 Heat Transfer data in Commercial Boilers

Industrial boilers operate at 830 to 880⁰C, but only few experimental studies have been carried out at high temperatures. Risers of commercial CFB boilers are usually rectangular in cross-section and are fabricated from membrane water walls. The membrane wall assemblies make it difficult to penetrate probes into the riser to make measurements of such factors as solids flux, solids holdup, local temperature and local pressure. The lower section is often tapered or constricted. In addition to primary gas from the bottom, secondary gas is commonly injected through nozzles at higher elevations. Because of these factors, data from laboratory CFB units cannot always be compared to heat transfer data in industrial scale CFB reactors. Heat transfer data from large combustors are still essential to supplement results from laboratory and pilot units.

Only a limited amount of data on heat transfer on the water wall in CFB boilers is available in the open literature due to experimental difficulties and proprietary safeguards. Table 2.4 gives a list of commercial boilers where experiments were performed, and the range of measured heat transfer coefficients. Each of these units has its horizontal cross-sectional dimensions greater than 1 m and its height substantially in excess of 10 m. The units range in capacity from 12 MW_{th} Chalmer University boiler unit (13.5-m tall) in Sweden to the large 125 MW_e Emile Huchet EDF power (height 33m). As indicated in the Table 2.4, conditions in different combustors varied through a limited range of bulk temperatures from 700 to 920⁰C, suspension densities from 2 to 10 kg/m³, superficial gas velocities between 3 to 6 m/s, and mean particle diameters from 140 to 440 μm. Above data are restricted to the water wall.

A wider range of data on heat transfer on the water wall in a commercial unit might be helpful to develop empirical correlations along with the reported data. No data on heat transfer into wing walls in a CFB boiler are reported in the open literature. Therefore, reliable data on wing wall is required to develop correlations and mechanistic models for

commercial CFB boilers.

Table 2.4. Geometric dimensions, operating conditions and measured heat transfer coefficients for large-scale CFB boilers (adopted from Basu and Nag, 1996; Golriz, 2002)

Unit, Reference	Output	Size of the furnace (m×m×m)	Sus. density (kg/m ³)	Bed temp (°C)	\bar{U}_g (m/s)	Wall Temp (°C)	Particle size (μm)	Heat Tr. Coeff. (W/m ² K)
Chalmers University, Sweden (Anderson, 1996)	12 MW _{th}	1.4×1.7 × 13.5	1.5-13	760-860	1.8-6.1	210	220	100-200
Jianjiang, China, Xiaozhong et al 1999	50 MW _{th}	3×6×20	14-52	920	5.1	290	400	200-300
Chatham, Canada, Couturier et. al 1993	72 MW _{th}	4×4×23	10.4	880	6.4	500	200	200
Flensburg, Germany, Werdermann and Werther, 1994	109 MW _{th}	5.1×5.1 ×28	6.1-9.2	860	6.3	340	209	165-173
VW Wolfsburg, Blumel et al., 1992	145 MW _{th}	7.6×5.2 ×31	2.3-5.2	850	6.2	340	NS	110-150
Orebro, Andersson et al., 1996	165 MW _{th}	4.6×12 ×33.5	n/a	700-860	3-5	360	280	NS
Duisberg, Germany (Werdermann and Werther, 1994)	226 MW _{th}	8(dia) ×32 (Horizontal tube bank)	n/a	850	5.3	650	177	445-596
Nucla, USA (Boyd and Friedman, 1991)	110 MW _e	6.9×7.4 ×34	n/a	774-913	2.6-5.1	330	150	143-197
Emile Huchet, France, (Jestin et al., 1992)	125 MW _e	8.6×11 ×33	5-11	800-860	NS	340	150	130-175

n/a: Not available

2.3.5 Mechanistic Model of Heat Transfer

In order to explain the parametric behaviour of heat transfer in a CFB furnace and help scale up heat transfer coefficients, several models have been proposed by a number of researchers (Basu. and Nag, 1996; Breitholtz., 2000). Table 2.5 shows a summary of mechanistic models proposed by different researchers for enclosing water walls in the combustor. These models were classified broadly under three groups, viz (a) single particle model, (b) continuous film model (b) cluster renewal model.

Single particle model:

The single particle model is an extension to circulating fluidized beds (CFB) of the model originally developed by Zeigler *et al* (1964) for bubbling fluidized beds. The primary concern of this model is the first layer of particles adjacent to the wall. Thus it ignores the thermal boundary layer. Here particles are assumed to travel down the wall with an initial temperature equal to the bulk bed. Heat is convected from the particles, closest to the wall, to the gas around it, which in turns transfer to the wall. It is further assumed that the heat flow to the wall is controlled by the heat transfer from the particle to the gas film surrounding it. This film is assumed to be at a mean temperature of the bed and the wall-an assumption yet to be verified.

Continuous film model:

This model assumes that walls of CFB boiler are always covered by a homogeneous film of gas and solid. The up-flowing gas does not come in contact with the wall. So, there is no need to consider separate convective gas heat transfer model. Mahalingam and Kolar (1991) considered the influence of the wall-layer by treating radiation and convection from a homogeneous layer of particles falling along the wall. The thermal radiation was estimated by an alternate slab method. The convective component was calculated by the analytical solution for transient conduction from the film. Chen and Chen (1992) used the above approach to calculate the heat transfer coefficient except that they neglected any

contact resistance on the wall, but used a contact time distribution function measured using an optical fibre probe. A major shortcoming of this model is that it fails to predict the effect of particle size, length of heat transferring surface etc.

Cluster renewal model:

This model, developed by Subbarao and Basu (1986), is the most commonly used model for CFB heat transfer. According to this model discrete clusters are swept to the wall and then they travel on the wall for a certain time. After a short moment, another cluster moves to the wall to renew the cluster wall contact. Heat is transferred from the clusters while they fall along the wall for a certain distance and are rejected from the wall afterwards. The heat transfer from the clusters is calculated as conduction from a semi-infinite body. Convection from the disperse phase and radiation are calculated as additive components. However, parameters like fractional wall coverage by the cluster in commercial boilers, thermal boundary layer in the wall layer of this widely accepted cluster-renewal model are still unknown. So there is the need for a model which will use refined values of wall coverage and cluster velocity.

Table 2.5. Review of mechanistic models of heat transfer in fast beds (adopted from Basu and Nag; 1996)

Authors	Particle Convection	Gas Convection	Contact Resistance
Subbarao and Basu (1986)	Cluster renewal	Conduction from gas bubble	None
Basu and Nag (1987, 1990)	Cluster renewal	Correlation of dust laden gas	10
Johnsson <i>et al.</i> (1987, 1988)	Single-particle contact	$\frac{h_g d_p}{k_g} = 0.009 \text{Pr}^{1/3} \text{Ar}^{1/2}$	Martin's (1984) model
Chen <i>et al.</i> (1988)	Uniform gas-solid suspension		
Glicksmann (1988)	Cluster renewal	Neglected	10

Lints and Glicksman (1994)	Cluster renewal	Neglected	$35.5(1 - \varepsilon)^{0.59}$
Yenming <i>et al</i> (1989)	Cluster renewal	Correlation for particles free gas	Wunschmann (1980)
Sekthira <i>et al.</i> (1988)	Single particle	Neglected	Particle renewal
Wu <i>et al</i> (1990b)	Cluster renewal	Equation for particle free gas	2.5
Leckner (1991)	Continuous gas-solid film near wall boundary layer	Heat transfer across time average thermal boundary layer	
Kudo <i>et al.</i> (1991)	Up-flowing uniform gas solid mixture	$\frac{h_g d_p}{k_g} = 0.009 \text{Pr}^{1/3} \text{Ar}^{1/2}$	Equation of motion, energy and continuity for dispersed gas-solid film
Mahalingam and kolar (1991a, b)	Continuous gas-solid film developing on wall	None	10
Chen and Chen (1992)	Continuous gas-solid film on wall	None	Neglected
Nowak <i>et al</i> (1992)	Single particle renewal	$40U_g^{0.37}$	2-10
Qi and farag (1993)	Single particle renewal in empty column	Correlation for gas only	Nil
Borodulya and Teplitsky (1999)	Two-zone film model	None	$34.8 \left(\frac{\rho}{\rho_p} \right)^{0.581}$
Golriz and Grace (2002)	Cluster renewal	Ditus Boelter equation $\text{Nu}_g = 0.023 \text{Re}_D^{0.8} \text{Pr}^{0.3}$	$35.5(1 - \varepsilon)^{0.59}$

2.4. Concluding remarks

In this chapter, a critical review of the present level of understanding of the heat transfer processes in the commercial CFB boilers is presented. A review of influencing parameters and available models is also summarized. This review focuses on three particular types of heat transfer, i.e., (1) fast bed to the furnace walls, (2) fast bed to the suspended bodies and (3) moving bed to the wall of the standpipe.

Based on the critical analysis conducted, the following conclusions are drawn

1. In a commercial CFB boiler, heat transfer coefficients depend on both suspension density and bed temperature of the combustor or riser. The vertical length of the heating surface does not have any effect on heat transfer coefficient because a fully developed flow is formed over it. The superficial velocity may have an effect on heat transfer when a surface is placed in the core of the riser.
2. Currently available empirical correlations for heat transfer on water walls predict the effect of suspension density alone. There is a need to develop one that also considers the other important variable, bed temperature.
3. Among the available mechanistic models, the cluster renewal model is found to be more relevant because of its capability of the core annulus hydrodynamic structure in the riser. However, a number of parameters of this model are yet to be determined for the commercial boiler and hence research is required in this direction.
4. The only investigation currently available is for the dense section of the standpipe with vertical heating tubes passing through it. This geometry is not conducive to its use for extraction of heat in standpipe as it may adversely affect the flow dynamics in the standpipe. Moreover, there is no investigation on the dilute section of the standpipe. Therefore, investigations in this direction are required.
5. No information on the wing wall and on the cavity-type inertial separator is presently available in the literature. So it is necessary to understand the mechanism of heat transfer on these surfaces and to generate at least some qualitative data.

Chapter 3

Overall heat transfer to water-walls and wing-walls of commercial CFB boilers

This chapter develops empirical correlations of heat transfer coefficients for water walls and wing walls. These are developed by analysing data on overall heat absorption rates, bed temperature and suspension density from two commercially operating CFB boilers (100 T/h and 700 T/h capacities). A methodology was developed to deduce heat transfer coefficients on wing walls from the measured overall heat duties of the entire evaporator. Correlations are developed relating the heat transfer coefficients, averaged over the entire height of the heat absorbing wall, with operating parameters. The correlations are tested against heat transfer coefficients measured and reported by other researchers. The deviation is within $\pm 15\%$ which is of the same order as the uncertainty in measured data.

3.1. Introductory remarks

The furnace temperature of a circulating fluidized bed (CFB) boiler is generally controlled by adjusting the heat transfer to the enclosing water-walls and to the suspended wing walls in the furnace. A wing wall can be either a part of the evaporator or superheater of the boiler. Typically wing walls or platen surfaces hang from the ceiling and extend from the front wall to some distance towards the opposite wall, where the furnace exit is located (Fig. 1.1 and 1.2). To absorb the required amount of heat, a CFB boiler often uses more than one wing wall. The amount of heat absorbed in the wing wall could be as high as 30% of that absorbed in the furnace walls. More information (Basu and Nag, 1996; Glicksman, 1997; Molerus and Wirth, 1997; Breitholtz 2000) is available on heat transfer on membrane-tube type water-walls of CFB boilers. A number of researchers (Table 2.1) proposed correlations for estimating average heat transfer

coefficients on water wall using the cross-section average suspension density as a variable. All of these data and studies pertain to the enclosing walls. Currently no correlation is available in the open literature, let alone any studies on average heat transfer on the wing walls. Wing walls operate in different hydrodynamic condition than that of water walls. Thus the information on water walls is not directly applicable to wing walls.

Furnaces as large as 250 MW_e capacity routinely use wing walls. Yet the knowledge on heat transfer rates on bed to wing walls was so inadequate that manufacturers had to revise wing wall surfaces in some instances. With time, the manufacturers have largely overcome design uncertainties they had in the initial stage. Still, no analysis of heat transfer to wing walls, theoretical or empirical is available in published literature.

Some manufacturers use division walls in the furnace as an alternative to wing walls. It is a vertical wall that effectively separates the furnace into two beds. Theoretically, this appears to be a sound idea, but its practical operation could be difficult: For instance, the air-solid flow may flip-flop between two sections creating non uniform hydrodynamic and heat transfer conditions. Wing walls, thus, remains the most reliable means for augmentation of furnace heat absorption. The present work, probably the first attempt in this area, might help optimize the design of wing walls on commercial boilers.

3.2. Data from commercial units

The analyses of failures and performance predictions of commercial boilers require meaningful scale up of data. Experimental data from bench-scale or laboratory-size units are often used to predict the performance of commercial units. However, commercial boilers are usually rectangular in cross-section compared to the circular diameter laboratory-size units. These boilers are fabricated from large membrane water walls. The membrane wall assemblies make it difficult to penetrate into the riser itself to make measurements of such factors as solids flux, solids holdup, local temperature and local

pressure. The lower section is often tapered or constricted. In addition to primary gas from the bottom, secondary gas is commonly injected through nozzles at higher elevations. Because of these factors, data from laboratory CFB units cannot always be related to heat transfer in industrial scale CFB reactors. Therefore, for a reliable prediction, heat transfer data from large combustors are essential to supplement results from laboratory and pilot units.

Thus, it is imperative that information on large commercial units be used to validate correlations. Such a validation is very difficult and at times impossible. In scientific experiments, the effect of one independent parameter on a dependent variable is generally studied by measuring the dependent variable for specific values of that influencing parameter while keeping all other parameters constant. Very few commercial units operate in ideal conditions. In commercial CFB boilers, it is very difficult to achieve such conditions. Most commercial boilers are operated by an automated control system. Thus, when one parameter is varied, several other parameters also change which makes it very difficult to assess the impact of the chosen parameter. Secondly, very few commercial CFB boilers are instrumented to measure all relevant parameters, like heat transfer coefficients or suspension densities etc.

These difficulties do not, however, diminish the importance of generation of data in commercial units, because that is the ultimate test of engineering models which are to be used for industrial designs. With this in mind, efforts were made to collect data from industrial units. Commercial secrecy and lack of proper instrumentation made it difficult to get access to a reliable set of data. However, some data on heat transfer coefficients were deduced from a set of measured operating parameters in two large commercial circulating fluidized bed boilers. One unit is in the range of 20 MW_e while the other one produces more than 170 MW_e power. Figure 3A and 3B show both general arrangement and simplified drawing of the boilers studied. Like any commercial unit, these boilers are operated under different loads at different times. Data logged at different loads were analyzed to deduce heat transfer coefficients at different conditions.

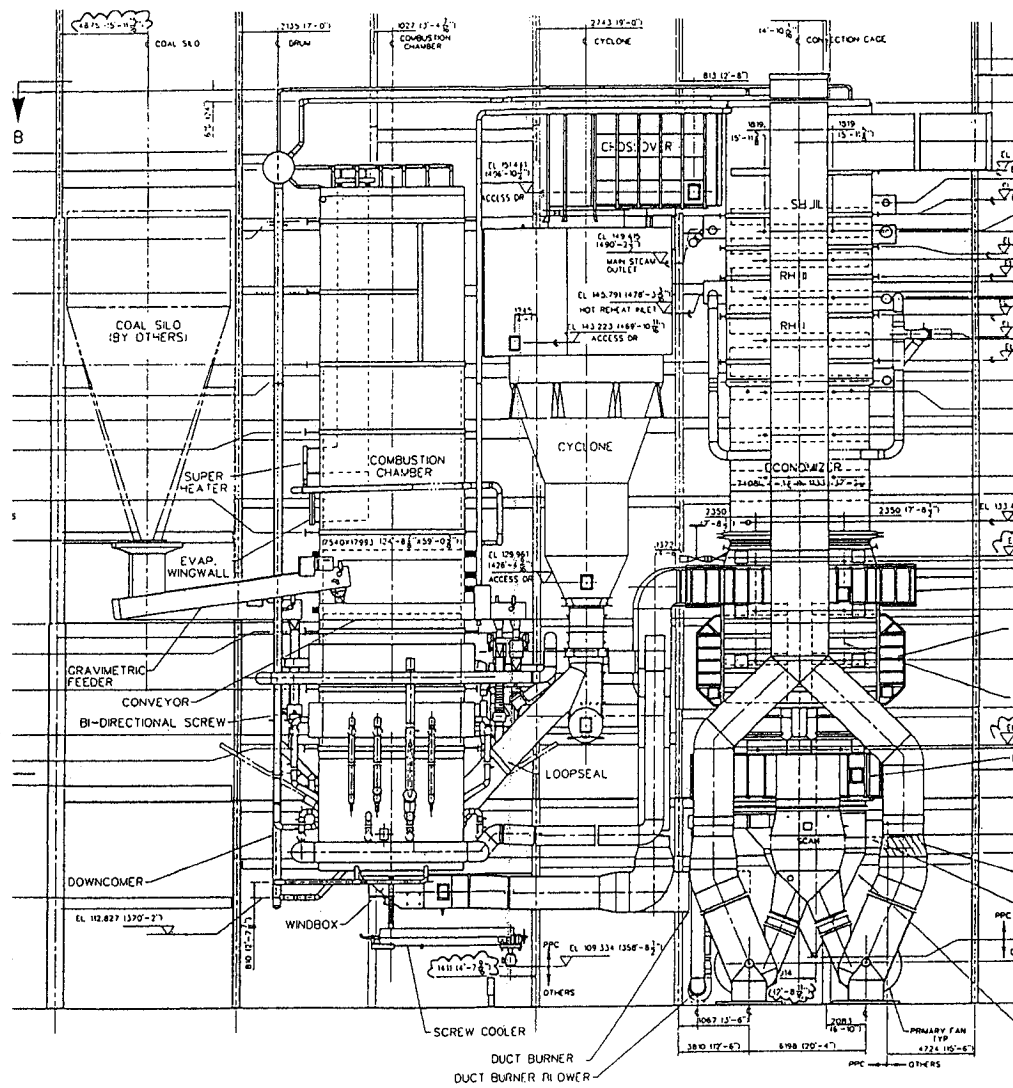


Figure 3A(1). General arrangement drawing of the 170 MW_e CFB boiler

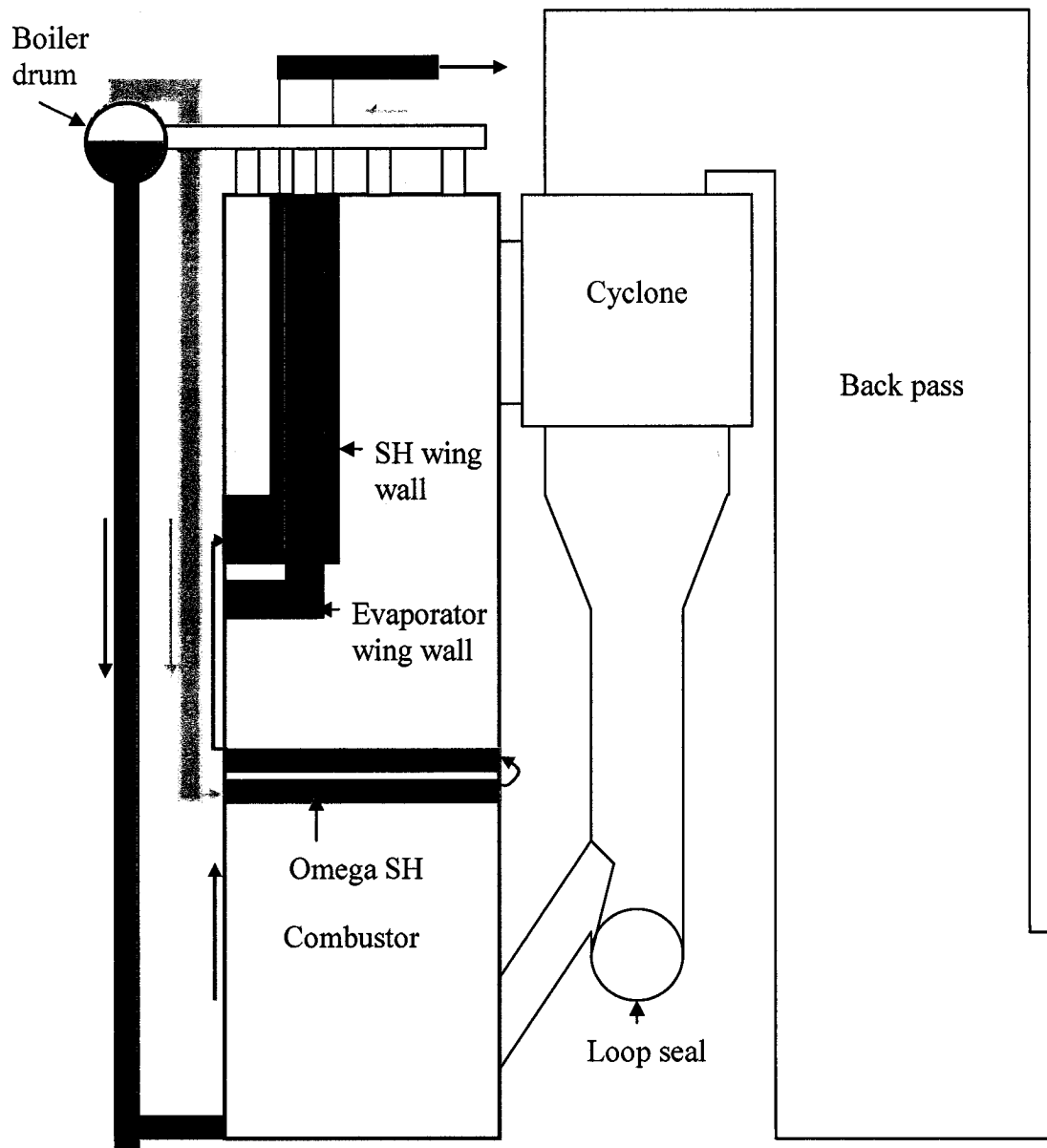


Figure 3.A(2). A simplified general arrangement side elevation of 170 MWe boiler

Flow Circuit	Locations	Color
High pressure water	• From drum to evaporator (water wall/wing wall)	————
High pressure steam/water	• From evaporator to drum	————
High pressure steam	• From drum to Omega SH	————
High pressure steam	• From wing wall SH to SHIII at the backpass	————

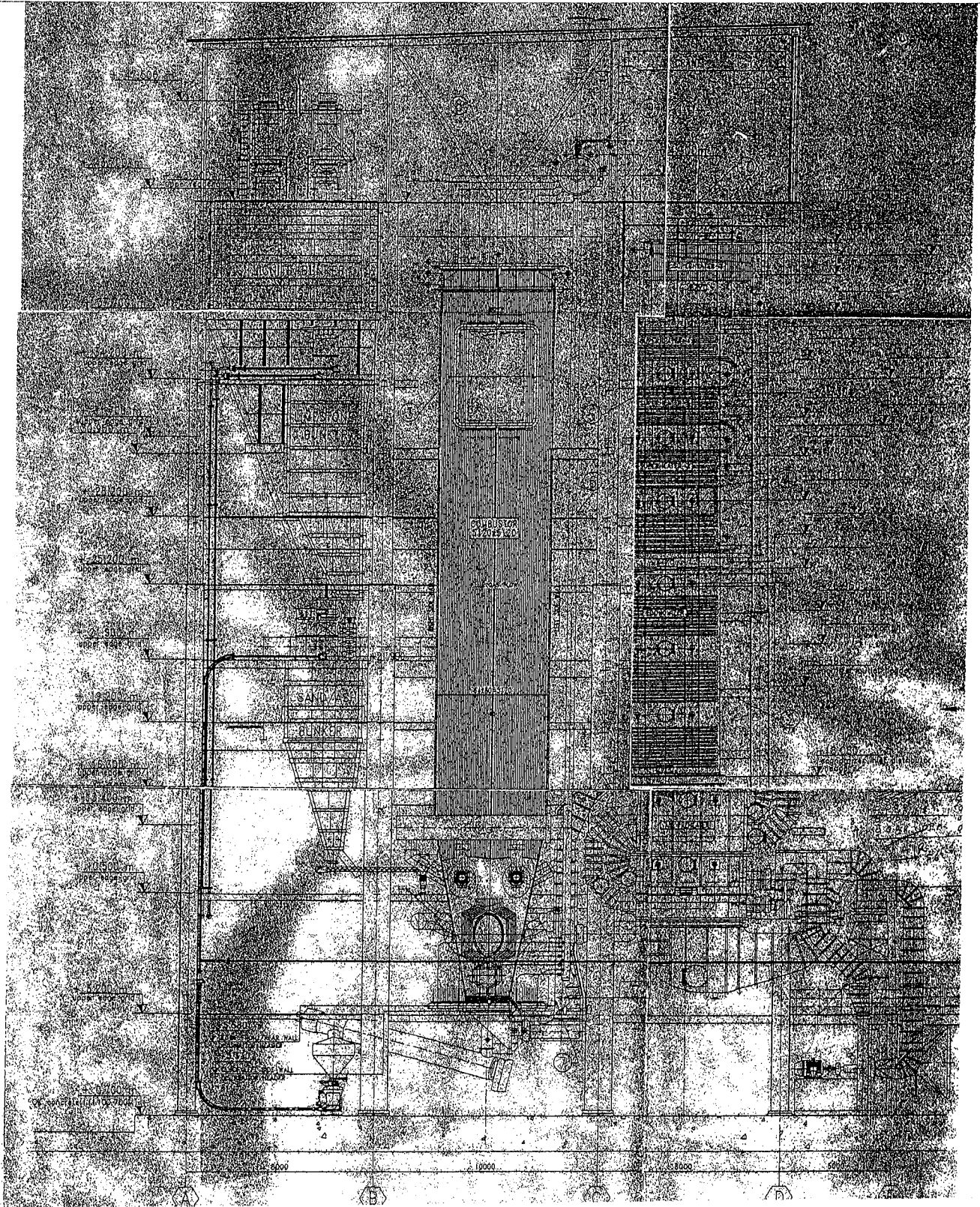


Figure 3B(1). General arrangement drawing of the 170 MW_e CFB boiler

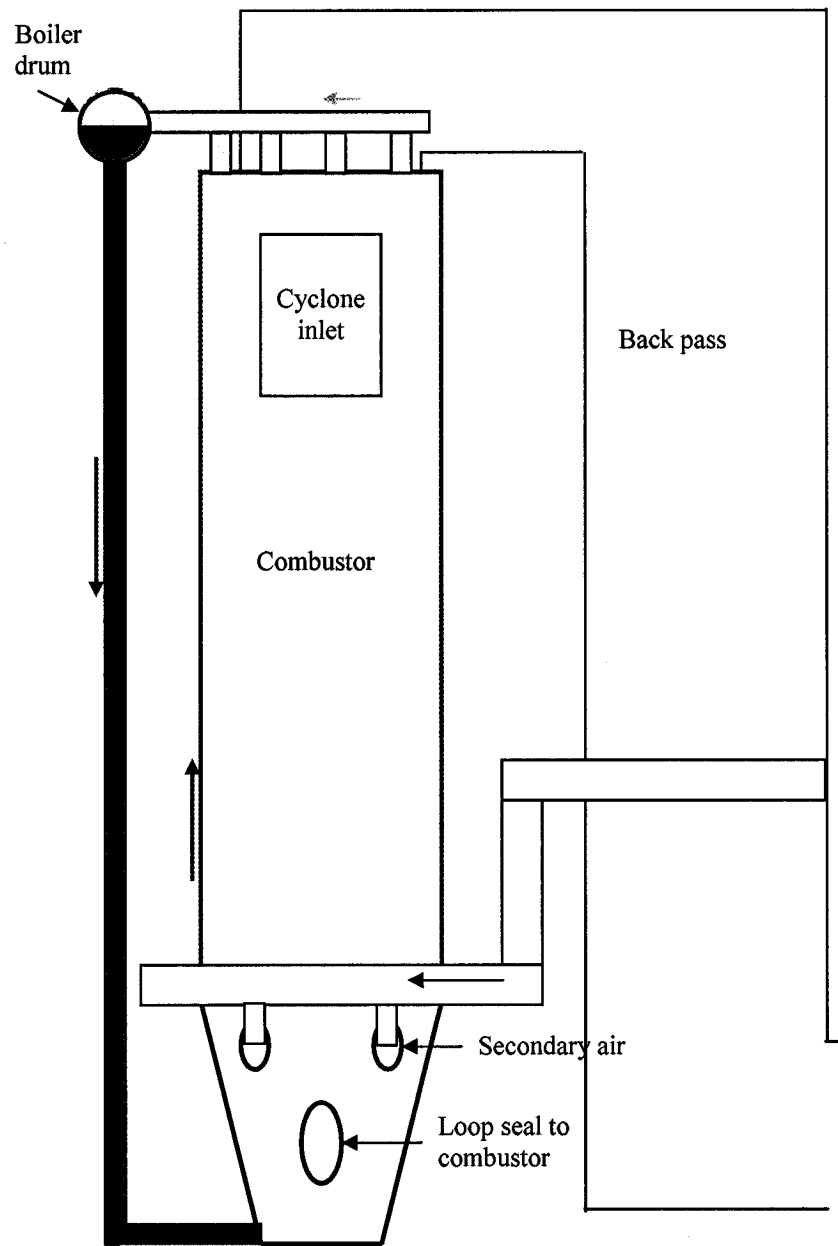


Figure 3.B (2). A simplified general arrangement side elevation of 20 MW_e boiler

3.3. Methodology for estimating heat transfer coefficient

Unlike laboratory test rigs, commercial boilers are not designed to gather scientific data. As such, they do not use pressure transducers, thermocouples, heat flux meters, or flow meters at every location. Thus, it is difficult to get a direct measure of the heat transfer coefficient on a commercial boiler. It has to be estimated indirectly. Heat balance over different sections of the boiler allowed us to measure heat absorption in individual group of heating surfaces (panels). The larger boiler, in question, used wing walls as both evaporative surface as well as superheater surface. Thus, the total evaporative load of the boiler does not give or measure the heat absorbed in the water walls. To compare the heat transfer to the wing walls with that to the water walls, one needs to calculate the heat transfer coefficient separately for each case at a specific operating condition. The heat transfer coefficient on the superheater wing wall could be easily deduced from its surface area as the temperatures of the steam entering and leaving the superheater wing wall were recorded in the control room. Although both types of wing walls are exposed to the same hydrodynamic conditions, the heat transfer coefficient for superheater wing wall may not be applicable directly to the evaporative wing wall because the surface temperature of the evaporative wing walls could be much lower than that of the superheater wing walls. So, one needs to determine the heat transfer coefficient for the evaporative wing walls from that on the superheater wing walls. The following assumptions were made to estimate the evaporative wing wall heat transfer coefficient.

1. The superheater and evaporator wing walls are arranged side by side in the upper parts of the furnace. Thus, both are exposed to the same hydrodynamic conditions. As the particle convection component of the heat transfer does not depend significantly on the surface temperature, it is assumed to be same on both types of wing wall.
2. The particle convection is constant and accounts for 20% of the total heat transfer in the upper zone of the CFB riser (Basu and Konuche 1988).

3. The average surface temperature of the superheater is 50⁰C above the average steam temperature (Basu *et al* 1999).
4. The average surface temperature of the evaporator is 25⁰C above the saturation temperature as per boiler design norm. (Basu *et al* 1999)

The total heat transfer coefficient in a CFB is the sum of convective and radiative component heat transfer (Basu and Nag 1987, Wu *et. al* 1987, Basu & Fraser, 1991). The ratio of the total heat transfer coefficient for the superheater wing wall, h_{swwall} , and evaporator wing wall, h_{ewwall} , is, therefore, written as

$$\frac{h_{swwall}}{h_{ewwall}} = \frac{h'_p + \frac{k(T_g^4 - T_{swwall}^4)}{(T_g - T_{swwall})}}{h''_p + \frac{k(T_g^4 - T_{ewwall}^4)}{(T_g - T_{ewwall})}} \quad (3.1)$$

After simplification, equation (3.1) can be written as

$$\frac{h_{swwall}}{h_{ewwall}} = \frac{h'_p + k(T_g^2 + T_{swwall}^2)(T_g + T_{swwall})}{h''_p + k(T_g^2 + T_{ewwall}^2)(T_g + T_{ewwall})} \quad (3.2)$$

where h'_p , h''_p are the particle convective component for superheater wing wall and evaporative wing wall respectively. T_g , T_{swwall} , T_{ewwall} are the bed temperature, surface temperature of superheater wing wall and surface temperature of evaporator wing wall respectively.

The overall heat transfer coefficient for the superheater wing wall was calculated by using the measured value of Q_{swwall} , T_g , T_{swwall}

$$h_{swwall} = \frac{Q_{swwall}}{A_{swwall}(\text{Projected})(T_g - T_{swwall})} \quad (3.3)$$

Using assumption (2), the particle convection for the superheater wing wall was estimated as

$$h'_p = 0.2 \times h_{swall} \quad (3.4)$$

Considering the total heat transfer coefficient as the addition of particle convection and radiation (Basu and Nag 1987, Wu *et. al* 1987), the constant k of the radiative term into wing walls (Stefan-Boltzmann constant, emmissivity, etc) was estimated from the equation (3.5).

$$k = \frac{h_{swall} - h'_p}{(T_g^2 + T_{swall}^2)(T_g + T_{swall})} \quad (3.5)$$

Using this value of k and the assumption (1) i.e., $h'_p = h''_p$, the evaporative wing wall heat transfer coefficient was then deduced from the equation (3.2).

The amount of heat absorbed by the evaporator water wall was estimated by subtracting the estimated evaporator heat duty of the wing wall from the calculated total evaporator duty.

$$Q_{wwall} = Q_{evaporator} - Q_{ewall} \quad (3.6)$$

The average water wall heat transfer coefficient was then estimated by using the same equation as that of step 1.

$$h_{wwall} = \frac{Q_{wwall}}{A_{wwall (Projected)} (T_g - T_{wwall})} \quad (3.7)$$

This gives the average heat transfer coefficient over the entire height of the water wall.

3.4. Results and discussion

3.4.1. Suspension density effect

Applying the above methodology, the average heat transfer coefficients to water walls and wing walls are estimated at different loads of the 170 MW_e boiler. The average heat transfer coefficients, suspension densities and bed temperatures are presented in non-dimensional form by dividing its maximum operating values. Fig. 3.1a and 3.1b show that non-dimensional heat transfer coefficients to the water wall and wing wall increases with non-dimensional suspension densities, measured across the entire upper section of the furnace at different loads. The effect of the bed temperature is not considered while fitting the curve as $h \sim \rho_{sus}^n$. The exponent n for the fitted curve is found to be 0.48. This exponent is close to that observed by Basu and Nag, (1996); Glicksman, 1988; Ebert *et al.*, 1993 who found it to be 0.5.

3.4.2. Temperature effect

Non-dimensional heat transfer coefficients to water walls and wing walls are also plotted against the non-dimensional bed temperatures in Fig: 3.2a and 3.2b. If radiation were the dominant factor, one would expect the heat transfer coefficient to be proportional to T_g^4 . But the exponent is found to be 1.5 instead of 4 as expected for pure radiation. Yet, this suggests that furnace temperature has a greater influence on the heat transfer coefficient than the suspension density has on it. Instead of choosing data for any temperature, if one uses value for a narrow range of bed temperature (930-940 °C), the exponent for the suspension density is found to be 0.21 for the water wall (Fig. 3.3a). It is interesting that this value is similar to that reported by Breitholtz *et. al* (1999), who proposed a correlation for commercial boilers by minimisation of the square of the deviations between the measured data and the correlations without considering bed temperature. The exponent for the wing wall in this case is found to be 0.11 (Fig. 3.3b), which suggests a lesser dependence on the average suspension density.

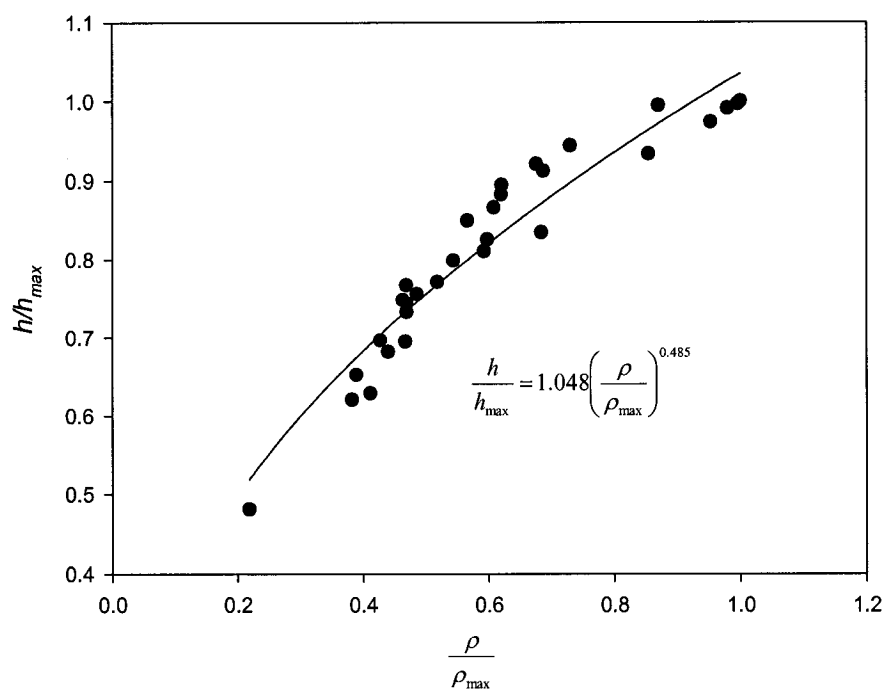


Figure 3.1a. Water wall heat transfer coefficient with non-dimensional suspension density (170 MW_e)

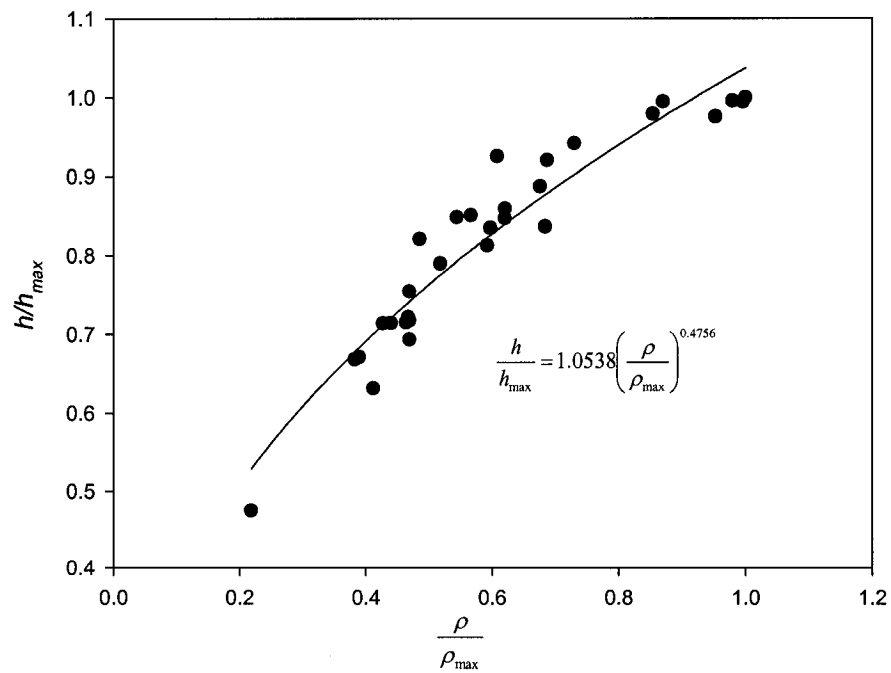


Figure 3.1b. Wing wall heat transfer coefficient with non-dimensional suspension density (170 MW_e)

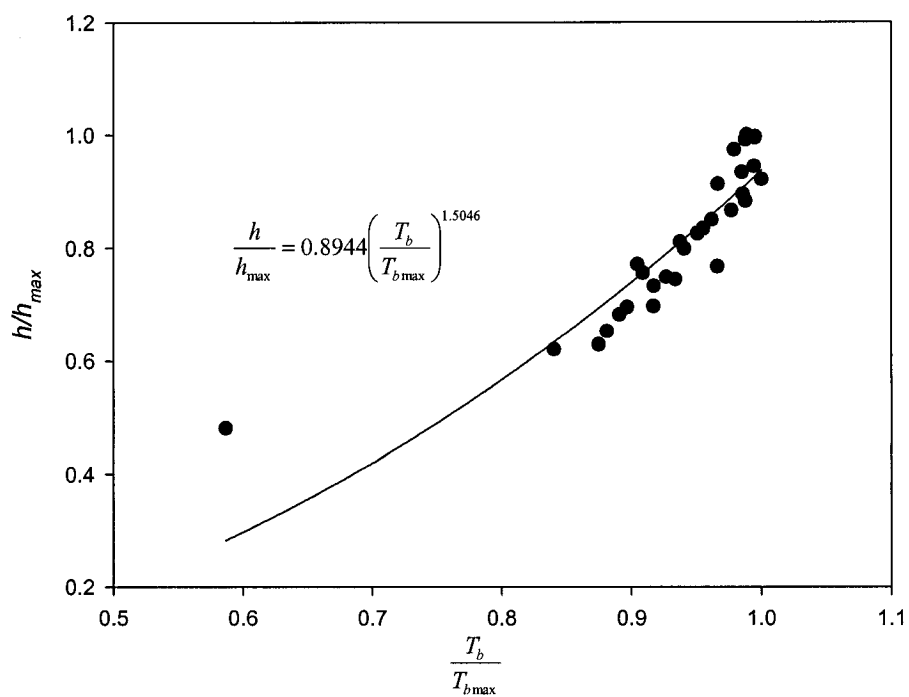


Figure 3.2a. Water wall heat transfer coefficient with non-dimensional bed temperature
(170 MW_e)

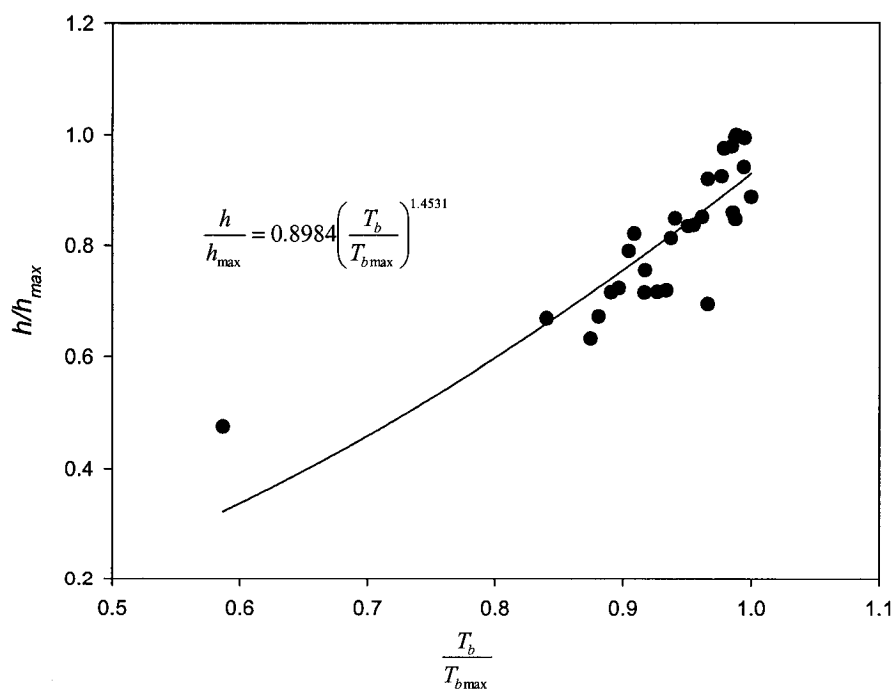


Figure 3.2b. Wing wall heat transfer coefficient with non-dimensional bed temperature
(170 MW_e)

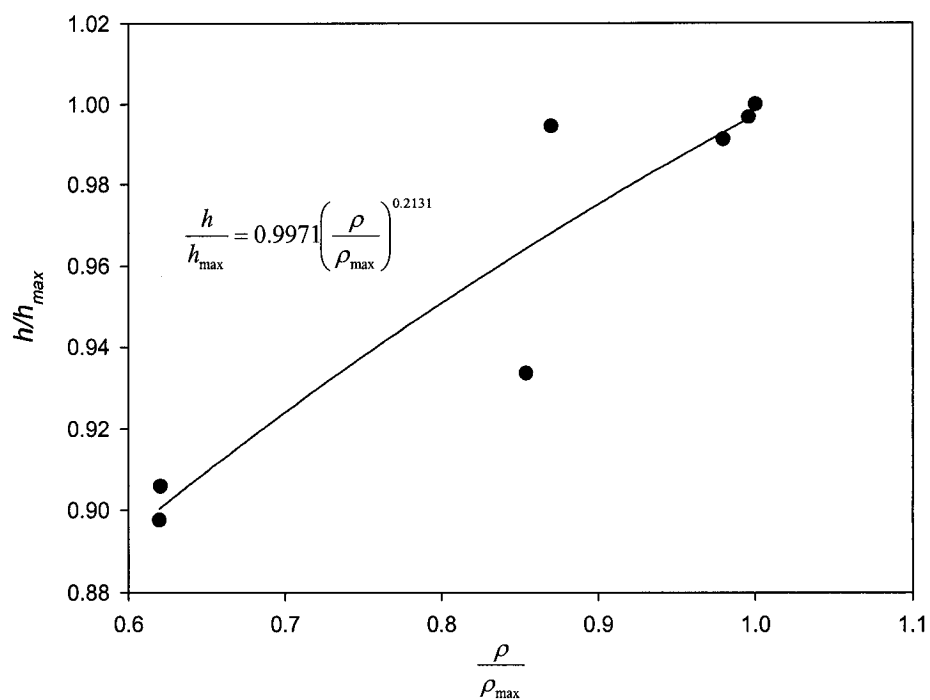


Figure 3.3a. Heat transfer coefficient for water walls of 170 MW_e boiler (Bed temperature 930-940⁰C)

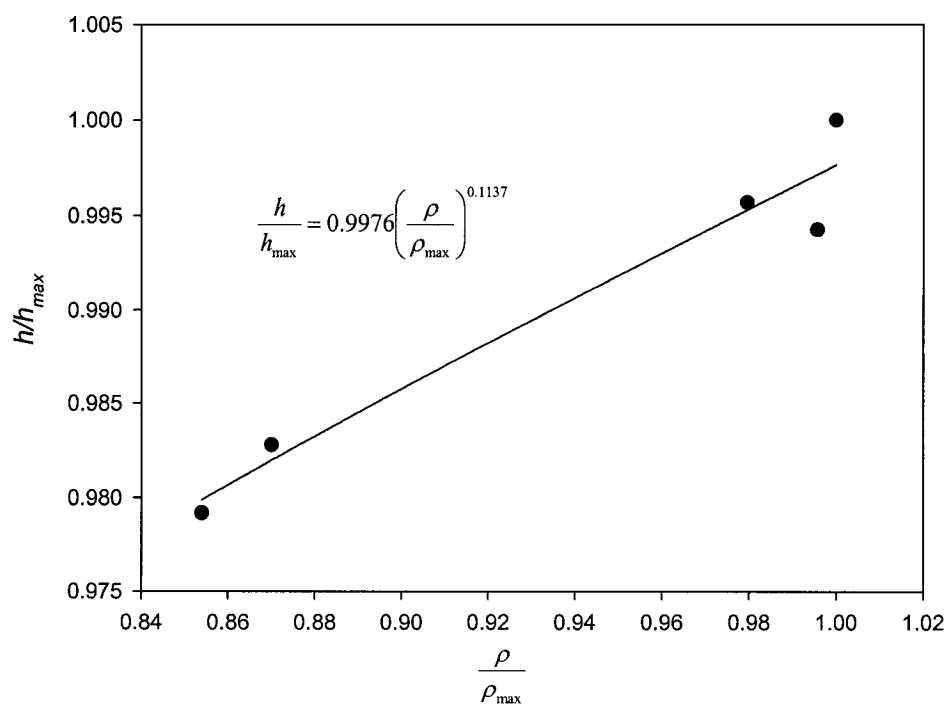


Figure 3.3b. Heat transfer coefficient for wing walls of 170 MW_e boiler (Bed temperature 930-940⁰C)

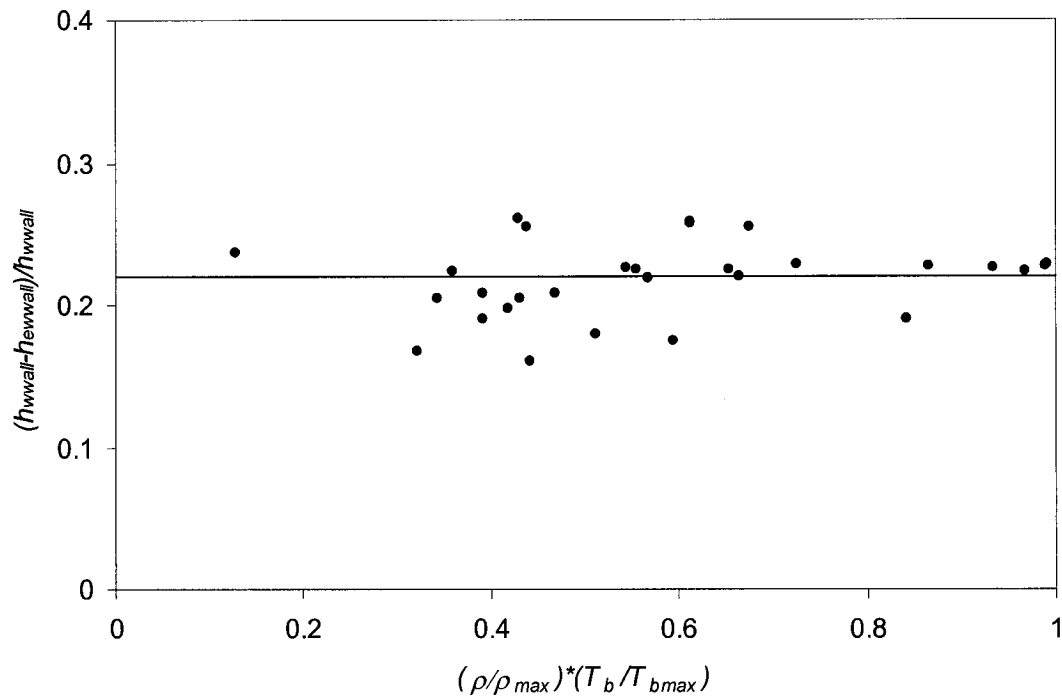


Figure 3.4. The percentage reduction of heat transfer coefficient between water wall and wing wall at different operating conditions

The heat transfer curves for both evaporative wing wall and water wall are nearly parallel to each other (Fig: 3.1 and 3.2). The absolute value of the heat transfer coefficient on the wing walls is found to be consistently lower than that on the water walls. In Fig: 3.4, the ratio of this difference and heat transfer to the water walls is plotted against non-dimensional suspension density and bed temperature. The ratio is found to be about 0.22 or 22% at different loads of the boiler which is more than the particle convective component of a CFB furnace (20%) operating at 800-900⁰C (Basu and Konuche 1988). Even an assumption that particle convective heat transfer on the wing wall is negligible, cannot account for this larger difference. So, one could speculate that both particle convective and radiative heat transfer are lower on the wing walls than what would be on water walls. The hydrodynamics on wall tubes are different from that on wing walls, which are exposed to relatively dilute up-flowing

solids. The heat transfer on wing walls is found to be dominated by forced convection from dilute suspension, while that on the water walls is dominated by down-flowing particle convection. As a result, there is higher particle convection on the water walls. Also, the water wall is exposed to the entire cavity of the furnace whereas the wing wall is exposed to the relatively narrow cavity between wings. For this reason, the mean beam length of the gas radiation in water walls is higher resulting in higher radiative heat transfer coefficient.

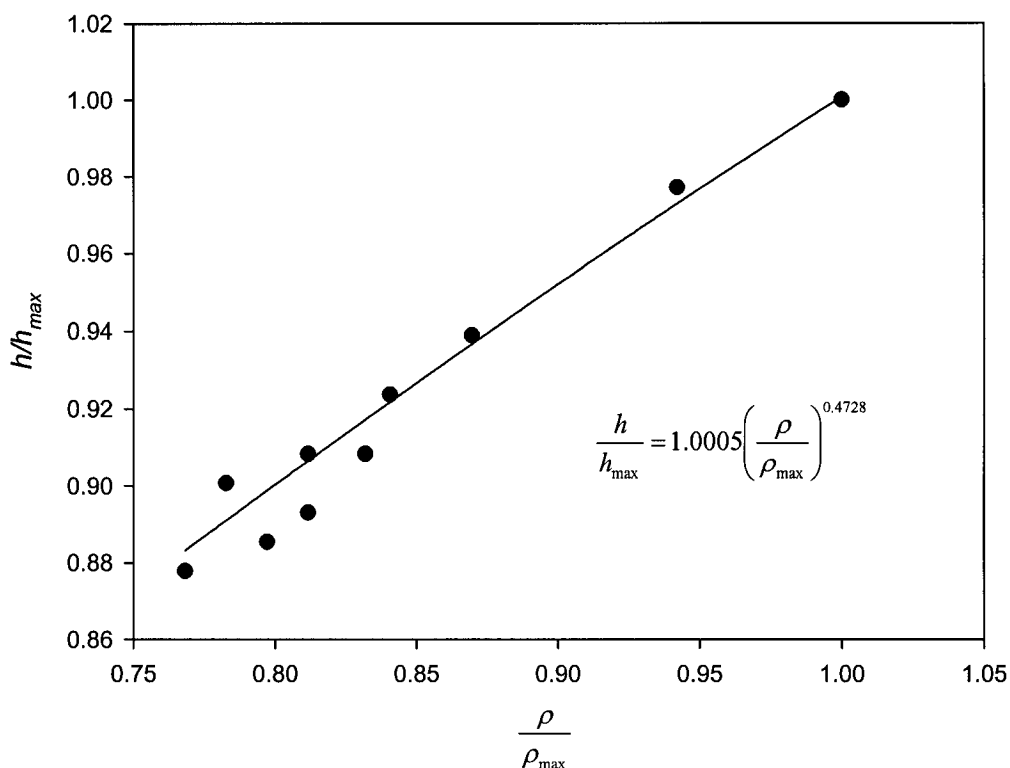


Figure 3.5a. Water wall heat transfer coefficient with non-dimensional suspension density (20 MW_e boiler)

Above discussions relate to data from the 170 MW_e unit. The data from the 20 MW_e boiler were analyzed in the same fashion. The 20 MW_e boiler does not have the wing wall. The results on water wall support the findings for the water wall of the 170 MW_e boiler. Results of heat transfer on the water walls of the 20 MW_e boiler are shown in Fig. 3.5a and 3.5b. The exponent for the fitted curve for non-dimensional heat transfer coefficients with non-dimensional suspension densities is 0.47 (Fig. 3.5a) whereas it is 1.52 for non-dimensional heat transfer coefficients with non-dimensional bed temperatures (Fig. 3.5b). These results are of the same order that is found for 170 MW_e (Fig. 3.1a and 3.2a).

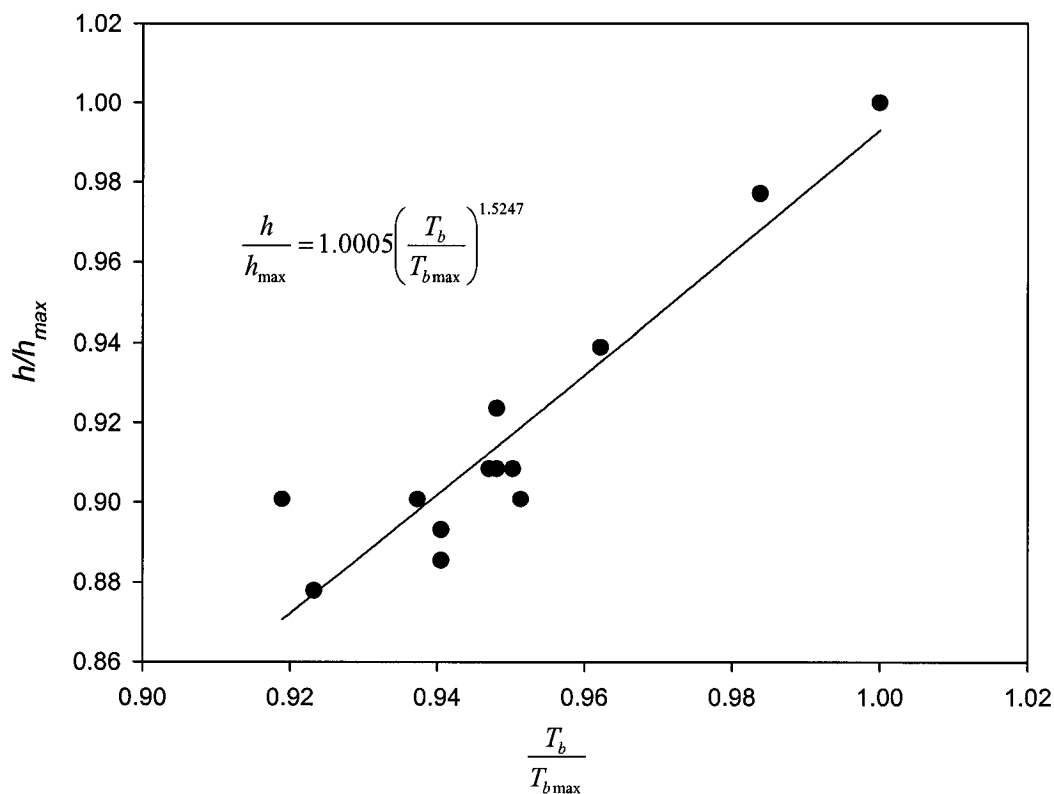


Figure 3.5b. Water wall heat transfer coefficient with non-dimensional bed temperature (20 MW_e boiler)

3.5. Empirical correlation of heat transfer coefficient

Presently no empirical correlation on heat transfer to wing walls is available in published literature. So, an effort is made here to develop a correlation which can be used to predict average gross value of heat transfer to wing walls and water walls. Fig. 3.1 and 3.2, show that total heat transfer coefficient depends on both suspension density and bed temperature. The average heat transfer coefficient, to the water wall and wing wall is correlated to the average suspension density ρ_{sus} and average bed temperature T_g , by a potential function,

$$h = \alpha \rho_{avg}^a T_g^b \quad (3.8)$$

Using Statistical Analysis Software (SAS), and by converting the non-linear equation to multiple linear equations, the values of the parameter in the correlation, α , a and b were found by regression analysis.

For the water wall the correlation is

$$h_{wwall} = 5 \times \rho_{avg}^{0.391} \times T_g^{0.408} \quad \text{W/m}^2.\text{K} \quad (3.9)$$

where ρ_{avg} is in kgm^{-3} and T_g in $^{\circ}\text{C}$.

whereas for wing wall, the correlation is

$$h_{ewwall} = 3.6 \times \rho_{avg}^{0.37} \times T_g^{0.425} \quad \text{W/m}^2.\text{K} \quad (3.10)$$

Fig. 3.6a and 3.6b compares heat transfer coefficients measured with those calculated by the above correlations. The agreement between measured and correlated values is within $\pm 5\%$ limit which is a good agreement for an empirical correlation.

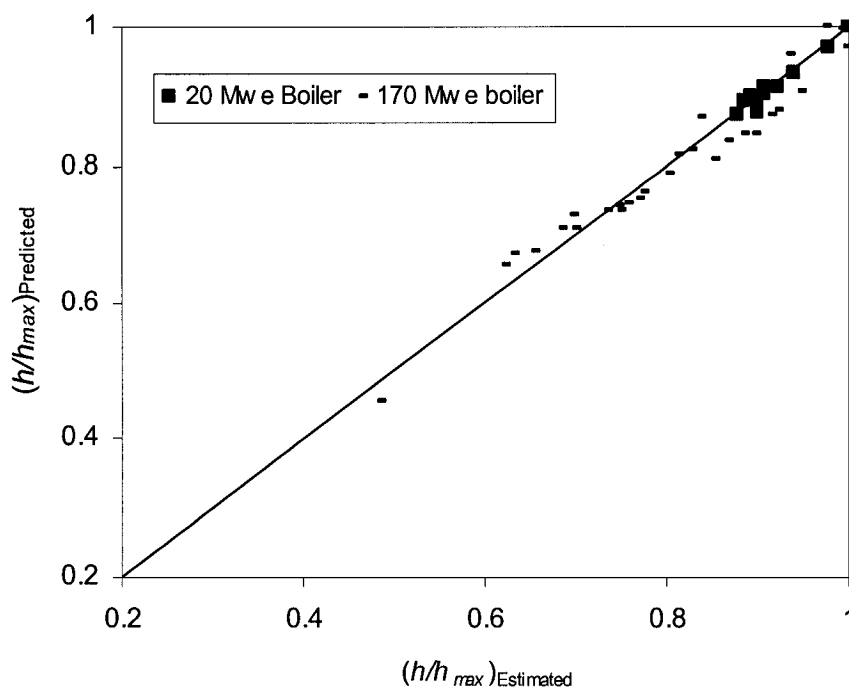


Figure 3.6a. Heat transfer coefficient to the water walls; estimated versus predicted

The correlation of average heat transfer coefficient to water walls is also validated with average water wall heat transfer coefficients for a number of commercial boilers reported (Table 2.4) by a number of researchers (Anderson 1996, Werdermann 1994, Couturier 1993, Jestin 1992, Blumel 1992, and Basu and Fraser 1991). Fig. 3.7 shows that the correlation is in good agreement with the reported values within $\pm 15\%$. As no data are available for wing walls in commercial boilers in the open literature, the correlation could not be validated against data from any other independent sources except for the ones used for developing the correlation. However, one can expect a similar agreement, like water walls.

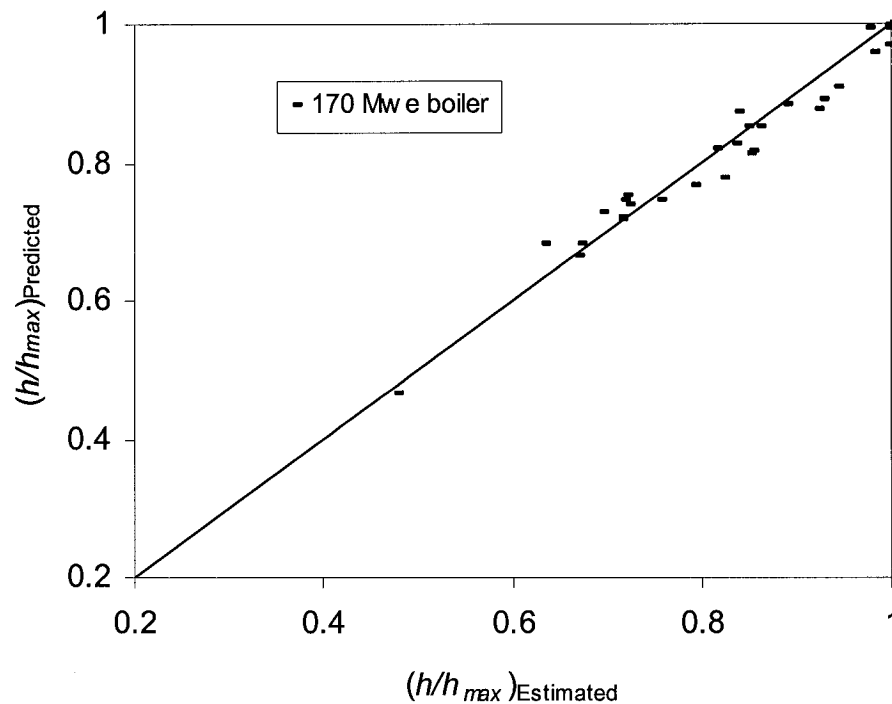


Figure 3.6b. Heat transfer coefficient to the wing walls; estimated versus predicted

3.6. Comparison of proposed empirical correlation with the ones reported by other researchers

The correlation developed for water walls (Eq 3.9) is compared with the correlations developed by other investigators reported in Table 2.1. Table 3.1 shows the sum of squares errors between measured and predicted values for a number of commercial boilers for different correlations. Definitely, the newly developed correlation, which includes temperature as a variable with suspension density appears to be promising for a wide range of operating conditions. However, the correlation developed by Baskakov et al (2001) can be used within a narrow range of operating conditions ($5 < \rho_{sus} < 10$ and $800 < T_b < 850$).

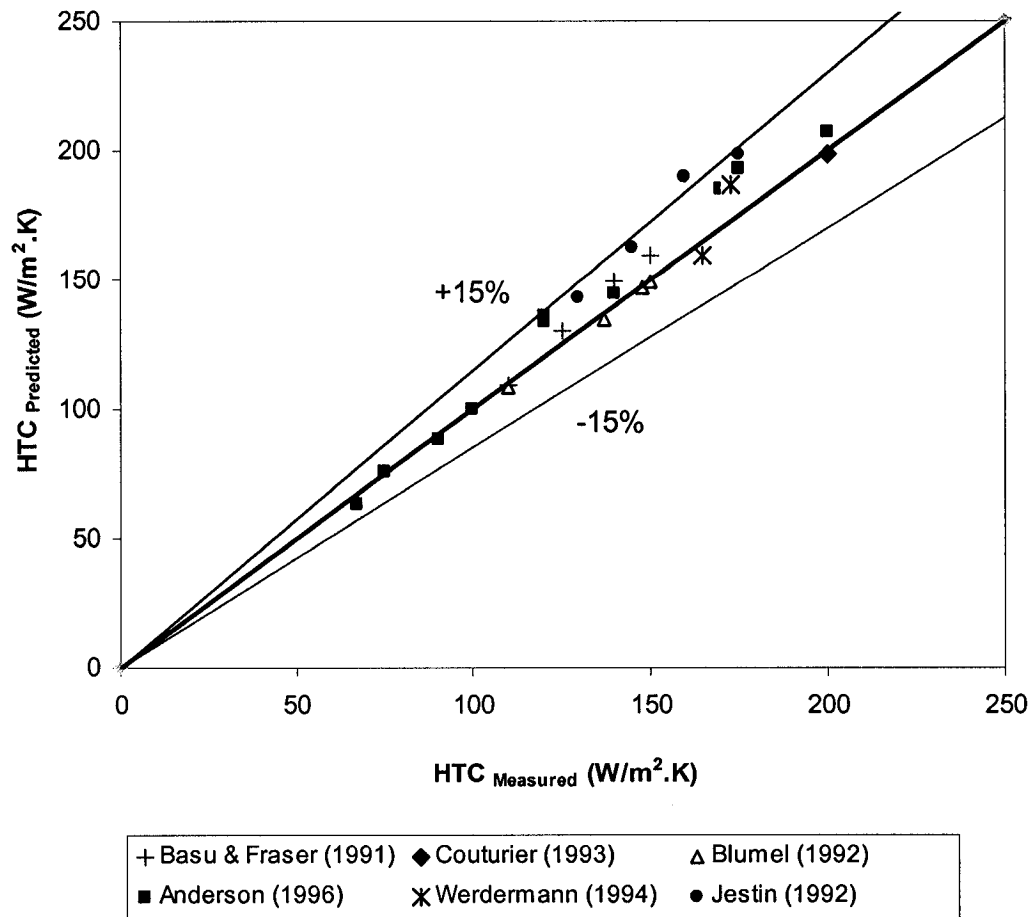


Figure 3.7. Reported versus predicted overall heat transfer coefficient for water walls

Table 3.1. Measurement of heat transfer on water wall in different commercial units

Experimental Unit, Reference	Plant Output	Sus. density	Bed temp	Anderson and Leckner (1992)	Golriz and Sunden (1994)	Anderson (1996)	Basu and Nag (1996)	Breitholtz et al (2000)	Baskakov et. al (2001)	This work
		Kg/m³	(°C)	W²/m⁴k²	W²/m⁴k²	W²/m⁴k²	W²/m⁴k²	W²/m⁴k²	W²/m⁴k²	W²/m⁴k²
Chalmers University, Sweden (Anderson 1996)	12 MW _{th}	1.5-13	760- 860	30,536	8,757	6,250	14,503	6000	575	543
Chatham, Canada, Couturier et. al 1993	72 MW _{th}	10.4	880	10,661	6,646	4,256	5,041	405	806	2
Flensburg, Germany, Werdermann and Werther, 1994	109 MW _{th}	6.1-9.2	860	1,500	6,054	4,834	7,053	22	408	227
VW Wolfsburg, Blumel et al., 1992	145 MW _{th}	2.3-5.2	850	23,294	4,112	6,728	12,567	615	285	9
Emile Huchet, France, (Jestine et al., 1992)	125 MW _e	5-11	800- 860	3,300	1,483	1,562	3,300	968	97	491
Basu and Fraser 1991	NS	2.5-6	800- 875	9,399	2,819	4,565	9,400	1,334	27	208
This work (Chapter 3)	170 MW _e	1.8-8.2	554- 940	201,584	55,528	130,262	107,272	6,164	7,021	732
This work (Chapter 3)	20 MW _e	2.7- 3.45	850- 925	62,570	3,580	24,917	35,727	3,870	215	15
Sum of all SSE*				342,844	88,979	183,374	194,863	19,378	9,434	2,227

* Sum of square error $SSE = \sum (h_{\text{exp}t} - h_{\text{pre}})^2$

3.7. Concluding remarks

This chapter presents a systematic approach for estimating heat transfer on wing walls and it compares that with heat transfer on water walls. Empirical correlations for water walls and wing walls are developed for predicting heat transfer coefficients. The main assumptions used for estimating heat transfer data on the wing walls are that particle convection constitutes about 20% of the total heat transfer in the upper zone of the riser and it is independent of the temperature of the heat transfer surface.

Based on the data generated, the following conclusions are reached:

1. The influence of suspension density and furnace temperature on the heat transfer on wing walls is similar to that on heat transfer on furnace water walls.
2. Heat transfer coefficients on wing walls are 22% lower than those on water walls regardless of the operating conditions.
3. Two empirical correlations are developed for estimation of the average heat transfer coefficients to water walls and wing walls. These relate heat transfer coefficients to average suspension density and average bed temperature in corresponding parts of the furnace.
4. The correlation developed predicts the heat transfer coefficients on the water wall of the commercial boilers with a $\pm 15\%$ error.

Chapter 4

An Experimental Investigation on Wing Walls in a CFB Boiler

This chapter describes an experimental investigation on wing walls in a circulating fluidized bed pilot plant of $1\text{ m} \times 0.5\text{ m}$ in cross section and 5 m in height operated at room temperature. A wing wall (918 mm [height] \times 500 mm [width]) was hung at two different positions in the riser. Investigations detected a net downward solids flow when the wing wall was located at the top of the riser, but no downward solids flow was observed on its surface when the wing wall was placed 1.3 m below the roof. It also showed that for a given operating condition, the heat transfer coefficient on the wing wall was higher when it was placed at the top of the riser than when located at mid-height. The difference in heat transfer between water wall and wing wall, as observed in the present experiment in the pilot plant, is similar to that noted in commercial boilers (Chapter 3).

4.1. Introductory remarks

Chapter 3 showed that heat transfer coefficients on wing walls are always lower than those on water walls (termed as walls) in a commercial boiler. The difference is nearly 22% of that of water wall heat transfer coefficient. This difference is higher than the contribution of the particle convection on heat transfer on the walls. The dynamics of solids and gas in the vicinity of the walls controlled the suspension-to-wall heat transfer (Basu and Fraser 1991, Glicksman, 1997). Wing walls, which are located away from the walls, may operate under hydrodynamic conditions different from those on the walls. Therefore, it is not known if available experimental data on water walls or mechanistic models (Table 2.5) for water walls can be applied directly to wing walls. The present work is conducted to investigate the physical phenomenon behind the mechanism of heat

transfer on wing walls. It provides preliminary data on heat transfer in wing walls measured in a large pilot plant operated at room temperature and compares measured data with those on vertical riser walls.

4.2. Experiments on Pilot Plant

4.2.1. Description of Pilot Plant

Experiments on the wing walls and the enclosing water wall were carried out using a closed loop cold-model circulating fluidized bed riser of $1\text{m} \times 0.5\text{m}$ rectangular cross-section. The system, illustrated in Fig. 4.1 consists of a riser, two separators, two standpipes for storing recirculating solids and a J-valve to feed solids back into the riser. Details are available in Appendix A. The riser is 5m in height. Clear plastic (LEXAN) was used on the front wall along the height of the riser column for visual observation whereas the other three walls were made of wood lined with aluminum sheets. The aluminum sheets were used to ensure a smooth surface, because roughness might affect the hydrodynamics within the riser. Pressure taps are located on the side wall of the riser column at 500 mm intervals (Table 4.1). Air was provided by a $2.5\text{ Nm}^3/\text{s}$, 11.2 kPa fan. Air enters the bottom of the riser through a multi-orifice (9 mm diameter) distributor of 20% opening area coupled with a fine wire mesh of 50% opening area. The superficial gas velocity was measured by both venturi meter and pitot tube arrangements. The highest superficial velocity in the experiments was 5 m/s.

At the top of the column, entrained solids were carried by air from the riser to the separators as shown in Fig. 4.1. Air leaving the secondary separator was led to the baghouse and then to the suction of the fan. Solids in the standpipe entered the riser from the J-valve through a 140 mm ID clear plastic (Acrylic) tube centered 700 mm above the distributor. The wing walls were hung at two positions marked as Case 1 and Case 2 as shown in Fig. 4.1.

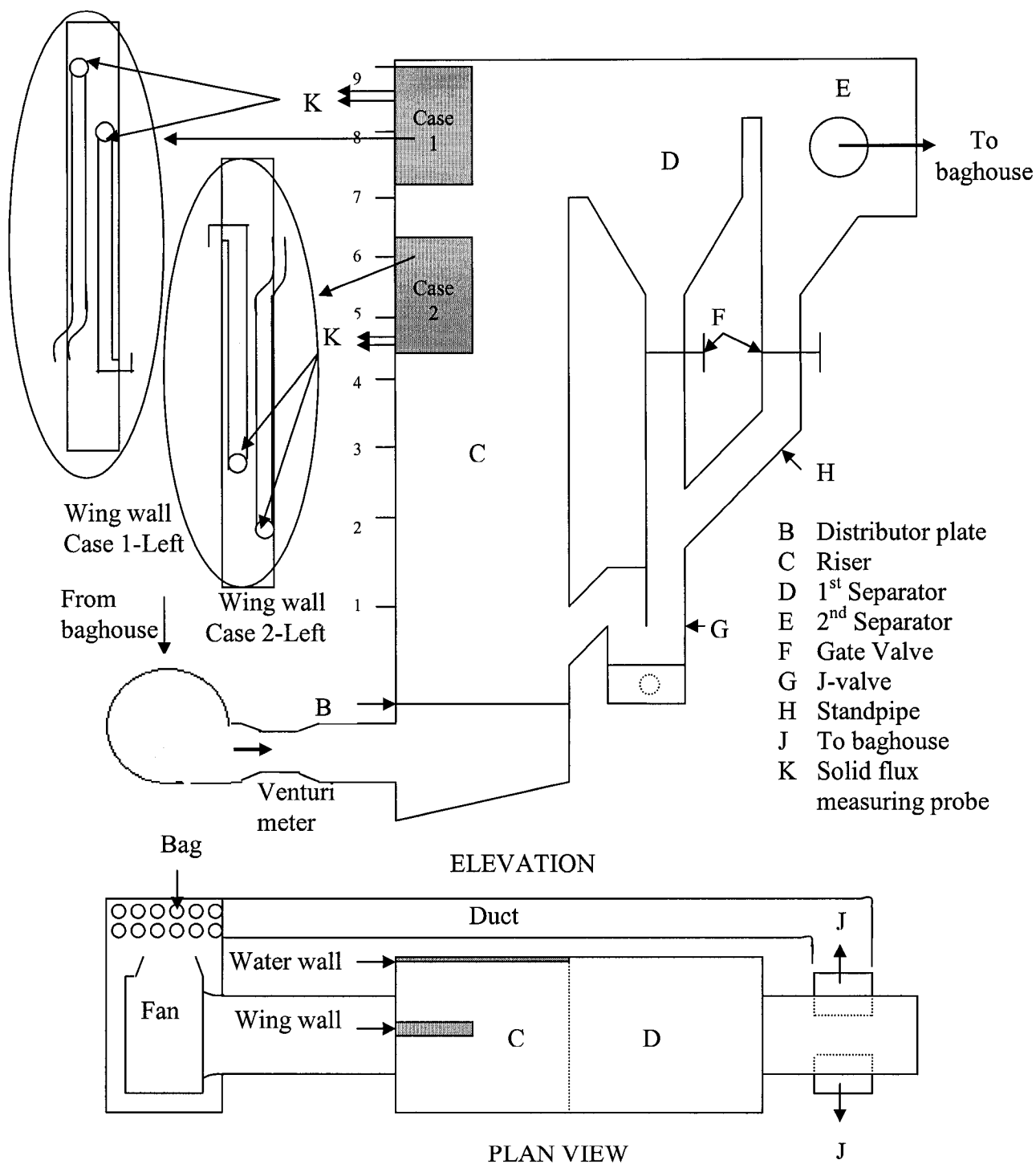


Figure 4.1. Schematic diagram of the experimental unit

4.2.2. Wing Wall

The wing wall was 918mm long, 500mm wide and 50mm thick. It had heaters placed on it in several locations as shown in Fig. 4.2. It was hung in the upper part of the fluidized bed riser at 1300 mm in Case 2, and at 50 mm in Case 1 below the roof of the riser (Fig. 4.1). The movement of the wing wall was restricted by holding it to the side wall with long wooden screws and coupling it with an extension rod from the front wall of the riser at its right bottom corner. This ensured a rigid and stable support when it was suspended in the riser.

The wing wall was fabricated of 6.25mm thick low conductivity Tivar 1000 antistatic UHMW polyethylene. It was made of two sheets of this material, one on each side of the wing wall supported by 37.5mm strips of the same material along the edge. Fiberglass-insulated flexible silicon rubber heaters of low thermal conductivity, were attached to each side of the wing wall. The heaters (2nos of 610 mm × 50 mm and 6nos of 50 mm × 152 mm) were installed on both sides of the wing wall (Fig. 4.2) to reduce heat loss from the walls. The heaters were placed in grooves on both surfaces, in such a way that they were flush with the surfaces. Double-sided insulating fiberglass tape was applied between the heaters and the surfaces within these grooves. These heaters are thermally insulated by fiberglass on all four sides.

The above heaters were chosen because they are very thin (0.7 mm) and are made of a material with a low thermal conductivity. Such heaters are known to have (Mosyak *et al* 2001) a constant heat flux. All the heaters were electrically connected in parallel with each other. The temperature distribution over the heated surface was measured from the outer side by 22 thermocouples. In the present study, Teflon coated T-Type thermocouples (0.3 mm thick) were attached to the heaters. These thermocouples have a resolution of 0.1°C and a response time of 0.3 seconds. Details of the thermocouples and their locations are shown in Fig. 4.2. The photograph shows the wing wall looking down

from the top for case 2 in Fig. 4.2a and from front for case 1 in Fig 4.2b. Two additional thermocouples were used to measure the gas-solid suspension temperature. Connecting leads for the thermocouples and the heaters were routed internally through the interior of the wing wall. This was done to keep the surface of the wing wall smooth. All wires were collected in one corner of the wing wall. From there, they ran first through the side of the wing wall and then through the sidewall of the fluidized bed riser. The heaters were connected with the power source through a wattmeter and an autotransformer (variac). The heat flux of the heaters was controlled by the variac.

4.2.3. Solids Flux Measuring System:

A non-isokinetic probe was used on each side of the wing wall to measure the upward and downward solids flux. They were located 310 mm from the sidewall of the riser and 1500 mm and 720 mm below the top of the roof for Case 2 and Case 1 respectively. Details are given in Table 4.1 and Figs. 4.1-4.3. As per the suggestion of Rhodes *et al.* (1988), the suction air velocity inside the probe was maintained within the range of 4-7 m/s. The probes were 7.5 mm inside diameter, with one opening on the outside of the wing wall, and the other opening within the wing wall. The opening on the inside was attached to flexible plastic tube. This tube first ran through the side of the wing wall and then through the side of the fluidized bed. Valves were attached to the end of each tube to control the flow of solids (Fig. 4.3).

4.2.4. Water wall:

A heating strip, 610 mm long and 50 mm wide, was attached to one side of the riser wall, 1.5 m below from the roof of the riser. This heating surface simulated the enclosing water wall. It was used to compare the heat transfer coefficient of the water wall with that on the wing wall (Case -2) at a specific height. The water wall test section was similar to the wing wall section except that it was flush with the sidewall of the riser instead of hanging from the roof. Details are given in Fig. 4.4.

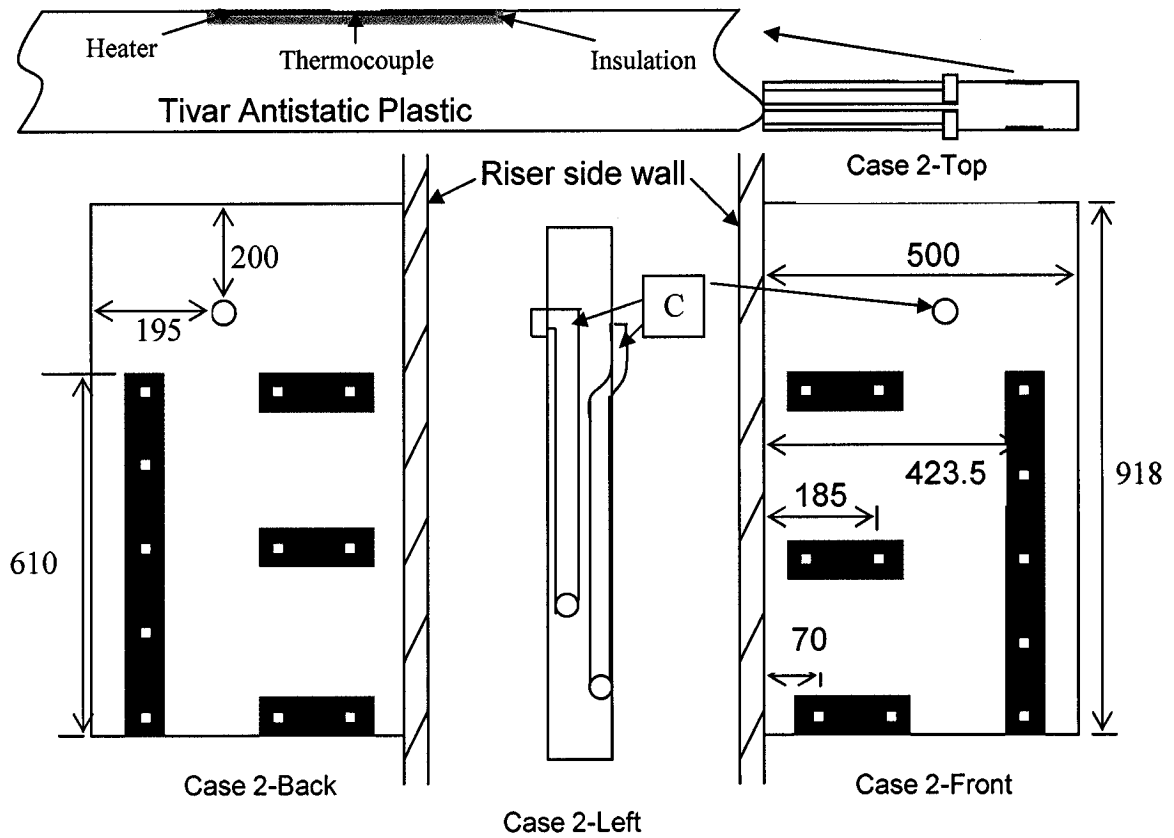


Figure 4.2a. Details of experimental set-up of wing wall when it is placed at 1300 mm below the roof (case-2)

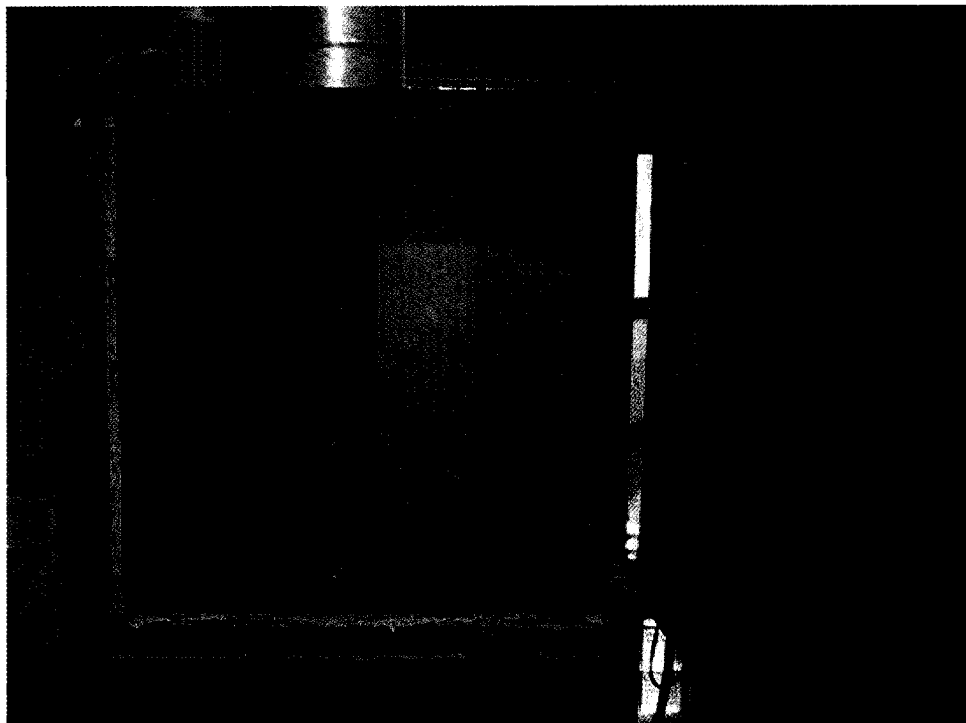
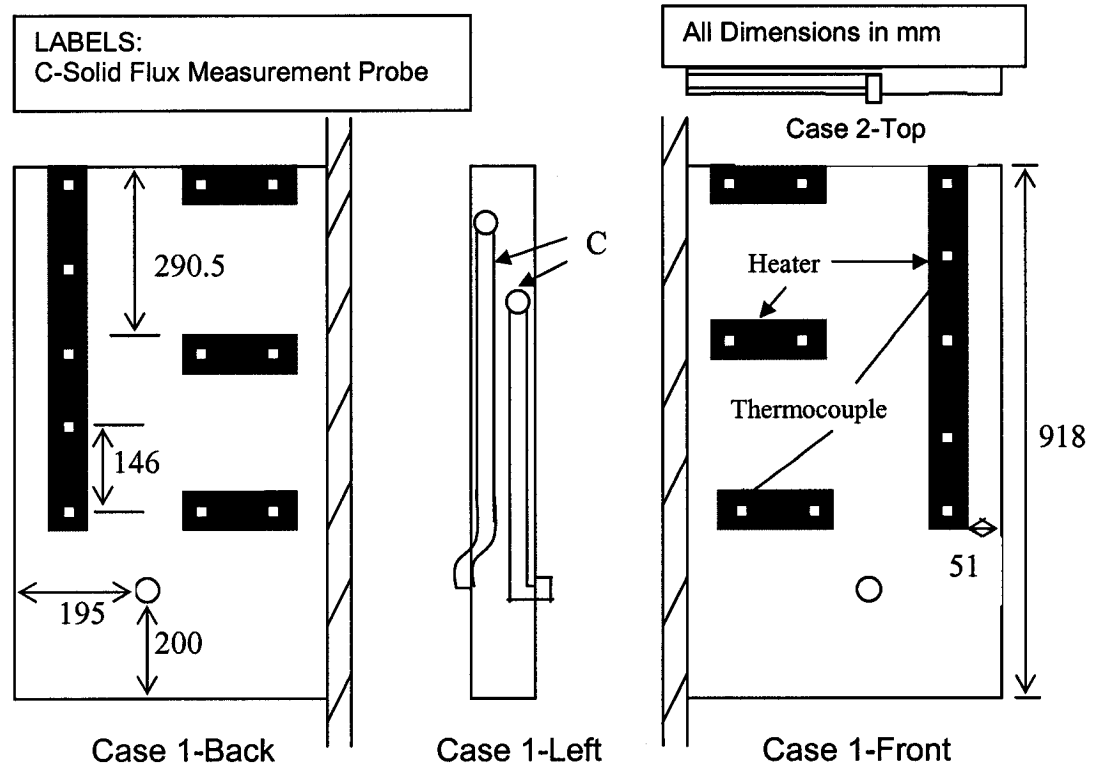


Figure 4.2b: Details of experimental set-up of wing wall when it is placed at the top of the roof (case-1)

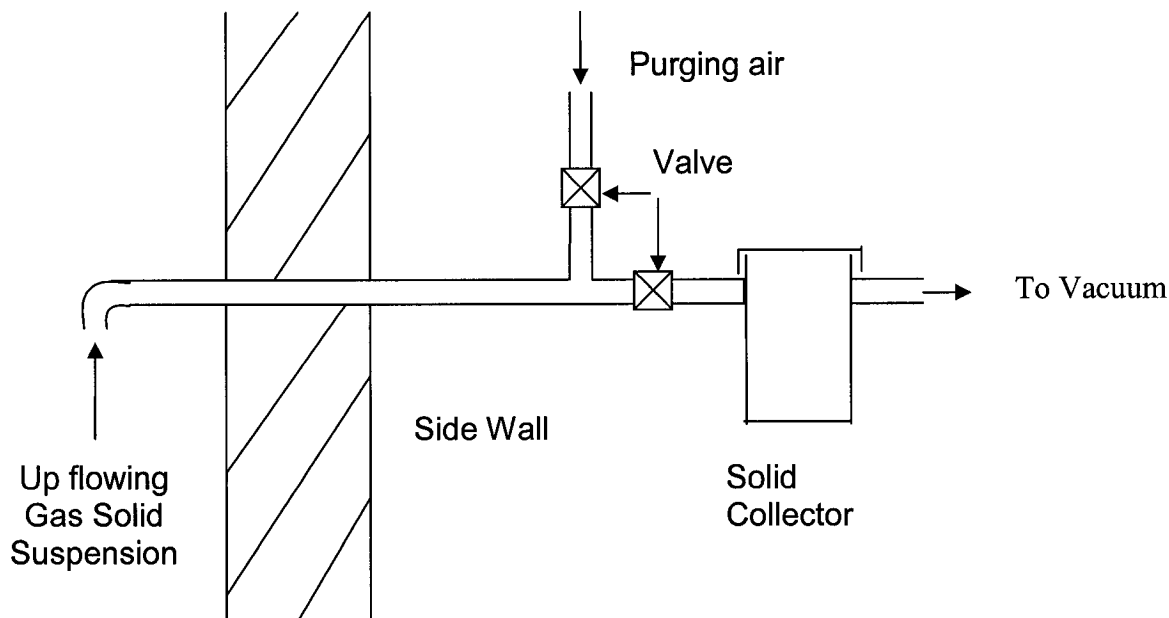


Figure 4.3. Schematic diagram of solid flux measuring probe

Table 4.1. Locations of pressure transducers in the riser
(a) *Differential pressure transducers*

Transducer No	Height, to midpoint of measurement section from distributor (m)
1	0.8
2	1.5
3	2
4	2.5
5	3
6	3.5
7	4
8	4.5
9	5
<i>(b) Absolute pressure transducers</i>	
At bottom	0.06 m
<i>(c) Solid flux measuring port</i>	
At the surface of the wing wall	
<i>Case 1</i>	
From Roof	720 mm
From Side wall	310 mm
<i>Case 2</i>	
From Roof	1500 mm
From side wall	310 mm

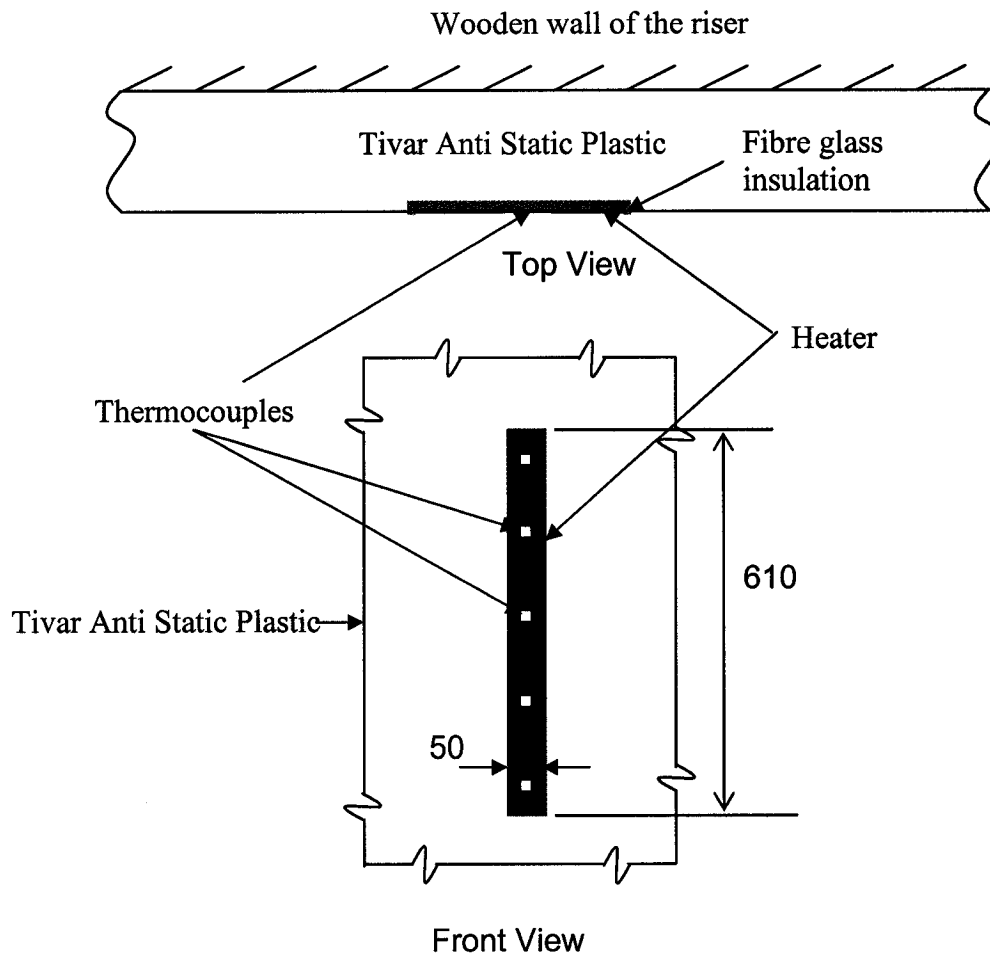


Figure 4.4. Details of experimental set-up of water wall

4.2.5. Experimental Techniques

To conduct the experiments, the wing walls were placed in two positions, referred here as Case 1 and Case 2 (Fig. 4.1). The test section, simulating the water wall, was kept on the sidewall of the riser at 1.5m below the roof. The temperatures were measured after a steady-state condition was reached. The gas-solid suspension was first allowed to flow over the heat transfer surface at a given superficial air velocity and then the power for the heater was switched on. Once the temperature of the surface reached a steady value, the

temperature measurements were carried out and the local heat transfer coefficient between walls and the bed was determined from the following equation

$$h_x = \frac{\dot{Q}}{(T_{wx} - T_b)} \quad (4.1)$$

where T_{wx} is local temperature on the wall and T_b is the average bed temperature.

The heat flux \dot{Q} is calculated by dividing the power input, P , by the heater area, A .

The input power, P , can be calculated by two different ways:

- a) By measuring the voltage across the autotransformer and the current by ammeter
- b) By reading values directly from the wattmeter.

Both methods gave similar results in all experiments. Therefore, the simpler method described in (b) was used to estimate the heat flux of the heating surface.

In the setup for solids flux measurements, solids were collected through the trap over a specified period of time. The probe was purged by a three way valve until sampling started. It also allowed the suction rate to be set before the start of the sampling period (Fig. 4.3). The solids flux rate was obtained by weighing the particles collected over a specified period of time. The net downward solids flux was obtained by subtracting the upward solid flux from the downward solids flux and vice versa. The probe was calibrated by integrating the flux profile over the cross sectional area of the riser and compared that with the externally measured solids flux.

The superficial velocity was measured in the riser using the venturimeter installed in the air duct. The solids circulation rate was measured by means of two knife valves in the upper part of the return legs, located just below the two separators. The solids circulation rate was calculated by measuring the time required for a known volume of solids to accumulate on top of the knife valve after the valve was closed.

For each experiment, the solids valve was opened allowing solids to flow into the riser. When the solid levels in both return legs remained unchanged for some period of time, the system was deemed to have reached a steady state condition.

4.2.6. Bed Material:

Nova Scotia sand having a mean (surface/volume) diameter 266 μm , particle density of 2564 kg/m^3 and bulk density of 1320 kg/m^3 was used as the bed material. The particle size distribution is given in Appendix B.

4.3. Results and discussion of data from CFB pilot plant:

This section presents results on hydrodynamic and heat transfer behavior of gas-solids on the wing walls. The data of the experiments are shown in Appendix D. The following discussions are carried out by analyzing those data.

4.3.1. Hydrodynamics:

The wing wall setup was hung from the top of the riser at two different locations;

1. Middle of the left wall and at the top of the riser and
2. Middle of the left wall and 1.3 m below from the top of riser.

4.3.1.1. CASE-1 (Top of the riser, Figure 4.2b)

In Case-1, the location of solids flux probe was 720 mm from the roof and 310 mm from the side wall. A net downward solids flow was noticed on the surface of the wing wall as shown in Fig. 4.5. Data, collected by the solids measuring probe, show that the net downward flux of solids increased with an increase in the external solid circulation. This

observation can be explained as follows. The upward moving gas turns 90° at the top of the riser to move towards the riser exit. So, a stagnant zone or cavity is created at the top corner of the riser just opposite to the exit to the cyclone. Though one could expect much eddies at the corner, the net upward gas velocity is zero in that area. The streamlines of gas carrying solids in this region was clearly visible through the transparent front wall. The test zone (wing wall) was observed to lie above this gas flow path. On the other hand, because of their higher inertia, the solids continued to move upwards. Some of them directly hit the roof of the riser while others gradually lost their momentum due to inertial effect and fell down in the cavity. The ratio of downward and upward fluxes gives the relative measure of downward solid flux. It was 1.6 while the external solid recycle rate was $2.0 \text{ kg/m}^2\text{.s}$. This ratio increased to 2.2 when external recycle rate was increased to $8 \text{ kg/m}^2\text{.s}$ (Fig 4.5b). This suggests a relatively mild influence of the recycle rate.

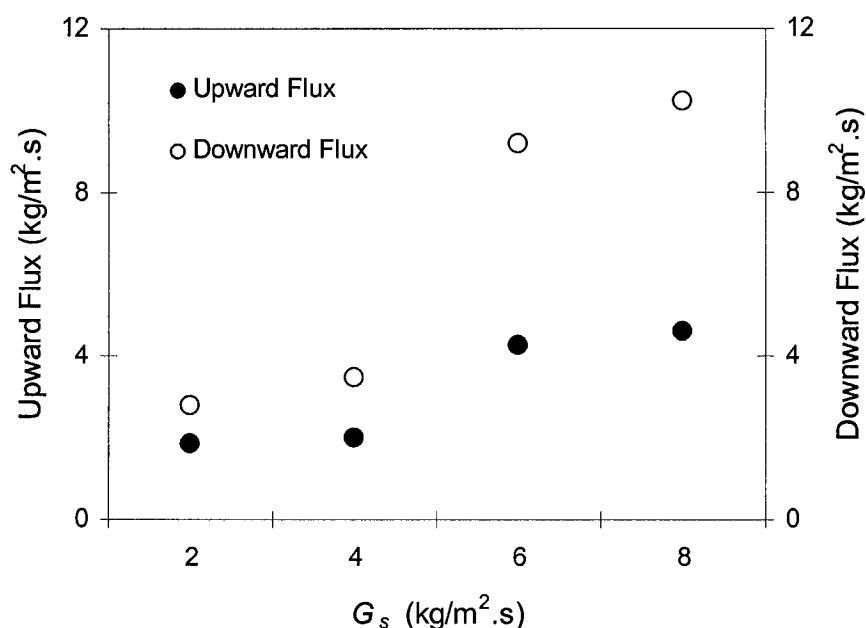


Figure 4.5a Variation of upward and downward solids fluxes with external solids circulation rates for a constant superficial velocity ($V_s = 3.9 \text{ m/s}$) for wing wall (Case-1).

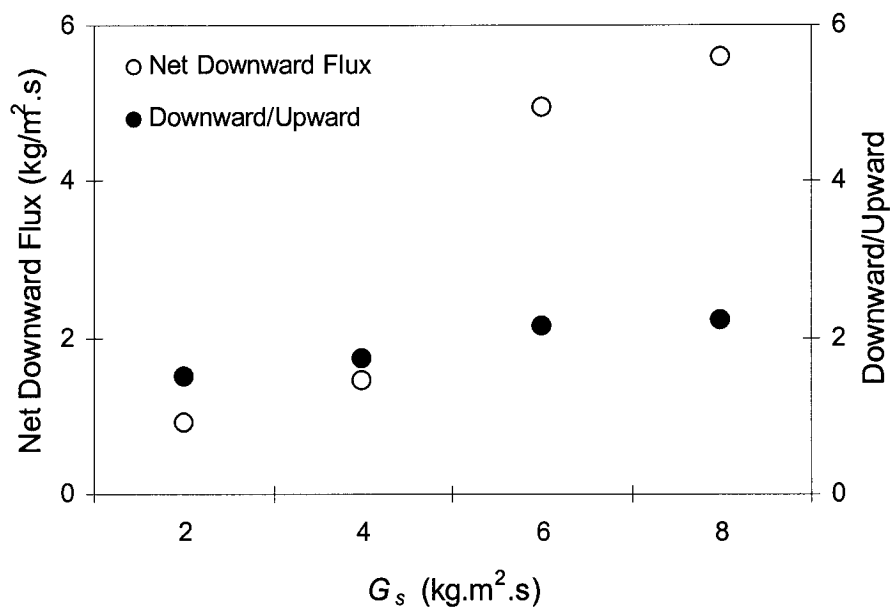


Figure 4.5b Variation of net downward fluxes and ratio of downward and upward fluxes with external solids circulation rates for a constant superficial velocity ($V_s = 3.9$ m/s) for wing wall (Case-1).

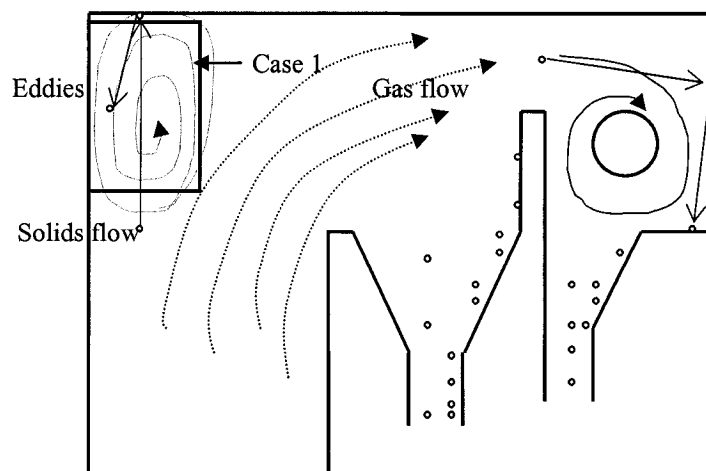


Figure 4.5c Expected gas solids motion on the top of the riser

4.3.1.2. CASE-II (1.3 m below the roof, Figure 4.2a)

In Case-2, the location of solids flux probe was 1500 mm from the roof and 310 mm from the side wall. This location was further down the riser than that of previous case, and same distance from the wall. Unlike the previous case, no net downward solids were noticed on the surface of the wing wall in this case (Fig 4.6a – 4.6b). This observation can be explained by the core annulus structure, the widely accepted hydrodynamic model for the CFB riser. According to this model, the solid concentration is very low at the center of a CFB riser and it increases exponentially towards the wall of the riser (Zhang, 1995). As the wing wall in the present experiment was located at the middle of the riser, one can expect a very low concentration of solid in that region. Moran and Glicksman (2001) reported that the gas velocity at the center of a CFB riser is as much as twice of the cross sectional average gas velocity (superficial velocity). Neither high upward gas velocity nor low concentration of solid favor formation of clusters, which flow downward on the wing wall. The presence of solids reduce the thickness of the boundary layer on the wall giving a flatter velocity profile in the radial directions compared to when gas alone is flowing (Rogers and Eaton, 1990; Rashidi *et al.*, 1990; and Hussainov *et al.*, 1998). For this reason, solids near the wing wall at the centre do not flow downward. However, when the solid concentration is increased, greater number and heavier clusters are formed. Consequently, solids tend to flow down more on the wing wall. Measured data showed (Fig. 4.6b) that the net upward flux of solids on the surface decreases with the increasing of external solid circulation. This was irrespective of superficial velocity.

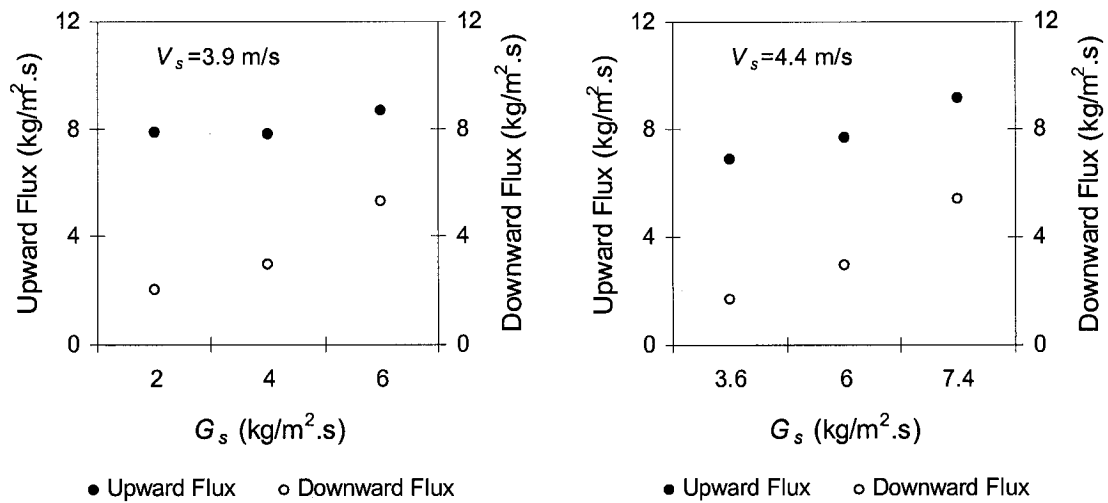


Figure 4.6a. Variation of upward and downward solids mass fluxes with external solids circulation rates at two different superficial velocities ($V_s = 3.9$ m/s, $V_s = 4.4$ m/s) for wing wall (Case-2).

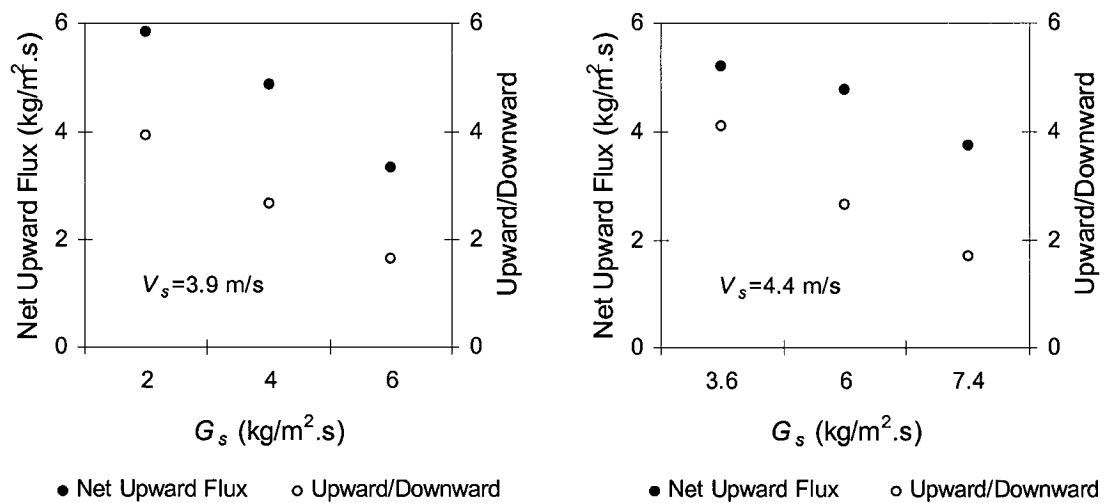


Figure 4.6b. Variation of net upward solids fluxes and ratio of upward and downward solids fluxes with external solids circulation rates at two different superficial velocities ($V_s = 3.9$ m/s, $V_s = 4.4$ m/s) for wing wall (Case-2).

4.3.2. Heat transfer:

4.3.2.1. Axial distribution of heat transfer coefficient

To study the effect of varying hydrodynamic conditions on the heat transfer, local heat transfer coefficients were measured on the wing wall at both upper and lower locations. Experiments were carried out at different external circulation rates and superficial velocities. The temperatures on both sides of the wall were found similar and local wall temperatures were estimated by averaging the recorded values from both sides (Appendix D). Results are shown in Figs. 4.7–4.9. These figures compare the results for both cases: i.e. the variation of heat transfer coefficients along the height of the wing wall at a fixed operating condition. For Case 1, (Fig. 4.7), at higher external circulation rates (8 and 6 $\text{kg/m}^2\cdot\text{s}$) the heat transfer coefficient decreased gradually from the top of the heating strips towards its bottom. This can be explained by the observed net downward solids flow (Fig. 4.5b) along the height of the wing wall. The net downward solid flux was in excess of 4 $\text{kg/m}^2\cdot\text{s}$. As the layer of particles sweeps down the heating strip, it gradually approaches thermal equilibrium with the surface. This reduces the thermal driving force which is the temperature differential across the gas film. This causes lower heat transfer and consequently lower heat transfer coefficient which is based on temperature difference between the wall and the average bed temperature. These results confirm the hydrodynamic behavior in the riser as observed by the solid flux measurement probe (Fig. 4.5b). Similar observations are also made on heat transfer to the water wall (Wu *et al.*, 1987, and 1989). These results also showed higher heat transfer coefficients at higher external solid circulation rates.

However as seen from Fig 4.7, at lower external solids circulation rates (2-4 $\text{kg/m}^2\cdot\text{s}$), the heat transfer coefficient on the lowest point of the wing wall is higher than that on the point just above it. The heat transfer in the cold bed comprises contributions of both gas convection and particle conduction. In the case of low external circulation rate, we can see from Fig. 4.5 that both upward and downward solid fluxes are very low. This gives a

low particle concentration in the upper bed. Thus, the gas convection from the upward gas flow is more dominant than the conduction from the moving particles. For instance, in case of forced convection on a flat plate, the heat transfer on the leading edge is the highest. Thus in the present case, the heat transfer at the bottom of the wall is highest. To verify this hypothesis, several tests were carried out without any solids in the riser. Results clearly show that for pure gas convection the heat transfer coefficient is highest at the lowest point of the wing wall.

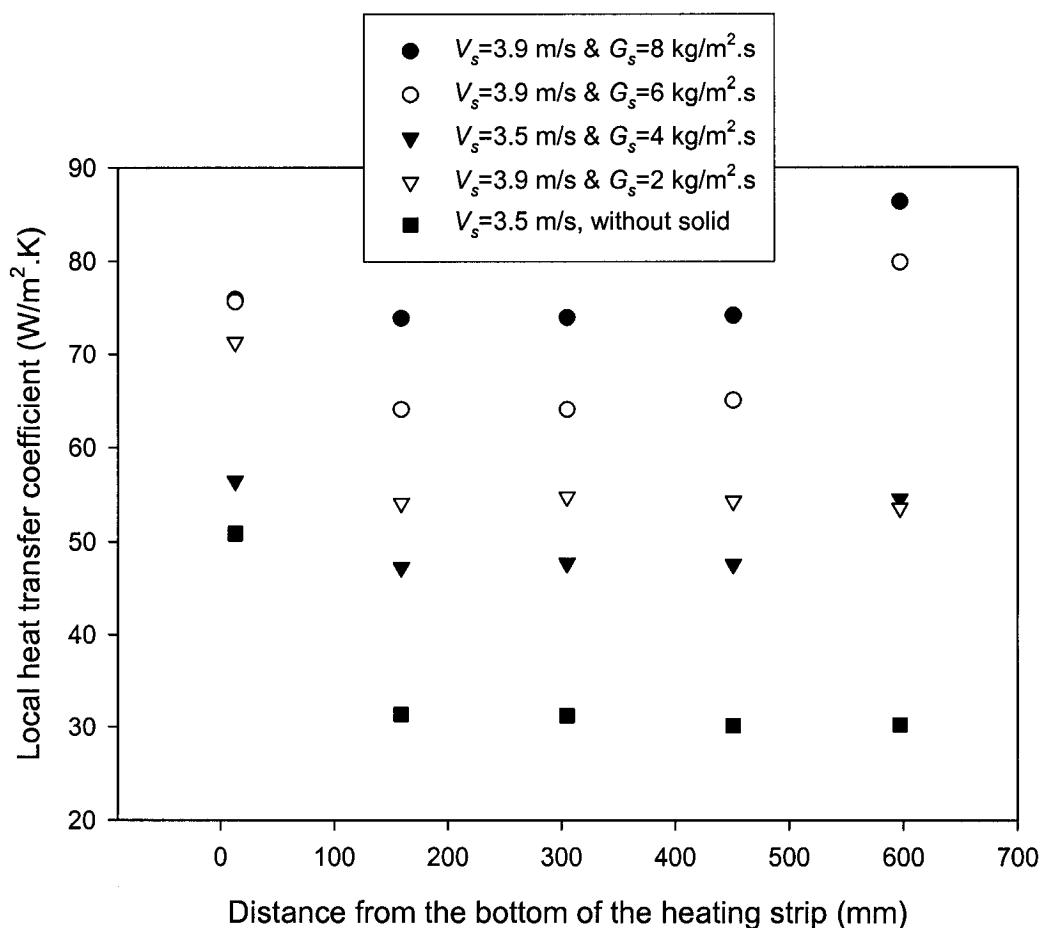


Figure 4.7. Local heat transfer coefficients measured along the height of the wing wall placed at the top of the roof at different operating conditions (Case-1)

Results from Case 2 where the wing wall was at 1300mm below the top of the roof (Fig. 4.8a) presents a different scenario. The heat transfer coefficient is higher at the bottom of

the heating strip at all external solids circulation rates. The heat transfer coefficient gradually decreases down to the heating strip. It suggests that there is no net downward solids flow along the wing wall at this position. Solids flux measurements (Fig. 4.6a), which showed that upward solids fluxes are greater than the downwards fluxes, supported these findings. In general, the heat transfer coefficient increases with increasing superficial gas velocity and external solids circulation rates. The difference in heat transfer coefficients between two superficial gas velocities (3.9 m/s and 4.4 m/s) at a fixed circulation rate of 6 kg/m².s is very large at the lowest point of the wing wall while at the top of the wing wall it is negligible (Fig. 4.8a). This suggests that at the lowest position the dominant effect is of the gas velocity. At a higher velocity, the Reynolds number is higher and the corresponding convective heat transfer coefficient will also be higher in this region of developing thermal boundary layer. However, further up in the developed region, due to the formation of the thermal boundary layer, the heat transfer coefficient is low and is nearly constant. The contribution of particle convection becomes also important here because of net upward solid flux. As the solid flux is upwards, the particle convection is also higher in the lower end. For the same reason the particle convection decreases towards the top. Owing to the particle convection, the heat transfer coefficient in this case is higher than the heat transfer coefficient measured (Fig. 4.8a) without solids in the bed. The contribution of particle convection increases with the increase in external solids circulation rates, hence suspension density in the riser.

Fig. 4.8b shows the ratio of average heat transfer for the wing wall (Case 2) with and without particles with average suspension density for a superficial velocity of 3.9 m/s. The Apparent cross-sectional-averaged solids hold-ups can be inferred by measuring average differential pressures across sections of the riser and equating the static pressure drop between the riser height of 2.5m to 5m to the bulk weight in the riser sections, i.e.,

$$\Delta P/\Delta z \cong [\rho_p(1-\varepsilon_{avg}) + \rho_g\varepsilon_{avg}]g \quad (4.2)$$

where, ΔP = differential pressure in N/m², Δz = height in m, ρ_p = density of particle in kg/m³ and ε_{avg} is the voidage

Wall friction for both gas and solids and solids acceleration is neglected because of their insignificant contribution on the pressure profile (less than 20%, Issangya *et. al.* 1999). Thus suspension density data are presented as apparent solids hold-ups, i.e. as $(1-\epsilon)$ calculated for equation (4.1), throughout the rest of this thesis.

As seen from Fig 4.8b, the proportionality exponent for the fitted curve is found to be 0.12, which is lower than the reported value of 0.5 for the water wall by other researchers (Basu and Nag, 1996; Glicksman 1988).

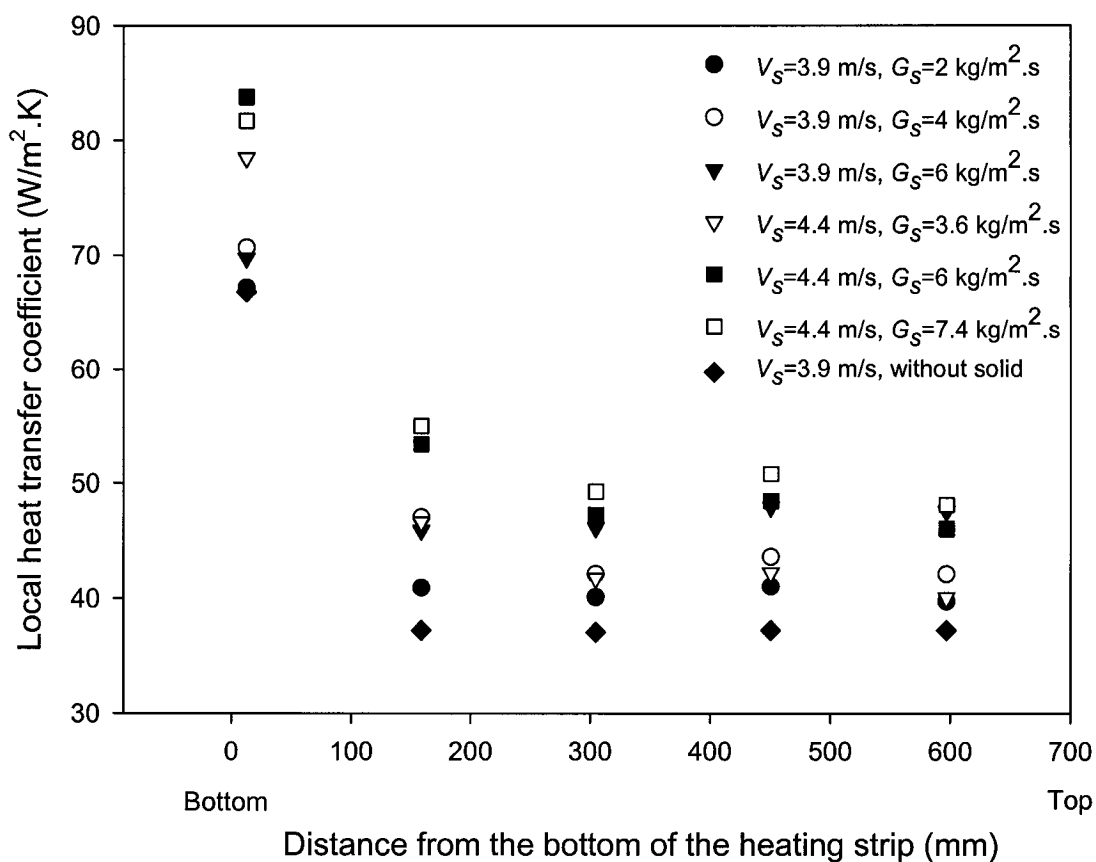


Figure 4.8a. Local heat transfer coefficients measured along the height of the wing wall placed 1300 mm below the top of the roof at different operating conditions (Case-2)

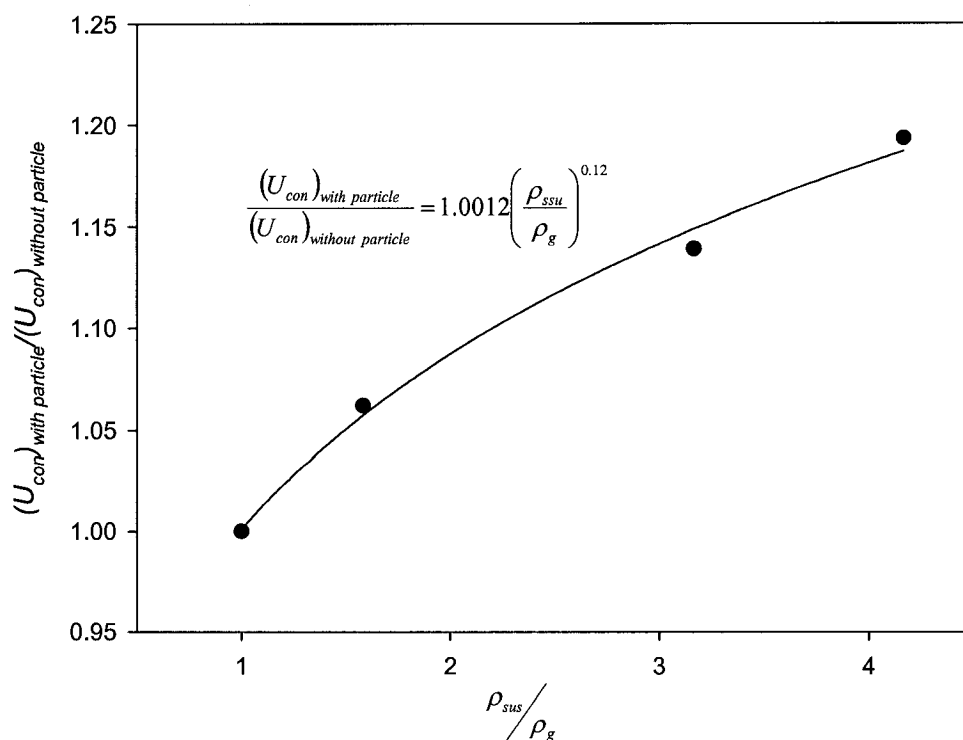


Figure 4.8b. The ratio of forced convection with and without particles increases with the ratio of suspension density and gas density. The graph is plotted for a superficial gas velocity of 3.9 m/s (Case-2).

The relative importance of downward solids flow, along the heating strips for a given velocity and circulation rate is shown in Fig. 4.9. In Case 1, at the highest point of the heating strip, the heat transfer coefficient is nearly 1.5 times the value recorded in the highest point of the wing wall in Case 2. However, at the lowest point where gas convection is dominant both have approximately similar heat transfer coefficients. The upper wing wall (Case-1) enables higher heat transfer in the upper end of the heating surface due to higher downward solids flux compared to that at the top of the lower wing wall (Case-2). However, as one moves down, the downward flux declines because the solids sweep upward over the upper wing wall due to higher local gas velocities at those positions. Therefore, the difference between heat transfer coefficients on the lower end of wing walls at two locations is low. Finally, the lowest point of the wing walls is influenced by the strong entry effect of upward moving gas and solids. Thus, both have higher but similar heat transfer coefficients.

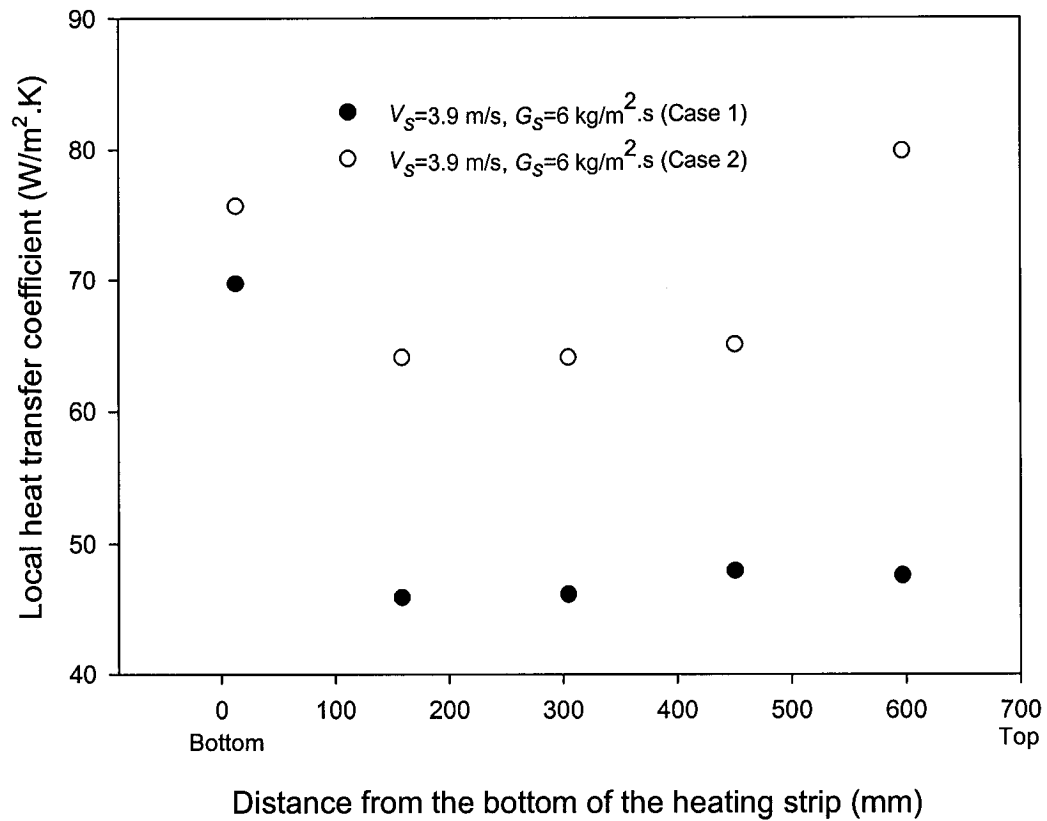


Figure 4.9. Comparison of local heat transfer coefficients profiles along the height of the heating strip between two positions of the wing wall for a specific operating condition.

4.3.2.2. Lateral distribution of heat transfer coefficients

The local heat transfer coefficient along the width of the wing wall is shown in Fig. 4.10. The local heat transfer coefficient is plotted for different operating conditions at three different heights measured from the bottom of the heating strip and along the width (distance measured from the sidewall) of the wing wall. Near the wall, the heat transfer coefficient is higher suggesting a greater solid concentration at the wall and on the corner.

As the external solid circulation increases, the heat transfer coefficient also increases due to the increase in suspension density as well as in solids concentration. In Case 1 (upper location), an interesting observation is made when the CFB unit was operating for two different external solids circulation rates (Fig. 4.10a -4.10b). At the top of the heating strip ($H=596.8$ mm), the heat transfer coefficient was higher than that at the bottom. This is due to a greater downward solids flow at higher circulation rates. On the other hand, at a lower circulation rate, the heat transfer coefficient at the bottom ($H=12.7$ mm) is higher than that at the top signifying an upward solid flow. A wide variation is observed at the position 423 mm from the sidewall of the riser. This can be attributed to the fact that the heating strip is a long (610 mm in height) one instead of short (50 mm in height) one, which forms thermal boundary layer on the heating surface along the height of the strip.

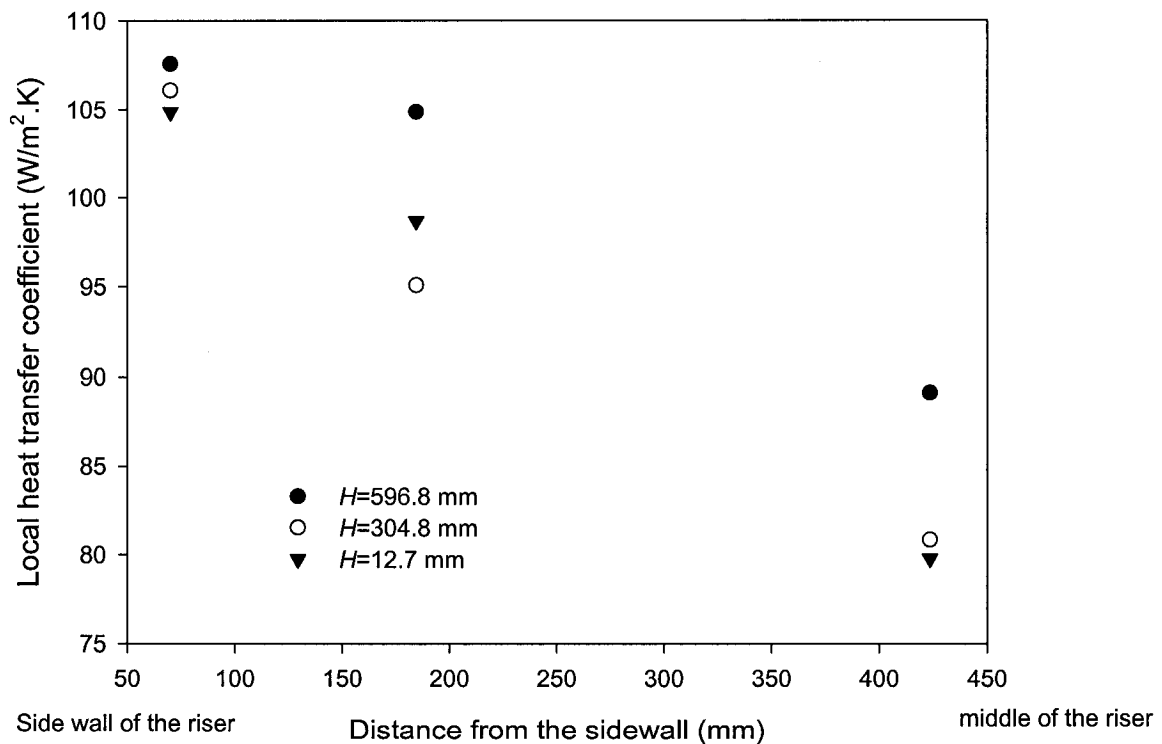


Figure 4.10a. Local heat transfer coefficients along the width of the wing wall for case-1 (a) $V_s=3.9$ m/s; $G_s=8$ kg/m².s, (case-1)

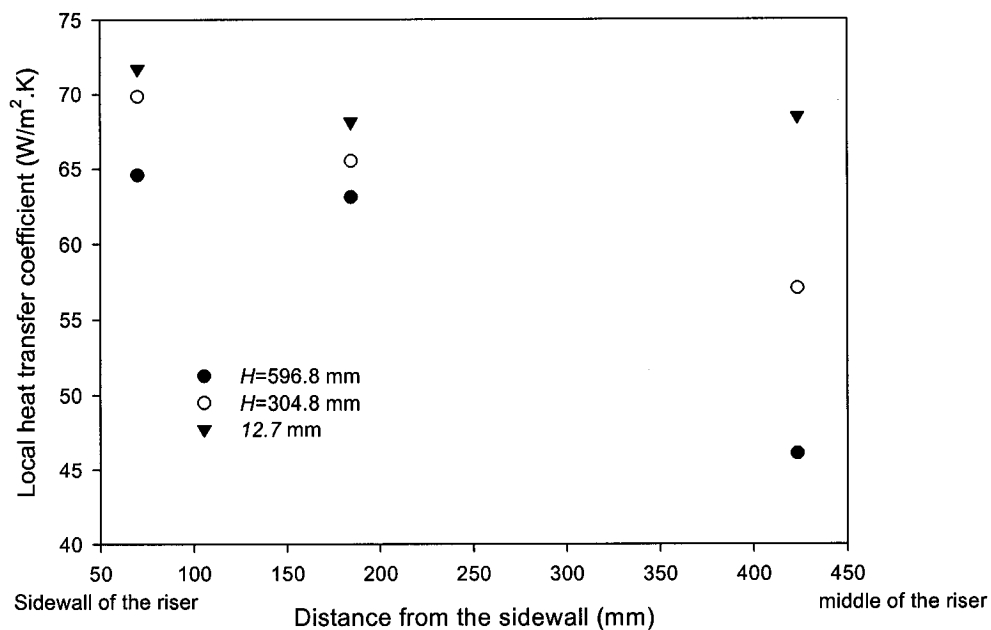


Figure 4.10b. Local heat transfer coefficients along the width of the wing wall for case-1 (b) $V_s=3.6$ m/s; $G_s=2$ kg/m².s

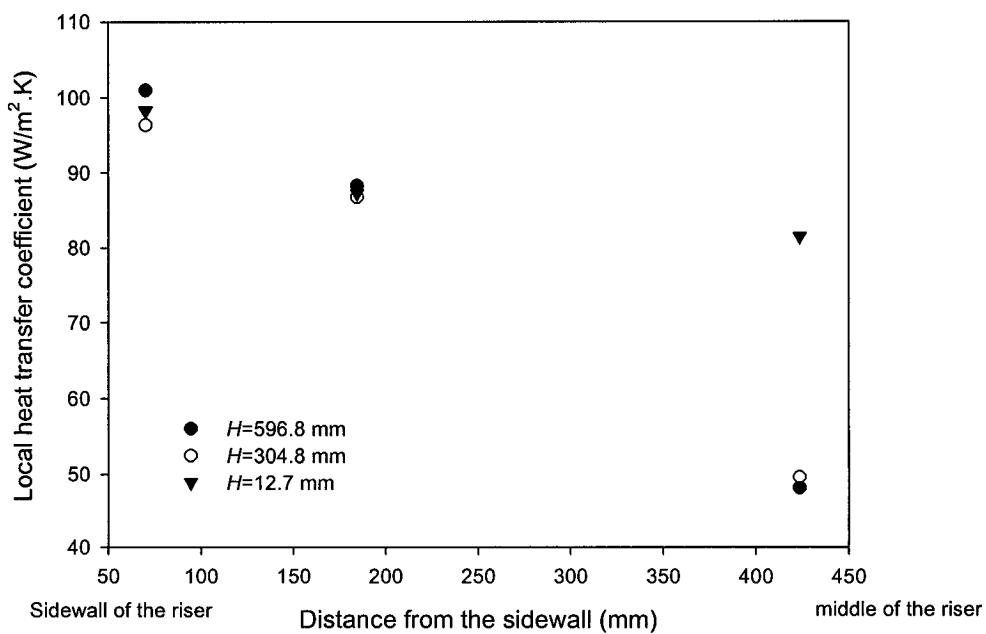


Figure 4.10c. Local heat transfer coefficients along the width of the wing wall for case-2 (c) $V_s=4.4$ m/s; $G_s=7.4$ kg/m².s

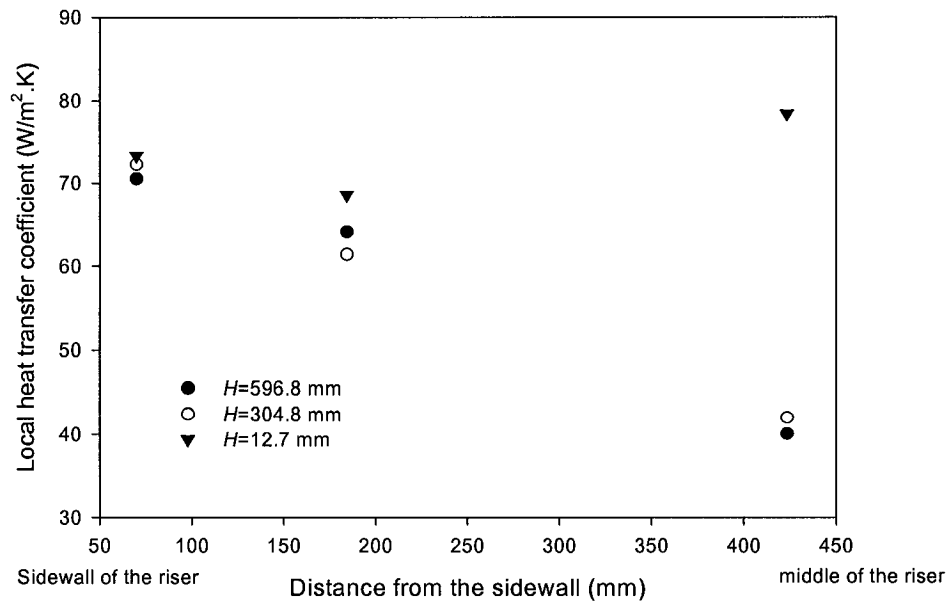


Figure 4.10d. Local heat transfer coefficients along the width of the wing wall for case-2 (d) $V_s=4.4$ m/s; $G_s=3.6$ kg/m².s

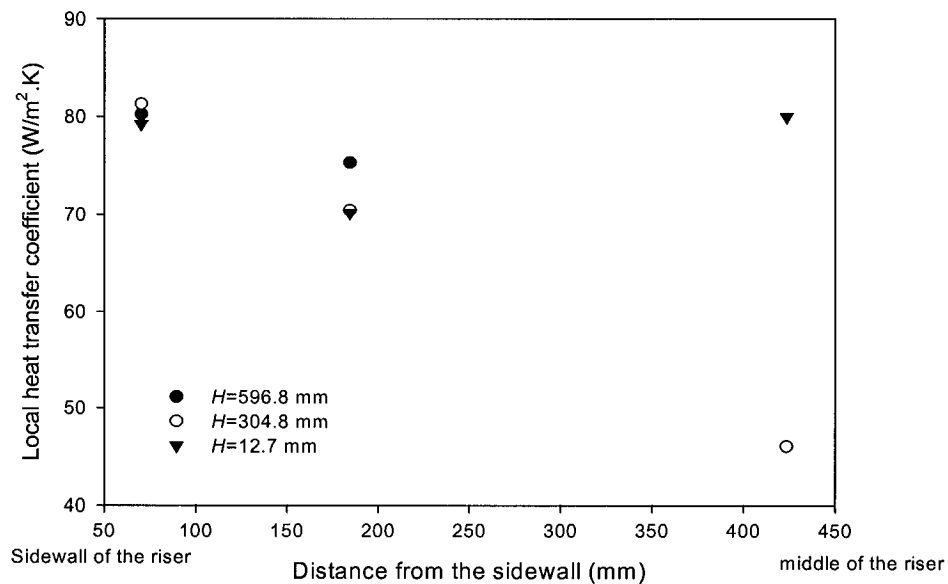


Figure 4.10e. Local heat transfer coefficients along the width of the wing wall for case-2 (e) $V_s=4.4$ m/s; $G_s=6$ kg/m².s

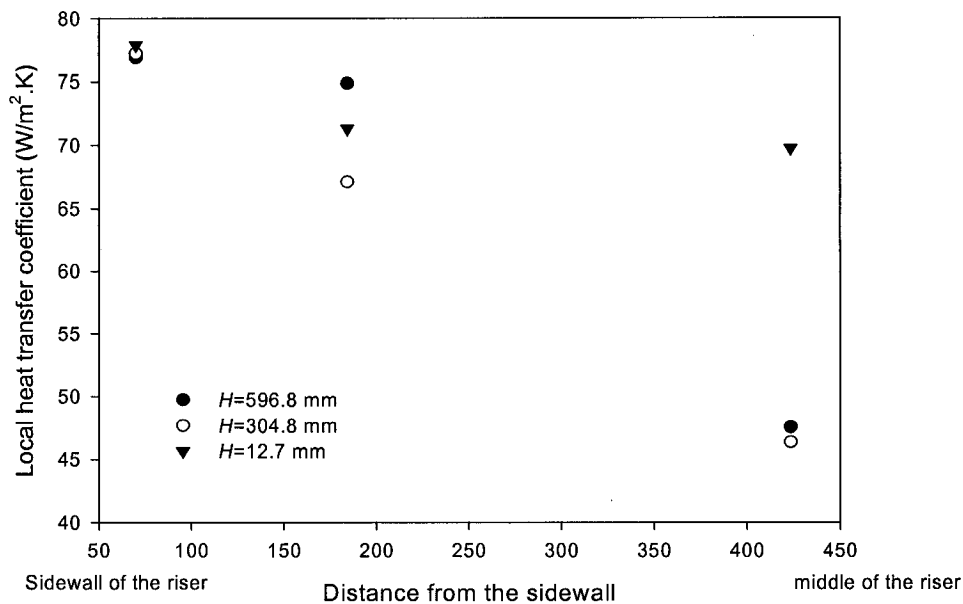


Figure 4.10f. Local heat transfer coefficients along the width of the wing wall for case-2 (f) $V_s=3.9$ m/s; $G_s=6$ kg/m².s

Within the range of operating parameters ($V_s = 3.5$ - 4.4 m/s and $G_s= 2$ - 7.4 kg/m².s) a net upward flux (Fig 4.6a – 4.6b) was always observed in Case 2 (Figs. 4.10c-4.10f). The hydrodynamic observation also supports the heat transfer measurements. Taken at specific points, for example, Figs. 4.10c-4.10e show that the local heat transfer coefficients near the corner (70 mm and 185 mm away from the side wall of the riser) increases with the external solid circulation rates. However, no noticeable change was observed for the position 423.5 mm away from the sidewall. However, in Figs. 4.10e-4.10f, due to the different superficial velocity, there was a noticeable change in heat transfer coefficient on that position. This is explained in a following fashion: In a CFB with rectangular cross-section, the corners have higher solids concentration (Zhou. J *et al* 1994). Therefore, the local heat transfer coefficient here depends more on the solid concentration than on the gas convection. The gas convection is more predominant in the middle of the riser. It is also seen that as the heating surface area decreases, the heat transfer coefficients increases. This supports the observations made by other researchers elsewhere (Luan *et al*, 1999)

4.3.3. Comparison between water wall and wing wall heat transfer

Local heat transfer coefficients along the water wall were obtained for different superficial velocities and external solids circulation rates. These are plotted in Fig. 4.11 where the distance along the water wall is measured from its bottom to the top. Similar to the trend reported earlier (Wu *et al* 1978 and 1989), the local heat transfer coefficient increases with the increase in distance from the bottom to top, suggesting a predominantly down-flowing solid layer next to the water wall surface, with fresh cold solids coming into contact with the top part of the surface.

Experiment shows that heat transfer coefficients increase with an increase in the solids circulation rates. More interestingly, for the same operating conditions, it is observed that heat transfer is higher on the water wall than that on the wing wall at a given elevation as shown for Case 2 in Fig. 4.12.

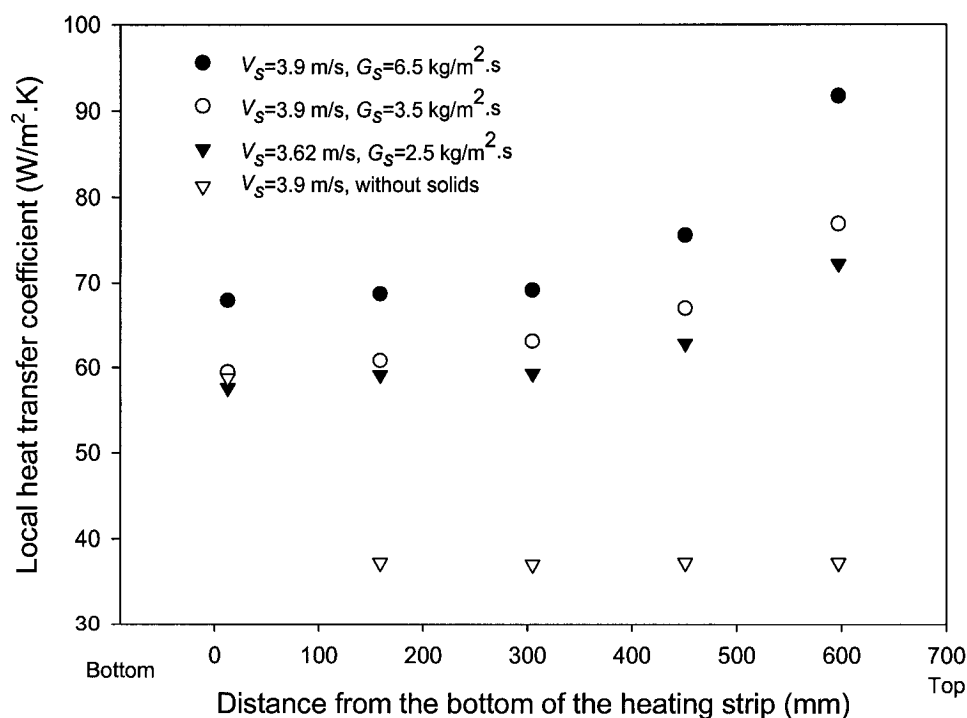


Figure 4.11. Local heat transfer coefficients measured along the height of the water wall at different operating conditions.

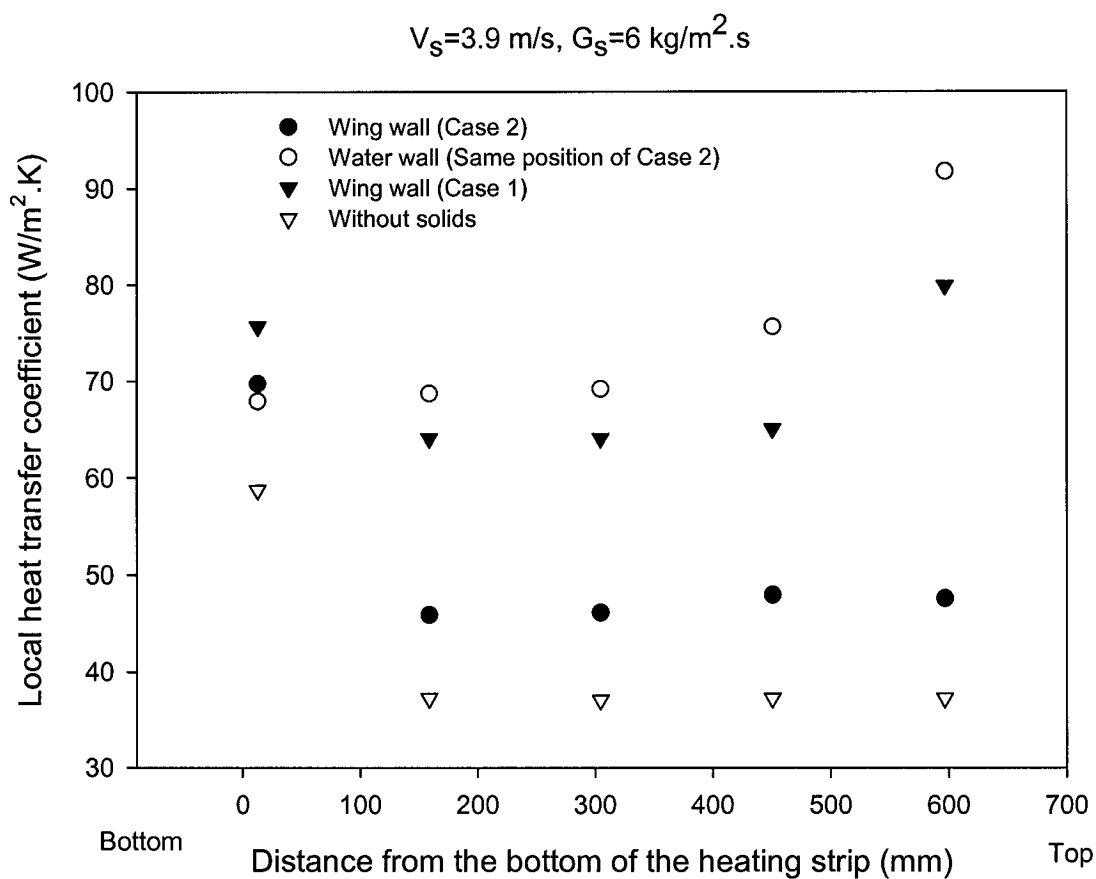


Figure 4.12. Comparison on local heat transfer coefficients along the height of the heating strips for wing wall (Case-1 and Case-2) and water wall at a specific operating condition.

The difference in heat transfer coefficients between water wall and wing wall is lower when the wing wall was at the top of the riser (Case-1). As mentioned earlier, the hydrodynamic condition on the wing wall in Case 1 is similar to that on the water wall which is characterized by a net downward solids flux. When the wing wall is placed at mid-height (Case-2), the hydrodynamics condition is marked by dispersed gas-solid flow with net upward solids flux. However, the heat transfer coefficient in Case-2 is greater than the heat transfer coefficient without solids because of a flatter boundary layer over the wing wall and total absence of particle convection.

4.4. Concluding remarks

This chapter reported experimental investigations on both hydrodynamics and heat transfer on wing walls in a circulating fluidized bed pilot plant operated at room temperature. Within the range of operating parameters (Superficial velocity 3.5 to 4.4 m/s and solid circulation rates of 2 to 6 kg/m²·s) the following conclusions are drawn.

1. The hydrodynamic condition on the wing wall is different from that on the water wall.
2. At any operating condition the heat transfer coefficient on the wing wall is lower than that on the water wall regardless of its position.
3. The position of the wing wall in the riser affects both hydrodynamics and heat transfer. A wing wall placed at the top of the CFB riser has higher heat transfer coefficients than that placed at the mid height of the CFB riser. This is due to downward solids flow at the top corner of the riser.
4. No net downward solids flow is present when the wing wall is placed at mid height.
5. While modeling heat transfer in a rectangular riser, the corner effect should be taken into consideration because of its influence on both hydrodynamics as well as on heat transfer rates.

Chapter 5

An Investigation on heat transfer to the standpipe of a CFB boiler

This chapter reports the results of an experimental and theoretical investigation on heat transfer to the walls of the standpipe. The heat transfer was studied at room temperature in a standpipe test section, which is 1940 mm in length and has a square cross-section of 100 mm. Solids used in this study were silica-alumina ceramic microspheres and sand with particle densities of 700 kg/m^3 and 2564 kg/m^3 , and sizes of 0.130 mm and 0.266 mm, respectively. The results show that for both types of particles, heat transfer is higher in dense section of the standpipe than in the dilute section. The heat transfer coefficient increases with increase in solid circulation rate. For a given circulation rate, finer particles yield higher heat transfer coefficients. This chapter also presents a mechanistic model of heat transfer in the standpipe. Heat transfer coefficients, predicted by the proposed model agree well with the experimental data.

5.1. Introductory remarks

Standpipes, which transfer solids from the cyclone to the loop seal, are traditionally refractory lined. For large capacity CFB boiler they offer an opportunity for additional heat transfer. Standpipes, with their refractory lined walls have high surface heat loss and high maintenance cost. Furthermore, besides adding to the weight of the standpipe assembly, their high thermal inertia severely restricts the fast light up of the boiler. Figure 1.1 and 1.5 shows the details of a conventional standpipe. Greenfield Research Inc. has developed a design to use the standpipe as a measure of heat absorbing medium. This was accomplished by replacing the thick refractory lined wall with thin membrane

type panels. To the author's knowledge, up to this time, no work on heat absorption in a standpipe has been either proposed or studied. So the present work is essentially an exploratory study into this new option.

The hydrodynamics of solids flow in the standpipe has been studied by a number of researchers (Knowlton, 1997; Basu and Fraser 1991; Jones and Leung 1985), however, a detailed study on heat transfer is still not available. Lehner and Wirth (1999) developed an empirical correlation based on their experimental data for calculating heat transfer in the downflow circulating fluidized bed based on normalized pressure drop number. One can assume that the hydrodynamic condition in the downflow CFB at zero superficial velocity resembles that in the dilute section of the standpipe. However, their correlation overpredicts the heat transfer coefficient when the normalized pressure drop number is unity. The earlier works by Liu *et al* (1999) and Colakyan and Levenspiel (1984) on the dense bed portion of the standpipe were based on the work done by Botterill and Desaim (1972), Denloye and Botterill (1977), Mickley and Trilling (1949), and Mickley and Fairbanks (1955). These works on moving bed flow, provide a useful starting point for understanding the heat transfer behavior in the dense section of the standpipe (Table 2.3). None of these mentioned works are on the walls of the standpipe. Most of the work on heat transfer has concentrated on vertical tubes passing through the standpipe. Such a configuration may affect free flow of solids down the standpipe as required in CFB boilers. So, there is a need to understand the phenomena of heat transfer between the solids and the standpipe walls. The present work proposes a rectangular cooled standpipe as used by GRI (Greenfield Research Inc.) for revamping old PC boilers. The objective of this work is to systematically obtain heat transfer data between the solids and the walls in the standpipe of a cold model CFB. Also, the findings were correlated and explained by available theory after simple modification.

5.2. Experimental set-up

The details of the CFB unit used is presented elsewhere (Basu and Cheng, 2000) and is shown in Figure 5.1. For this experiment, an instrumented test section of 100 mm square cross section and 1940 mm high is placed between the top of the existing loop seal i.e., supply chamber of the CFB unit and the bottom of the cyclone (Figure 5.2). Wear resistant clear plastic (LEXAN) was used for the front surface along the height of the standpipe for visual observation whereas the other three surfaces were made of low density wood. There were pressure taps on the sidewall of the standpipe at 450 mm intervals. Two flat silicon flexible electric resistance heaters (609 mm × 50.8 mm) were used as heating surfaces on the back wall of the standpipe; at locations between 10 mm to 620 mm and 1250 mm to 1860 mm from the entrance of the existing loop seal. The installation took the form of grooves on the back surface of the standpipe, made in such a way that the heaters were flush with the surface. Double-sided insulating fiberglass tapes were applied between the heaters and the surfaces within these grooves. These heaters are thermally insulated by Teflon on all four sides.

These heaters were chosen because they are very thin (0.7 mm) and are made of a material with a low thermal conductivity. Such heaters are known (Mosyak *et. al.* 2001) to have a constant heat flux. Both heaters were electrically connected in parallel with each other. The temperature distribution over the heated surface was measured from the outer side by 10 thermocouples. In the present study, Teflon coated T-Type thermocouples (0.3 mm thick) were then attached to the heaters. These thermocouples have a resolution of 0.1°C and a response time of 0.3 second. Details of the thermocouples and their locations are shown in Figure 5.2. Two additional thermocouples were used to measure the gas-solid suspension temperature.

The heaters are connected to the power source through a wattmeter and an auto transformer (variac). The heat flux of the heaters was controlled by the variac.

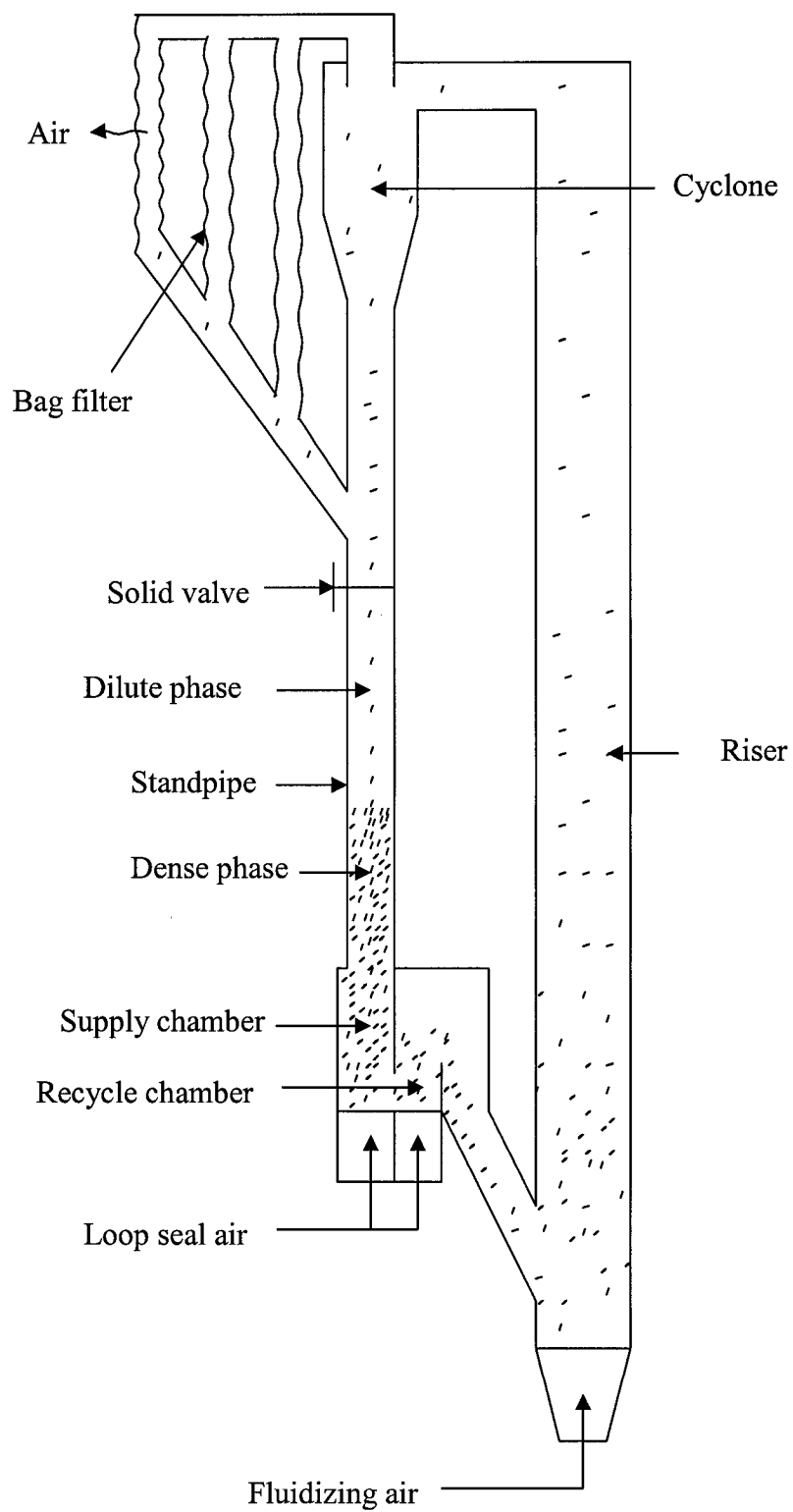


Figure 5.1. Schematic diagram of the experimental unit

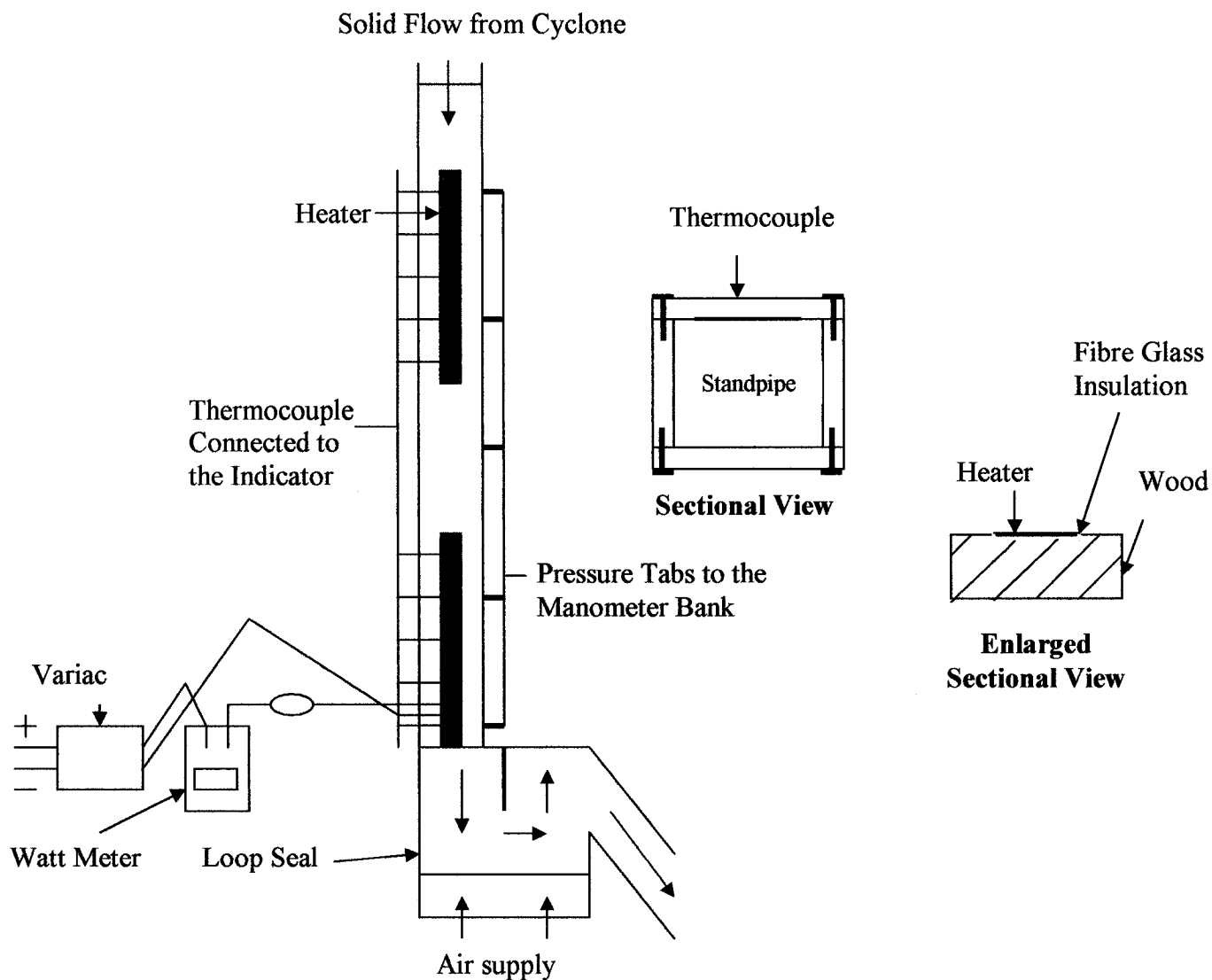


Figure 5.2. Schematic diagram of the experimental set-up

When the CFB units operates, solids collected in the cyclone and the bag filters flow down the standpipe (Figure 5.1), which in turn feeds it into the loop seal. The loop seal feeds the solids to the base of the riser. Thus, the solids move in an endless loop.

5.3. Experimental procedure and measurement techniques

The heat transfer coefficient was calculated by steady-state temperature measurement. At the start of each experiment, the solids valve (Figure 5.1) was kept open to allow solids to flow freely through the standpipe. Some solids begin building-up at the bottom of the standpipe (Figure 5.1). The loop seal draws the solids from its bottom and feeds them into the riser. A dynamic equilibrium is created in the standpipe when the solid flow rate into the standpipe (from the cyclone and baghouse) is equal to the solid withdrawal rate by the loop seal. Under this condition, a dense moving bed of solids is created in the standpipe with a dilute phase of raining solids above it. When the solid level in standpipe remained unchanged at a location between the two heating strips, the system was deemed to have reached a steady state or dynamic equilibrium condition. Once the temperatures at different measuring locations of the heated surface reach steady values, the local heat transfer coefficient between walls and the bed is determined according to the following relation:

$$h_i = \frac{\dot{Q}}{(T_{w_i} - T_b)} \quad (5.1)$$

where $\dot{Q} = \frac{E}{A}$ and A is the surface area of the heater on the stand pipe wall and T_b and T_{w_i} are the average suspension temperature and local wall temperature.

The electric heat input, E , can be calculated in two different ways:

- a) By reading the voltage from auto-transformer and current from the ammeter. The power consumed is determined by multiplying current with voltage.
- b) By reading the value of power consumption directly from the wattmeter.

For all experiments, both methods gave similar results. Therefore, the simpler method described in (b) was used to measure the heat flux of the heating surface.

The cross-sectional-averaged solids hold-ups in the dilute section of the standpipe can be inferred from the average pressure drop differential measured across the dilute section. The measured static pressure drop is equated to the bulk weight of the gas and solids in the standpipe sections, neglecting acceleration effects: i.e.,

$$\frac{\Delta P}{L} \cong [\rho_p (1 - \varepsilon_{avg}) + \rho_g \varepsilon_{avg}] g \quad (5.2)$$

where, ΔP = differential pressure in N/m^2 , L = height between measuring points in m, ρ_p = density of particle in kg/m^3 , ρ_g = density of gas in kg/m^3 and ε_{avg} is the voidage

In the dense section of the standpipe, particles move down slowly as a moving packed bed. The Ergun (1952) equation as modified by Basu and Cheng (2000) is used to estimate the average void concentration, ε_s of the dense section of the standpipe.

$$\frac{\Delta P}{L} = \frac{150(1 - \varepsilon_s)^2}{\varepsilon_s^3} \frac{\mu_g (\Delta u)}{(\phi_s d_p)^2} + \frac{1.75(1 - \varepsilon_s)}{\varepsilon_s^3} \frac{\rho_g (\Delta u)^2}{\phi_s d_p} \quad (5.3)$$

where Δu is the relative velocity of gas with respect to the solid

$$\Delta u = u_o + U_s$$

Here u_o is the upward velocity of gas and U_s is the downwards velocity of solids.

The superficial gas velocity in the loop seal was measured using a rotameter installed in the air line feeding the loop seal. This refers to air flow in the supply chamber of the loop

seal (Figure 5.1) divided by the cross sectional area of the standpipe. The actual velocity may be slightly lower due to some flow diversion into the recycle chamber.

The solids circulation rate was measured by a gate valve in the upper part of the standpipe, just below the cyclone and bag house. The solids circulation rate was calculated by measuring the time for a known volume of solids to accumulate on top of the gate valve after the valve was closed.

5.4. Model for heat transfer in the standpipe

A number of researchers (Knowlton, 1997; Basu and Fraser, 1991; Jones and Leung, 1985; Lehner and Wirth, 1999; Liu *et. al*, 1999) indicated that the standpipe is made of two hydrodynamic regions; a moving packed bed section and a dilute phase section. The latter region has the greatest concentration of solids near the wall.

In an extreme case of very low solids circulation rate, the dense-phase region may disappear, resulting in a whole dilute phase spread over the entire standpipe. In the other extreme case of very large circulation rate, the entire standpipe could be covered by the dense phase. Both extremes are undesirable for the smooth operation of a CFB boiler.

5.4.1. Predictive Model for Dense Section

The scenario of this section is similar to that of a moving packed bed. The instantaneous convective heat transfer coefficient h_i , can be calculated considering the solids and the interstitial gas as a single entity, sweeping over the heat transfer surface with a uniform velocity. This assumption is a modification of the widely used “packet” theory of Mickley and Firbanks (1955) and used by Denloye and Botterill (1977), Colakyan and Levenspiel (1984) and later by Liu *et. al* (1999). According to this theory, the heat

transfer takes place across two thermal resistances, shown by R_c and R_e . So, the heat transfer coefficient at a certain height h_i is:

$$h_i = \frac{1}{R_c + R_e} \quad (5.4)$$

where R_c is the contact resistance and defined as:

$$R_c = \frac{d_p}{\delta k_g} \quad (5.5)$$

where δ is non-dimensional gas layer thickness between the wall and moving solid which can be approximated by the expression given by Lints and Glicksman (1994)

$$\delta = 0.0282(1 - \varepsilon_s)^{-0.59} \quad (5.6)$$

and R_e is the thermal resistance of solids,

$$R_e = \sqrt{\frac{\pi L}{k_e \rho_e C_e U_s}} \quad (5.7)$$

where L is the height of the heat transferring surface

The average heat transfer coefficient, h , over the entire length can be approximated by

$$h = \frac{1}{R_c + \frac{1}{L} \int_0^L h_i dx} = \frac{1}{R_c + 0.5 \sqrt{\frac{\pi L}{k_e \rho_e C_e U_s}}} \quad (5.8)$$

The downwards solid velocity, U_s , can be approximated by using the following relationship:

$$U_s = \frac{G_s}{\rho_e} \quad (5.9)$$

where ρ_e is the bulk density of the dense phase in kg/m^3

The downward solids velocity can also be measured by setting a graduated ruler at the side transparent window of the standpipe and measuring the time taken for the particles to flow down. Both techniques assume solids to flow in plug flow.

The effective thermal conductivity of the solids emulsion, k_e , is the sum of two components k_e^0 and k_e^t reported by a number of researchers (Yagi and Kunii 1957; and Gelperin and Einstein 1971):

$$k_e = k_e^0 + k_e^t \quad (5.10)$$

where k_e^0 , is the conductivity of a fixed bed with motionless fluid which is given by Deissler and Boegli (1958) as:

$$\frac{k_e^0}{k_g} = \left(\frac{k_s}{k_g} \right)^{\left[0.28 - 0.757 \log_{10} \varepsilon - 0.057 \log_{10} \left(\frac{k_s}{k_g} \right) \right]} \quad (5.11)$$

where k_g and k_s are the thermal conductivity of gas and solids, respectively and ε is the voidage.

and k_e^t , the radial transfer of heat by turbulent diffusion is estimated by a slight modification on velocity term of the equation reported by Xavier and Davidson (1985):

$$k_e^t = 0.1 \rho_g C_g d_p (\Delta u) \quad (5.12)$$

where Δu is the relative velocity of gas with respect to the solid.

$$\Delta u = u_0 + U_s$$

The specific heat of the emulsion can be calculated as a lumped property instead of using an emulsion heat capacity (Breitholtz, and Leckner, 1997):

$$\rho_e C_e = (1 - \varepsilon_s) \rho_p C_p + \varepsilon_s \rho_g C_g \quad (5.13)$$

where ε_s is average voidage in the dense section.

So the overall heat transfer coefficient, h , can be expressed as:

$$h = \frac{1}{\frac{\delta d_p}{k_g} + 0.5 \sqrt{\frac{\pi L}{k_e \rho_e C_e U_s}}} \quad (5.14)$$

5.4.2. Predictive Model for Dilute Section

Lehner and Wirth (1999), Zhang *et. al.* (2001) reported that in a dilute phase the highest solids concentration is obtained in the vicinity of the wall. Even increased solids circulation rate does not change this shape of the radial solids concentration profile in a downflow CFB for a superficial gas velocity less than 2m/s. This flow pattern is very similar to the solids concentration distributions reported in the risers of up-flow CFBs. So, the model proposed by Basu and Nag (1987), Glicksman (1997) for the up-flow riser can be used to estimate the heat transfer coefficient in the dilute section of the standpipe. The overall heat transfer coefficient, h in the dilute phase is made up of the contributions of gas, h_g and solids h_p .

$$h = f h_p + (1 - f) h_g \quad (5.15)$$

where f is the fractional wall coverage by the solids.

Similar to the dense section, the dilute phase also has a contact resistance (R_w) due to the separation of the cluster from the wall by a thin gas layer and a resistance (R_{cl}) due to the transient heat conduction in the cluster. The exact expression for transient conduction from a semi-infinite body to a surface with a series resistance is complicated. However, experimental measurements (Gloski *et. al.*, 1984) have shown that a close approximation to the actual heat transfer coefficient from a cluster is given by assuming that these two mechanisms, the contact resistance and the transient conduction to a cluster of particles, act independently and in series with each other. Therefore, h_p which represents the particle convection component, can be expressed as:

$$h_p = \frac{1}{R_w + R_{cl}} \quad (5.16)$$

The expression for contact resistance due to gas layer is given as

$$R_w = \frac{\delta d_p}{k_g} \quad (5.17)$$

where δ is non-dimensional gas layer thickness between the wall and cluster which can be approximated by the expression given by Lints and Glicksman (1994) similar to the considering in dense section modeling.

$$\delta = 0.0282(1 - \varepsilon_{avg})^{-0.59} \quad (5.18)$$

The particle convection heat transfer coefficient, which is the combination of cluster and conduction gas gap heat transfer coefficients, is then expressed as:

$$h_p = \frac{1}{\frac{0.0282(1 - \varepsilon_{avg})^{-0.59} d_p}{k_g} + 0.5 \sqrt{\frac{\pi L}{k_c \rho_c C_c U_s}}} \quad (5.19)$$

The thermal conductivity of the cluster (k_c) is calculated from the equation provided by Gelperin and Einstein (1971) for packet heat transfer.

$$\frac{k_c}{k_g} = 1 + \frac{M}{N} \quad (5.20)$$

where M and N are given below.

$$M = (1 - \varepsilon_c) \left(1 - \frac{k_g}{k_s} \right)$$

$$N = \left(\frac{k_s}{k_g} \right) + 0.28 \varepsilon_c^{0.63} \left(\frac{k_g}{k_s} \right)^{0.18}$$

for particle diameter less than 0.5mm and $k_s/k_g < 5000$.

The specific heat of the cluster can be calculated as a lumped property instead of using an emulsion heat capacity (Breitholtz and Leckner 1997)

$$\rho_c c_c = (1 - \varepsilon_c) \rho_p c_s + \varepsilon_c \rho_g c_g \quad (5.21)$$

The cluster density can be estimated as;

$$\rho_c = (1 - \varepsilon_c) \rho_p + \varepsilon_c \rho_g \quad (5.22)$$

where ε_c is cluster voidage and is calculated from the equation provided by Lints and Glicksman (1994)

The effect of cross sectional average volumetric solid concentration on the cluster solid fraction is accounted for as follows:

$$\begin{aligned} \text{Cluster solid fraction } c_{sf} &= 1.23c^{0.54} \\ c_{sf} &= 1.23(1 - \varepsilon_{avg})^{0.54} \end{aligned} \quad (5.23)$$

where ε_{avg} is cross sectional bed average voidage. The cluster voidage ε_c is given by

$$\varepsilon_c = 1 - c_{sf} \quad (5.24)$$

Visual observation shows that, solids accumulated in the cyclone, generally fall through the dilute phase in the form of cluster or group of particles. One can approximate the falling velocity of cluster over the heat surface by the following equation:

$$U_s = \frac{G_s}{\rho_p(1 - \varepsilon_{avg})} \quad (5.25)$$

G_s is the solids mass flux as $\text{kg/m}^2\text{s}$.

The gas convection heat transfer from the bed to the wall of the riser is estimated by Wen Miller(1961) equation. However, as the velocity of gas in the dilute section of standpipe is very small, the Wen Miller equation significantly overpredicts the gas convection.

As an alternative, the present work plotted the measured overall heat transfer coefficient, which is the sum of gas convective and particle convective, against solids fraction in the dilute phase (Figure 5.10a) can be used. Since gas convection is the only component remaining when there are no solids, the plot of Figure 5.10a was extrapolated to 0.01%, which is approximately the solids concentration in the dispersed phase beyond the transport disengaging height. This value is a good first estimate of the gas convective component of the dilute phase in the standpipe.

The fraction of the wall covered by clusters is given by Lints and Glicksman (1994):

$$f = 3.5(1 - \varepsilon_{avg})^{0.37} \quad (5.26)$$

5.5. Results and discussion

This section presents results on hydrodynamic and heat transfer behavior of gas-solids on the wing walls. Experiments were carried out by two types of particles designated as 'A' (128 μm size and 700 kg/m^3 density) and 'B' (266 μm size and 2564 kg/m^3 density). The material properties and particle size distribution for both particle types are shown in Appendix B. The mean particle sieve diameter, d_p , was defined as:

$$d_p = \frac{1}{\sum \left(\frac{x_i}{d_{pi}} \right)} \quad (5.27)$$

The data of the experiments are shown in Appendix E. The following discussions are carried out by analyzing those data.

5.5.1. Hydrodynamics in the Dense Section:

Solids volume concentration of the dense section of the standpipe is calculated by Equation 5.3. This section is an expanded packed bed section. Figures 5.3a & 5.3b show solid concentration and suspension density profiles along the height of the standpipe. The solid concentration in this section is slightly higher for the fine particles 'A' than that for the coarse particles 'B'. However, the suspension density of particles 'A' is significantly lower than that for particles 'B'. In a fixed volume bed; fine particles would have more particles packed in than coarse particles would. This gives higher solids concentration with fine particles. The particle type B, is more than three times denser than the particle type A. Therefore B shows higher suspension density.

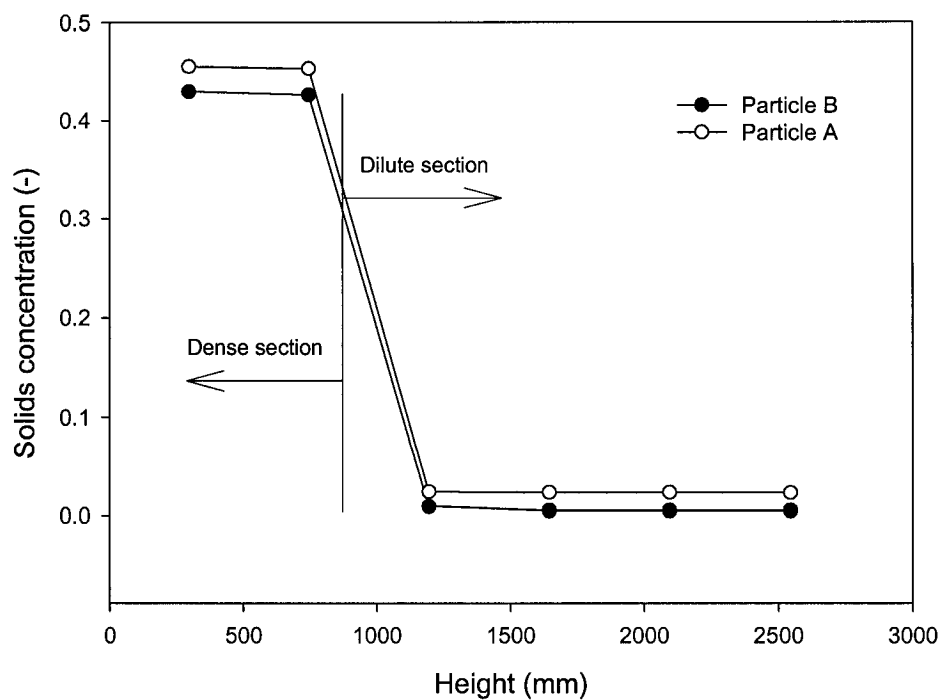


Figure 5.3a. Solids volume concentration profile measured along the standpipe
 $G_s=18 \text{ kg/m}^2 \cdot \text{s}$

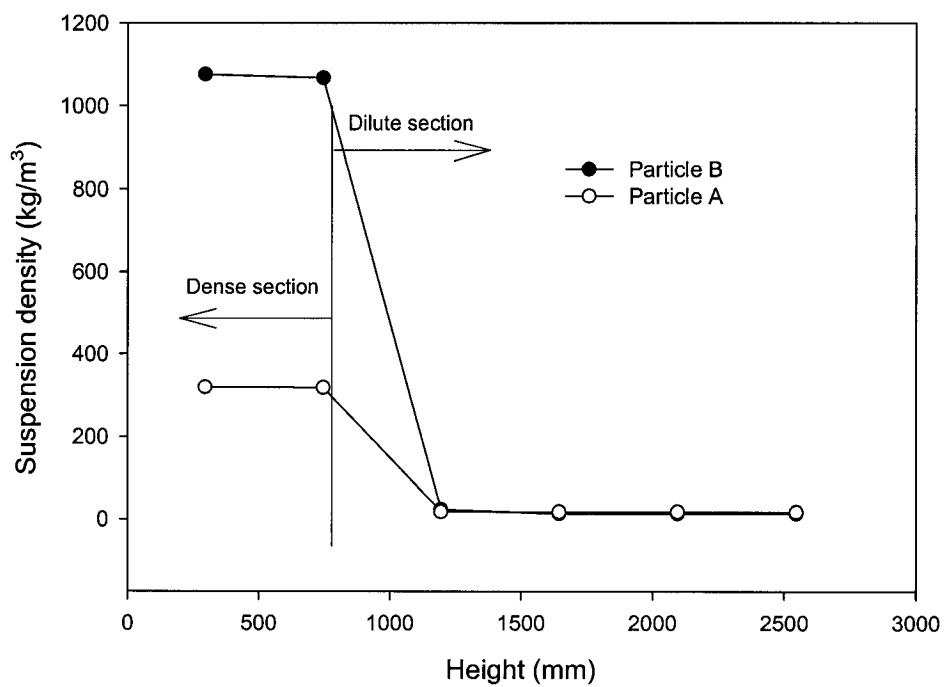


Figure 5.3b. Suspension density profile measured along the standpipe
 $G_s=18 \text{ kg/m}^2 \cdot \text{s}$

5.5.2. Hydrodynamics in the Dilute Section:

In case of dilute section, the observations on solids concentration and suspension density were found different from those made on the dense section. Fig. 5.3a shows that for a given circulation rate of $18 \text{ kg/m}^2\cdot\text{s}$, the solids concentration in the dilute section is higher in case of particles 'A' than that for particles 'B'. However, the suspension density in the dilute phase is similar for both types of particles as the contribution of higher concentration and lower particle density on suspension density are opposed to each other.

5.5.3. Heat Transfer in the Dense Section

Measured local heat transfer coefficients in the dense section of the stand pipe are shown in Figure 4a and 4b for both types of particles. Values are shown at different solid circulation rates. It is observed that the local heat transfer coefficient is higher at the top of the heating strip and it decreases gradually towards the bottom. This observation is similar to that observed on wing walls at the top of the riser of a circulating fluidized bed (Chapter 4). It is also observed that the local heat transfer coefficient increases with the solid circulation rate i.e. with the solid velocity down the pipe. This can be explained in the following fashion. The non-fluidized moving bed in a standpipe exhibits a plug flow (Jones and Leung 1985). Hence the local solids velocity is uniform and is equal to the mean solids velocity, despite the friction on the standpipe wall. At the top, relatively cold solids come in contact with the heated wall element, and then they get heated while traveling along the heated strip. This reduces the thermal driving force which is the temperature differential across the gas film. Due to the reduced thermal driving force, a lower heat transfer coefficient is calculated towards the bottom than at the top. However, it is also seen from the Figure 5.4a and 5.4b that heat transfer coefficients increase with the increase in solid circulation rate. The reason behind this is that the heat transfer coefficient also depends on the contact time between solids and the heated surface.

Higher circulation rates reduce the contact time and hence the heat transfer coefficient increases.

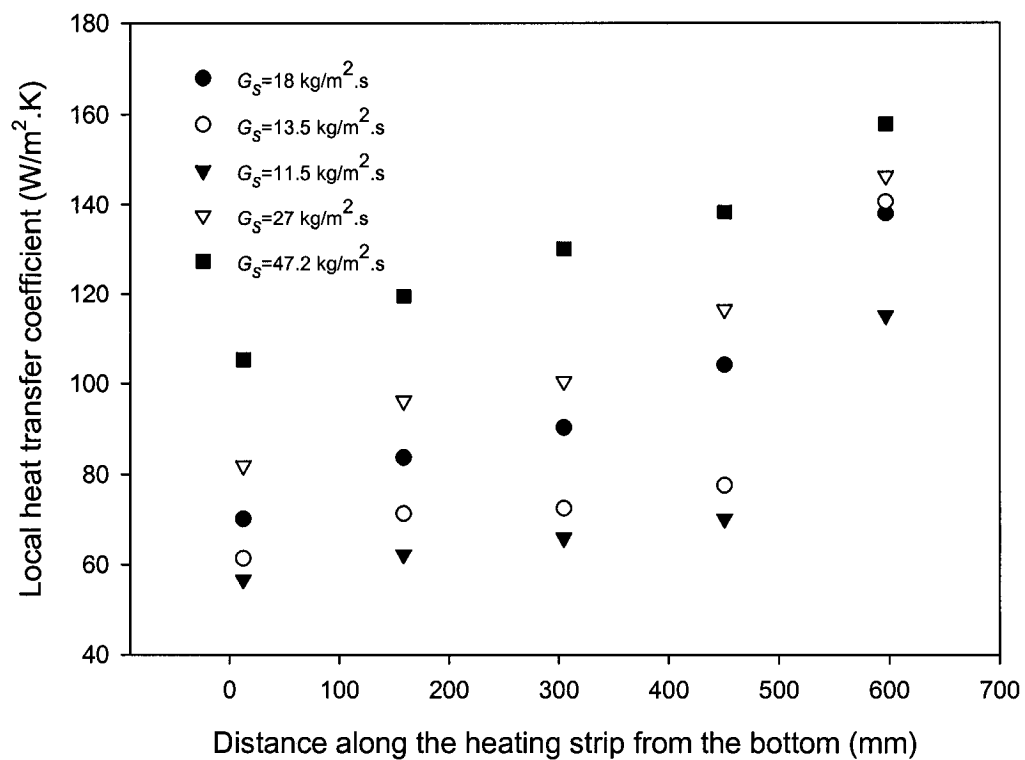


Figure 5.4a. Local heat transfer coefficients measured along the height of the dense section at different solids circulation rates (Particle B)

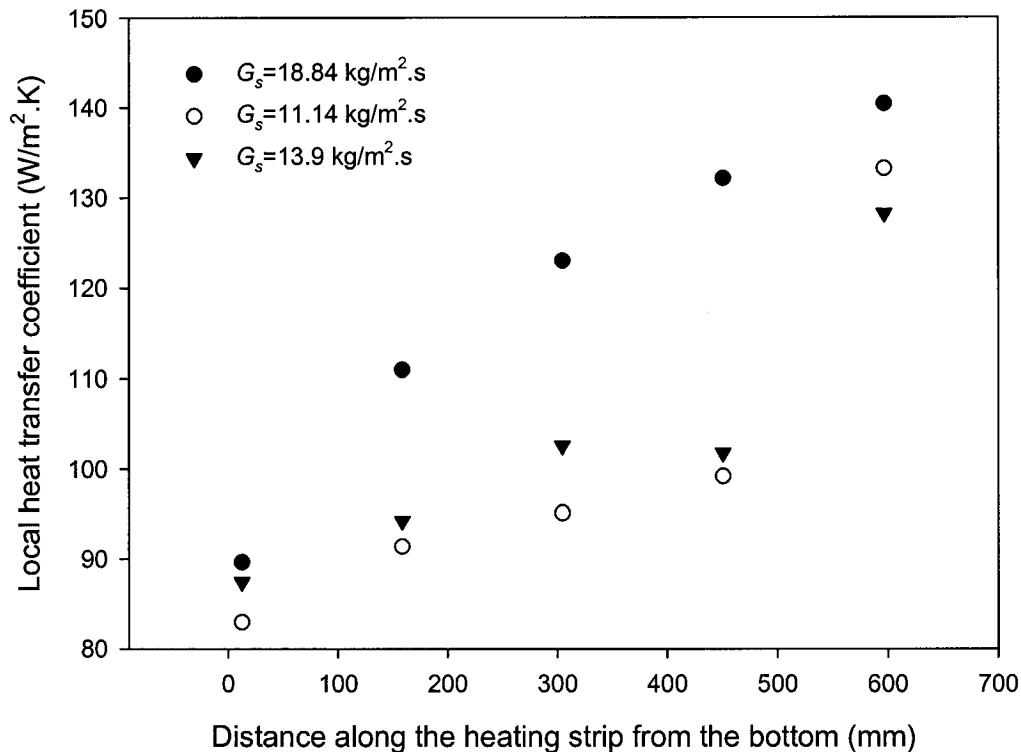


Figure 5.4b. Local heat transfer coefficients measured along the height of the dense section at different solids circulation rates (Particle A)

Figure 5.5 shows a comparison of local heat transfer coefficients measured for two types of particles for a constant circulation rate of $18 \text{ kg/m}^2.\text{s}$. As can be seen from the figure, the heat transfer coefficient is higher for finer particles. Finer particles have a larger contact surface area per unit volume which shorten the transfer paths between particle and the heat transfer area. Moreover, a higher downwards velocity of the finer particle 'A' at a constant solid circulation rate, reduces the contact time between the particles and the heated surface by a factor of approximately 3; $\left(\frac{\rho_B}{\rho_A} = 3.2\right)$ times. This results in a higher heat transfer coefficient of particles 'A', compared to particles 'B'. Figure 5.5 also shows

the predicted local heat transfer coefficient curve by using Equation 4. It agrees well with the experimental results.

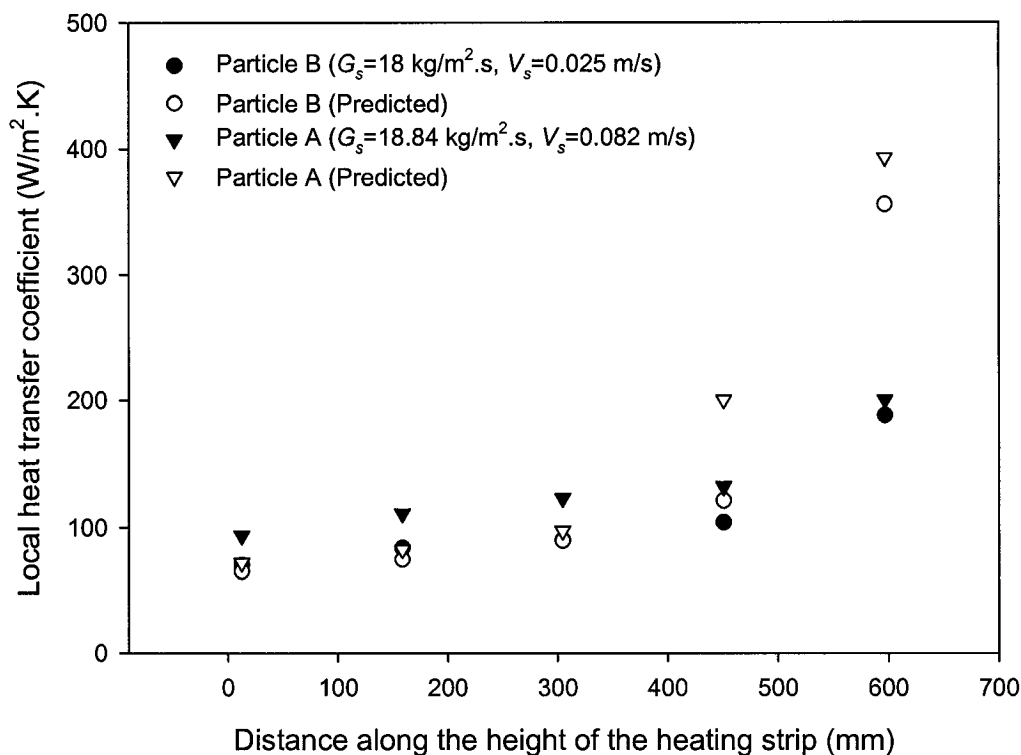


Figure 5.5. Comparison of local heat transfer for dense and light particles in the dense section. Predicted values are also shown for comparison

The results for the height average heat transfer coefficients measured for both types of particles in the dense section are shown in the Figure 5.6a and 5.6b. As we have seen in Figure 5.5, particles 'A' yields higher overall heat transfer coefficients for any circulation rate (Figure 5.6a). When the data is plotted against solids velocity, a different trend is noted. Figure 5.6b shows that for a constant solid downwards velocity particles 'B' has higher heat transfer coefficient than particles 'A'. Heat transfer coefficients between heated surface and solids depends on contact time, contact area and heat content of the particles. For a constant solid circulation rate of $18 \text{ kg/m}^2\cdot\text{s}$, lighter solids (particles 'A') would have higher solid velocity (0.082 m/s for particles 'A' and 0.025 m/s for particles

'B'). Hence particles 'A' would have a shorter contact time, resulting in a higher heat transfer coefficient. Also, the smaller particles have a large contact surface area per unit volume which shorten the transfer paths between particle and the heat transfer area. However, heat transfer also depends on the parameter (ρC_p) i.e., density of the particle. For a constant solid velocity, the heat content is higher for the denser particle and it results in higher heat transfer coefficient. The net effect would depend on which effect was stronger.

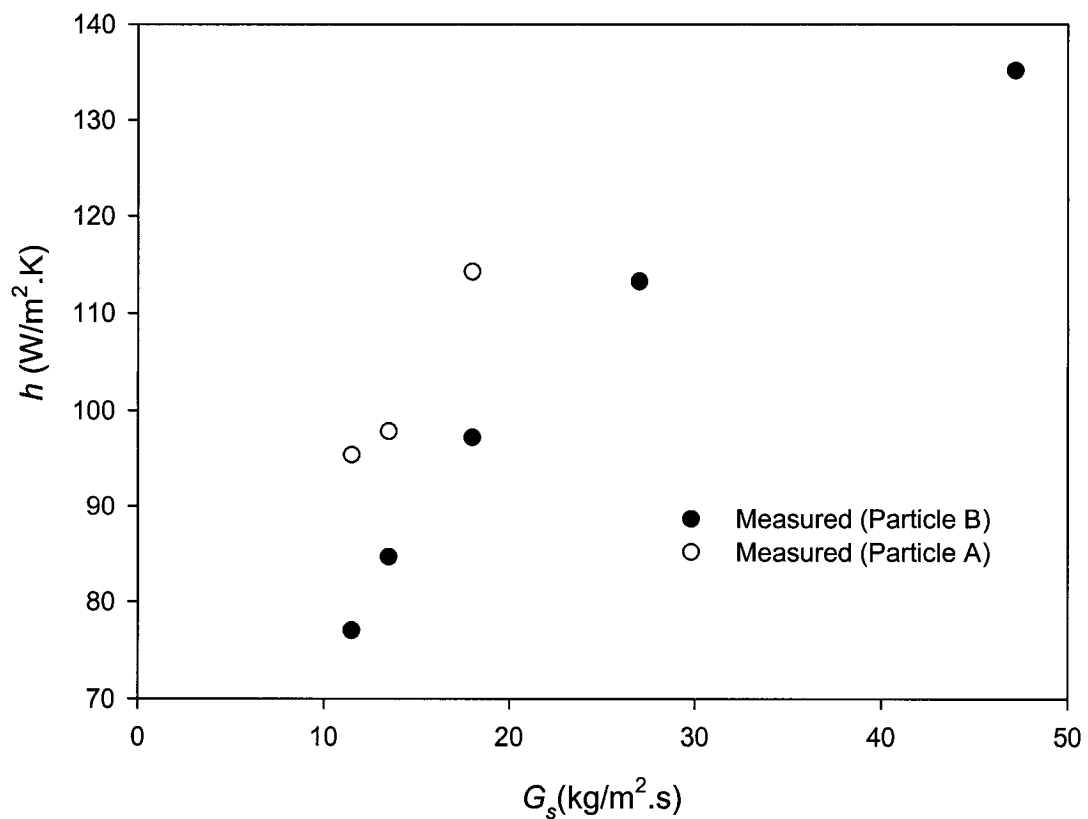


Figure 5.6a. Average heat transfer coefficients versus external solids circulation rates

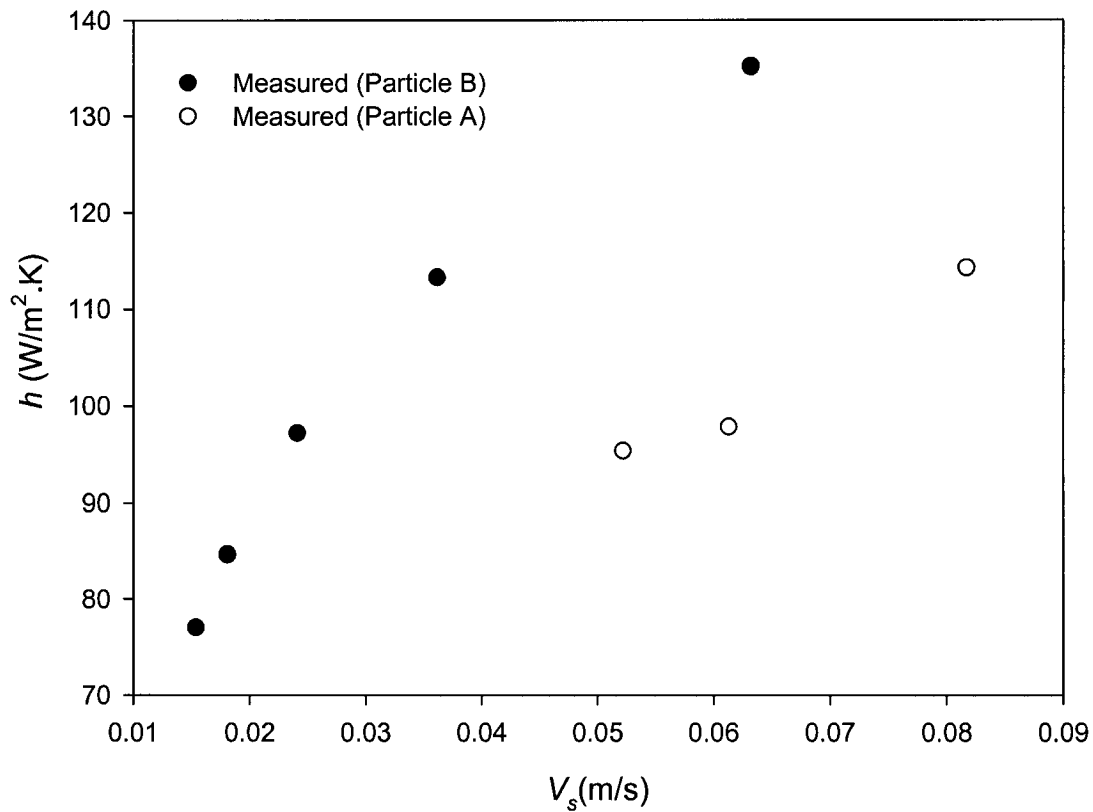


Figure 5.6b. Average heat transfer coefficient versus solids velocity

The experimental results for the height-average heat transfer coefficients are shown in Figure 5.7 together with values predicted by Equation 5.14. For the lower circulation rates, the ratio between measured and predicted heat transfer coefficient varies from 0.95 to 1.12 and decreases as the solid circulation rates increases. Increase in solid circulation rates results in an increase in gas-solid relative velocity in the standpipe, which causes a greater interaction between gas and solids. This interaction possibly causes a reduction in the solids volume concentration, resulting in a reduction in heat transfer. Similar observation is also reported by Liu *et al* (1999).

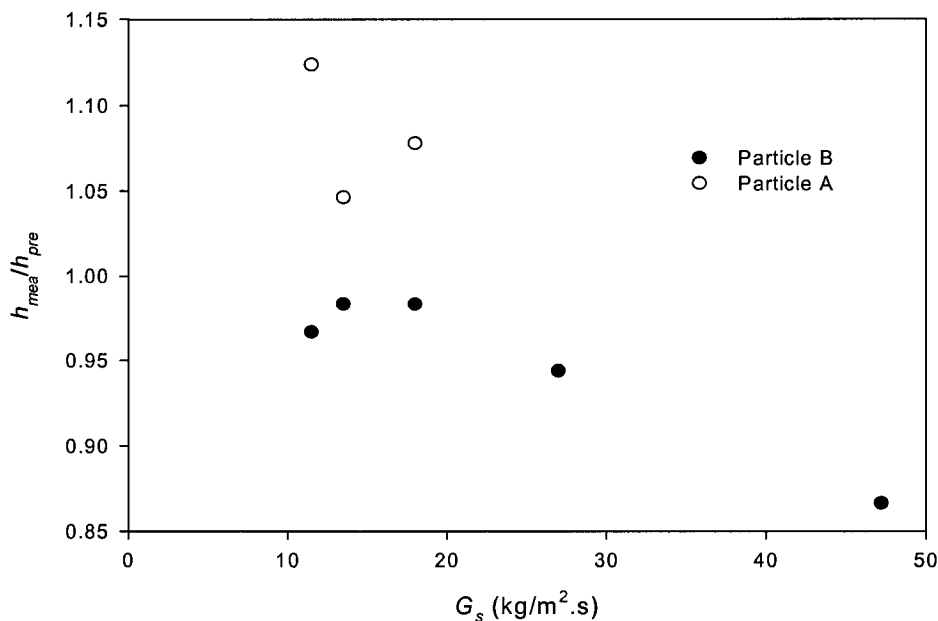


Figure 5.7 Ratio of measured and predicted heat transfer coefficients versus external solids circulation rates in dense bed.

5.5.4. Heat Transfer in the Dilute Section

Hydrodynamically the dilute section of the standpipe may be represented by a downflow CFB. The solids concentration profile of a downflow CFB is similar to the solids concentration distributions reported for the CFB risers (Lehner and Wirth, 1991; Zhang *et al.*, 2001). Figure 5.8a and 5.8b show local heat transfer coefficients measured along the height of the heating strip. Similar to the riser (Wu *et. al* 1987, 1989a), local heat transfer coefficient at the top of the heating strip is the highest and gradually decreases towards the bottom. For a constant circulation rate of 18 kg/m².s (Figure 5.9), particles ‘A’ exhibits higher, about twice the heat transfer coefficient, recorded for particles ‘B’. In the hydrodynamic section we have seen that, for a constant circulation rate, finer particles give lower voidage. Lower voidage and finer particle size, which give lower contact resistance, together yield higher heat transfer coefficient.

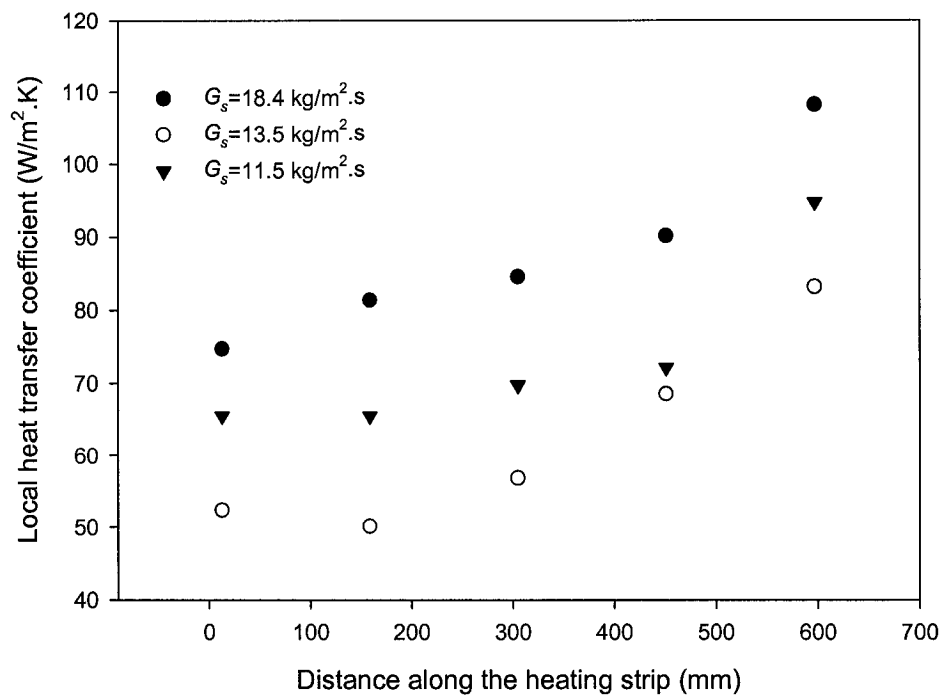


Figure 5.8a. Local heat transfer coefficients against height of the dilute section (Particle A)

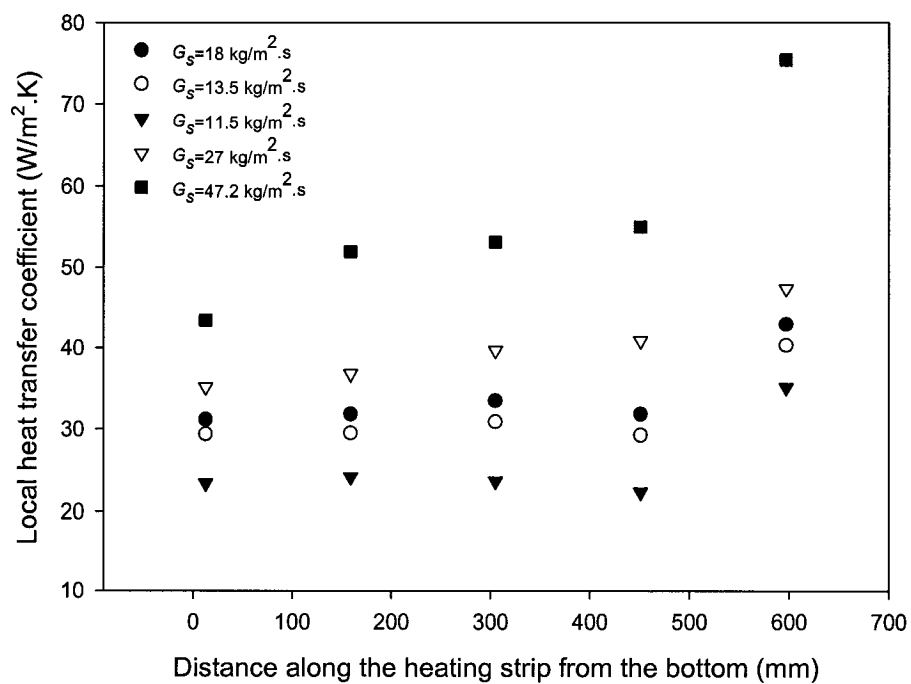


Figure 5.8b. Local heat transfer coefficients against height of the dilute section (Particle B)

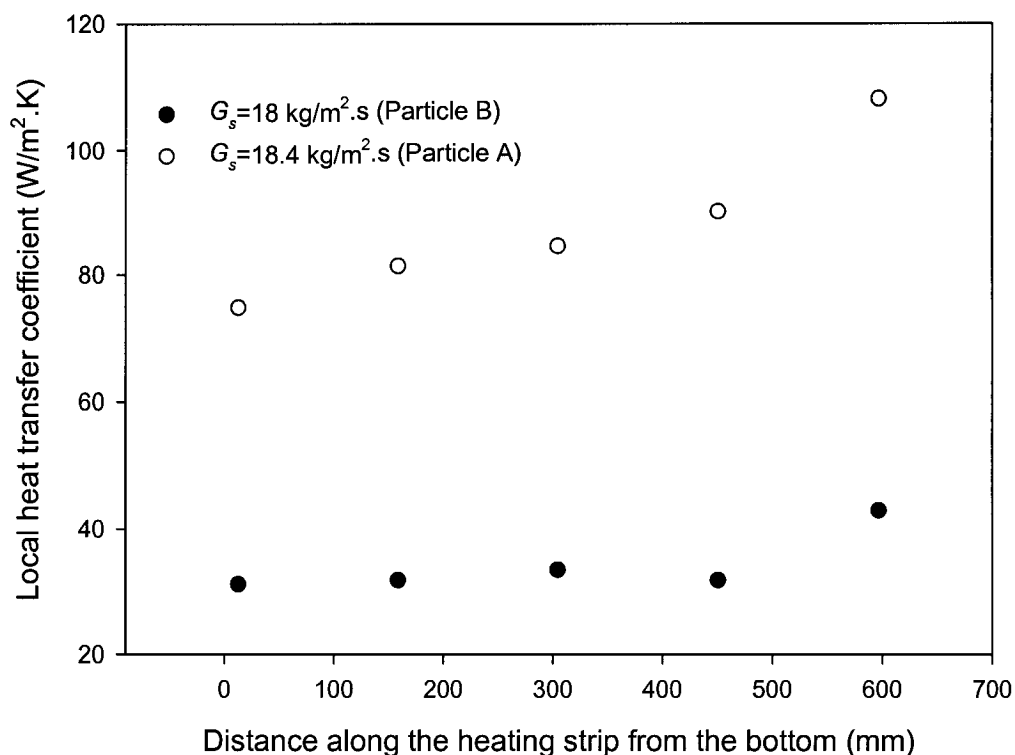


Figure 5.9. Comparison on local heat transfer coefficients in the dilute section for two types of particles

In the Figure 5.10a and 5.10b, the average heat transfer coefficient is plotted against the solid volume concentration and suspension density for both types of particles. It shows that the heat transfer coefficient increases with average solid concentration in the dilute section for both types of particles. The heat transfer coefficient is found proportional to the square root of the solid concentration. This observation is analogous to the observation reported for the riser (Basu and Nag, 1996; Glicksman, 1988; Ebert *et. al*, 1993). Similar observation is also reported for the downflow CFB at a gas velocity of less than 2 m/s (Liu *et al*, 1999). However the proportionality constant for the particles 'A' is higher which suggests that smaller particles have higher heat transfer coefficients than that of coarse ones. It is interesting to note that when plotted against solids volume concentration (Figure 5.10a) both particles fall on one line. Thus the heat transfer coefficient can be expressed by one equation.

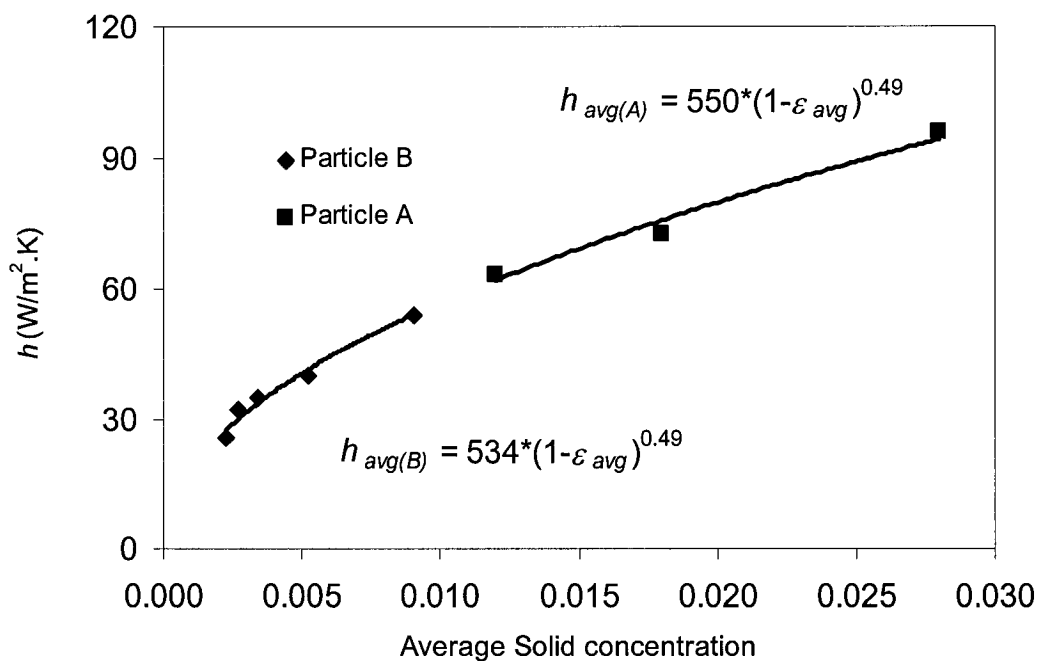


Figure 5.10a. Average heat transfer coefficients with average solids concentration at dilute section for both types of particles

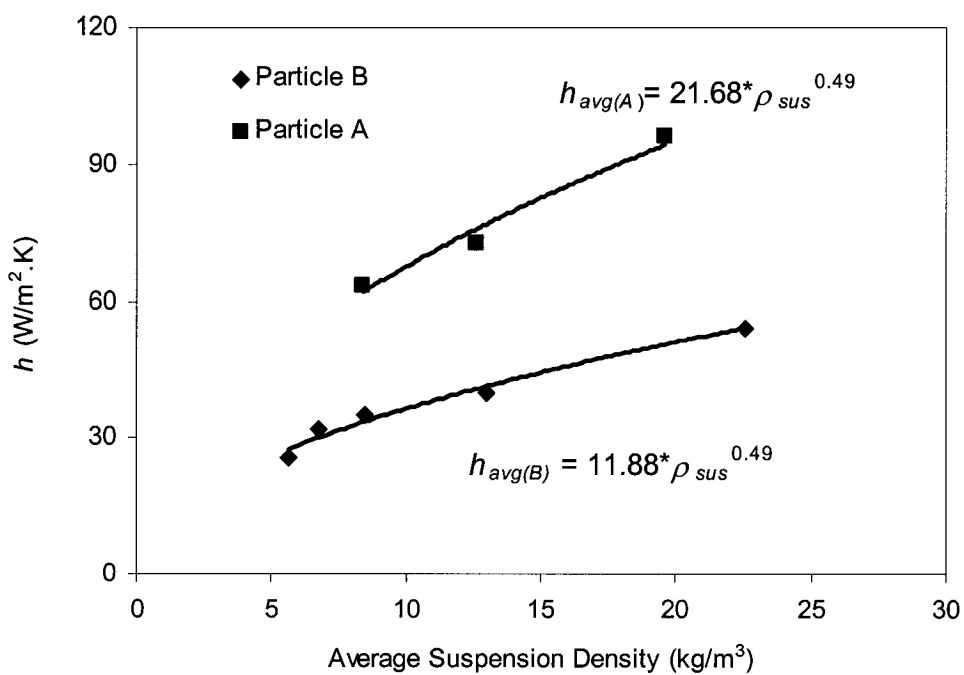


Figure 5.10b. Average heat transfer coefficients with average suspension density at dilute section for both types of particles.

Figure 5.11 shows both measured and predicted heat transfer coefficients against the external circulation rates. It is apparent that the predictive model agrees well with the measured data. For lower circulation rates, the model agrees well with the measured heat transfer coefficient. However, it overpredicts the heat transfer coefficient as the circulation rate increases. Accurate estimation of the wall coverage is required to predict an average heat transfer coefficient (Lints and Glicksman, 1994; Basu and Nag, 1987). Wall coverage is estimated by Equation 5.26 which was developed on the basis of experimental data achieved from a 20 cm diameter column (Lints and Glicksman, 1994). There is an influence of column diameter on wall coverage which is not included in the correlation and a larger diameter column would be prone to have higher coverage than the smaller one for a constant solid circulation because of lower (perimeter)/(cross sectional area) ratio. The discrepancy would be more as the cross section average solid fraction increases. The hydraulic diameter of our test section is 10 cm. Perhaps, this overpredicts the heat transfer coefficient as the solid circulation increases.

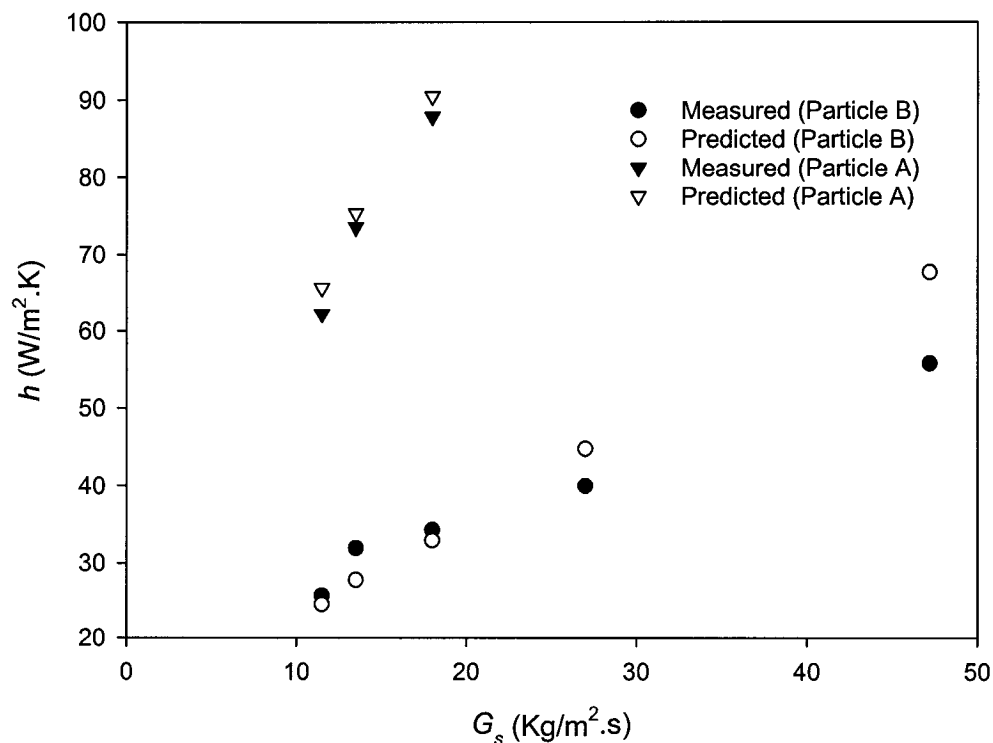


Figure 5.11. Predicted and measured heat transfer coefficients in the dilute section with external solids circulation rates

5.5.5. Comparison of Heat Transfer Between Dense and Dilute Section

It can be seen from the Figure 5.12 that for a given circulation rate the dense section always exhibits a local heat transfer coefficient higher than shown by the dilute section. It shows that the difference in local heat transfer coefficients between two types of particles is greater in the dilute section than that in the dense section. It also shows that the difference between dense and dilute section for particles 'A' is less than that of particles 'B'. For a more explicit discussion, the ratio of average heat transfer coefficient in dense section with that in the dilute section is plotted against the solid circulation rate in the Figure 5.13. For particles 'B', the ratio is found to be about 3 whereas for particles 'A', it is about 1.5. It also seen from Figure 5.13 that the ratio decreases with the increase of solid circulation, but scatter in the data is too large to draw a definite conclusion.

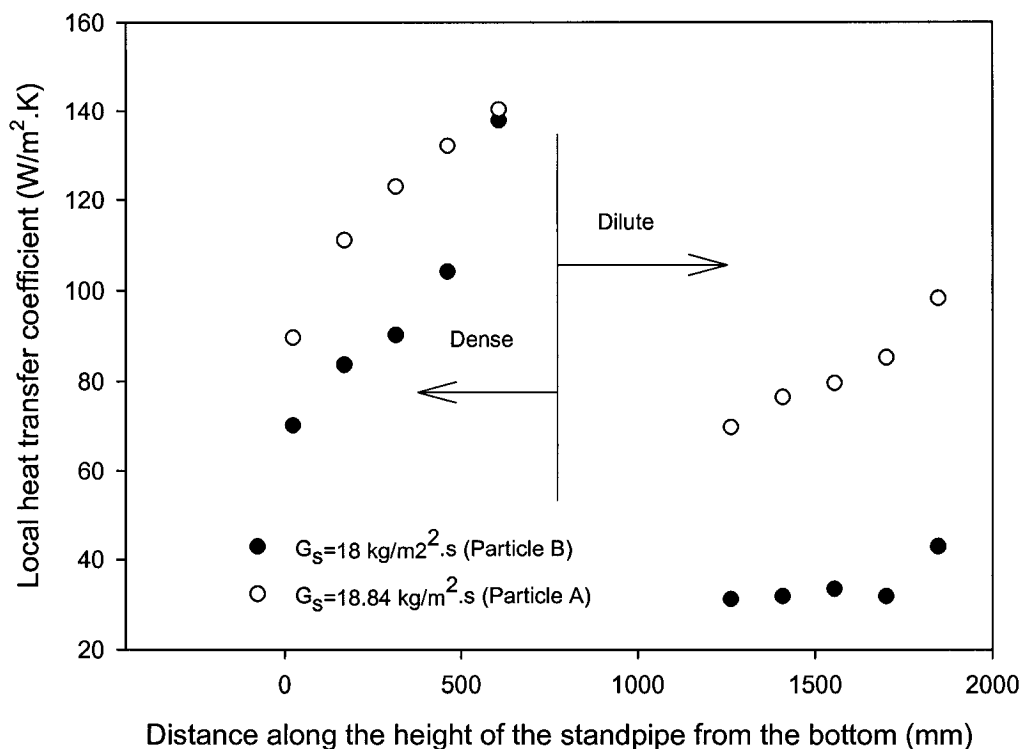


Figure 5.12. Comparison of heat transfer between dense and dilute sections for both types of particles

Wall coverage and thermal capacity are two important parameters in the heat transfer coefficients. Particle 'A' is finer and lighter. Predicted wall coverage of this particle in the dilute phase (0.7-0.9) is close to that in dense phase (Figure 5.14). Thus the difference between dense and dilute phase heat transfer coefficients is lower in particle 'A' (Figure 5.13). For dense particle 'B', the predicted wall coverage in dilute phase is very low (0.35-0.5). Thus the difference between dilute and dense phase heat transfer coefficient is much higher here.

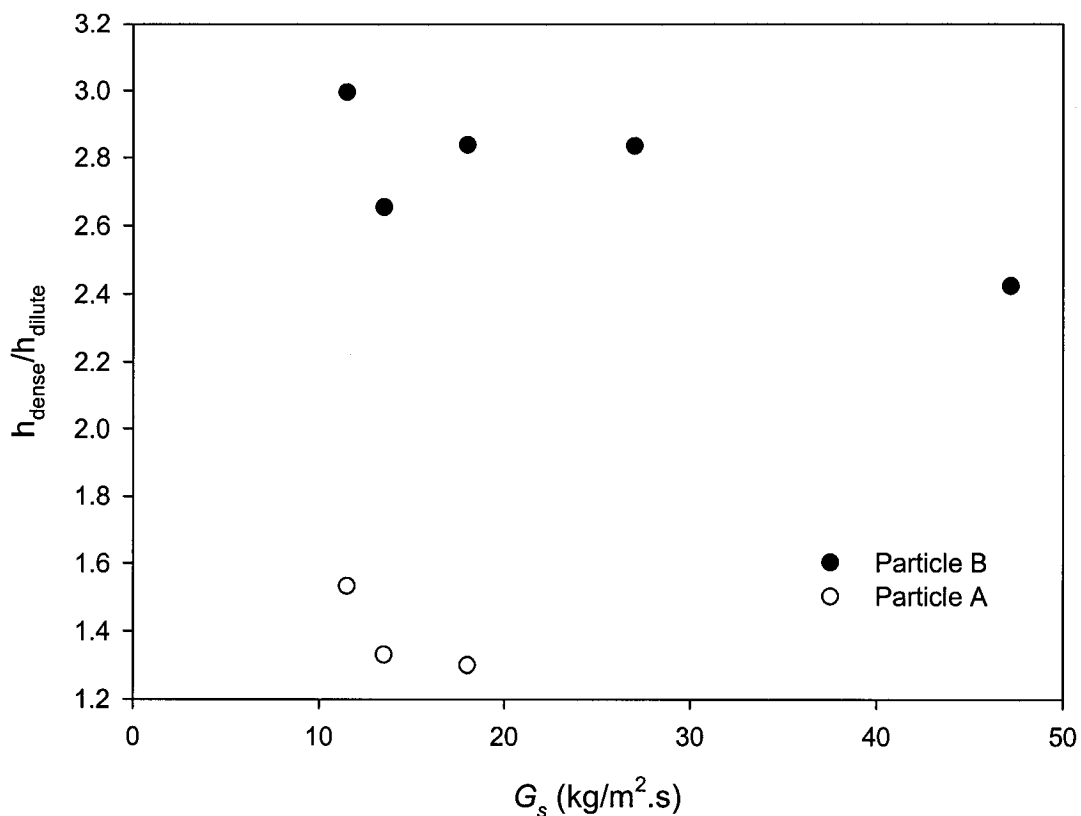


Figure 5.13. Ratio of average heat transfer coefficients in dense and dilute phase plotted against solids circulation rates

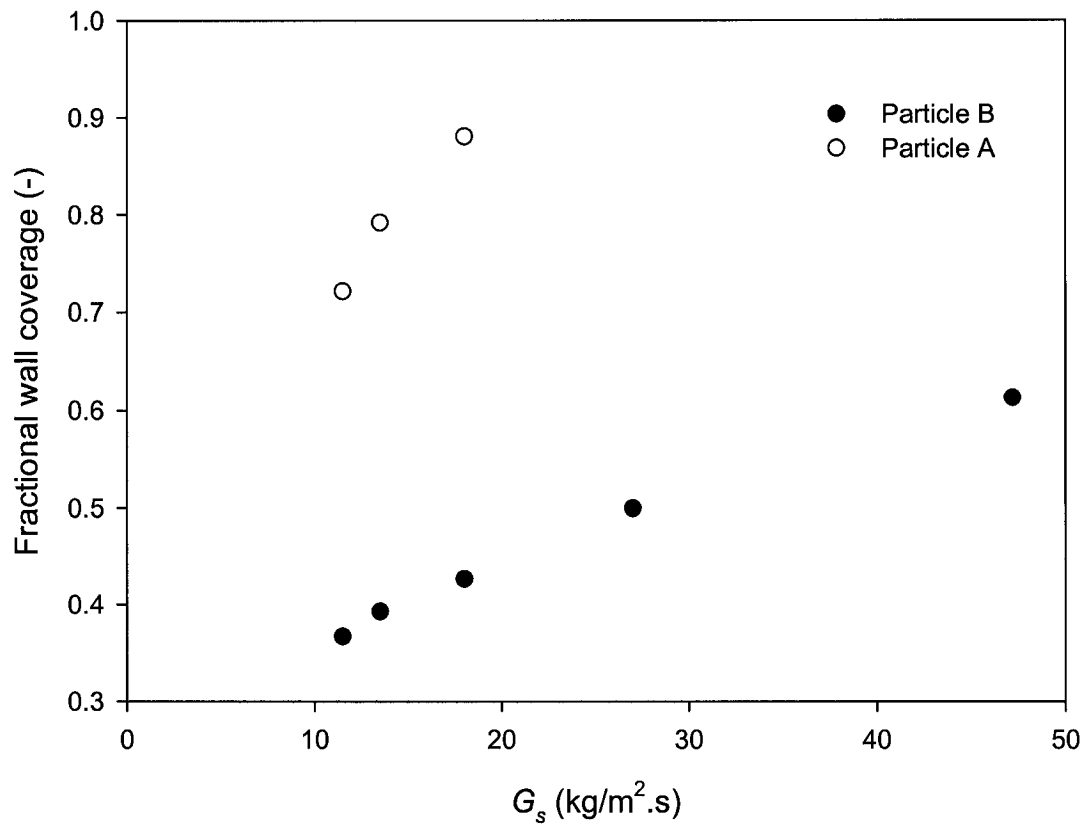


Figure 5.14. Predicted fraction wall coverage versus solids circulation rates

5.6. Concluding remarks

In this chapter, both experimental and theoretical analyses of heat transfer on the wall of a standpipe are presented. The experimental investigation was carried out in a circulating fluidized bed pilot plant operated with two types of solids (A and B) at room temperature. Within the range of operating parameters (superficial velocity 0.016 to 0.085 m/s and solid circulation rates of 9 to 47.2 kg/m²s) the following conclusions are drawn.

1. The standpipe may be divided into two hydrodynamic regimes: moving dense bed and downflowing dilute phase.
2. The hydrodynamic condition of the dense section resembles that of a downflow moving packed bed. The dilute section of the standpipe is similar to the downflow CFB (downer reactor) with a superficial gas velocity less than 2m/s.
3. Heat transfer coefficient in the dense section is higher than that in the dilute section under all conditions. The heat transfer coefficient increases with the solid circulation rate. For a given circulation rate, finer particles show higher heat transfer coefficients than the coarser ones. This is observed in both dilute and dense sections.
4. The local heat transfer coefficient in both dense and dilute sections decreases with distance down the pipe. The average heat transfer coefficient in the dilute section is proportional to the square root of average solid concentration.
5. Both local and average heat transfer coefficients are affected by the properties of solids, such as the particle size, specific heat, and thermal conductivity. The proposed model agrees well with the experimental values.

Chapter 6

Heat Transfer on Cavity-type Inertial Separators in a CFB boiler

This chapter presents experimental investigations on the hydrodynamics and heat transfer behavior of cavity-type inertial separators in a circulating fluidized bed. Three rows of cavity-type inertial separators were hung from the roof of a pilot plant where one row was kept inside the riser (simulating the furnace) and the other two rows were kept in the primary chamber, located between the back-pass and the riser. The pilot plant was operated at room temperature. Parameters measured were average suspension density and lateral solids flux in the riser, and axial solids flux and heat transfer coefficient on cavity-type inertial separators. It is shown that the presence of cavity-type inertial separators not only provides additional heat transfer surfaces but also indirectly increases the heat transfer coefficients on the riser wall.

6.1. Introductory remarks

Provision of required amounts of heating surfaces inside the furnace of a circulating fluidized bed (CFB) boiler is an important design issue especially in large capacity boilers. In large boilers, the enclosing wall, which constitutes the heat transfer surface, needs to be supplemented with additional heating surfaces in the form of wing walls, division walls, or external heat exchangers. However, all of these additional heat absorption surfaces are expensive and, additionally do not contribute to the collection of solids. An alternative design for additional heat transfer surfaces has been developed by Greenfield Research Inc. (Patent, 2001), which is less expensive than its alternatives and at the same time captures a significant amount of solids entrained from the CFB furnace,

obviating the need for expensive large cyclone. This type of separator different from conventional impact type separator is used in many boilers. Impact separators comprise steel beams, which are not cooled with nearly equal sides placed in the path of gas-solid flow.

The new system is, instead, a set of heat absorbing panels, which are arranged so as to form a deep cavity, i.e., depth of the cavity is greater than its width (Fig. 1.6). Such a cavity affects separation primarily by inertia; as opposed to impaction. It is therefore, called inertial-cavity separator. These vertical cavities are placed near the exit of the furnace. Solids exiting the furnace are trapped and separated in the arrays of cavities. Thus, a relatively clean gas flows to the convective section of the boiler. The bulk of the solids separated from the gas drop into the furnace. Besides acting as an efficient heat exchange surface, the cavity-type inertial separators also contribute to a reduction in the loop seal duty by separating solids within the furnace. It, therefore, comes in handy to the designer of CFB plants, making the design more compact and cost effective than conventional CFB boilers. The latter aspect of the cavity type separator is successfully demonstrated in a commercial CFB boiler using impact type U-beam separators in the furnace (Belin *et al*,1999).

The objective of the present work is to study the hydrodynamics and heat transfer behavior of the cavity type inertial separator and to have a quantitative assessment of heat transfer between the solids and both inner and outer walls of this cavity-type inertial separator. Furthermore, the effects of the presence of inertial-cavity type separators on cross sectional average suspension densities are studied.

6.2. Experimental Unit

Experiments were carried out using a 5-m tall closed-loop cold-model circulating fluidized bed riser of rectangular ($1\text{m} \times 0.5\text{m}$) cross-section operated at room temperature (Fig. 4.1). The details of the unit are presented in section 4.2 and Appendix A.

The gas-solids suspension leaving the riser enters the first or primary separation chamber ($1\text{m} \times 0.6\text{m} \times 0.5\text{m}$), in which the cavity-type inertial separators are installed. After this, the gas-solids mixture enters another novel type of gas-solids separation device located in the second separation chamber. This separation device is discussed in Saha, Dutta, and Basu, (2002) and Appendix A. Air leaving the secondary or second chamber enters a baghouse from where it is drawn into the suction of the fan. Solids collected in the standpipe are fed into the riser by a loop-seal through a 140 mm diameter clear acrylic inclined tube centered 700 mm above the distributor.

6.2.1. Experimental Set-up

The cavity type separators are placed inside the riser as well as in the primary chamber (Fig 6.1 and Appendix A). The exit area from the riser to the primary cyclone chamber is 1-m high and 0.5-m wide. The flow area between the primary chamber and the secondary chamber is 350 mm (high) \times 260 mm (wide). Three rows of cavity-type separators were hung from the roof, one inside the riser and the other two inside the primary chamber (Fig 6.1). The separators, shown in Fig. 6.2, were in staggered arrangement. They were held rigidly to the riser by making all the separators of a row as one assembly with a rod attached to the bottom of the back end of the separators and attached to the two side walls of the riser. The separators were 920 mm high, 250 mm deep and approximately 115 mm wide. The model of the separator was made of galvanized iron sheet, to avoid the static charge problem of LEXAN. Its surface was covered with heaters as needed.

Three flat heating surfaces were fabricated for simultaneous measurement of heat transfer on three different locations of the separators. Two of them were placed in the first row (inside the riser) and the other was placed in the second row of the separators as shown in Fig. 6.2. In the first row, one heating surface was placed covering the inner surface of one separator and the other covering the outer surface of another separator. This arrangement provided information on the heat transfer mechanism on both inside and outside surfaces of the 1st row and 2nd rows of separators.

Two sides of the separators were 920 mm long, 250 mm wide and 6.26 mm thick and had heaters placed on them at the locations shown in Fig. 6.2 (b & c). The heaters were flush with the top of the frame of the separator elements, which were made of galvanized iron sheet.

The flat heating panels were fabricated of 6.25mm thick low conductivity Tivar 1000 antistatic UHMW polyethylene. Fiberglass-insulated flexible silicon rubber heaters of low thermal conductivity were attached to the top of them. Grooves were made on the surfaces in such a way that when the heaters were mounted on the panels the heaters were flush with the surfaces. Double-sided insulating fiberglass tapes were applied between the heaters and the grooves on the Tivar surfaces. These heaters are thermally insulated by fibreglass on all four sides. The heaters were very thin (0.7 mm). Such heaters (thin and made of material with low thermal conductivity) are known to have a constant heat flux. All heaters were electrically connected in parallel with each other.

Two types of experiments were carried out. In the first case, the temperature distribution was measured over the heated surface by 15 thermocouples along the vertical height of the heating strip (609.6 mm) (Fig 6.2b). In the second case, the temperature distribution along the width (152.4 mm) of the heating strip was measured by 9 thermocouples (Fig 6.2c). Teflon coated T-Type thermocouples (0.3 mm thick) were attached to the heaters. These thermocouples have a resolution of 0.1°C and a response time of 0.3 second. Details of the thermocouples and their locations are shown in Fig. 6.2.

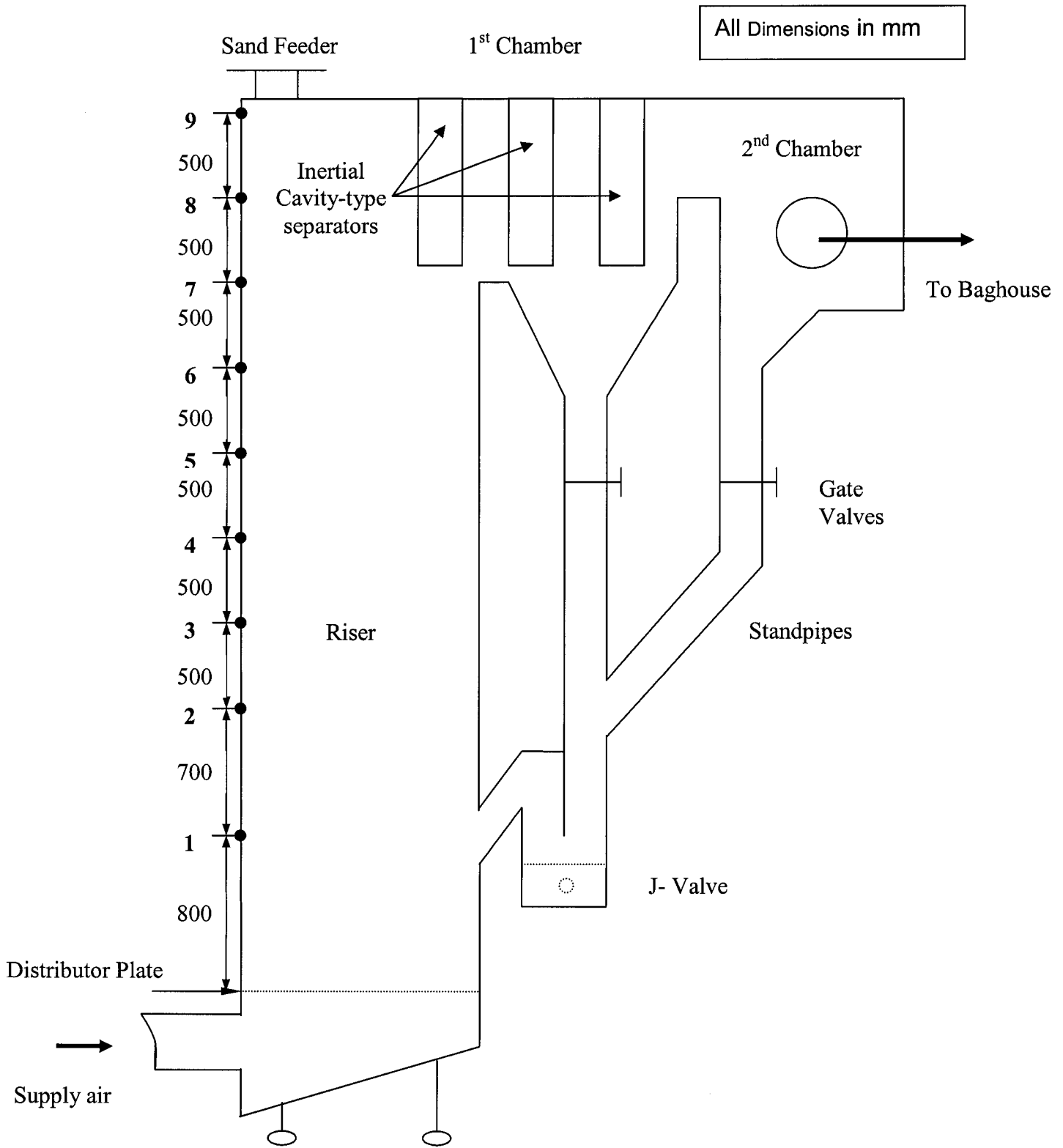


Figure 6.1 Schematic diagram of the experimental unit

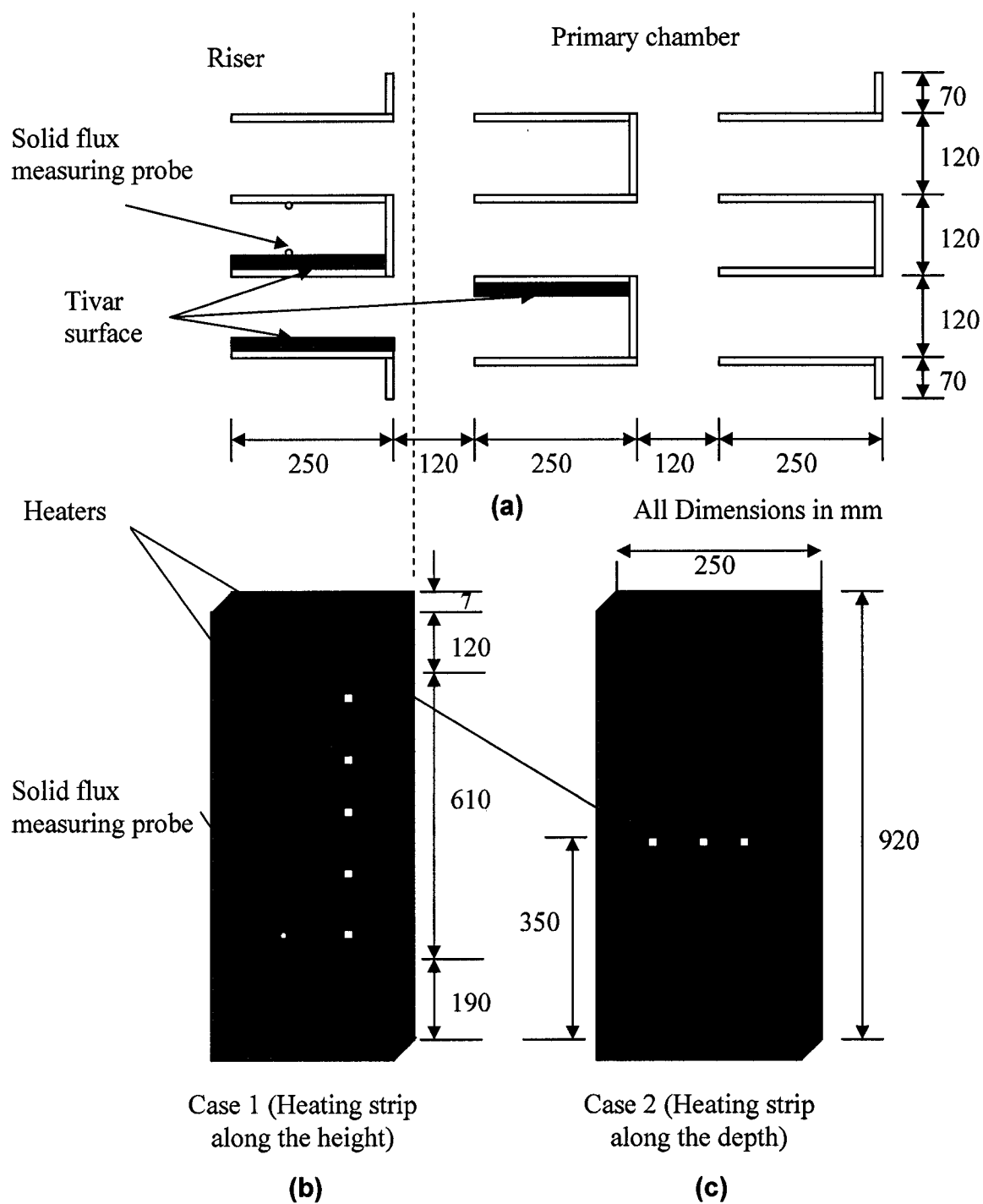


Figure 6.2 Details of experimental set-up of inertial separators:
 (a) arrangements of the separators
 (b) position of heating strip along height
 (c) position of the heating strip along depth

Two additional thermocouples were used to measure the gas-solids suspension temperature. Connecting leads for the thermocouples and the heaters were routed through the interior of the heating surface and the structure. This was done to keep the heating surface smooth. All wires were collected in one corner of the surface. From there, they were run through the front wall of the fluidized bed riser. The heaters were connected to a power source through a wattmeter and an autotransformer (variac). The heat flux of the heaters was controlled by the variac.

6.2.2. Solids Flux measuring system

Two probes were used to measure i) the axial solids flux inside the separator walls and ii) lateral solids flux in the riser

6.2.2.1. Axial solids flux measuring probe

Similar to that described in section 4.2, a non-isokinetic probe was used to measure the upward and downward solids flux inside the separator wall. They were located 120 mm from the edge of the separator entrance, 690 mm from the top of the roof. As per suggestion of Rhodes *et al.* (1988), the suction air velocity inside the probe was maintained between 4-7 m/s. The probes, as shown in Fig. 6.2a and Fig. 4.2, were 3.5 mm inside diameter with valves attached to the end of each probe to control the flow of solids.

6.2.2.2 Lateral solids flux probe

The schematic diagram of lateral solids flux probe is illustrated in the Fig. 6.3 which is essentially identical to that used by Zhou *et al.* (1995) and Jiang and Fan (1999). A 10-mm I.D stainless steel tube was introduced into the riser at an angle of 45° . The opening

face was cut vertically to ensure that only particles travelling laterally were captured. A small obstruction at the top of the opening prevented solids, that entered the tube, from bouncing back. As the outward lateral solids flux was measured alone, the probe was traversed between the entry port and the riser centerline. Purge air was supplied to the probe to maintain it free from solids before the actual measurement. No gas flow through the sampling tube was allowed during the sampling period. Lateral solids flux was obtained by measuring the sampling period and weighing the sampled particle.

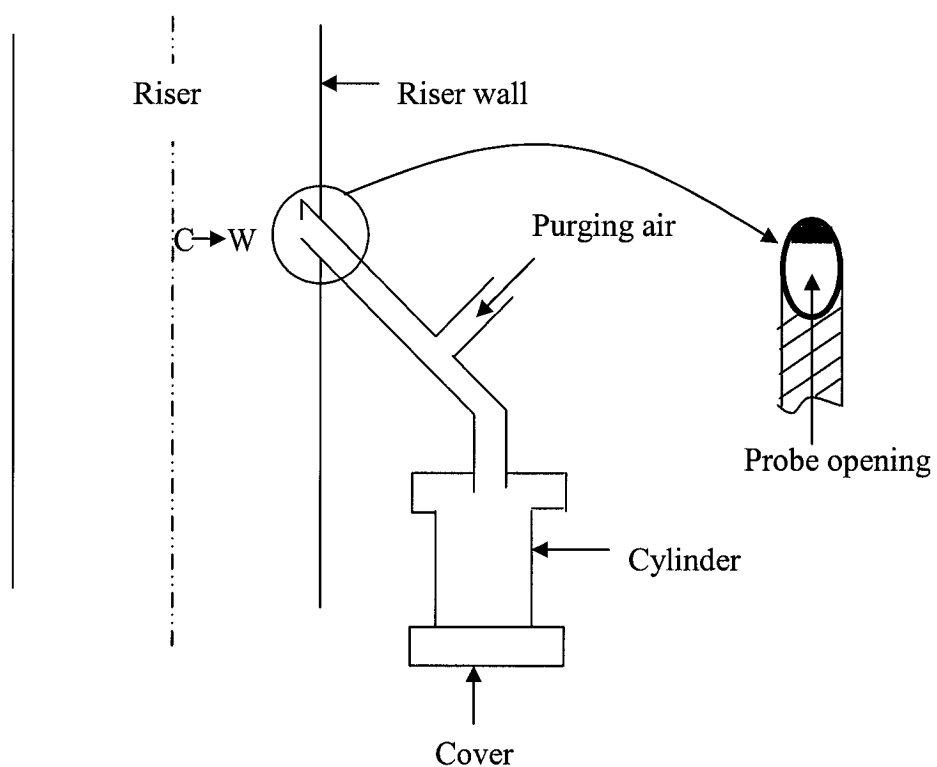


Figure 6.3 Schematic Diagram of the Lateral Solids Flux Measuring System (Core to Wall)

6.2.3. *Experimental Techniques:*

Techniques, applied for the experiments, were similar to those discussed in section (4.3). To conduct the experiments, heaters were placed in three different positions on the Tivar surface in two arrangements. They are referred as Case 1 (Fig. 6.2b) and Case 2 (Fig. 6.2c). The steady-state temperature measurements were carried out to calculate heat transfer coefficient. The gas-solids suspension was first allowed to flow over the heat transfer surface at a given velocity and then the power for the heater was switched on. Once the temperature of the surface reached a steady value, the local heat transfer coefficient between surfaces and the bed was determined according to the following formula:

$$h_x = \frac{\dot{Q}}{(T_{wx} - T_b)} \quad (6.1)$$

For each experiment, the solids valve in the standpipe was opened, allowing solids to flow into the riser. When the solids levels in both return legs remained unchanged, the system was deemed to have reached steady state condition.

6.2.4. *Bed Material:*

Nova Scotia sand of mean diameter 266 μm , particle density of 2584 kg/m^3 and bulk density of 1321 kg/m^3 was used as bed material. Details are presented in Appendix B.

6.3. Results and Discussion:

This section presents results on hydrodynamic and heat transfer behavior of gas-solids on the cavity-type inertial separators in the riser. The data of the experiments are shown in Appendix F. The following discussions are carried out by analyzing those data.

6.3.1: Gas solids suspension flow

This section discusses the effect of the presence of cavity-type inertial separator on the suspension density and lateral solids flux distribution on the riser. The results of hydrodynamics of gas solids suspensions in and around cavity-type inertial separators are also discussed.

6.3.1.1 Suspension densities:

Figures 6.4a and 6.4b show vertical profiles of the apparent suspension density, as determined from the axial pressure gradient, at superficial air velocities, 3.5 m/s and 4.4 m/s, and solids circulation rates 3 kg/m².s and 5.7 kg/m².s respectively. First set of experiments were carried out without the presence of the inertial separators inside the riser. The second set was with the separators in the riser. In both sets, an exponential profile or a profile with a dense bottom zone and an upper dilute region can be seen depending on the adjusted operating conditions.

A higher solids concentration i.e. suspension density is seen along the riser column when the inertial separators are present. Inertial suspended surfaces contribute to a greater solids hold-up along the riser column. One of the reasons is that solids collected in the separators cavity lose their momentum and fall down to the riser rather than flowing out of the riser to the primary cyclone. Solids form a thicker boundary layer along the height of the inertial surfaces.

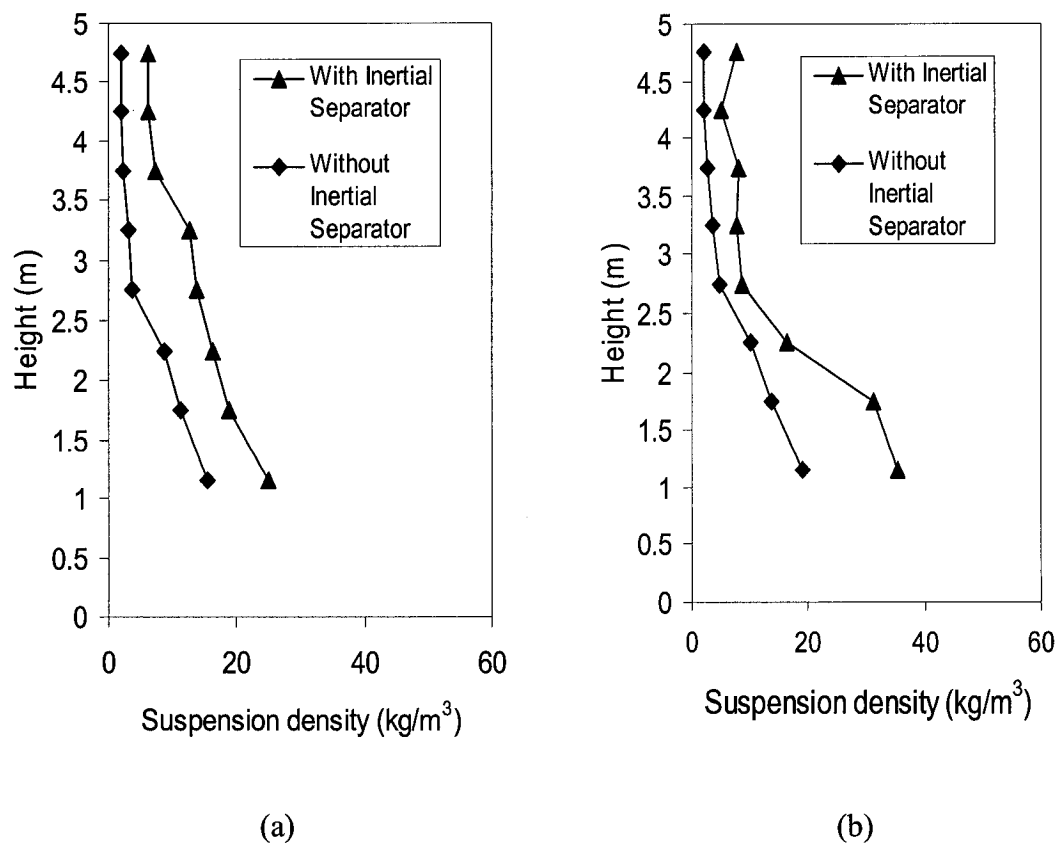


Fig 6.4: Suspension density profile along the riser column.

(a) $V_s = 3.6$ m/s and $G_s = 3$ kg/m².s, b) $V_s = 4.4$ m/s and $G_s = 5.7$ kg/m².s

At higher solid circulation rate and higher superficial velocity, the aforementioned effect is even greater. It is shown that suspension density increases in this section with height. It is because many particles which hit the inclined surfaces and the top of the inertial surfaces tend to rebound and, therefore, the particle concentration near the exit becomes high. The region of influence is further extended due to the corners in the rectangular column. Corners can shelter particles rebounding from the suspended surfaces because downward moving particles from the corners are more difficult to strip than those travelling downwards when the surface is smooth. Particles in the corner region moving downwards have been visually observed just as has been experienced by Zhou *et. al* (1994).

6.3.1.2 Lateral solids flux distributions:

The variations in the lateral solids flux were examined in the upper dilute region of the riser 1.3 m from the top and at the middle of the front face. The experiments were conducted at the same superficial velocity and solid circulation rate mentioned above. Only outward solids fluxes were measured with suspended surfaces hanging from the top of the riser.

When there are no separators, the lateral fluxes are low at the central dilute region, gradually increasing towards the wall (Fig 6.5a). This trend was observed for both operating conditions, but it is in contradiction to the measurements of Jiang and Fan (1999), who reported a gradually increasing solids flux towards the wall, reaching a maximum, and then decreasing. The reported (Jiang and Fan) non-dimensional value near to the wall was 0.9, which still shows an increase in lateral outward solids flux near the wall. However, the trend of the present investigation agrees with the measurements of Qi and Farag (1993), who reported a monotonic increasing trend along the radial direction towards the wall. Their reported non-dimensional value near to the wall was 0.97, which was the same as in the present study. The value of lateral flux for either operating condition does not exceed the respective solid circulation rate.

Figure 6.5b shows the comparison of non-dimensional lateral solids mass fluxes investigated by the above two researchers with the present investigation. An increase in non-dimensional lateral fluxes towards the riser wall is observed for all the cases. Because of the wider variety of operating conditions and particles used, it is difficult to make a definite conclusion on those data. However, it could be seen that for a larger diameter riser, values are higher from a non dimensional position of 0 to 0.75. This could be explained by the core-annular structure in the riser. As the diameter increases, ratio of perimeter/cross-sectional area decreases and one could have a higher lateral solids flux towards the wall.

Fig 6.5a shows an interesting phenomenon for the suspended inertial cavity type separator in the riser. At some points, the flux shows local peak values. This can be explained by the core-annulus theory. In the suspension density profile, a higher solids concentration was observed in the upper zone. It is expected that additional boundary layers are formed along the wall of the inertial separators. Each U-beam separator might act as a small CFB riser with a core-annulus structure. The higher peak points are just below the wall of the U-beam separators. Further research is needed to establish this fact. In summary, it can be concluded from the present work that the lateral flux may also depend on parameters like the suspended surfaces in the riser, riser geometry and operating conditions.

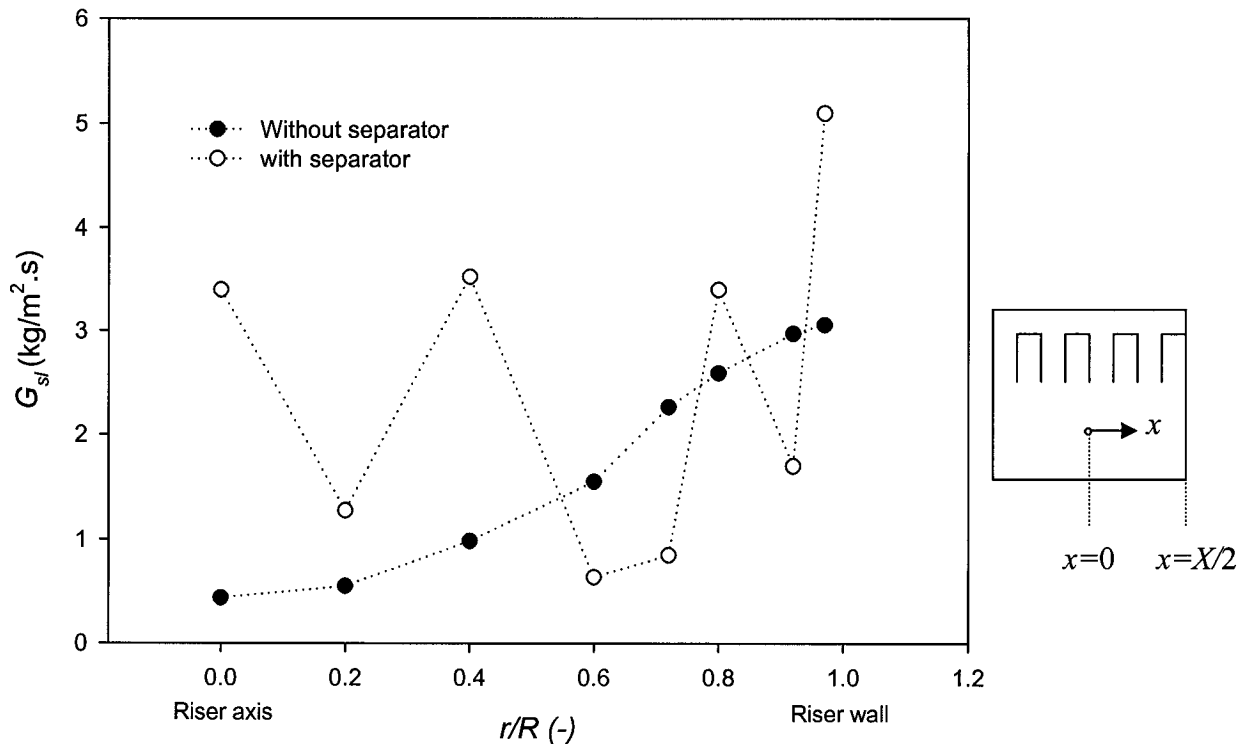


Figure 6.5a. Lateral outward solids mass fluxes ($V_s=4.4$ m/s and $G_s=5.7$ kg/m².s)

- Qi and Faraq, 1993 (14 cm dia, $V_s=3.9$ m/s and $G_s=21.3$ kg/m².s, glass beads, 200 mm, 2500 kg/m³)
- Jiang and Fan, 1999 (10 cm dia, solids concentration 0.48%, FCC, 87 mm, 1500 kg/m³)
- ▼ This work (67 cm hydraulic dia, $V_s=4.4$ m/s and $G_s=5.7$ kg/m².s, sand, 266 mm, 2600 kg/m³)

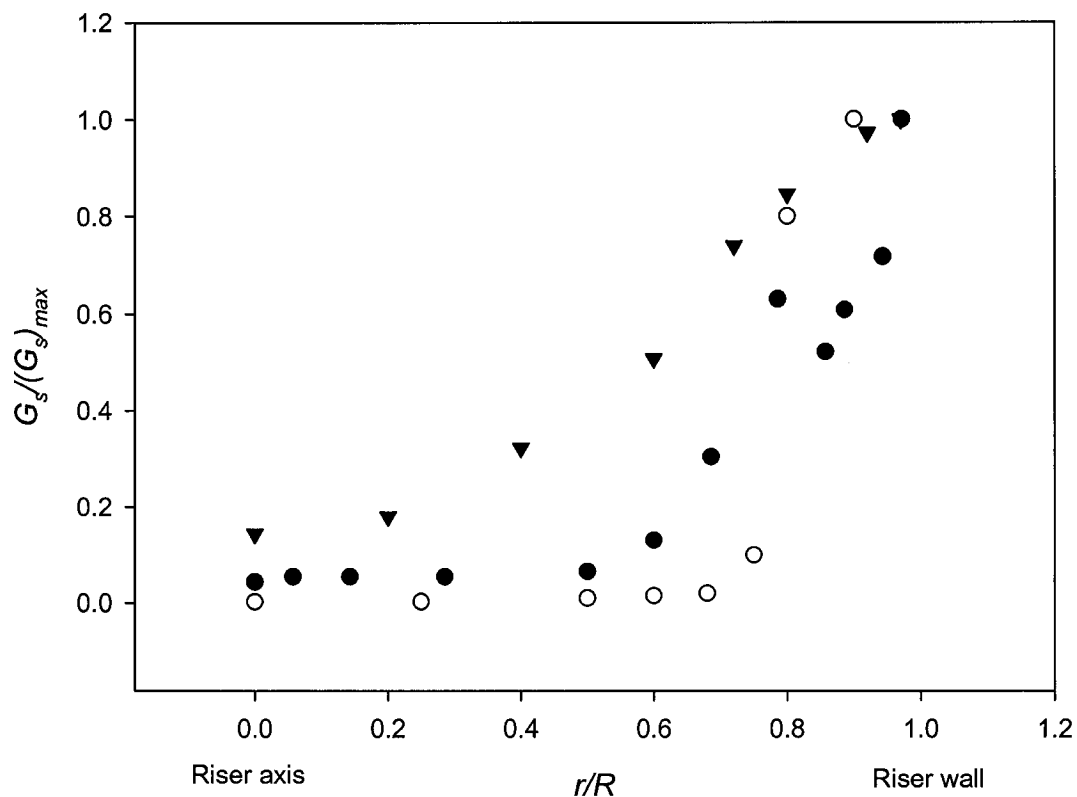


Figure 6.5b. Comparison of non-dimensional lateral core to wall solids mass flux for different riser diameters

6.3.1.4. Axial solids flux in the 1st row of the separator (in the riser)

Both downward and upward solids fluxes were measured at different operating conditions on the inside surface of one of the inertial separators (Fig 6.2a). The solids flux probe was located 230 mm away from the bottom and 120 mm from the front of that separator (Fig: 6.2b). No upwards solids flux was observed at the surface. Only a downward solids flux was observed at all operating conditions (Fig. 6.6). Observations showed that the downward solids fluxes increased with the increase of external solids circulation rate.

The increase was steady up to $3 \text{ kg/m}^2\cdot\text{s}$ and then tapered off. An effort was made to detect the downwards solids flux on the outside of that separator. However, no downward solids fluxes were observed.

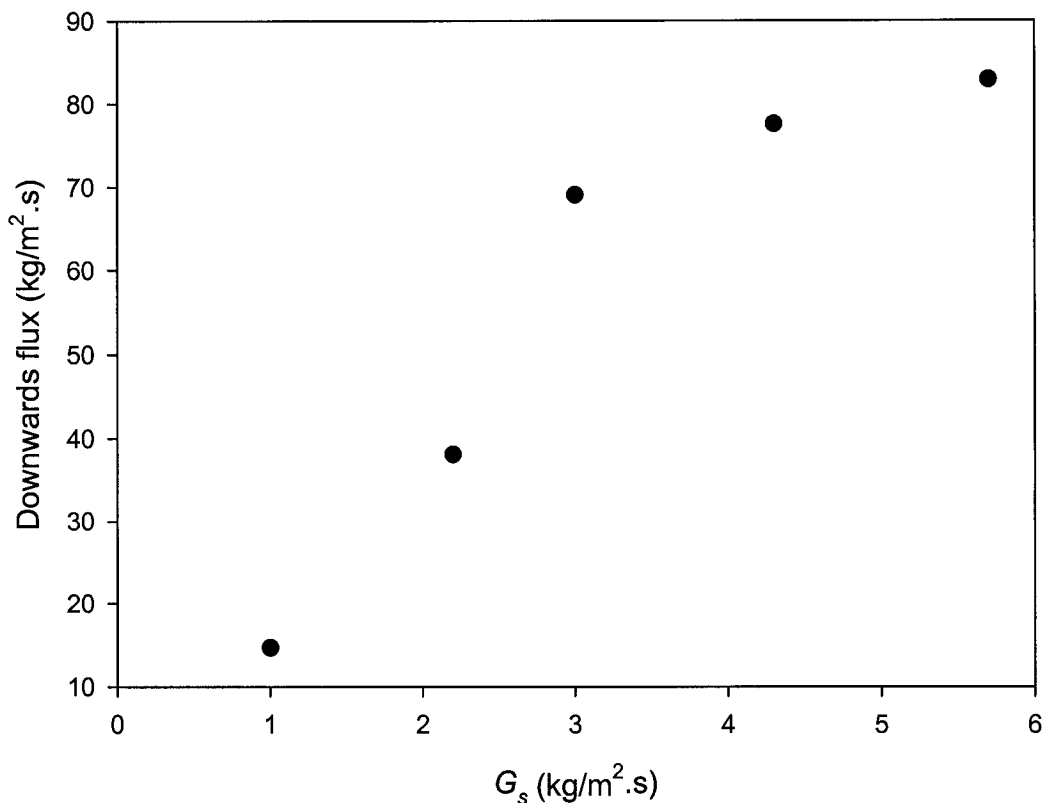


Figure 6.6. Downwards solids flux with solids circulation rates on the inner walls of the separator in the 1st row

6.3.1.5. Solids collection in the 2nd row of the separator (in the primary chamber)

The configuration of the experimental set-up did not allow to measure the solids flux on the surface of separators placed in the second row; however, it allowed to measure the collection efficiency in the primary chamber (Fig. 6.1). Two staggered rows of separators were placed in the primary chamber as shown in Fig. 6.2a. The path of the gas solids

suspension was observed to be nearly horizontal. However, since the exit to the secondary chamber is in the upper half of the rear wall, some diagonal flow may be expected. Also, a stagnant zone may be created at the bottom of the rear wall of the separator due to the gas exiting from the upper section of this wall. When the superficial velocity was varied from 3.6 to 4.4 m/s, the overall collection efficiency of solids, varied from 75 to 81 % based on the external solids circulation rate. (Fig: 6.7).

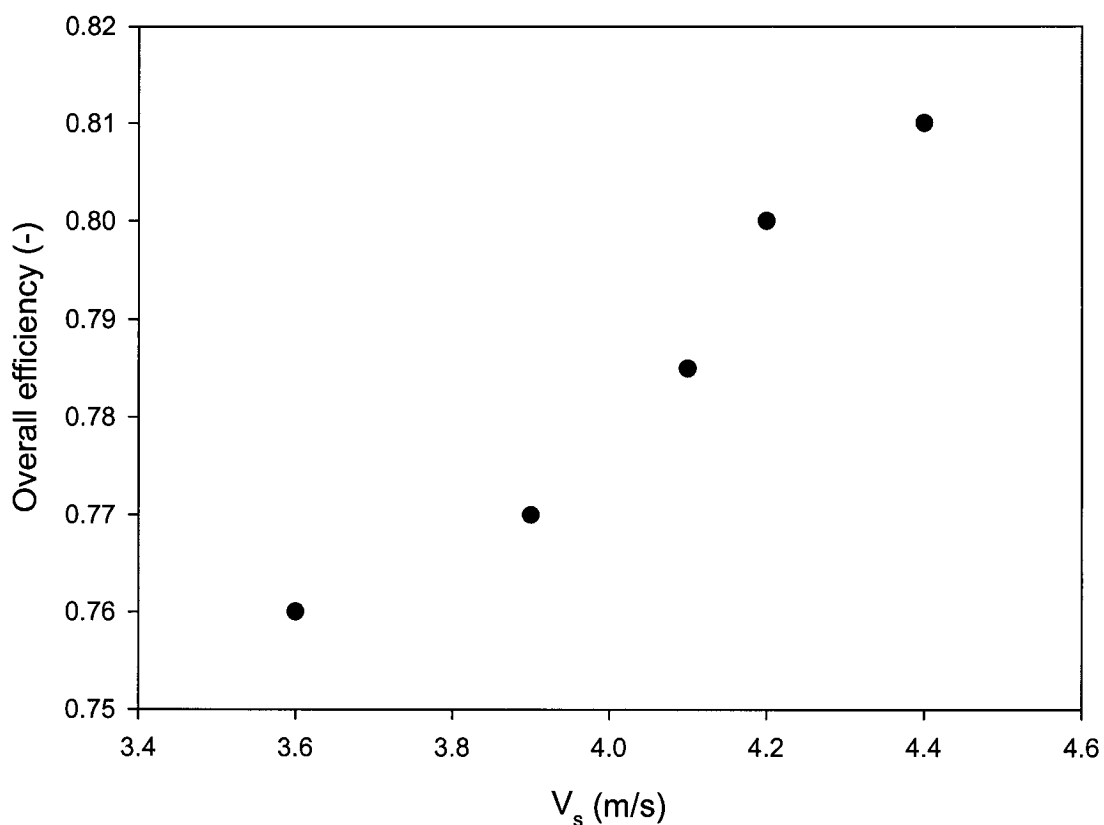


Figure 6.7. Overall efficiency of the inertial separators in the primary chamber plotted against superficial velocity

6.3.2. *Expected Mode of solid separation*

6.3.2.1. 1st row of inertial separator (in the riser)

Separators in this section were placed at the top of the riser and near to its exit where the direction of the gas-solids suspension flow was visibly diagonal. However, a stagnant zone of gas was created inside the separator where separation of solids took place due to the following two reasons:

1. The gas may turn 90^0 and flow towards the exit, but the solids directly hit the roof of the riser due to their higher momentum. Rebounded solids drop in the cavity. After this fall, the solids travel along the height of the separator until another upward gas-solids suspension moves it away.
2. Solids enter the cavity owing to their inertia, but the gas velocity in it is too weak to carry them out further. Thus, they drop inside the cavity.

The vertical component of the diagonal gas-solids suspension flow contributes to the first reason, while the horizontal component contributes to the second one. In the riser, the contribution to the first reason could be more predominant than the second one. It is due to the upward flow component. Solids flux measurement in this section shows a downward solids flux, which supports this observation. In subsequent rows, outside the riser, the second reason may be predominant as there is no upward flow there.

6.3.2.2. 2nd row of the separator (in the primary chamber)

The motion of the gas-solids suspension in the primary chamber was nearly horizontal. In this case, solids are expected to be separated by inertial separation (Second reason). In the present design, the gas exit is on the upper part of the rear wall. So the lower part of this section of the separators is expected to be in a stagnant or eddy flow. This helps the separation to occur.

6.3.3. Heat transfer to inertial-cavity separators

To study the effect of varying hydrodynamic conditions on heat transfer, local heat transfer coefficients were measured inside the inertial separators. Experiments were carried out at different external circulation rates and superficial velocities. Results are shown in Fig. 6.8 – 6.14. The locations of heating strips on all three surfaces were: (i) 190 mm from the bottom and ran 800 mm along the height of the separator (Case 1) (Fig 6.2b) and (ii) the other strips ran from 50 mm to 200 mm along the width of the separator at a height of 350 mm from the bottom of the separator (Case 2) (Fig 6.2c). The first configuration would provide information on local heat transfer coefficients along the height whereas the second configuration would give local heat transfer coefficients along the width of the separator.

6.3.3.1. Inside the inertia-cavity separator (1st row)

This section discusses heat transfer to the inner walls of the cavity separator. The heat transfer declines moderately from the top of the heater at 600 mm to a point 450 mm under all operating conditions except when the solids re-circulation is stopped (Fig. 6.8). This variation in local heat transfer coefficients along the height of the inertial separator can be explained by the downwards solids flow observed earlier (section 6.3.2.1). As the layer of particles sweeps down the heating strip, it gradually approaches thermal equilibrium with the surface. This reduces the thermal driving force between the particles and the cavity surfaces, which in turn reduces the heat transfer and therefore the heat transfer coefficient. A similar observation was also made on the surface of the wing wall placed at the top of the riser. This was observed in a separate experiment but on the same riser (Chapter 4). These results showed higher heat transfer coefficients at higher external solids circulation rates. The decline in heat transfer beyond 400 mm is very modest and even shows an increase at its bottom, which is explained in the following paragraph.

At a lower external solid circulation rate ($1-3 \text{ kg/m}^2\text{s}$), the heat transfer coefficient on the lowest point of the separator is slightly higher than that on the point just above it. This could be due to the contribution of gas convection, which is one component of the combined gas convection and particle conduction modes of heat transfer. In the case of low external circulation rates, downward solids fluxes are low. This gives a low particle concentration in the upper bed. Thus, here the gas convection from the upward gas flow is more dominant than the conduction from the moving particles. In forced convection on a flat plate, for instance, the heat transfer on the leading edge is the highest. Thus, in the present case, the heat transfer coefficients at the bottom of the wall are higher than those on the point just above it. It is especially noticeable at low solids circulation rates. To verify this hypothesis, several tests were carried out without any solids in the riser. Results (Fig: 6.8) show that for pure gas convection, the heat transfer coefficient is highest at the lowest point of the inner wall of the separator. It is further observed that in all intermediate points i.e., 450 mm to 150 mm height, heat transfer coefficients are nearly the same under all conditions. It could be a combined result of decreasing particle conduction and increasing gas convection.

Fig. 6.9 presents data for the inner surface but along the depth of the separator (Case 2). It was observed that the local heat transfer coefficient was invariant with the depth of the separator. However, the heat transfer was higher at higher solids circulation rates. As the particle movement on the heater is only downward and there is no boundary layer formation along the depth, one does not expect much variation in heat transfer in this direction. One experiment was carried out without solids to estimate the pure gas convection heat transfer coefficient in this case, which was $45 \text{ W/m}^2\text{K}$ at all points. Comparing this with those measured with external solids circulation of $5.8 \text{ kg/m}^2\text{s}$, it was found that the particle convection was in the range of $27-30 \text{ W/m}^2\text{K}$, which is about 60 % of the gas convection (Fig. 6.9). The gas convection was assumed same because same superficial gas velocity was used for both cases.

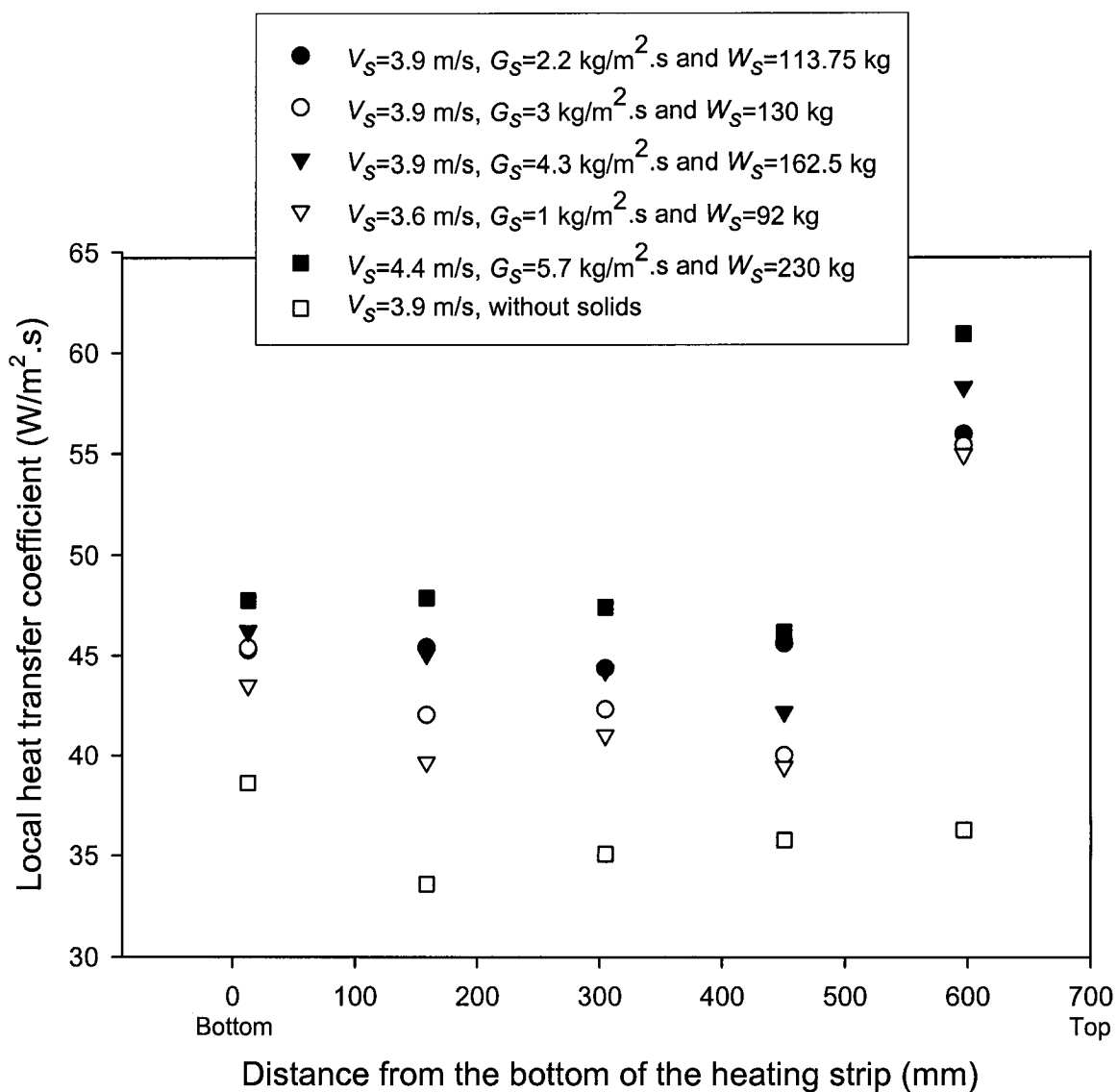


Figure 6.8 Local heat transfer coefficients measured along the height (Case-1) of the inner wall of a separator placed at the riser.

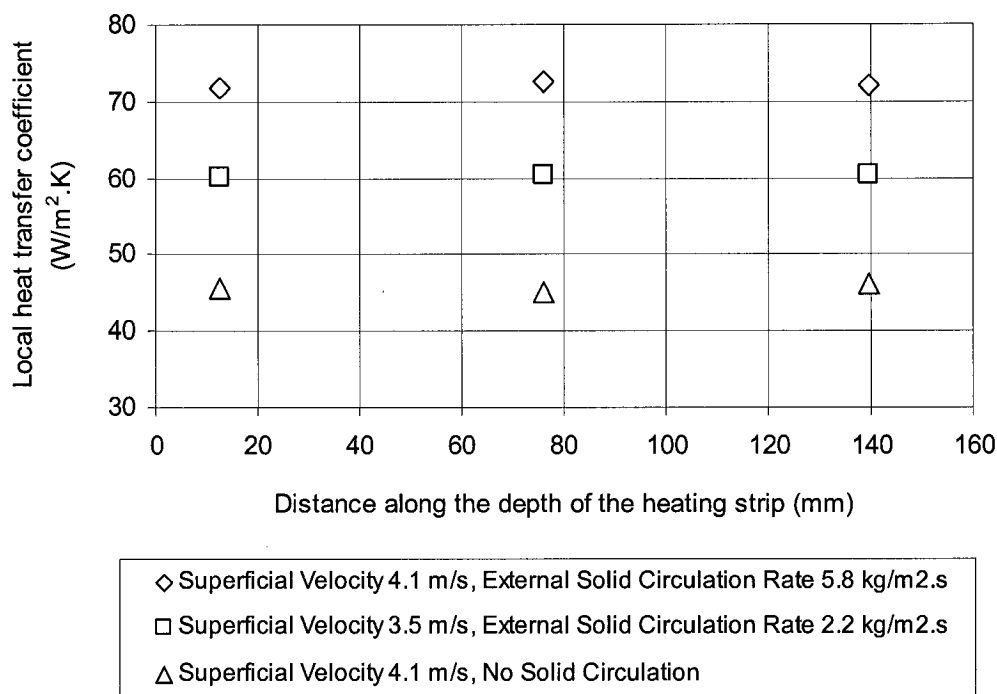


Figure 6.9. Local heat transfer coefficients measured along the depth (Case-2) of the inner wall of a separator placed at the riser

6.3.3.2. Outer wall of the inertial-cavity separator (1st row)

In a CFB boiler, inertial-cavity separators would be made of boiler tubes, as such both sides of the separator are heat absorbing. So, information is needed on heat transfer coefficients on both inner and outer surface of the separator. Fig. 6.10a shows local heat transfer coefficients at different heights of the outer wall (Case 1).

A heating strip was located on the outer wall of the separator (Case 1). At the top of the heating strip, higher local heat transfer coefficients were observed for all operating conditions, including a case without solids circulation. This can be explained by the fact that the exit path to the secondary separator is located at the top (Fig. 6.1). Therefore, one expects a velocity distribution in the primary chamber with the highest value at the top.

This results in a higher convective heat transfer coefficient from the top of the hanging separators.

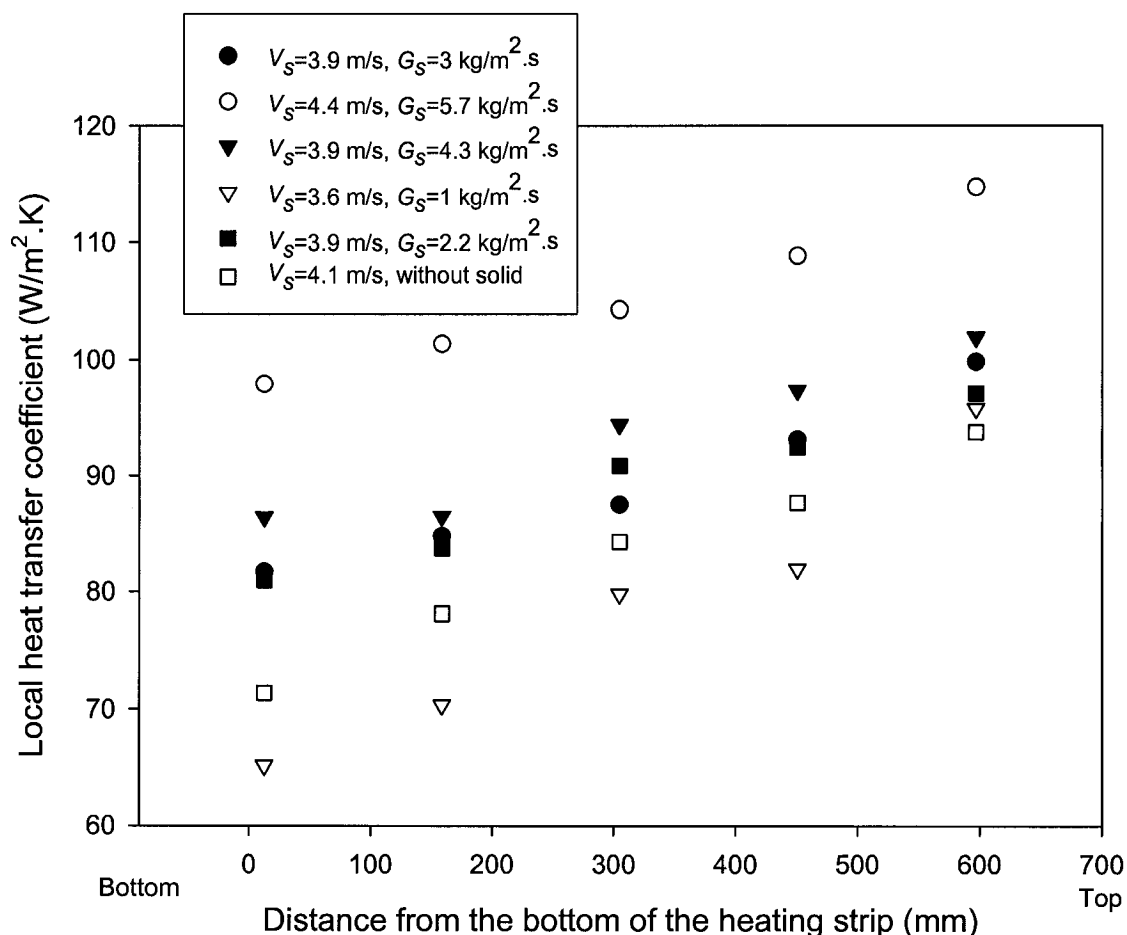


Figure 6.10a Local heat transfer coefficients measured along the height (Case-1) of the outer wall of a separator placed at the riser

In the absence of solids flow, the “height” average heat transfer coefficient on the outer surface of the separator is about 130 % higher than that on the inside. This suggests a strong effect of forced convection on the outer wall where the superficial gas velocity increases from 4.1 m/s to 9.5 m/s due to passage restriction. The effect of particle contribution can be estimated from Fig. 6.10 by subtracting the heat transfer coefficients calculated based on the experiment with empty riser (no solids) from those calculated based on the experiments with solids. Figure 6.10b represents the ratio of convection

with particle and convection without particles with average suspension density for a superficial velocity of 3.9 m/s. The proportionality exponent for the fitted curve is found to be 0.11, which is much lower than the reported value of 0.5 for the water wall by a number of researchers (Basu and Nag, 1996, Glicksman 1988) as similar to that on the wing wall (Chapter 4). The ratio of convection with particles to pure gas convection increases from 15% to 25 % when the solids circulation rate increases from 2.2 to 4.3 kg/m².s causing ρ_{sus}/ρ_g to change from 2.5 to 6.5.

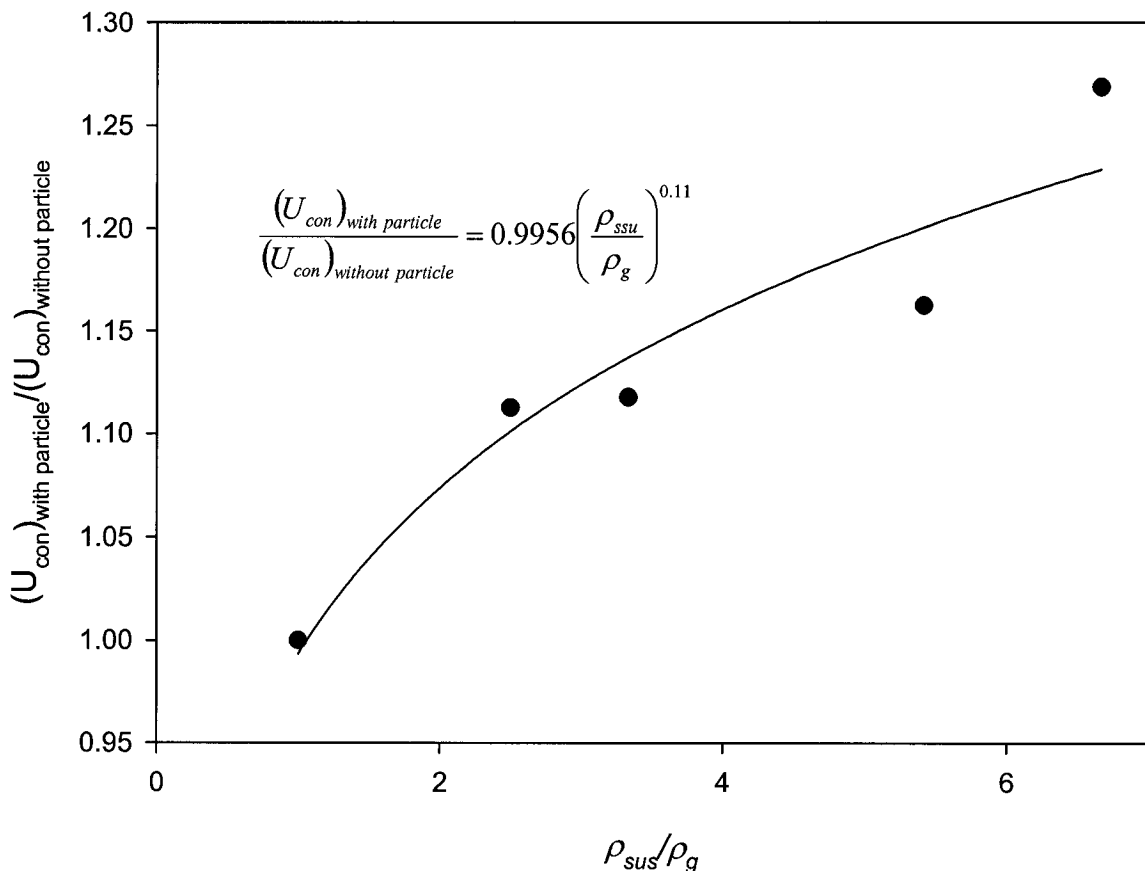


Figure 6.10b. Ratio of forced convection with particles and without particles with the ratio of suspension density and gas density for a superficial gas velocity of 3.9 m/s (Case-2).

Fig. 6.11 shows local heat transfer coefficients along the depth of a heating strip (Case 2). The dimension of this strip was 150 mm × 50 mm, which was not long enough to form a fully developed flow along the downstream. However, still, within this developing region, local heat transfer coefficients decrease along the depth of the surface of the inertial separator, which supports the supposition that the passage of the gas-solids suspension over the heating strip is horizontal rather than vertical. From Fig 6.11, it is also seen that when the solids circulation rate is increased to 5.8 kg/m².s, the increase in “depth” average heat transfer coefficient is 26%. This suggests that the gas convection component outside the separator has more effect on the heat transfer coefficient than particle convection.

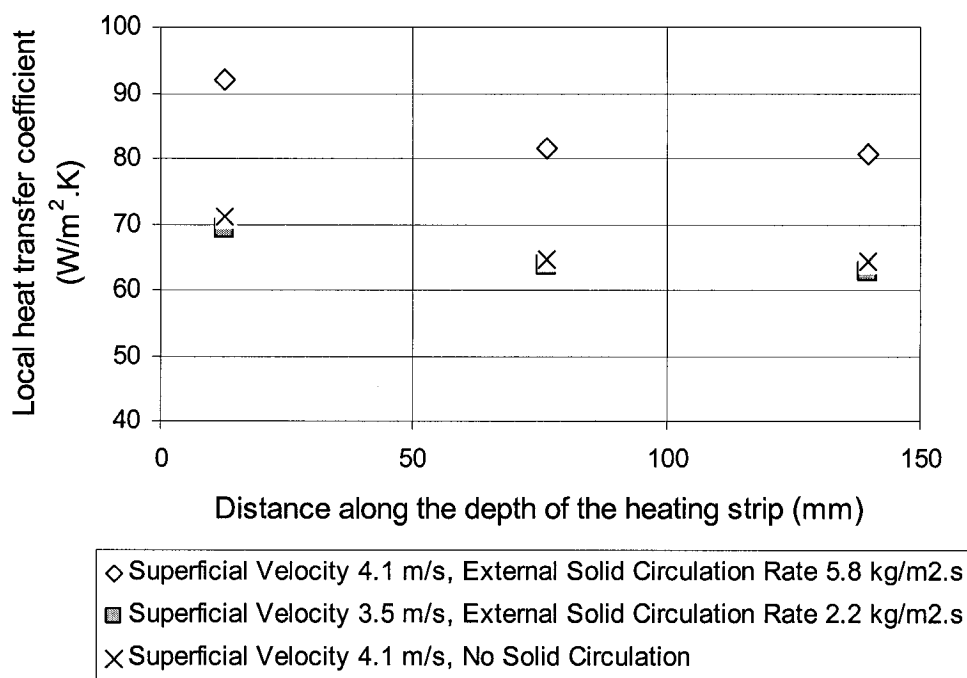


Figure 6.11. Local heat transfer coefficients measured along the depth (Case-2) of the outer wall of a separator placed at the riser

6.3.3.3. Comparison of heat transfer for both surfaces (1st row)

Fig. 6.12 shows a comparison of local heat transfer coefficients along the height between the inside and outside walls of the separator for a solids circulation rate of $4 \text{ kg/m}^2 \cdot \text{s}$ and varying superficial velocities. The “height” average heat transfer coefficients on the outside of the separator are 1.69 to 1.76 times higher than those on the inside, as the superficial velocity increases from 3.5 to 3.9 m/s. However, for a given superficial velocity of 4.1 m/s and without solids circulation, the ratio is 2.3. The implication is that, with solids circulation, the contribution from the solids is higher inside the separator than outside. In other words, the heat transfer on the inner wall is dominated by solids flow on it.

Comparing the local heat transfer coefficient along the depth, as can be seen from Fig. 6.9 and Fig 6.11 that, for a superficial velocity of 4.1 m/s, the ratio of “depth” average heat transfer coefficient between outside and inside walls of the separators decreases from 1.46 to 1.17 when solids circulation rate increases to $5.8 \text{ kg/m}^2 \cdot \text{s}$. This also supports the view that solids have greater influence on heat transfer coefficient inside the separator.

The difference in ratios between “height” average and “depth” average heat transfer coefficients can be explained by the pattern of gas solids suspension flow observed in the riser. The flow inside the separator is vertical whereas it is horizontal outside. One would expect a boundary layer formation along the height of the inside wall of the separator whereas it may be along the depth of the outside wall. The higher heat transfer coefficients result from the smaller heating surfaces along the flow path of the gas-solids suspension (Luan *et al*, 1999).

Also, inside the separator, one can see that the superficial velocity does not have a significant effect on the heat transfer coefficient, whereas it has a significant effect on heat transfer outside. As the analysis in the preceding section showed, the contribution of

the particles to heat transfer inside the separator is higher than that outside. For example, the particle contribution is 25-30 W/m².K inside the separator and 15-20 W/m².K outside.

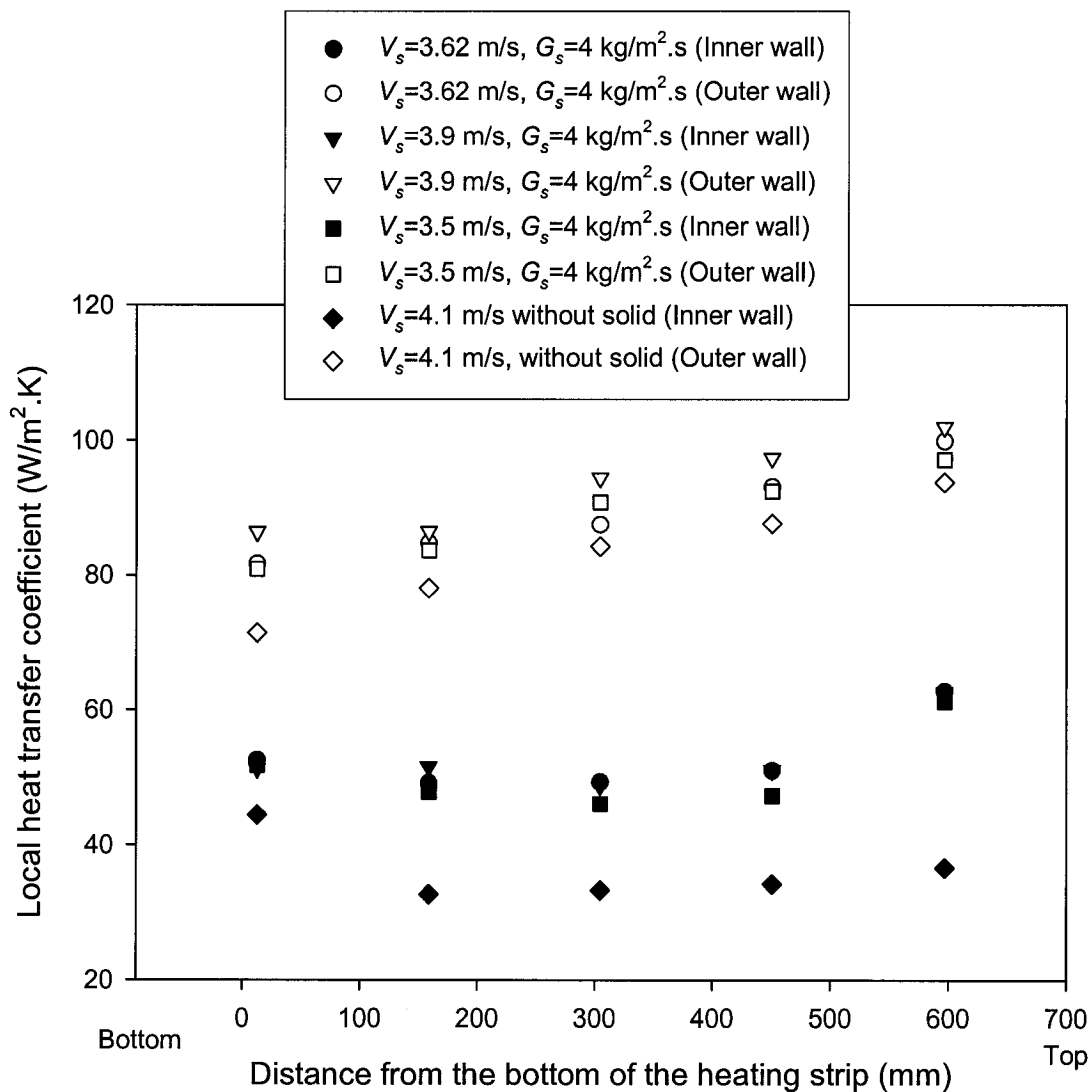


Figure 6.12. Comparison of local heat transfer coefficient measured along the height for both inner wall and outer wall of the separators placed at the riser(Case 1)

6.3.3.4. Inside the inertial-cavity separator (2nd row)

Fig. 6.13 (Case 1) shows results in separators located outside the riser but inside the primary chamber (Fig. 6.1).

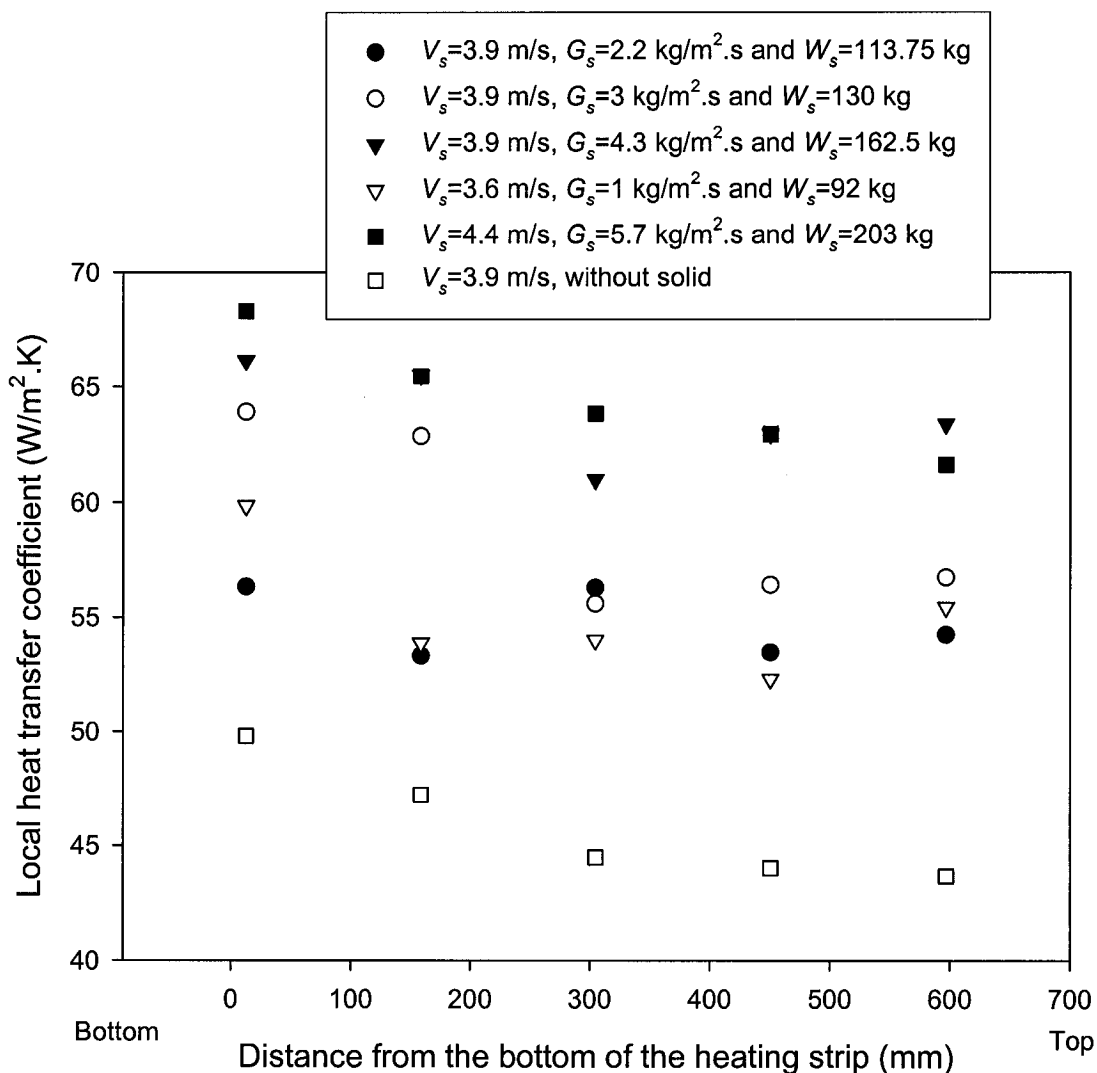


Figure 6.13. Local heat transfer coefficients measured along the height (Case 1) of the inner wall of a separator placed at the primary chamber.

It should be noted that, the local heat transfer coefficients increase gradually from the top of the heating strips towards its bottom for all operating conditions. This is expected

since the solids concentration is higher at the bottom of the heating strip due to an expected stagnant zone. The contribution of particle convection to the “height” average heat transfer coefficient in this section is 39% of that of gas convection when the solids circulation rate increases to $4.3 \text{ kg/m}^2\cdot\text{s}$ for a given superficial velocity of 3.9 m/s . The local heat transfer coefficients along the depth of the heating strip indicate the formation of a boundary layer in the second row where local heat transfer coefficients decrease gradually along the depth of the heating strip (Fig. 6.14). The “depth” average heat transfer coefficient increases by 57% when solids circulation rate increases from $0 \text{ kg/m}^2\cdot\text{s}$ to $5.8 \text{ kg/m}^2\cdot\text{s}$.

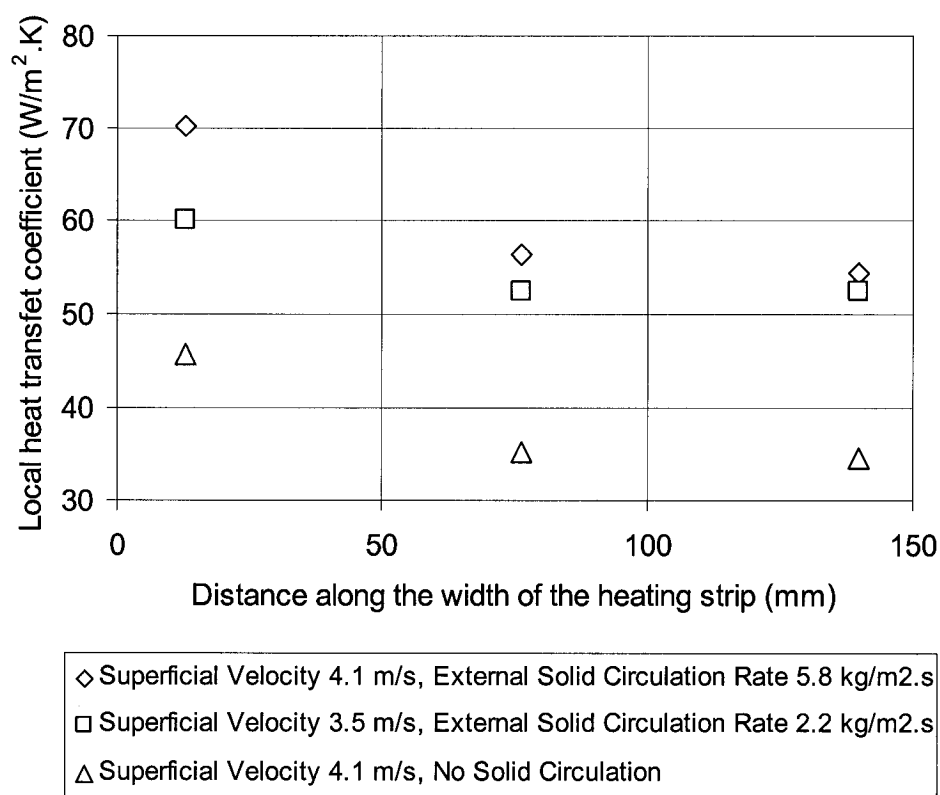


Figure 6.14. Local heat transfer coefficients measured along the depth (Case-2) of the inner wall of a separator placed at the primary chamber.

6.3.3.5. Comparison of heat transfer for both 1st and 2nd row (Inner wall)

The heat transfer coefficient in the 2nd row was found to be higher than that in the 1st row (Fig. 6.8 and Fig. 6.13). More interestingly, higher heat transfer is observed at the bottom of the 2nd row compared to the top for the 1st row. This is due to different hydrodynamic conditions existing in the two rows. For a cold bed, solids concentration on the surface governs the heat transfer. In the 1st row, a higher solids concentration is obtained at the top whereas in the 2nd row, it is obtained at the bottom. Also, the positions of heating strips on the gas-solids suspension flow direction play an important role. In the 1st row, gas-solid suspension forms a boundary layer over the heating surface (because the direction of flow is along the height, which is 609.6 mm) whereas in the 2nd row, there was no boundary layer formation over the heating strip (because the direction of flow is along the depth, which is 50.8 mm). To verify this hypothesis, Case (2) study was performed. Fig. 6.9 and Fig. 6.14 show that local heat transfer coefficients are higher inside the 1st row of the separator and are nearly constant over the depth of the strip. However, there is an indication of the formation of a boundary layer in the 2nd row where local heat transfer coefficients decrease gradually along the depth of the heating strip. Fig. 6.9, Fig. 6.11 and Fig. 6.14 also show that local heat transfer coefficients are higher in the outer wall of the separator, i.e., in the gas pass for all operating conditions among all three heating surfaces.

6.3.3.6. Comparison of heat transfer with the water walls

The use of inertial separators for heat absorption is a novel idea described in patents (GRI 2001), but no data is available in published literature to indicate how effective this option is compared to the walls of CFB risers. Therefore, an attempt is made here to compare the heat transfer coefficients on inertial separators with those on the walls (Table 6.1). As no heat transfer probe was mounted on the wall in the present series of experiments, data was taken from a previous series of experiments on the same riser (Chapter 4).

Table 6.1: Comparison of height average heat transfer coefficient in the experimental unit

Location of Heat transfer surfaces	Operating condition	Average suspension density (kg/m ³)	Average HTC (W/m ² .K)
Water wall • Without in-furnace separator	• $V_s=3.9$ m/s and $G_s=5.7$ kg/m ² .s	3.51	75 (Section 4.3.3)
	• With in-furnace separator	• $V_s=4.4$ m/s and $G_s=5.7$ kg/m ² .s	8.02 113* Projected)
Inner surface of in-furnace separator	$V_s=4.4$ m/s and $G_s=5.7$ kg/m ² .s		50 (Section 6.3.3.1)
Inner surface of 2 nd row separator	$V_s=4.4$ m/s and $G_s=5.7$ kg/m ² .s		64.4 (Section 6.3.3.4)
Outer surface of in-furnace separator	$V_s=4.4$ m/s and $G_s=5.7$ kg/m ² .s		105 (Section 6.3.3.2)

* Projected heat transfer coefficient was estimated by the equation $h = 40\rho_{sus}^{0.5}$, which was proposed by Basu and Nag (1996) and verified by our experimental data.

Under a given operating condition, the present experiments showed suspension densities higher than those in earlier experiments when the separator inside the furnace was absent. This is due to the presence of these in-furnace separators. For instance, for an operating condition of $V_s=4.4$ m/s and $G_s=5.7$ kg/m².s, the average suspension density in the riser increased by 128% of the value without in-furnace separators. As we have seen in section (2.3.1.1) that heat transfer coefficients are strongly influenced by the suspension density, so the previous data of “height” average heat transfer coefficients on water walls measured in the previous experiment (Section 4.3.3) were extrapolated to the higher suspension density of the present series of experiments. It shows that for a given operating condition, the “height” average wall heat transfer coefficient is increased by 50% over that of the original ones. The heat transfer coefficients on the inner surface of the separators are 44% (1st row) and 57% (2nd row) of that of the original heat transfer coefficients on the enclosing wall. The heat transfer coefficient on the outer surface of the separator is 93% of that of the enclosing wall. Thus, the presence of heat absorbing

inertial separators in the furnace not only increases the heat transfer surfaces in the CFB loop but also enhances the heat transfer rate to the existing walls of the furnace.

6.4. Concluding remarks

This chapter presents a detailed experimental investigation on both hydrodynamics and heat transfer on cavity-type inertial separators. The experiments were conducted in a circulating fluidized bed pilot plant operated at room temperature within a range of operating parameters (superficial velocity 3.5 to 4.4 m/s and solids circulation rates of 1 to 5.8 kg/m².s). Within this range, the following conclusions were drawn.

1. The heat transfer coefficient inside the separator is lower than that on the outside irrespective of its position.
2. The position of the separator, whether inside or outside the riser, affects both hydrodynamics and heat transfer. Inside the separator, heat transfer on the 2nd row is higher than that on the 1st row. This is due to a higher solids concentration on the second row where there is an absence of upward gas flow.
3. Superficial gas velocity does not have much effect on the heat transfer inside the separator. However, it affects the heat transfer outside the separator. Solids circulation has a major effect on heat transfer to the inside wall of the separator.
4. The presence of heat absorbing separators in the riser not only adds to the heat transfer surfaces of the boiler but also enhances the heat absorbed by the enclosing walls of the riser due to increase in average suspension density in the riser.
5. The hydrodynamic condition inside the separator is different from that outside the separator.

Chapter 7

Models for the vertical walls of CFB boilers

This chapter presents mechanistic models for water walls and wing walls of commercial CFB boilers. It also presents a mechanistic model for the cavity-type inertial separators and validates it against the experimental data from a pilot plant operated at elevated temperature. The physical model for the water walls modifies the cluster renewal model, by including recent findings on thermal boundary layer in the combustor, cluster velocity and gas gap. Furthermore, a correlation for wall coverage in large commercial boilers is developed. The model proposed for both the wing walls and cavity-type inertial separators, is based on the hydrodynamic conditions that were observed at chapter 4 and chapter 6 of this thesis respectively.

7.1 Model for water walls:

7.1.1 Background

A considerable amount of work, mostly measurements on heat transfer in the large circulating fluidized bed combustors has been carried out (Table 7.1). The energy released in a CFB combustion chamber is typically exchanged with water tubes that comprise the walls of the riser. So the mechanisms for heat transfer can be described by the interactions between the bed material, the gas and the wall. As seen in the upper portion of a CFB (Fig 2.1), the flow of bed material near the wall is predominantly downward in agglomerations of particles known as clusters in a core-annular flow regime

(Glicksman, 1998). The recent results (Breitholtz, 2000) show that the radiative constituent of heat transfer depends on the optical thickness of a particle boundary layer, and that the convective constituent can be related to the average cross sectional suspension density.

A summary of different mechanistic models for calculating heat transfer on the water walls is presented in the Table 2.4. Although a number of alternative models have been proposed so far to calculate the heat transfer coefficient on the water wall, cluster renewal model of Subbarao and Basu (1986) appears to hold ground. However, there are areas to improve this mechanistic model by incorporating detailed behaviour of the fluid-dynamics of the combustor such as: thickness of the gas-gap between the wall and the particle suspension, the wall coverage, the temperature boundary layer, cluster concentration, cluster velocity etc.

Some correlations are available for most of these unknown parameters; however, no data for wall coverage in commercial boilers are available. An effort is made to deduce data for wall coverage by applying cluster renewal model with those recent findings from the reported heat transfer coefficients on commercial CFB boilers. A correlation for wall coverage in commercial boilers is proposed hereafter and the modified cluster renewal model is validated with the data reported in the literature (Table 7.1).

Table 7.1: Measurement on heat transfer in different commercial units

Unit, Reference	Plant Output	Size of the furnace (m)	Sus. density (kg/m³)	Bed temp (°C)	Wall Temp (°C)	Particle size (µm)	HTC W/m².K
Chalmers University, Sweden (Anderson 1996)	12 MW _{th}	1.4×1.7×13.5	1.5-13	760-860	210	220	100-200
Jianjiang, China, Jin et al 1999	50 MW _{th}	3×6×20	14-52	920	290	400	200-300
Chatham, Canada, Couturier et. al 1993	72 MW _{th}	4×4×23	10.4	880	500	200	200
Flensburg, Germany, Werdermann and Werther, 1994	109 MW _{th}	5.1×5.1×28	6.1-9.2	860	340	209	165-173
VW Wolfsburg, Blumel et al., 1992	145 MW _{th}	7.6×5.2×31	2.3-5.2	850	340	NS	110-150
Orebro, Andersson et al., 1996	165 MW _{th}	4.6×12×33.5	NS	700-860	360	280	NS
Duisberg, Germany (Werdermann and Werther, 1994)	226 MW _{th}	8(dia)×32 (Horizontal tube bank)	NS	850	650	177	445-596
Nucla, USA (Boyd and Friedman, 1991)	110 MW _e	6.9×7.4×34	NS	774-913	330	150	130-188
Emile Huchet, France, (Jestine et al., 1992)	125 MW _e	8.6×11×33	5-11	800-860	340	150	130-175
This work (Chapter 3)	170 MW_e	7.5×18×36	1.8-8.2	554-940	360	240	87-181
This work (Chapter 3)	20 MW_e	5.2×5.2×32	2.7-3.45	850-925	343	230	115-131

7.1.2 Model Development:

A physical model is adopted, which resembles the cluster renewal model where the following assumptions were made:

1. Existence of a temperature profile in a horizontal section of the riser which shows a difference between the bed core temperature (T_b) and the temperature of the first (from the heat transfer surface) row of particles (T_s); (Fig 7.1)
2. A linear profile of temperature in a gas film where temperature varies from T_w to T_s (Fig. 7.1)

Golriz (1995), presents the results of an experimental study on radial temperature distribution in a 12 MW_{th} CFB boiler at different furnace elevations. The data was generalized by Borodulya *et. al* (1999) in the following form:

$$T_s = T_w + 1.29 \left(\frac{\rho}{\rho_s} \right)^{0.13} (T_b - T_w) \quad (7.1)$$

7.1.2.1 Heat transfer mechanism:

The heat transfer is frequently described as the sum of three mechanisms: Gas convection, particle convection and radiation. The mechanisms are not strictly additive, but it is a common simplification to assume that they can be treated separately.

$$h_{tot} = f(h_{con} + h_{rad})_{cluster} + (1 - f)(h_{con} + h_{rad})_{dilute} \quad (7.2)$$

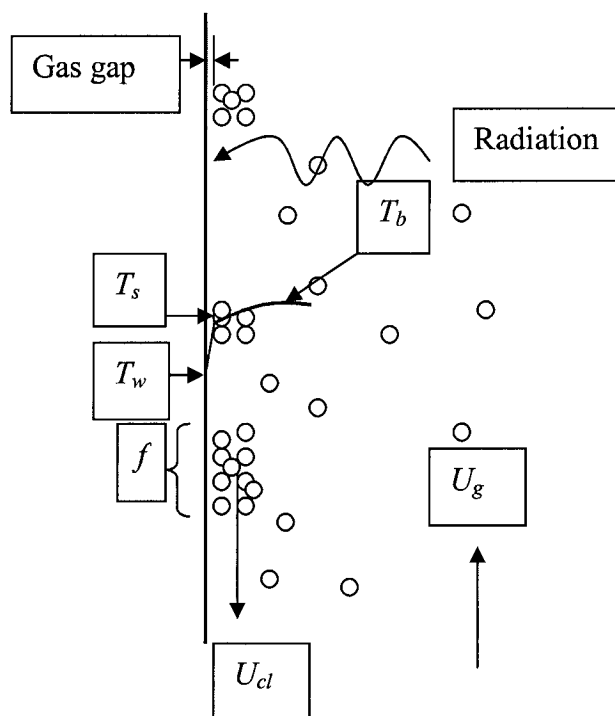


Figure 7.1. Heat transfer mechanism

The Biot number for particles is higher than that of the gas. Therefore, the particles are superior heat carrier between the core and the wall of a CFB riser. Consequently, a higher concentration of particles results in higher heat transfer. However, the contact time and contact area between the particles and the wall are small, and the direct heat transfer from the particles to the wall through the point of contact is negligible. Majority of the heat is transferred through conduction across the gas-gap. Thus, the thermal conductivity of the gas determines the heat transfer between the gas-particle suspension and the wall. The gas-gap is often modeled as an almost particle-free gap, the thickness of which decreases with an increase in the local suspension density at the wall. The particle volume fraction at a flat wall is about three times the cross-section average, and in the region between two tubes at a membrane tube wall it is about ten times the cross-sectional average (Glicksman, 1997). Since the particle volume fraction at the wall is proportional to the

one in the core, the cross sectional average suspension density represents the condition at the wall, which in turns affects the heat transfer through the particle coverage of the wall.

Mickley and Fairbanks (1955) proposed the packet theory for bubbling fluidized beds. Subbarao and Basu (1986) extended the basic model of Mickley and Fairbanks (1955) along with the other relevant information to predict bed to wall heat transfer in a circulating fluidized bed. A core-annulus model is discussed in section 2.2 which is the basis of the cluster-renewal model.

Agglomeration of solid particles into clusters or strands is a major characteristic feature in a CFB process. Figure 7.1 shows the cluster renewal heat transfer mechanism in the core annulus structure in a CFB riser column. The heat transfer model is based on the transient heat conduction in strands or clusters travelling downwards along the heat transfer surface. The clusters are assumed to travel a certain distance, disintegrate and reform periodically in the annular layer of the furnace. The influence of the down-flowing clusters on heat transfer is predominant at the wall surface. When the clusters slide over the wall, an unsteady heat conduction takes place from the clusters to the wall surface. The time averaged cluster-wall heat transfer coefficient is given by the following equation (Mickley and Fairbanks, 1955). Figure 7.1 and 7.2 show the cluster renewal heat transfer mechanism.

$$h_{cluster} = \left[\frac{4k_c(\rho c)_c}{\pi t_c} \right]^{0.5} \quad (7.3)$$

The thermal conductivity of the cluster is calculated from the equation provided by Gelperin and Einstein (1971) for packet heat transfer.

$$\frac{k_c}{k_g} = 1 + \frac{M}{N} \quad (7.4)$$

where M and N are given below.

$$M = (1 - \varepsilon_c) \left(1 - \frac{k_g}{k_s} \right)$$

$$N = \left(\frac{k_s}{k_g} \right) + 0.28 \varepsilon_c^{0.63} \left(\frac{k_g}{k_s} \right)^{0.18}$$

for particle diameter less than 0.5mm and $k_s/k_g < 5000$.

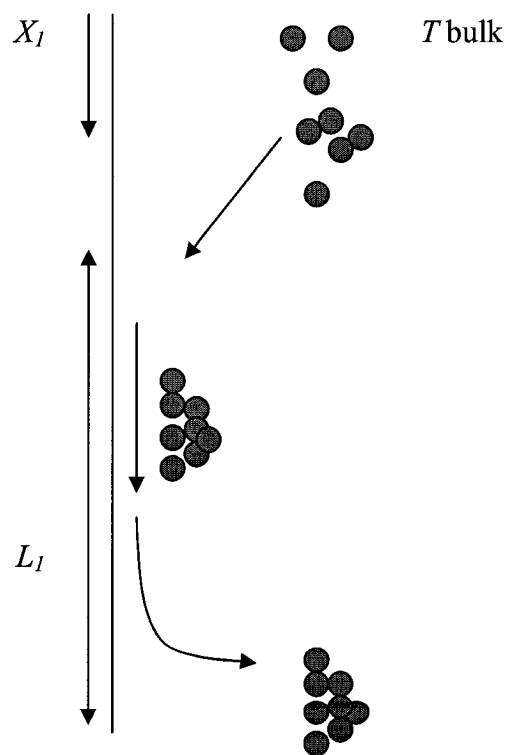


Figure 7.2. Single cluster at the wall showing deposition locations and contact length

The specific heat of a cluster is calculated based on more relevant form of lumped property instead of using an emulsion heat capacity (Breitholtz and Leckner 2000) and cluster density and is estimated from the following relation:

$$(\rho c)_c = (1 - \varepsilon_c) \rho_p c_p + \varepsilon_c \rho_g c_g \quad (7.5)$$

where ε_c is cluster voidage and is calculated from the equation provided by Lints and Glicksman (1994). The effect of cross sectional average volumetric solid concentration on cluster solid fraction is accounted for.

The relation between cluster solid fraction and cross section average volumetric solid concentration in an atmospheric CFB is given by Lints and Glicksman (1994).

$$\text{Cluster solid fraction} \quad c_{sf} = 1.23(1 - \varepsilon_{avg})^{0.54} \quad (7.6)$$

where ε_{avg} is cross sectional bed average voidage. The cluster voidage ε_c is given by

$$\varepsilon_c = 1 - c_{sf}$$

At the top of the wall surface, a strand or cluster is formed or comes in contact with the wall. While swept on the wall, the cluster first accelerates to a steady velocity and decelerates in the vertical direction before it moves away from the wall. So it is assumed that it travels downwards along the wall surface with an average velocity U_{cl} for a characteristic length L_c before disintegrating (Fig. 7.1). The residence time for each cluster (t_c) at the wall surface is given by

$$t_c = \frac{L_c}{U_{cl}} \quad (7.7)$$

The cluster velocity can be estimated by the following correlation proposed by Noymer and Glicksmann (2000).

$$U_{cl} = 0.75 \sqrt{\frac{\rho_p}{\rho_g} g d_p} \quad (7.8)$$

The characteristic length (L_c) is estimated from the literature (Wu *et al*, 1990).

$$L_c = 0.0178(\rho_{sus})^{0.596} \quad (7.9)$$

In addition to the resistance due to transient heat conduction in the cluster, the separation of the cluster from the wall by a thin gas layer will introduce another resistance to heat transfer from the cluster. The exact expression for transient conduction from a semi-infinite body to a surface with a series resistance is complicated. However, experimental measurements (Gloski *et al*, 1984) have shown that a close approximation to the actual heat transfer coefficient from a cluster is given by assuming that these two mechanisms, the contact resistance and the transient conduction to a cluster of particles, act independently and in series with each other.

The expression for heat transfer coefficient due to conduction through a gas layer is given as:

$$h_w = \frac{k_g}{\delta d_p} \quad (7.10)$$

where δ is non-dimensional gas layer thickness between the wall and cluster. δ could be calculated by the expression given by Lints and Glicksman (1994).

$$\delta = 0.0282c^{-0.59} \quad (7.11)$$

where c is cross section average volumetric solid concentration.

So, the cluster convective $[(h_{con})_{cluster}]$ heat transfer coefficient, which is the combination of cluster convection and gas gap conduction heat transfer coefficients is given below:

$$(h_{con})_{cluster} = \left[\frac{1}{h_{cluster}} + \frac{1}{h_w} \right]^{-1} \quad (7.12)$$

$$(h_{con})_{cluster} = \frac{1}{\left[\frac{\pi}{4k_c(\rho c)_c} \right]^{0.5} + \frac{\delta d_p}{k_g}} \quad (7.13)$$

The radiation heat transfer from the cluster to the wall may be considered to be that between two parallel plates. So the cluster radiation component of the heat transfer coefficient is estimated from the equation given below:

$$(h_{rad})_{cluster} = \frac{\left\{ \sigma (T_s^4 - T_w^4) \right\}}{\left(\frac{1}{e_c} + \frac{1}{e_w} - 1 \right)} (T_s - T_w) \quad (7.14)$$

here T_s is the cluster layer temperature, which can be estimated from equation 7.1. e_c and e_w are the emissivities of the cluster and wall, respectively.

The cluster emissivity, e_c is estimated from the following relation (Grace, 1982):

$$e_c = 0.5(1 + e_p) \quad (7.15)$$

The CFB furnace comprises dense clusters and upflowing dispersed medium. So, while not in contact with the clusters, the wall is in contact with the gas with dispersed solids. The convective heat transfer from this dispersed medium is calculated using the modified equation of Wen and Miller (1961) which is given by Basu and Fraser (1991) as:

$$(h_{con})_{dilute} = \left(\frac{k_g}{d_p}\right) \left(\frac{c_p}{c_g}\right) \left(\frac{\rho_{dis}}{\rho_p}\right)^{0.3} \left(\frac{U_t^2}{gd_p}\right)^{0.21} \text{Pr} \left(\frac{\rho_g}{\rho_{go}}\right)^{0.2} \quad (7.16)$$

where ρ_{dis} is the density of the dispersed phase and is given by

$$\rho_{dis} = \rho_p Y + \rho_g (1 - Y) \quad (7.17)$$

Y represents the volumetric concentration of particles in the dispersed phase. The value of Y is recommended as 0.001% (Basu and Fraser 1991)

However when applying this heat transfer coefficient to the cluster renewal model, it over predicts the experimental results. A number of researchers, for example Golriz and Grace

(2002) have applied Dittus Boelter (1930) Equation $h_d = 0.023 \frac{k_g}{D_{eq}} \text{Re}_D^{0.8} \text{Pr}^{0.3}$ to estimate

the convection from the dispersed medium. The dispersed phase contains a small concentration of particles, which would have an effect on the heat transfer coefficient. Therefore, the heat transfer coefficient for longitudinal sweeping wall proposed by Basu *et al* (1999) is considered with a correction factor for particle presence (C) in the dilute phase as follows:

$$(h_{con})_{dilute} = 0.023 C C_1 C_t \frac{k_g}{D_{eq}} \text{Re}^{0.8} \text{Pr}^{0.4} \quad (7.18)$$

where C_t is the correction factor for the temperature difference between wall and medium, which can be calculated as (Basu *et al*, 1999):

$$C_t = \left(\frac{T_b}{T_w} \right)^{0.5}$$

C_l is the correction factor of tube length, when $\frac{L}{D_{eq}} > 50$, $C_l = 1$. When the entrance effect is predominant, it is common to correlate the entrance effect by the following equation noted in (Perry *et al.*, 1984)

$$C_l = 1 + F \left(\frac{D_{eq}}{L} \right)$$

Some selected values of F are noted as follows:

Flow condition	F
Fully developed velocity profile	1.4
Abrupt contraction entrance	6
90 ⁰ right-angle bend	7
180 ⁰ round bend	6

The correction factor for the presence of particles in the dilute phase can be assumed as:

$$C=1.1$$

Radiation between the suspension (dilute phase) and the bare wall is estimated from the usual expression for parallel surfaces, i.e.

$$(h_{rad})_{dilute} = \frac{\{\sigma(T_b^4 - T_w^4)\}}{\left(\frac{1}{e_b} + \frac{1}{e_w} - 1\right)}(T_b - T_w) \quad (7.19)$$

where e_w and e_b are the wall and dilute phase emissivities at T_w and T_b , respectively, with e_b , for a large boiler, estimated from the correlation of Brewster (1986):

$$e_b = \left[\frac{1.5e_p}{(1-e_p)} \left\{ \frac{1.5e_p}{(1-e_p)} + 2 \right\} \right]^{0.5} - \frac{1.5e_p}{(1-e_p)} \quad (7.20)$$

Experimental data on the wall coverage plotted by Glicksman (1997) shows a strong influence on column diameter and he proposes a correlation for a 20 cm diameter experimental unit. However, the correlation omits the dependence of the wall coverage on column diameter, and is therefore unsuitable for a large unit. Golriz and Grace (2002) proposed a correlation based on data from the laboratory unit (0.09 m – 0.30 m) which accounts the size effects of the boiler as:

$$f = 1 - \exp\left\{-25,000\left[1 - \frac{2}{e^{0.5D} + e^{-0.5D}}\right](1 - \varepsilon)\right\} \quad (7.21)$$

While applying Equation [7.21] to the commercial unit with an equivalent diameter of 3 m and higher with a solid concentration of 0.0004 (suspension density of 2 kg/m³) and higher, wall coverage approaches unity. However, it is reported by different researchers (Divilio and Boyd, 1994, Baskakov *et al*, 2001) that for a commercial boiler, radiation is

the dominant factor (upper two thirds of the combustor) in the heat transfer in the dilute region (suspension density below 5 kg/m^3). However, the above equation can predict the wall coverage for small laboratory units, for which it was actually developed. In addition, for a CFB, it is understood from the hydrodynamic point of view that, the average solid concentration, the most dominant contributor for the wall coverage, also varies exponentially with the height of the furnace. Therefore, it is worthwhile to include height as a variable into the correlation along with average solid concentration and size of the riser. Considering the above analysis, a correlation for estimating fractional wall coverage is proposed as follows, where size and height of the riser is used in a non-dimensional form (D/H):

$$f = 1 - \text{Exp} \left(-a \{1 - \varepsilon\}^b \left\{ \frac{D}{H} \right\}^c \right) \quad (7.22)$$

Data from several commercial boilers were analyzed to derive values of the coefficients of a , b , and c . Heat transfer measurements of four commercial units of equivalent size of 1.7 m, 5.2 m, 6.18 m 10.6 m with different heights (above the secondary air supply) of 11.5m, 25 m, 26 m, and 30 m were used to deduce the data for fractional wall coverage by applying the equation (1-20). Coefficients were estimated using multiple regression analysis:

$$a = 4300, b = 1.39, c = 0.22$$

Finally, for a commercial boiler, the average heat transfer coefficient for the water wall can be estimated by Equation [7.2].

7.2 Model for wing walls:

7.2.1 Background

In chapter 4, it is shown that the mechanism of heat transfer on the wing wall is different from that on the water wall. No net downwards solids flux was observed on the wing wall except for the top where one can assume a stagnant zone. So, one needs to use a separate model to estimate the heat transfer coefficient on the wing wall, which is different from the water walls. The subsequent sections will discuss that in a systematic way.

7.2.2 Model development

The wing wall panel of the boiler is located on the upper part of the furnace (Fig. 2.1). In case of industrial circulating fluidized bed boilers, the suspension density on the upper part of the boiler is very low (Divilio and Boyd, 1994). Zhang (1995) shows the radial voidage profile in the riser by the following equation that requires the cross-sectional average voidage, ε_{av} , and the radial location r/R as an input.

$$\varepsilon_i = \varepsilon_{av} \left(0.191 + \left(\frac{r}{R} \right)^{2.5} + 3 \left(\frac{r}{R} \right)^{11} \right) \quad (7.23)$$

For a rectangular section of riser (Fig. 7.3), the hydraulic radius can be estimated by following equation:

$$R = \frac{4 \times (L_x \times L_y)}{4 \times (L_x + L_y)} \quad (7.24)$$

The ratio (r/R) can be estimated by the following way:

The following relationship can be used for the specific case shown in the Fig. 7.3

$$\frac{H_x}{H_y} = \frac{L_x}{L_y}$$

$$r = \frac{4 \times H_x \times \frac{H_x \times L_y}{L_x}}{4 \times \left(H_x + \frac{H_x \times L_y}{L_x} \right)} \quad (7.25)$$

Equation 7.24 can be achieved placing $H_x=L_x$

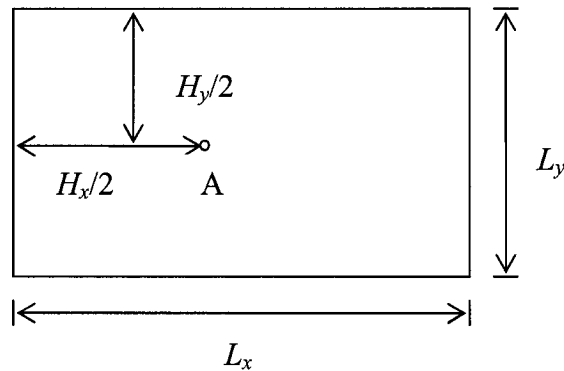


Figure 7.3. Most common rectangular cross-section of a riser

Applying Equation 7.23, one can find that the particle concentration at the core of a riser is very low. This supports the findings reported in chapter 4, where no downward solids flux was observed on the wing wall. Therefore, cluster convection can be neglected in this case due to its negligible presence in the core. Considering this special hydrodynamic condition of the wing wall, the heat transfer between the flue gas and the wing walls surfaces may be taken to be mainly due to dilute convection and radiation.

$$h_{total} = h_{dilute\ convection} + h_{dilute\ radiation} \quad (7.26)$$

7.2.2.1 Dilute Convection:

Similar to the dilute phase for the water wall, the heat transfer coefficient for longitudinal sweeping wall proposed by Basu *et al* (1999) is considered:

$$h_{gas\ convection} = 0.023C_i C_t \frac{k_g}{D_{eq}} Re^{0.8} Pr^{0.4} \quad (7.27)$$

where C_i and C_t have similar values to those reported for the water wall dilute section.

Due to the presence of particles, the gas dilute convection heat transfer coefficient can be estimated from Figure 4.8b by the following equation:

$$h_{dilute\ convection} = h_{gas\ convection} \left(\frac{\rho_{sus}}{\rho_g} \right)^{0.12} \quad (7.28)$$

At this point, the Reynolds number is proposed to be calculated based on the gas velocity at the core and the hydraulic diameter of the combustor. In a single phase flow, the thickness of the boundary layer increases from the entrance of a duct until the flow becomes fully developed. Then for given developed flow conditions, the Fluid-dynamic Boundary Layer (FBL) thickness solely depends on the column diameter. However, in two phase flow the interaction between downward flow of particles and the upward flow of gas creates an initial velocity profile that may result in an optimistic development of FBL thickness along the wall, i.e. the thickness decreases as the gas flows up depending on how strong the particle downflow is. Zhang *et al* (1995) reported the boundary layer by correlating it with the equivalent bed diameter based on both their experimental as well as on literature data. It is given as follows:

$$\delta = 0.05D_{eq}^{0.74} \quad (7.29)$$

where D_{eq} is the hydraulic diameter which can be calculated as

$$D_{eq} = \frac{4 \times L_x \times L_y}{2 \times (L_x + L_y)}$$

By assuming zero air velocity within the boundary layer, the gas velocity at the core can be estimated by the following equation:

$$U_{gc} = \frac{Q_{air}}{\left\{ (L_x - 2\delta) \times (L_y - 2\delta) - \frac{N\pi d_t^2}{4} \right\}} \quad (7.30)$$

$$\text{i.e; } U_{gc} = \frac{U_g \times \left(L_x \times L_y - \frac{N\pi d_t^2}{4} \right)}{\left\{ (L_x - 2\delta) \times (L_y - 2\delta) - \frac{N\pi d_t^2}{4} \right\}} \quad (7.31)$$

where N is the number of vertical tubes and d_t is the tube diameter of the wing wall and U_{gc} is the gas velocity at the core of the riser

7.2.2.2 Radiation:

Similar to the water wall, the dilute phase radiation heat transfer coefficient to the wing wall can be estimated from the following relation.

$$h_{dr} = \frac{\left\{ \sigma (T_b^4 - T_w^4) \right\}}{\left(\frac{1}{e_d} + \frac{1}{e_w} - 1 \right)} (T_b - T_w) \quad (7.32)$$

where e_d is the emissivity of the dilute phase. The emissivity of ash/gas mixture will be less than the sum of emissivity of the two considered separately. This is due, both to the spectral overlap of the emission of each as well as to the scattering by the ash of radiation emitted by the gas. For a very dilute medium, the effect of gas radiation can be taken into account by the following equation [Andersson *et al*, 1986].

$$e_d = (e_g + e'_p - e_g e'_p) \quad (7.33)$$

For a very dilute medium i.e., at the upper part of the riser, the effective emissivity of a particle cloud is estimated by the following equation (Glicksman 1988):

$$e'_p = 1 - \text{Exp}\left(-1.5e_p Y' \frac{L_e}{d_p}\right) \quad (7.34)$$

Considering an infinite parallel surface, the mean beam length (L_e) of the wing wall, can be estimated as (Holman, 1999):

$$L_e = 1.8 * L \quad (7.35)$$

where L is the distance between the two walls.

For a first hand approximation, the voidage in the riser interior Y' can be estimated by

$$Y' = 1 - \varepsilon_{r/R=0.5} \quad (7.36)$$

where $\varepsilon_{r/R=0.5}$ can be calculated from equation 7.23.

$$\varepsilon_{r/R=0.5} = \varepsilon_{av}^{0.369} \quad (7.37)$$

7.3 Models for Cavity Type Inertial Separator

7.3.1 Model development

The mechanistic model for the cavity-type inertial separator is based on the hydrodynamics of the separator explored and discussed in chapter 6. As the solids movement outside and inside of the separator is different, the heat transfer mechanism would also be different. The formulation of the model is discussed below.

7.3.1.1. Inside the inertial separator:

Figure 7.4 shows the expected mode of heat transfer mechanism inside the separators. A downward solids flux on the inner wall of the separator resembles the solids flow distribution on the water wall (Chapter 6). The separation of solids on the deep cavity of the separator is taking place due to the inertial effect of the solids. One can expect a negligible gas velocity inside the separator. Therefore, the expected mode of heat transfer on the inner wall of the separator can be treated as separate in the following form:

$$h_i = f(h_{con} + h_{rad})_{cluster} + (1 - f)h_{gas\ radiation} \quad (7.38)$$

The particle convection can be estimated as convection due to cluster similar to the wall. To estimate the cluster contribution, Equations [7.1-7.14] can be used and the gas radiation can be estimated by Equation 7.31.

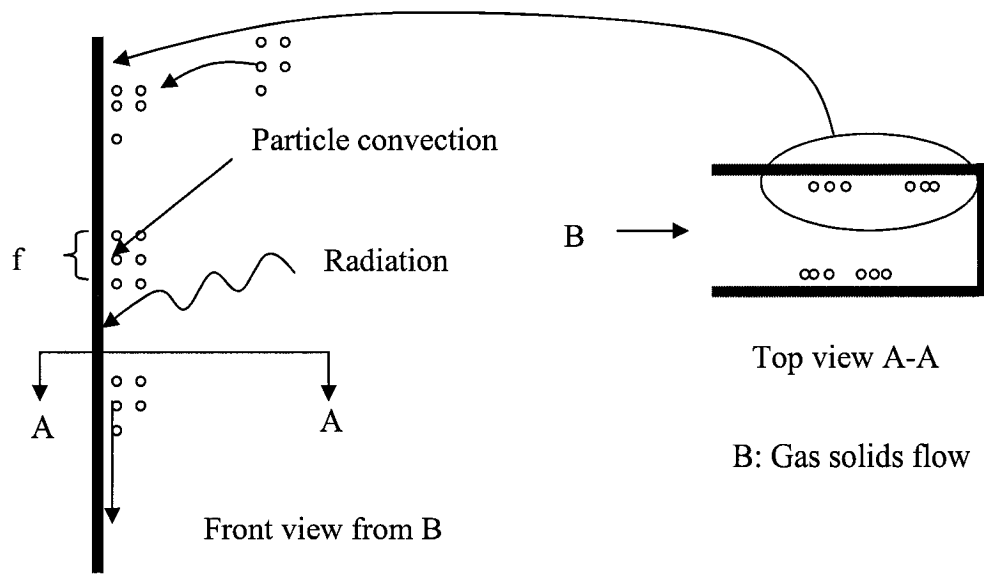


Figure 7.4. Proposed heat transfer mechanism inside the separator

7.3.1.2. Outside the inertial separator:

On the outer wall of the separator, no downwards solids flux was observed. However, the presence of separators at the exit of the riser to the solids recycle system narrows down the flow area and results in a very high gas velocity. This high velocity dominates the heat transfer mechanism which is termed as forced convection. The presence of solids (of the order of 0.001%) in this region also enhances the heat transfer on the surface.

Therefore, the mode of heat transfer outside the separator can be addressed in the form of addition of both forced convection and radiation from the gas as shown in Fig 7.5.

$$h_o = h_{dilute\ convection} + h_{dilute\ radiation} \quad (7.39)$$

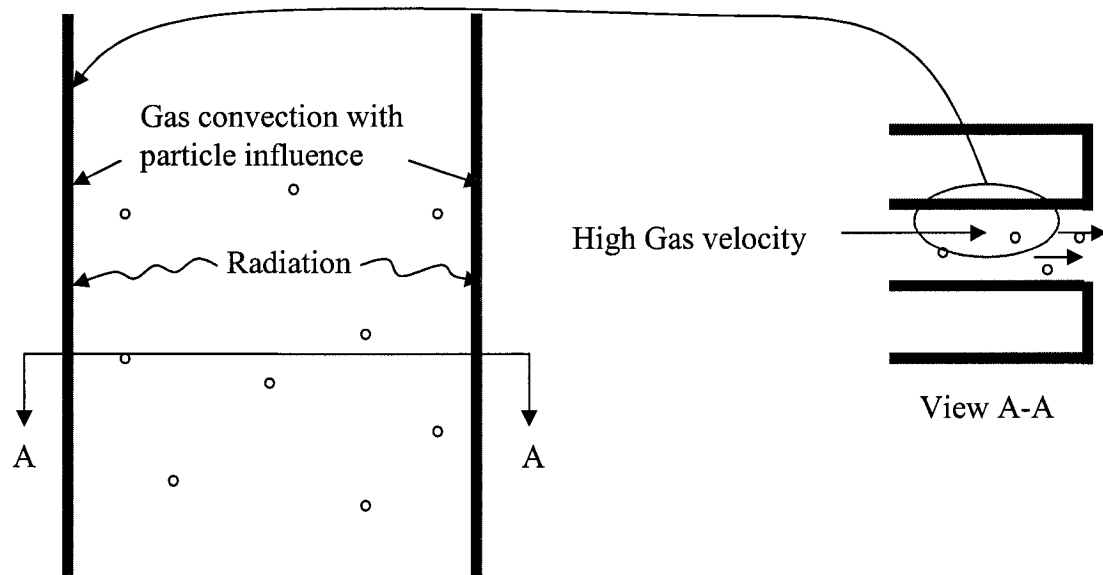


Figure 7.5. Proposed heat transfer mechanism outside the separator

For estimating gas convection, Equation 7.27 can be used by replacing D_{eq} as $D_{eq \text{ separator}}$.

$$h_{\text{gas convection}} = 0.023 C_i C_t \frac{k_g}{D_{eq \text{ separator}}} \text{Re}^{0.8} \text{Pr}^{0.4} \quad (7.40)$$

By assuming zero air velocity within the boundary layer and inside the separator, the gas velocity outside the separator can be estimated by the following equation:

$$U_{\text{separator}} = \frac{Q_{\text{air}}}{\{(L_x - 2\delta) \times (L_y - 2\delta) - NA_{\text{inertial separator}}\}} \quad (7.41)$$

$$\text{i.e; } U_{\text{separator}} = \frac{U_g \times (L_x \times L_y - NA_{\text{inertial separator}})}{\{(L_x - 2\delta) \times (L_y - 2\delta) - NA_{\text{inertial separator}}\}} \quad (7.42)$$

where N is the number of inertial separators inside the riser and

$A_{inertial\ separator}$ is the cross sectional area of the separator.

Therefore, the average heat transfer coefficient on the outer wall can be estimated by incorporating the particle contribution from the equation of Figure 6.10b as:

$$h_{dilute\ convection} = h_{gas\ convection} \left(\frac{\rho_{sus}}{\rho_g} \right)^{0.11} \quad (7.43)$$

For the radiation part, the same equation developed for the wing wall can be used. While calculating the mean beam length, L should be taken as the distance between the two separators.

So, the average heat transfer coefficient on the inertial separator will be:

$$h_{avg} = \frac{h_i + h_o}{2} \quad (7.44)$$

7.4 Results and discussion:

7.4.1. Water wall:

Comparison of two models based on data from commercial boilers is plotted in Figure 7.6. The deviation lies within $\pm 10\%$.

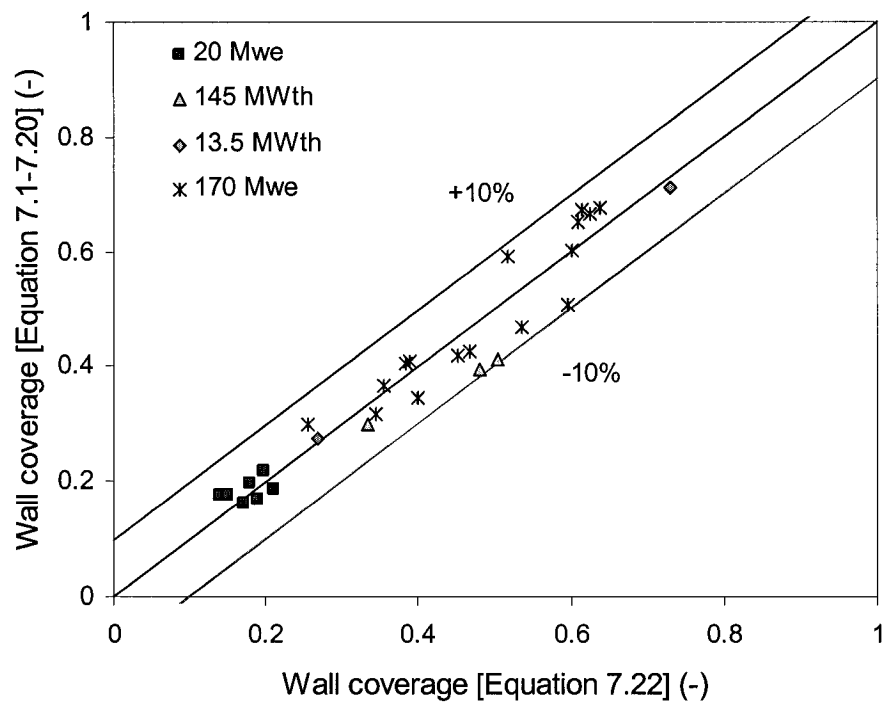


Figure 7.6. Comparison of estimated (Equations 7.1-7.20) versus predicted (Equation 7.22) wall coverage for a number of commercial boilers.

Figure 7.7 presents the predicted heat transfer coefficient with experimental data for the water wall reported by different researchers. A very good agreement is observed which varies within 10%.

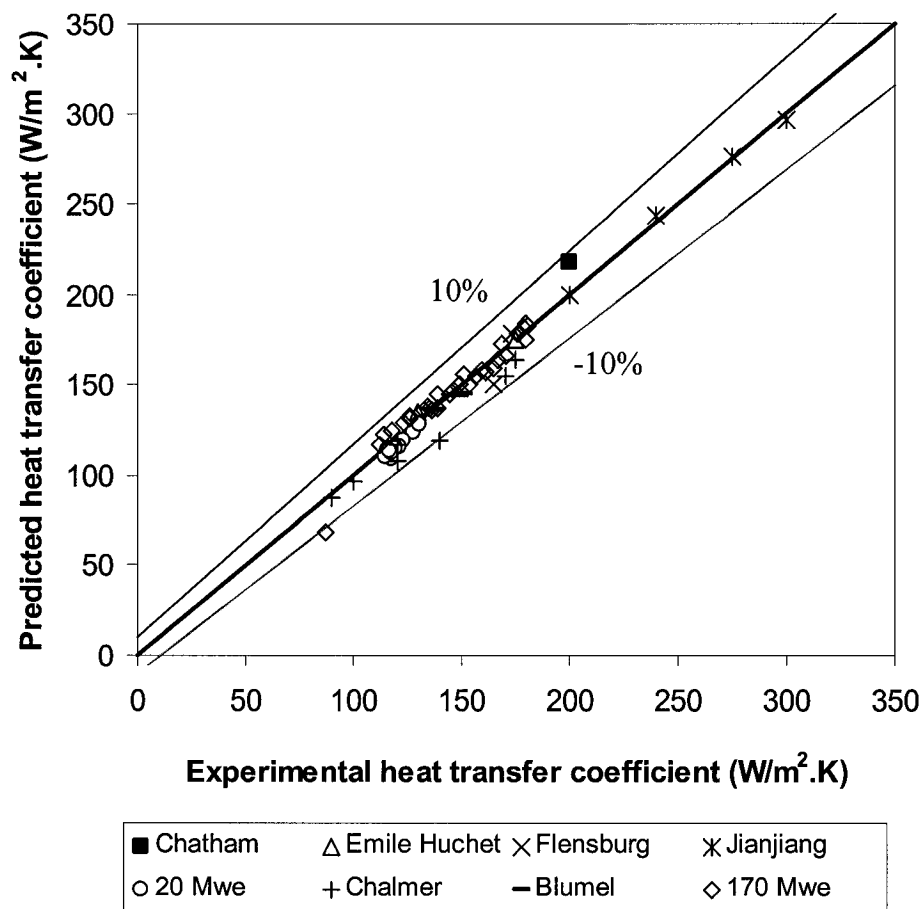


Figure 7.7. Predicted heat transfer coefficient with measured heat transfer coefficient.

7.4.2. Wing wall:

Figure 7.8 shows non-dimensional experimental with non-dimensional predicted heat transfer coefficient for the wing wall of a 170 MW_e power plant (Chapter 3). It agrees well within the experimental uncertainties of 15%.

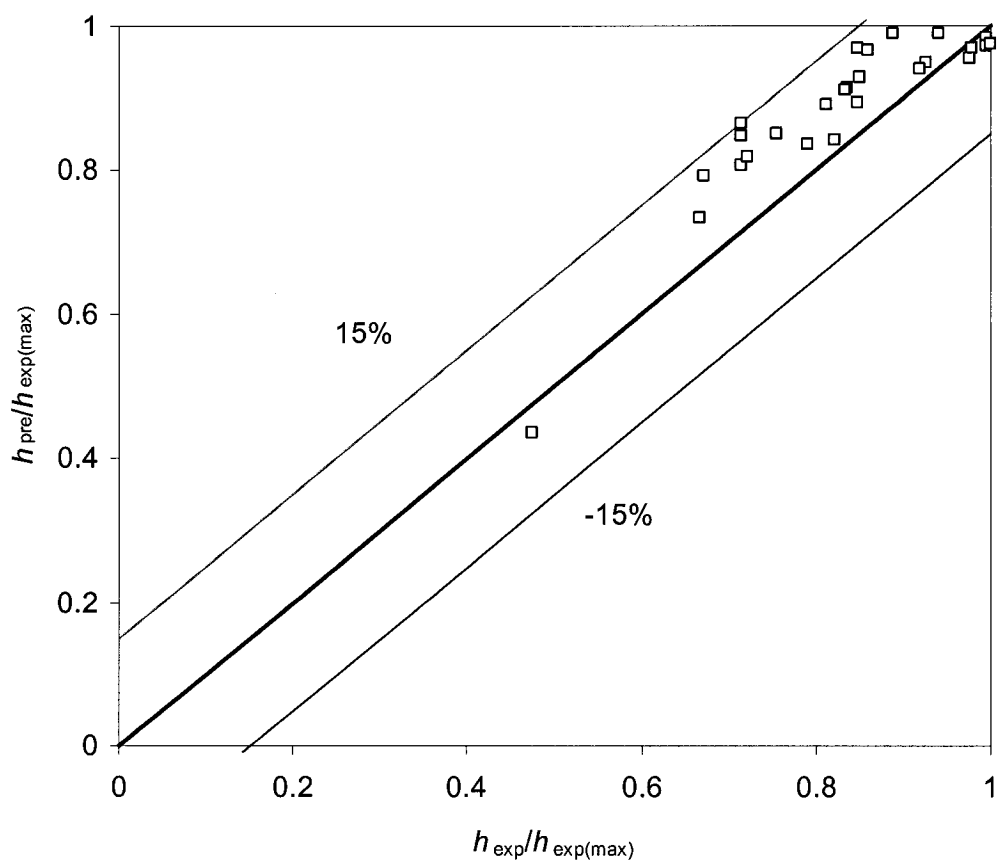


Figure 7.8. Experimental versus predicted heat transfer coefficient for the wing wall

7.4.3. Cavity type inertial separator.

The only available heat transfer data at elevated temperature for this new surface is shown in Table 7.1 (Winaya, 2000).

Table 7.1. Heat transfer data for cavity type inertial separator in a 0.3 MW_{th} pilot plant.

No of test	Superficial velocity (m/s)	Suspension density (kg/m ³)	Bed temp. (C)	Wall temp (C)	Average heat transfer coefficient (W/m ² .C)
1	5.34	6.16	477.3	15	61.52
2	6.11	11.86	477.3	15	72.75
3	7.09	18.97	477.3	15	85.21
4	7.68	23.25	477.3	15	99.6

Figure 7.9 represents predicted heat transfer coefficients with the experimental ones for cavity-type inertial separators. An excellent prediction is observed for the proposed mechanistic model.

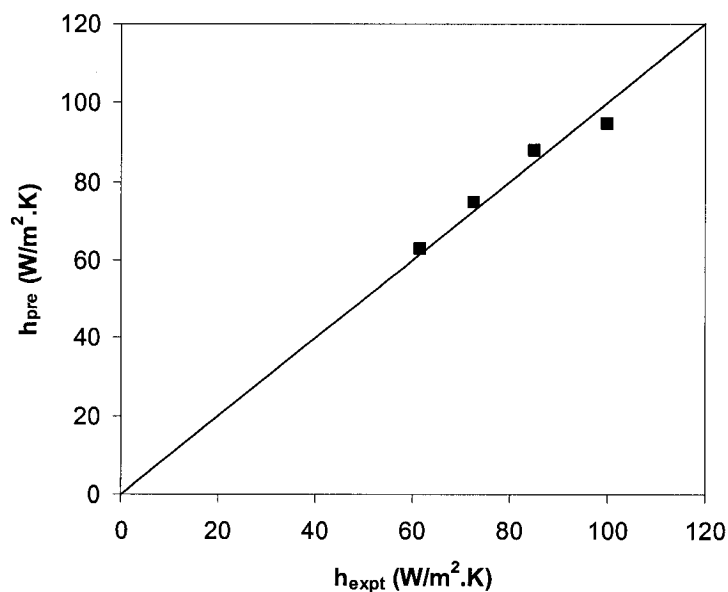


Figure 7.9. Experimental versus predicted heat transfer coefficients for cavity type inertial separators

7.5. Concluding remarks

In this chapter, mechanistic models for wing walls and cavity type inertial separators are developed. A correlation for fractional wall coverage of the water wall is also developed for the commercial boilers by applying the modified Subbarao and Basu (1986) model with recent findings on thermal boundary, non-dimensional gas gap, cluster velocity etc. The following conclusions are drawn.

1. The correlation for fractional wall coverage, developed on the basis of solids concentration averaged over the height of the heat transfer surface and non-dimensional diameter (hydraulic diameter/height of the furnace from secondary air supply) shows a good agreement with the estimated values for a number of boilers.
2. The modified cluster renewal model predicts the heat transfer coefficients for the water walls within $\pm 10\%$ error
3. The mechanistic model for predicting heat transfer coefficient on the wing walls could not be validated against data from independent sources. However, it agrees within $\pm 15\%$ error with the data deduced in chapter 3.
4. The mechanistic model for heat transfer on cavity-type inertial separator predicts very well with the only reported data for a 0.3MW_{th} pilot plant.

Chapter 8

8.0 Overall conclusions and recommendations

The objective of this work was to improve the understanding of the heat transfer mechanisms on different heat transfer surfaces in the CFB loop. Surfaces investigated were wing walls, standpipe walls and innovative cavity-type inertial separators. Based on experimental investigations on those surfaces theoretical models were proposed. In this chapter, the conclusions drawn from the results of three investigations are stated, followed by a discussion of the achievement of the objectives and recommendations for future work.

8.1 Overall Conclusion

In chapter 3, analyses of the data from the commercial units have shown that heat transfer coefficients on the wing wall are always smaller than the heat transfer coefficients on the water wall. The influence of suspension density and furnace temperature on the heat transfer to the wing walls is similar to that on the water walls. Empirical equations developed from the data on commercial units predict heat transfer coefficients on water walls and wing walls within $\pm 15\%$ error.

The chapter 4 considers a CFB pilot plant with a rectangular cross section. The riser has a lower height to hydraulic diameter ratio to simulate an industrial CFB boiler. Experimental investigations has revealed that hydrodynamic conditions on the wing wall are different from that on the water wall. Heat transfer from gas convection is found to be the dominating factor on the wing walls whereas particle convection dominates on the water wall. However, gas convective heat transfer coefficients on the wing wall are found to be higher than those in a single phase flow without free-stream turbulence.

Position of the wing wall in the riser also plays an important role on both hydrodynamics and heat transfer characteristics on the wing wall. A net downwards solids flux is observed when the wing wall is placed at the top whereas a net upwards solids flux is observed when it is placed at the middle of the riser. Due to formation of a stagnant zone, a higher heat transfer coefficient is found at the top corner of the riser. Local lateral heat transfer coefficients on the wing wall show higher values near the wall of the riser than those of the middle, which confirms that a core annulus structure is established in the riser.

Both experimental and theoretical investigations on a square section of a standpipe are presented in chapter 5. Heat transfer coefficients on the dilute section of the standpipe are found lower than those of the dense section for both types of particles investigated. However, heat transfer coefficients on the dilute section of the standpipe are comparable with those on the wing wall. The heat transfer mechanisms on the standpipe are also explored and mechanistic models are proposed, which agree well with the experimental data.

Exploratory research on new heat transfer surface cavity-type inertial separators, are performed in a CFB unit with a rectangular riser in chapter 6. A net downwards solids flux is observed on inner wall of the separators, however no downwards solids flux is observed on the outer wall of the separators. Heat transfer coefficients on the outer wall of the separators are found higher than those on the inner wall of the separators, which is attributed to the gas convection with higher velocity outside the separator. Presence of cavity-type inertial separator in the riser also enhances the heat transfer coefficient on the enclosing water wall. The average heat transfer coefficients on the inertial separator are comparable to those obtained for wing wall and standpipe.

In chapter 7, detailed mechanistic models on the basis of experiments in the pilot plant are developed and used to predict the heat transfer on vertical wall and wing wall in commercial boilers within $\pm 10\%$ error. The mechanistic model proposed for the cavity-

type inertial separators predicts the experimental results from a pilot plant within $\pm 5\%$ error.

8.2. Closure

The objective of this thesis was to understand the heat transfer mechanisms on different available and new heat transfer surfaces in the CFB loop. The purpose was to pinpoint the problems for available heat transfer surfaces and understand their underlying heat transfer mechanisms associated with larger capacity boilers and come up with constructive ideas for new heat transfer surfaces for further improvements. It has been shown that the thesis helped develop some understanding of the heat transfer processes and contributed some data in fields where nothing was available.

Tables 8.1 and 8.2 show the summary of the results of investigations to fill the gap regarding the underlying heat transfer mechanisms. For instance, to overcome design uncertainties of wing wall heat transfer surfaces both empirical correlations and mechanistic models are developed. A further improvement on both empirical correlations and mechanistic models for the water wall is also made.

Two new heat transfer surfaces standpipe and cavity-type inertial separators in the CFB loop of a CFB boiler are proposed and exploratory research is conducted. Mechanistic models are proposed and experimental results of heat transfer on these surfaces are encouraging for an arrangement of these types of heat transfer surfaces in the CFB loop to be worthwhile for a large CFB boiler. Presence of inertial separators in the furnace is also found to enhance the heat transfer on the enclosing wall.

Table 8.1. Summary of the results on cold bed pilot plant and their comparison for a given operating condition

Unit	Location of heat transfer surfaces	Operating condition	Nature of investigation	Average HTC (W/m ² K)	Mode of heat transfer	Reference sections
Pilot plant	Wing wall a) at the top of the riser b) at the middle of the riser	Superficial velocity =3.9 m/s and circulation rate=6 kg/m ² .s	Experimental	a) 69.7 b) 51.4	a) Particle convection Dispersed convection and Radiation b) Dispersed convection and radiation	Section 4.3.3
Pilot plant	Water wall (same position of wing wall at case b)	Superficial velocity =3.9 m/s and circulation rate=6.5 kg/m ² .s	Experimental	75	Particle convection, Dispersed convection and Radiation	Section 4.3.3
Pilot plant	Cavity type inertial separator a) Inner wall of in-furnace separator b) Outer wall of in-furnace separator c) Inner wall of 2 nd row separator	Superficial velocity =4.4 m/s and circulation rate=5.7 kg/m ² .s	Experimental and theoretical	a) 50 b) 105 c) 64.4	a) and c) Particle convection and Radiation b) Dispersed convection and radiation	a) Section 6.3.3.1 b) Section 6.3.3.2 c) Section 6.3.3.4
Standpipe	a) dense section b) dilute section	For Type B, Circulation rate=18 kg/m ² .s	Experimental and theoretical	a) 97 b) 34	a) Particle convection and radiation b) Particle convection, dispersed convection and radiation	Section 5.5.5

Table 8.2. Summary of results on commercial boilers and hot bed pilot plant.

Unit	Location of heat transfer surfaces	Operating condition	Empirical correlation and mechanistic model on average heat transfer coefficients (W/m ² K)	Error
Commercial boiler	Water wall	Part load to full load	Empirical correlation: $h_{ewall} = 3.6 \times \rho_{avg}^{0.37} \times T_g^{0.425}$ (Section 3.5) Mechanistic model: $h_{tot} = f(h_{con} + h_{rad})_{cluster} + (1-f)(h_{con} + h_{rad})_{dilute}$ (Section 7.1.2.1) where $f = 1 - Exp\left[-a\{1-\varepsilon\}^b \left\{\frac{D}{H}\right\}^c\right]$ and $a=4300, b=1.39, c=0.22$.	±15% ±10%
			Wing wall	Part load to full load
0.3 MW _{th} pilot plant	Cavity-type inertial separator	Table 7.1	a) Inside inertial separator: $h_i = f(h_{con} + h_{rad})_{cluster} + (1-f)h_{gas\ radiation}$ (Section 7.3.1.1) b) Outside inertial separator $h_o = h_{dilute\ convection} + h_{dilute\ radiation}$ (Section 7.3.1.2) $h_{dilute\ convection} = h_{gas\ convection} \left(\frac{\rho_{sus}}{\rho_g}\right)^{0.11}$	±5%

8.2 Recommendations for Future Work

The recommendations for future work are as follows:

- a) In order to describe the detailed hydrodynamics of gas solids flow in a CFB riser, a mathematical model needs to be developed with suspended surfaces (wing wall, inertial separators) at the top of the riser.
- b) Since the experimental results on heat transfer for two additional surfaces, inertial separators and standpipe show encouraging results, it is worth carrying experiments in a demonstration plant of a CFB boiler which can be operated at combustion temperature.
- c) More data on heat transfer to the wing walls from large number of commercial units will refine or enhance confidence on the empirical relation developed here.
- d) The investigations on the unit for both wing walls and inertial separators were carried out within a small operating range of operating parameters ($V_s=3.5-4.4$ m/s, $G_s=1-5.8$ kg/m².s). It is recommended to conduct all the experiments for a wider range of operating parameters.
- e) The experiments were carried out for only primary air flow from the bottom of the bed. It is recommended to conduct experiments with secondary air injection to simulate the CFB boilers.
- f) A cost benefit analysis is recommended for use of the cavity-type inertial separators in a CFB both as a heat transfer surfaces and particles separation systems with a view to build a subcompact CFB unit in future.

Literature Cited

- Abrahamsen, A.R., Geldart, D., "Behaviour of gas-fluidized beds of fine powders- part I: homogeneous expansion", *Powder Technology*, vol 26, pp 35, 1980.
- Andersson, B.-A., "Effect of bed particle size on heat transfer in circulating fluidized bed boilers", *Powder Technology*, 87 pp 233-238, 1996.
- Andersson, B.-A., and Leckner B., "Local lateral distribution of heat transfer on tube surface of membrane walls in CFB boilers", in A.A. Avidan (ed.), Proc. 4th Int. Conf. Circulating Fluidized Beds, Hidden Valley, PA, pp 311-318, 1994.
- Andersson, B.-A., and Leckner, B., "Experimental methods for estimating heat transfer in circulating fluidized bed boilers", *Int. J. Heat and Mass Transfer*, 35, 3353-3362, 1992a.
- Andersson, B.-A., and Leckner, B., "Bed-to-wall heat transfer in circulating fluidized bed boilers", Presented at 2nd Minsk International Heat and Mass Transfer Forum, Minsk, USSR, May 1992b.
- Andersson, B. A., Johnsson, F., and Leckner, B., "Heat flow measurements in fluidized bed boilers", in *Proceedings of the 9th International Conference on Fluidized Bed Combustion*, ed. J. P. Mustonen, ASME, New York, 592-598, (1986).
- Bader, R., Findlay, J., and Knowlton, T. M., "Gas/Solid flow patterns in a 30.5-cm-diameter circulating fluidized bed", in: P. Basu, J. F. Large (Eds.), Proceedings of Second International Conference on Circulating Fluidized Beds, Compiègne, France, pp. 123-137, 1988.
- Baskakov, A., Leckner, B., Breitholtz, K., "Complex heat transfer furnaces with a circulating fluidized bed", *Heat Transfer Research*, 32, (7 & 8), pp. 343-348, 2001.
- Basu, P., "Heat transfer in fast fluidized bed combustors", *Chem. Eng. Sci*, 45, 3123-3136, 1990
- Basu, P., and Cheng, L., "An analysis of loop seal operations in a circulating fluidized bed", *Chemical Eng. Res. and Design*, 78 (7), pp. 991-998, 2000.
- Basu, P., and Fraser S. A.; Circulating Fluidized Bed Boilers-Design and Operation, Butterworths-Heinemann, Stoneham, 1991.
- Basu, P., and Konuche, F., in P. Basu and J.F. Large (eds.), "Circulating Fluidized Bed Technology II", Pergamon, Oxford, pp 245, 1988.

- Basu, P., and Nag P.K., "Heat transfer to walls of a circulating fluidized-bed furnace", *Chemical Eng. Sci.*, 51 (1), pp 1-26, 1996
- Basu, P., Kefa, C., and Jestin, L.; "Boilers and Burners Design and Theory", Springer, New York, 1999.
- Basu, P., and Talukder, J., "Revamping of a 120 MW_e pulverized coal fired boiler with circulating fluidized bed firing", paper no 127, 16th International Conf. on FBC, Reno Nevada, USA, 2001.
- Basu, P; Personal communication; 1999
- Basu, P., Nag, P.K.; An investigation into heat transfer in circulating fluidized beds, *International Journal of Heat and mass Transfer* 30 (11) 2399-2409, 1987.
- Belin F., Kavidass, S., Marymchik, M., Walker, D.J., Mandal, A.K., and Price, C.E.; "Update of operating experience of B & W IR-CFB coal fired boilers", 15th International Conf. on FBC, Savannah (FBC 99-0082)USA, 1999
- Berruti, F., Chaouki, J., Godfroy, L., Pugsley, T.S., and Patience, G.S.; "Hydrodynamics of circulating fluidized bed risers: A review", *The Canadian Journal of Chemical Engineering*, 73, pp. 579-602, 1995.
- Bi, H., Jin, Y., Yu, Z., and Bai, D., "An investigation on heat transfer in circulating fluidized bed", in Circulating Fluidized Bed Technology III (Edited by P. Basu, M. Horio, and M. Hasatani), pp. 233-238, Pergamon Press, Oxford, 1991.
- Blumel, W.P., Kaferstein, P., Rummel, A., and Morl, P.; "Wirbelschichtsysteme", VGB conference, 1992.
- Bolton, L.W., and Davidson, J.F., "Recirculation of particles in fast fluidized bed risers" in Circulating Fluidized Bed Technology II (Edited by P. Basu, J.F. Large), pp. 139-146, Pergamon Press, Oxford, 1988.
- Borodulya, V.A., and Teplitsky, Yu.S.; "Prediction of average heat transfer coefficients between a riser's wall and circulating fluidized bed: effect of pressure and temperature", Circulating fluidized bed technology VI, Werther, J (Eds.) (DECHEMA, Germany) pp. 379-384, 1999.
- Botterill, J.S.M, and Desaim, M.; "Limiting factors in gas-fluidized bed heat transfer", *Powder technology*, 6, pp. 231-238. 1972.
- Botterill, J.S.M. and L.N. Hampshire, "The gap between surface and particles in relative motion", *Chem. Eng. Sci.*, 23, pp. 400, 1968.

- Botterill, J.S.M., M.H.D. Butt, G.L. Cain and K.A. Redish; "The effect of gas solids thermal properties on the rate of heat transfer to gas fluidized beds", International Symposium on Fluidization, Netherlands University press, Amsterdam, pp.442, 1967.
- Botterill, J.S.M., M.H.D. Butt, G.L. Cain, R. Chandrasekhar and J.R. Williams; "Enhanced heat transfer by the control of particle circulation past heat transfer surfaces in gas fluidized beds", International Symposium on Fluidization, Netherlands University press, Amsterdam, pp.458, 1967.
- Boyd, T.J., and Friedman, M.A.; "Operation and test program summary at the 110 MWe Nucla CFB", in Circulating Fluidized Bed Technology III (Edited by P. Basu, M. Horio, and M. Hasatani), pp. 297-312, Pergamon Press, Oxford, 1991.
- Breitholtz, C., and Lackner, Bo.; "Heat transfer in circulating fluidized bed boilers-do we know sufficiently?", Trends in Heat, Mass & Momentum Transfer, 3, pp. 85-104, 1997.
- Breitholtz, C., Leckner, B., and Baskakov, A.; "Wall average heat transfer in CFB-boilers", Proc. III European Conf. on Fluidization, Toulouse-France, 2000
- Breitholtz, C.; "Heat transfer in circulating fluidized bed boilers", PhD thesis, Chalmers University of Technology, Goteborg, Sweden, 2000.
- Brewster, M.Q., "Effective absorptivity and emissivity of particulate medium with application to a fluidized bed", Trans. Of ASME, New York, 108, August, pp. 710-713, 1986
- Caloz, Y., Reh, L., Cahen, C., Evrad, R., and Piedfer, O., "Local solids velocities and their fluctuations in CFB units of different sizes", in Circulating fluidized bed technology VI, Werther, J (Eds.) (DECHEMA, Germany) pp. 849-854, 1999.
- Chen, C.C, and Chen, C.L; "Experimental study on the bed-to-wall heat transfer in a circulating fluidized bed", Chem. Engg. Sci. 47, 1017-1025, 1992.
- Chen, J.C., Cimini, R. J. and Dou, S. S.; "A theoretical model for simultaneous convective and radiative heat transfer in circulating fluidized bed, in Circulating Fluidized Bed Technology II (Edited by P. Basu and J. F. Large), pp. 255-262, Pergamon Press, Oxford, 1988.
- Colakyan, M., and Levenspiel, O.; "Heat transfer between moving bed of solids and immersed cylinders", Klinzing, G.E. (Eds), Fluidization and fluid particle systems: Recent Advances, AIChE Symposium Series, (Twin Production and Design, USA) pp. 156-168. 1984.

- Couturier M.F, Steward F.R., and Poolpol, S.; “Experimental determination of heat transfer coefficients in a 72 MW_t circulating fluidized bed boiler”, in L. Rubow and G. Commonwealth (eds.), Proc. 12th Int. Conf. Fluidized Bed Combustion, ASME, pp 1215-1222, 1993.
- Deissler, R.G., and Boegli, J.S.; “An investigation of effective thermal conductivities of powders in various gases” *Trans. ASME* 80, 1417, 1958.
- Denloye, A.O.O., Botterill, J.S.M.; “Heat transfer in flowing packed bed”, *Chem. Eng. Sci.* 32, pp 461-465, 1977.
- Dittus, F. W and Boelter, L. M. K., “Heat transfer in automobile radiators of the tubular type”, *Univ. Calif. Pub. Eng.*, 13, 443, 1930.
- Divilio, R.J., and Boyd T.J.; “Practical implications of the effect of solids suspension density on heat transfer in large-scale CFB boilers”, in Proc. 4th Int. Conf. Circulating Fluidized Beds, Hidden Valley, PA, pp. 334-339, 1994.
- Ebert. E.R., Glicksman. L.R., and Lints, M.; “Determination of particle and gas convective heat transfer component in circulating fluidized bed”, *Chemical Engineering science* 48, 1993, pp. 2179-2188, 1993.
- Ergun, S., 1952, “Fluid flow through packed columns”, *Chemical Engg. Progress*, 48 (2), pp. 89-94.
- Fraley, L.D., Lin, Y.Y., Hsiao, K.H. and Slobakken, A., “Heat transfer coefficient in a circulating fluidized reactor”, ASME paper 83-HT-92.
- Furchi, J.C.L., Goldstein, L., Lombardi, G. and Mosheni, M., “Experimental local heat transfer in circulating fluidized bed”, in Circulating Fluidized Bed Technology II (Edited by P. Basu and J. F. Large), Pergamon press, Oxford, pp. 263-270, 1988.
- Gelperin, N. I., and Einstein, V. G.; “Heat transfer in fluidized beds”, in Fluidization, ed. J.F. Davidson and D. Harrison, Chapter 10, Academic press, New York, (1971)
- Gidaspow, D., Tsuo, Y.P., and Luo, K.M., “Computed and experimental cluster formation and velocity profiles in circulating fluidized beds”, in Fluidization VI (Edited by J.R. Grace, L.W. Shemilt and M.A.Bergougnou), Engineering Foundation, New York, 1989.
- Glicksman, L.R.; “Circulating fluidized bed heat transfer”, in Circulating Fluidized Bed Technology II (Edited by P. Basu and J. F. Large), Pergamon press, Oxford, pp. 13-29, March, France, 1988.

- Glicksman, L.R., Westphalen, D; "Lateral solid mixing measurements in circulating fluidized beds" *Powder Technology*, 82, pp. 153-167, 1994.
- Glicksman, L.R.; "Heat transfer in circulating fluidized beds", in: J.R. Grace, A.A. Avidan, TM Knowlton (Eds.), Circulating Fluidized Beds, Chapman & Hall, London, pp. 261-310, 1997.
- Gloski, D., Glicksman, L.R. and Decker, N.; "Thermal resistance at a surface in contact with fluidized bed particles", *International Journal of Heat and Mass Transfer*, 27, 599-610, 1984.
- Golriz, M.R., and Sunden, B., "An experimental investigation of thermal characteristics in a 12 MW_{th} CFB boiler", *Expt. Heat Transfer*, 7, 217-233, 1994.
- Golriz, M.R., "Thermal boundary layer in circulating fluidized bed boilers", In. Proc. Int. Sump. Eng. Foundation "Fluidization VIII", Tours, V. 1, pp. 185-192, France, 1995.
- Golriz, M.R., and Grace, J.R.; "Predicting heat transfer in large-scale CFB boilers", Circulating fluidized bed technology VII, (Grace, J.R., Zhu, J., and Lasa, H.d) (Eds.) (Niagara Falls, Canada) pp. 121-128, 2002.
- Greenfield Research Inc; "Method of adopting fossil fuel fired boilers into CFB and novel CFB firing boilers", patent no: 2,159,949, Canada, 2002.
- Harakas, N.K., and K.O. Beaty, Jr.; "Moving bed heat transfer: effect of interstitial gas with fine particles", *Chem. Eng. Prog. Symp. Ser.*, 59, (41), pp.122-128, 1963.
- Harris, B.J., Davidson, J.F., and Xue, Y.; "Axial and radial variation of flow in circulating fluidized bed risers", in Proc. 4th Int. Conf. Circulating Fluidized Beds, Hidden Valley, PA, pp. 103-110, 1994.
- Hartge, E.-U., Rensner, D., and Werther, J., "Solids concentration and velocity patterns in a circulating fluidized beds", in: P. Basu, J. F. Large (Eds.), Proceedings of Second International Conference on Circulating Fluidized Beds, Compiegne, France, pp. 165-180, 1988.
- Hartge, E-U., Werther, J., and Wiesendorf, V., "The influence of scale on solids flow and solids concentration at the wall of a CFB combustor", in Circulating fluidized bed technology VII, (Grace, J.R, Zhu, J, and Lasa, H.D.) J (Eds.) (Niagara Falls, Canada) pp. 325-332, 2002.
- Holman J. P., "Heat Transfer" 8th Edition, McGRAW-HILL, INC. 1997.
- Horio, M; "Hydrodynamics", in: J.R. Grace, A.A. Avidan, TM Knowlton (Eds.), Circulating Fluidized Beds, Chapman & Hall, London, pp. 21-85, 1997

- Horio, M., Morishita, K., Tachibana, O., and Murata, N., "Solid distribution and movement in circulating fluidized beds", in Circulating Fluidized Bed Technology II (Edited by P. Basu and J. F. Large), Pergamon press, Oxford, pp. 147-154, March, France, 1988.
- Hussainov, M., Kartushinsky, A., Mulgi, I. A., Shcheglov, S. Tisler; "Experimental study of two-phase flow past various bodies and deposition of solid particles on the surfaces", Advances in Engineering Heat transfer pp. 267-276.
- Issangya, A.S., Bai, D., Bi, H.T., Lim K.S., Zhu. J., and Grace J.R., "Suspension Densities in a High Density Circulating Fluidized Bed Riser", Chemical Engineering Science, 54, pp 5451-5460, 1999.
- Ishii, H., Nakajima, T., & Horio, M.; "The clustering annular flow model of circulating fluidized beds", Journal of Chemical Engineering of Japan, 22, pp. 484-490, 1989.
- Jestin L, Meyer P., Schmitt C. and Morin J.X.; "Heat transfer in a 125 MWe CFB boiler", in the *proceedings of the VII International Conference on Fluidization*, May, Broadbeach, Australia, 1992.
- Jiang, P. and Fan, L.S., "On the Turbulent Radial Transfer of Particles in a CFB Riser", 6th Int. Conf. Circulating Fluidized Beds, Ed. J. Werther, DECHEMA, Frankfurt, pp. 83-88, 1999
- Johnsson, F., Andersson, B. A., and Lackner, B.; "Heat transfer in circulating fluidized bed boilers", Minsk International Heat and mass transfer Forum, May, Minsk, USSR, 1988.
- Johnsson, F., Andersson, B. A., and Lackner, B.; "Heat transfer in FBB-discussion on models", Presented at IEA Meeting on mathematical Modeling on AFBC in Boston, May 1987.
- Jones P.J. and Leung L.S.; "Downflow of solids through pipes and valves", in J.F. Davidson, R. Clift, D. Harrison (Eds.), Fluidization, Chapter 8, Academic Press Inc. London, 1985,
- Kiang, K.D., Liu, K.J., Nack, H. and Oxley, J.H., Fluidization Technology, Vol. II (Edited by D.L. Kearins), Hemisphere, Washington-DC, pp. 471, 1976.
- Knowlton, T. M.; "Standpipes and return systems", in: J.R. Grace, A.A. Avidan, T.M. Knowlton (Eds.), Circulating fluidized beds, Chapter 7, Chapman & Hall, London, pp. 214-260, 1997.

- Kobro, H., and Brereton, C., "Control fuel flexibility of circulating fluidized beds", in Circulating Fluidized Bed Technology (Edited by P. Basu), Pergamon Press, Toronto, pp. 262-272, 1986.
- Kolar, A.K, and Sundaresan, R., "Surface length effect on heat transfer in the core of a circulating fluidized bed riser", Circulating fluidized bed technology VII, (Grace, J.R., Zhu, J., and Lasa, H.d) (Eds.) (Niagara Falls, Canada) pp. 105-110, 2002.
- Kudo, K., Taniguchi, H., Kaneda, H., Yang, W., Zhang, Y., Guand, K. H. and Matsumura, M., "Flow and heat transfer simulation in circulating fluidized beds", in Circulating Fluidized Bed Technology III (Edited by P. Basu, M. Horio, and M. Hasatani), pp. 269-274, Pergamon Press, Oxford, 1991.
- Kunii, D., and Levenspiel, O.; "Effect of exit geometry on the vertical distribution of solids in circulating fluidized beds. Part I: solution of fundamental equations; Part II: analysis of reported data and prediction", Powder Technology, 84, pp. 83-90, 1995.
- Leckner, B., and Andersson, B.A; "Characteristic features of heat transfer in a circulating fluidized bed boilers", Powder Technology, 70, pp. 303-314, 1992.
- Leckner, B.; "Heat transfer in circulating fluidized bed boilers", in Circulating Fluidized Bed Technology III (Edited by P. Basu, M. Horio, and M. Hasatani), pp. 27-38, Pergamon Press, Oxford, 1991.
- Lehner, P., and Writh, K.E.; "Heat transfer in a co-current downflow circulating fluidized bed", Circulating fluidized bed technology VI, Werther, J (Eds.) (DECHEMA, Germany) pp. 337-342, 1999.
- Leu, L.P., Hsia Y.K., and Chen, C.C.; "Wall to bed heat transfer in a turbulent fluidized bed", AICHE Symposium Series, 93 (317), pp. 83-86, 1997.
- Lim, K. S., Zhu, J. X., Grace, J. R.; "Hydrodynamics of Gas-Solid Fluidization" Int. J. Multiphase Flow vol 21, pp. 141-193, Pergamon. 1995
- Lim, K.S., Zhou, J., Finley, C., Grace, J.R., Lim, C.J., and Brereton, C.M.H.; "Cluster descending velocity at the wall of circulating fluidized bed risers", Proceedings of the 5th International Conference on Circulating Fluidized Beds, Beijing, China, 1996.
- Lints, Michael. C., and Glicksman, L. R., Parameters governing particle to wall heat transfer in a circulating fluidized bed, Circulating Fluidized Bed Technology IV, ed. A. A. Avidan, 297-304, 1994.
- Liu, J, P., Galvin, K. P., Tian, J., and Huan, B.; "Tube to solids heat transfer rate in the solids return standpipe of a circulating fluidized bed", Circulating fluidized bed technology VI, Werther, J (Eds.) (DECHEMA, Germany) pp. 343-348, 1999.

- Luan, W., Lim, C. J., Bereton, C. M. H., Bowen, B. D., Grace, J. R.; "Experimental and theoretical study of total and radiative heat transfer in circulating fluidized beds", *Chemical Engineering science* 54 3749-3764, 1999.
- Mahalingam, M. and Kolar, A. K.; "Heat transfer model for the membrane wall of a high temperature circulating fluidized bed", in Circulating Fluidized Bed Technology III (Edited by P. Basu, M. Horio, and M. Hasatani), pp. 239-246, Pergamon Press, Oxford, 1991a.
- Mahalingam, M. and Kolar, A. K.; "Emulsion layer model for wall heat transfer in a circulating fluidized bed", *A.I.Ch.E. J.* 37, 1139-1150, 1991b.
- Martin, H., "Heat transfer between gas fluidized beds of solid particles and the surfaces of immersed heat exchanger elements", *Chemical Engineering Progress*, 18, 157-223, 1984.
- Mickley, H.S., and Fairbanks, D. F.; "Mechanism of heat transfer to fluidized beds", *AIChE Journal*, 1, pp. 374-384, 1955.
- Mickley, H.S., Trilling, G.C. A.; "Heat transfer characteristics of fluidized beds", *Ind. Engg. Chem.* 41, pp 1135-1147, 1949.
- Molerus O. and Writh, K.-E.; "..." in Heat transfer in fluidized beds, 1st ed., Chapman & Hall, London, pp. 111-151, 1997.
- Moran, J. C., and Glicksman, L. R.; "Gas velocities and gas boundary layers inside a riser of a circulating fluidized bed", in: Donald W. Geiling (Ed.), 16th FBC Conference on Fluidized Bed combustion, (FBC 01-0027) Reno, Nevada 2001.
- Mosyak, A., Pogrebnyak, E., Hetsroni, G.; "Effect of constant heat flux boundary condition on wall temperature fluctuations", *Journal of Heat Transfer* 123 (2) 213-218, 2001.
- Muchowski, E. and E. Mannchen, "Heat transfer from the bottoms of vibrated vessels to stirred packings of spheres at atmospheric pressure under vacuum" *Int. Chem. Eng.*, 20, 577, 1980.
- Nag, P.K., and Ali Moral, M.N., "Effect of probe size on heat transfer at the wall in circulating fluidized beds", *Int. J. Energy Res.* 14, pp. 965-974, 1990a.
- Nag, P.K., and Ali Moral, M.N., "The influence of rectangular fins on heat transfer in circulating fluidized beds", *J. Inst. Energy, London*, 63, pp. 143-147, 1990b.

- Nowak, W., Arai, N., Hasatani, M., Bis, Z. and Busoul, M., "Stochastic model of heat transfer in circulating fluidized bed", Proceedings of the 4th SCEJ Symposium on Circulating Fluidized Bed, Tokyo, December, pp.19-29, 1991.
- Noymer, P. D., and Glicksman, L. R.; "Cluster motion and particle convective heat transfer at the wall of a circulating fluidized bed", *Int. J. Heat Mass Transfer*, 41 (1), pp. 147-158, 1998.
- Noymer, P.D., and Glicksman, L.R.; "Descent velocities of particle clusters at the wall of a circulating fluidized bed", *Chem. Eng. Sci.*, 55, pp. 5283-5289, 2000.
- Perry, R.H., Green, D.W. and Maloney, J.O., "Heat Transmission" in Perry's chemical engineering hand book, sixth edition, pp 10-17, 1984.
- Qi, C. and Farag, I. H., "Heat transfer mechanism due to particle convection in circulating fluidized bed, preprint volume, 4th International Conference on CFB, Aug 1-5, Pittsburg, USA, pp. 396-401, 1993.
- Qi, C. and Farag, I.H., "Lateral particle motion and its effect on particle concentration distribution in the riser of CFB", *AIChE Symp. Ser.* 89, pp 73-80, 1993
- Rashidi, M., Hetsroni, G., Banarjee, S.; "Particle-turbulence interaction in a boundary layer", *Int. J. Multiphase Flow* 16 (5) 935-949, 1990.
- Rhodes, M.J., Laussmann, P., Villain, F., Geldart, D.; "Measurement of radial and axial solids flux variations in the riser of a circulating fluidized bed", in: P. Basu, J. F. Large (Eds.), Proceedings of Second International Conference on Circulating Fluidized Beds, Compiègne, France, pp. 155-164, 1988.
- Rhodes, M.J., "Modeling the flow structure of upward flowing gas-solid suspensions", *Powder Technology*, 60, pp. 27-38, 1990.
- Rhodes, M., Mineo, H., and Hirama, T.; "Particle motion at the wall of a circulating fluidized bed", *Powder Technology*, 70, pp. 207-214, 1992.
- Rogers, C. B., Eaton, J. K.; "The behavior of solid particles in a vertical turbulent boundary layer in air", *Int. J. Multiphase Flow* 16 (5) 819-834, 1990.
- Saha, S.K., Basu, P. and Dutta, A., "Performance of a novel horizontal gas-solid separator in a circulating fluidized bed riser", in the Proceedings of Circulating Fluidized Bed Technology VII Conference edited by Grace, J. R., Zhu, Z-X and Lasa H. D., Niagara falls, Ontario, Canada, 2002.

- Sekthira, A., Lee, Y. Y. and Genetti, W. E.; "Heat transfer in circulating fluidized bed", Proceedings of the 25th National Heat Transfer Conference, Houston, Texas, 24-27 July, 1988.
- Stromberg, L., "Fast fluidized bed combustion of coal", in Proceedings of the 7th International Conferences on Fluidized Bed Combustion, DOE/METC-83-48, NTIS, Vol.2, pp. 1152-1163, 1983
- Subbarao, D. and Basu, P.; "A model for heat transfer in circulating fluidized beds", *Int. J. Heat and Mass Transfer* 29, 487-489, 1986
- Sullivan, W.N. and R.H. Sabershy; "Heat transfer to flowing granular media", *Int. J. Heat and Mass Transfer*, 18, 97, 1975.
- Tang J.T., and Engstrom, F.; "Technical assessment on the Ahlstrom pyroflow circulating and conventional bubbling fluidized bed combustion systems", Proc. 9th Int. Conf. Fluidized Bed Combustion, 1, ASME, New York, pp 38-54, 1987
- Wang, T., Lin, J., Zhu, J., Liu, D.C., and Saxena, S.C., "Particle velocity measurements in a circulating fluidized bed", *A.I.Ch.E. Journal*, 39, pp. 1406-1410, 1993.
- Wen, C. Y., and Miller, E.; "Heat transfer in solid-gas transport lines", *Journal of Industrial Engineering Chemistry*, 53, 51-53, 1961.
- Werdermann, C.C. and Werther J., "Heat transfer in large scale circulating fluidized bed combustors of different sizes, in *Circulating Fluidized Bed Technology IV* (ed. Avidan), pp. 428-435, AIChE, New York, 1994.
- Winaya. N. S., "Heat transfer investigations in atmospheric and pressurized circulating fluidized bed units" M. Sc. Thesis, Dalhousie University, 2000.
- Wirth, K.E., and Seiter, M., "Solids concentration and solids velocity in the wall region of circulating fluidized beds, *Proceedings of the 1991 International Conference on Fluidized Bed Combustion* (Edited by E.J. Anthony), Vol. 1, pp. 311-316, Montreal, 1991.
- Wu, R. L., Lim, C. J., Chaouki, J., Grace, J. R.; "Heat transfer from a circulating fluidized bed to membrane waterwall surfaces", *AIChE Journal* 33 1888-1893, 1987.
- Wu, R.L., Grace, J.R, and Lim, C.J.; "A model for heat transfer in circulating fluidized beds", *Chem. Eng. Sci.* 45, 3389-3398, 1990b.
- Wu, R.L., Grace, J.R, Lim, C.J., and Brereton, C.M.H.; "Suspension to surface heat transfer in a circulating fluidized bed combustor", *AIChE Journal* 35 (10) 1685-1691, 1989a.

- Wu, R.L., Lim, C.J., and Grace, J.R.; "The measurement of instantaneous local heat transfer coefficients in circulating fluidized bed", *Canadian J. Chem. Eng.* 67 301-307, 1989b.
- Wu, R.L., Lim, C.J., Grace, J.R., and Brereton, C.M.H.; "Instantaneous local heat transfer and hydrodynamics in a circulating fluidized bed", *Int. J. Heat and Mass Transfer*, 34 pp. 2019-2027, 1990a.
- Wunschmann, J. and E.U. Schlunder; "Heat transfer from heated surfaces to spherical packings", *Int. Chem. Eng.*, 20, 555, 1980.
- Xavier, A.M., and Davidson, J.F.; "Heat transfer in fluidized beds: Convective heat transfer in fluidized beds", in J.F. Davidson, R. Clift, D. Harrison (Eds.), Fluidization, Chapter 13A, Academic Press Inc. London, pp, 443, 1985.
- Xiaozhong, J., Junfu, L., Quing, L., Yong, Li., Jiansheng, Z., Xing, X., and Guangxi, Y.; "Investigation on the heat transfer in a CFB boiler", Circulating fluidized bed technology VI, Werther, J (Eds.) (DECHEMA, Germany) pp. 355-360, 1999.
- Xu, G., Nomura, K., Nakagawa, N., and Kato, K.; "Hydrodynamic dependence on riser diameter for different particles in circulating fluidized beds", *Powder Technology*, 113 pp. 80-87, 2000.
- Yagi, S., and Kunii, D.; "Studies on effective thermal conductivities in packed beds", *AIChE Journal*, 3, pp. 373-380, 1957.
- Yang, Y., Jin, Y., Yu, Z., Wang, Z. and Bai D., "The radial distribution of local particle velocity in a dilute circulating fluidized bed, ", in Circulating Fluidized Bed Technology III (Edited by P. Basu, M. Horio, and M. Hasatani), pp. 201-206, Pergamon Press, Oxford, 1991a.
- Yang, H., and Gautam, M., "Experimental study on the interface of core-annulus flow in the riser of a circulating fluidized bed", *Powder Technology*, 85, pp. 57-64, 1995.
- Yenming, Z., Gantang, C. and Zhangmao, W.; "A model for bed-to-surface heat transfer in circulating fluidized beds", *J. Chem. Ind. Engg (China)*, 1-11, 1989.
- Zevehoven, R., Kohlmann, J., Laukkanen, T., Tuominen, M., and Blomster, A.M., "Suspension-to-wall heat transfer in CFB combustion: near wall particle velocity and concentration measurements at low and high temperatures", in Circulating fluidized bed technology VI, Werther, J (Eds.) (DECHEMA, Germany) pp. 349-354, 1999.
- Zhang, H., Huang, W.X., and Zhu, J.X.; "Gas-solids flow behavior: CFB riser vs. downer", *AIChE Journal*, 47 (9), pp. 2000-2011, 2001.

- Zhang, W., "Fluid dynamic of the transport zone of circulating fluidized beds-with application to boiler", PhD thesis, Chalmers University of Technology, Goteborg, Sweden, 1995.
- Zheng, Q., Wang, X., and Li, X., "Heat transfer in circulating fluidized beds", in Circulating Fluidized Bed Technology III (Edited by P. Basu, M. Horio, and M. Hasatani), pp. 263-268, Pergamon Press, Oxford, 1991a.
- Zhou, J., Grace, J.R., Qin, S., Brereton, C.M.H., Lim, C.J. and Zhu, J., "Voidage Profiles in a Circulating Fluidized Bed of Square Cross-Section", Chem. Engg. Sci., Vol. 49, No. 19, pp 3217-3226, 1994.
- Zhou, J., Grace, J.R., Brereton, C.M.H., and Lim, C.J., "Particle velocity profiles in a circulating fluidized bed riser of square cross-section", Chem. Engg. Sci., Vol. 50, pp 237-244, 1995.
- Ziegler, E.N., Koppel, L. B. and Brazelton, W. T., "Effects of solid thermal properties on the heat transfer to gas fluidized beds", Ind. Eng. Chem. Fund. 3, 324-328, m. Fund. 3, 324-328, 1964.

Appendices

Appendix A

Construction of CFB pilot Plant at CFB Laboratory

1. Introduction

A multipurpose test rig was designed and constructed with which studies will be made that lead to better appreciation of the revamping technology. The end uses of the test rig are:

1. To gain understanding of the complex hydrodynamics of the CFB technology by visualization and to do some research on its parameters (ex: solid circulation rate, bed inventory, fluidization velocity etc.).
2. To do research on the influence of different parameters on material failure.
3. To understand the revamping technology.
4. To understand some key components of CFB (new as well as revamped) boilers (ex: inertial separator, horizontal cyclone, loopseal).

Since the unit was to be sent to India ultimately, measures were taken to build a modular model with flexible joints that allowed easier assembling and disassembling. Clear plastic (plexi-glass, Lexan) is used to visualize the complex hydrodynamics inside the unit. The major change required to revamp from a PC boiler to a CFB boiler is the incorporation of the cyclone. The difficulties associated with conversion are making room for the cyclone in an old PC boiler without major change of the space envelope. In a revamping project modifications should also be made with a minimum level of investment. To accommodate these restrictions, a horizontal cyclone was designed at the Dalhousie University CFB lab. The compact size of this cyclone made it more attractive to use in a revamping project.

This report lays out the design criteria and construction of the cold multipurpose test rig and gives the procedures for operating the rig. Finally it describes the commissioning of the rig.

2 Design Constraint:

The unit was built in the CFB lab at DalTech which had space limitations. Modifications to the lab space (example: the coal crusher and lime stone room was converted into a bag house) were made. After taking necessary measurements it was found that it was possible to build a rectangular cross section of 500 (mm) X 1000 (mm) and a riser column of 5000 (mm) height along with other accessories in the available space.

3 Design and Construction:

3.1 Fan selection:

Once the cross section of the riser column was determined it was easier to select a fan with respect to flow rate by assuming a superficial air velocity. The more difficult part was the pressure head that is required at the designed flow rate. Through various experiments and past experience a fan of 5400 CFM with the delivery head of 45 inch water column was chosen for this experimental set-up. It was possible to operate the fan at the desired flow rate within the limit. A fan characteristic curve is attached. Fan parameters are given in Table-A1.

Table-A1: Fan parameters

Volume (ACFM)	ΔP (inch w.g)	BHP	RPM	Density of air (lb/cu.ft)	Temp. (F)	Alt (ft)
5,400	44.93	59	3,550	0.075	70	0

Manufacturer: Northern Industrial

Model No: 2612A60

Motor Mounting 60 HP 3600 RPM 3/60/575 ODP Motor

3.2 Riser column:

A rectangular cross-section riser column was selected because furnaces of real boilers are rectangular in shape. For better appreciation and understanding of the circulating fluidized bed technology, visualization of results of different operating techniques will play a major role. Keeping this in mind measures were taken to build a test unit which would allow visualization of the complex flow pattern of the gas solid (hydrodynamics). Also the essential shifting of the unit to India when the project is completed had to be considered. There were three ways to construct the unit.

1. Make the four walls of the riser column of clear plastic (LEXAN).
2. Make the three walls of the riser column of mild steel and front wall with clear plastic (LEXAN).
3. Make the three walls of the riser column of wood and front wall with clear plastic (LEXAN).

The last of the above was considered best for two reasons. Firstly, the construction cost is less due to material cost and the labour cost. Secondly, assembling and disassembling will be easier because of flexible joints. So the body of the riser column is constructed with

angle bar (steel), wood and aluminum sheet and clear plastic (LEXAN). Channel bars and flat bars are used as reinforcement for the front face. The pressure drop in the riser column is estimated as 23 inch of H₂O. See drawing no A1 and A2 for detailed construction.

3.3 Windbox:

This is made of 3-mm thick mild steel sheet. Reinforcement is used to increase its strength. For uniform distribution of the air in the windbox, the bottom surface is inclined. A sand-removing gate is installed to remove the sand from the box after operating the unit if there is any. A detailed drawing is attached in drawing A2 (C(2-3), D(2-3) and E(2-3)).

3.4 Distributor plate:

There are different types of distributor plates available at present. Effort had been given to design and fabricate the simplest distributor plate and a perforated grid type distributor plate was designed and fabricated. A 10 mm thick mild steel plate was used and 1377 holes of 9.5 mm (3/8 inch) diameter were made which resulted in a percentage of open space of the plate of 20%. A wire mesh of 60 meshes per lineal inch with 21.3% open area was clamped on the top of the distributor plate to restrict the downwards sand flow. The plate is press fit with windbox and the riser. Provision was made for easy handling of the distributor plate if required. A detailed drawing is attached in drawing A2 (1(2-3) and 2(2-3)).

3.5 Inertial separator and Horizontal cyclone

A solids separator is an integral part of a CFB boiler. In the revamping technology of a PC boiler to a CFB boiler, it is the area where innovative ideas can be used. Two separators are recommended in series an inertial separator and a horizontal cyclone.

The inertial separator separates solids from the gas through impingement on collecting bodies arranged across the path of the gas solids mixture. Low thermal inertia, simpler construction, low pressure drop, easy scale up and lower cost are major attractions of inertial separators. The disadvantage is their lower efficiency of collecting particles.

The main attraction associated with the horizontal cyclone is its compactness, high efficiency (virtually 97.5% to 99.5% for 220 μm sand for a laboratory unit). The disadvantage of this cyclone is its relatively higher pressure drop than that of the inertial separator (500-200 Pa). This is a newly designed cyclone which is not available in CFB literature as well as in commercial boilers.

An innovative idea in the revamping process is that one can use these solid separators for two purposes.

1. Collecting particles
2. Heat transfer surfaces (super heater, reheater)

The rationale of item no 2 is that it significantly reduces the size of the CFB boiler for the same throughput resulting in cost reduction. A detailed drawing is shown in drawing; CFB unit details section (Horizontal cyclone)

4.6 Loopseal and return leg (Stand pipe)

Loopseals (non mechanical valves) are devices that allow the flow of solids between the return leg (stand pipe) and the furnace without any external mechanical force. Air facilitates the movement of solids in these valves. A loopseal was designed and fabricated with clear plastic (Lexan). The return leg (standpipe) is also made of clear plastic (Acrylic pipe). The bottom of the standpipe need not be fluidized, but it may need only a small amount of air. A detailed drawing is shown in drawing A2.

3.7 Ducting

The ducting was designed by considering the minimum pressure drop in the line and space availability. A 16" diameter pipe of 16 gauge galvanized iron was used as the return duct whereas a 3 mm thick mild steel pipe of same diameter was used as supply duct.

3.8 Baghouse

The baghouse is one of the main components for the CFB boiler. Its importance is increased significantly if one wants to recycle the air. A bag house was designed and constructed in the simplest way. See drawing no A3.

4 Instrumentation

Instrumentation is the key item for receiving instantaneous data from the unit while doing experiments. A number of pressure transducers are required to get the profile of suspension density. To get response with minor change of experimental parameters a highly sensitive pressure transducer is required. Therefore, a computer integrated OMEGA data acquisition system was installed. The configurations of the systems are as follows:

1. Computer: Dell Dim L400C Computer L 400
Special Feature: 17 " monitor, 64 MB RAM, 6.4 GB HD, CD ROM
2. OMB-DAQ-56: 20 channel 22 Bit DAS system
3. OMB-DAQ-SW-PLUS: OMB-DAQ-SW-PLUS Enhanced Personal DAQVIEW
4. Pressure Transducer: PX164-010D5V, PX142-002G5V, PX142-002D5V
5. USB Cable: OMB-CA-179-1
6. Motor Actuator: Honeywell ML6184 A1003
24 VAC 50/60 Hz 5VA Class2 90Sec@60 Hz
150 lb-in

5 Commissioning the System:

The test rig was first actuated on February 29, 2000. No major problem was noticed except for a few leaks. Efforts were made to eliminate these. During the period of testing, the horizontal cyclone burst due to high fluctuations of the pressure drop in the cyclone. To resist the observed pressure gradients across the wall a clear plastic such as LEXAN was used. As safety was a first priority of the laboratory later on, reinforcement was provided around the cyclone as well as the lower bed of the riser column. The pressure loss in the unit can be as measured in previous experiments on the test rig as follows:

Windbox with pipe and fittings:	2 inch of H ₂ O
Distributor plate:	8 inch of H ₂ O
Riser column:	22 inch of H ₂ O
U-Beam separator:	2 inch of H ₂ O
Horizontal cyclone:	8 inch of H ₂ O
Filter bags (baghouse):	3 inch of H ₂ O

5.1 Operation stability and system performance:

Operational stability is defined as the stability of the system to operate with fast bed conditions as designed. It was found that when the size distribution of sand fed is well controlled, the system behavior is sensitive to fluidizing velocity, solid circulation rate and total bed inventory in the riser.

In desired normal operation, the flow structure of fast fluidization is characterized by

1. Local two-phase structure consisting of a solid-rich dense phase and a gas-rich dilute phase;

2. Two region coexistence in the axial direction – a dilute region at the top and a dense region at the bottom;
3. Radial heterogeneous distribution with a dilute region in the core and a dense region near the wall;
4. Both local and overall heterogeneities are subject to operating conditions, material properties and boundary conditions.

One can propose the designation of the complicated variation of the flow structure in the following four categories:

Phase: State of particle aggregation

	Continuous		Discontinuous
Dense:	emulsion	or	clusters
Dilute:	broth	or	bubbles

Regime: Configuration of phase combinations is dependent on operating parameters: bubbling, turbulent, fast, transport.

Pattern: Constitution of regime spectrum dependent on material properties: bubbling/transport for coarse G/S systems; particulate/bubbling/turbulent/fast/transport for FCC catalyst/air systems; particulate only for most L/S systems.

Region: Spatial distribution of phases dependent on boundary conditions: top and bottom; core and wall.

It is possible to judge situations when the stable operation of the system cannot be expected. If the fluidizing velocity is greater and solid circulation is less, entrained solid might accumulate in the standpipe. If that happens, after a few minutes solids might block

the horizontal cyclone. So one might need to look at the amount of solids in the standpipe.

For visual inspection of the pressure profiles a manometer bank was used and it ensured that the system was running in fast bed condition.

Performance data of the newly designed test rig and its respective optimal operating regimes for sand particles of 250 μm average.

Table 2: Operating settings

Parameter	Fast bed configuration
Smallest fluidizing velocity (m/s)	2
Maximum fluidizing velocity (m/s)	5
Minimum solid inventory (kg)	50
Maximum solid circulation rate (kg/s)	3.5

7 Operating procedure of the test rig

The following procedures are to be followed

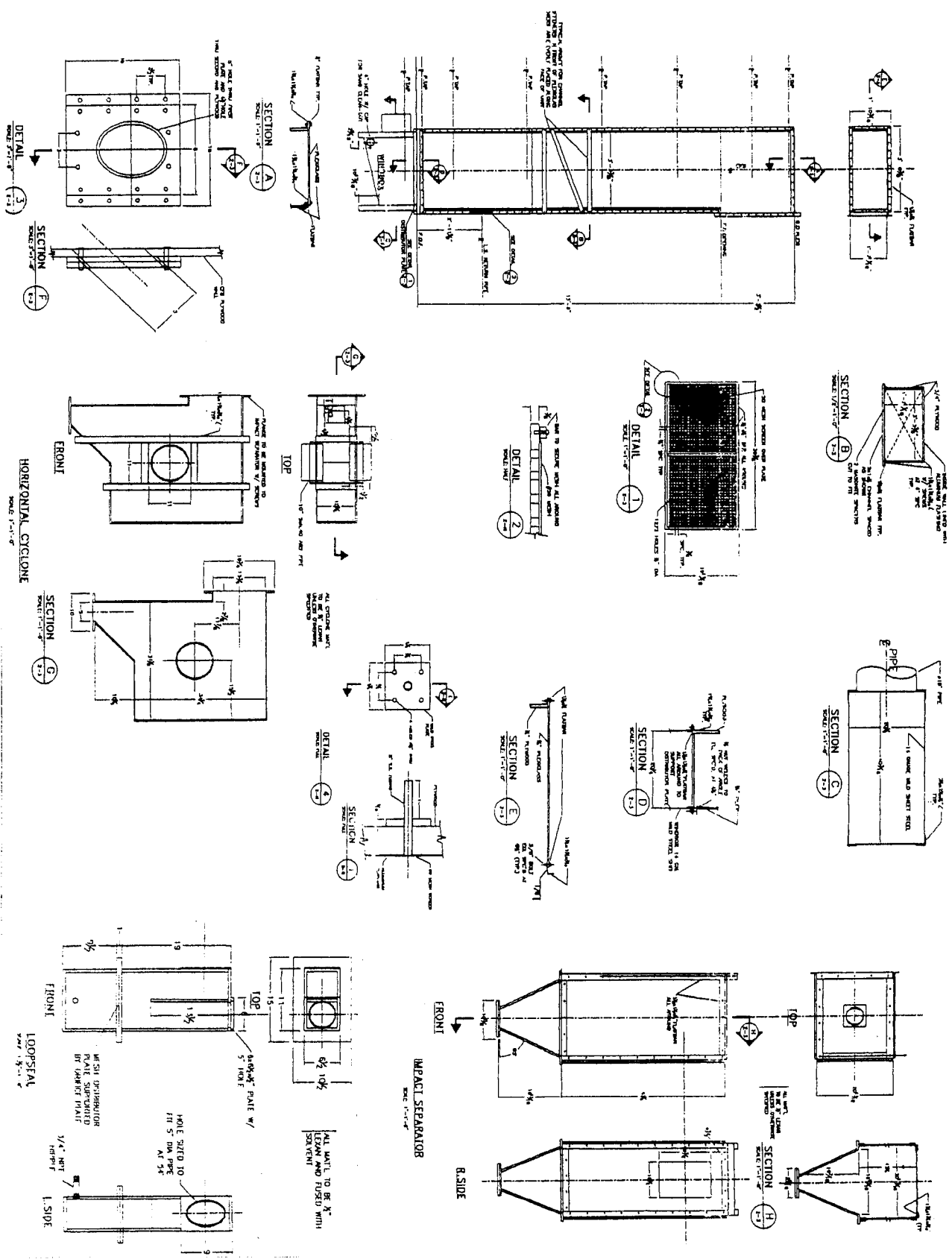
- (i) *When turning on*
 - a. Take the key of the blower from the Laboratory manager/CFB secretary
 - b. Check both that the valves in the stand pipe are open
 - c. Check that the valve for the sand feeding is closed
 - d. Check that the damper for the blower is in closed position (0^0)
 - e. Check the availability of compressed air in the loop seal from the facility line
 - f. Make sure the electrical extension line is available for the actuator of the damper

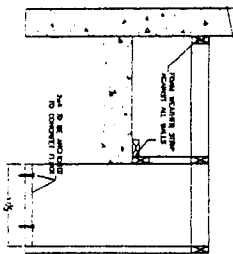
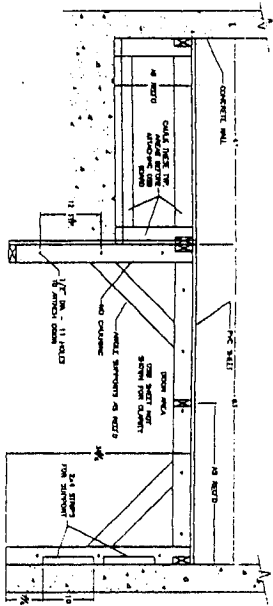
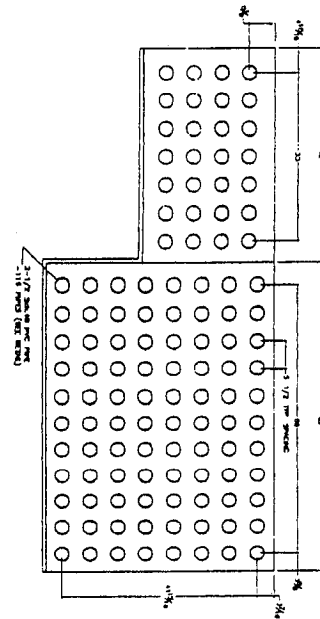
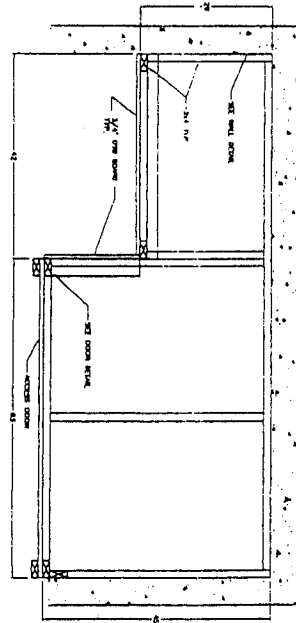
- g. Make sure that the differential manometers/transducers are properly connected
- h. Turn on the circuit breaker (main switch) for the blower.
- i. Turn on the blower.
- j. Gradually open the damper of the blower by actuator until fast bed regimes is achieved (can be seen from the differential manometer; it is established at 30 % opening of the damper)
- k. Turn on the loop seal air supply valve for the desired circulation

(ii) *When turning off*

- a. Gradually close the damper of the blower
- b. While there is no circulation, turn off the loop seal air supply valve
- c. Turn off the blower
- d. Turn off the circuit breaker/main switch
- e. Lock the main switch by the key-lock
- f. Hand over the key to Laboratory Manager/CFB secretary

A2: Drawings of CFB unit details and section





A3: Details drawing of baghouse

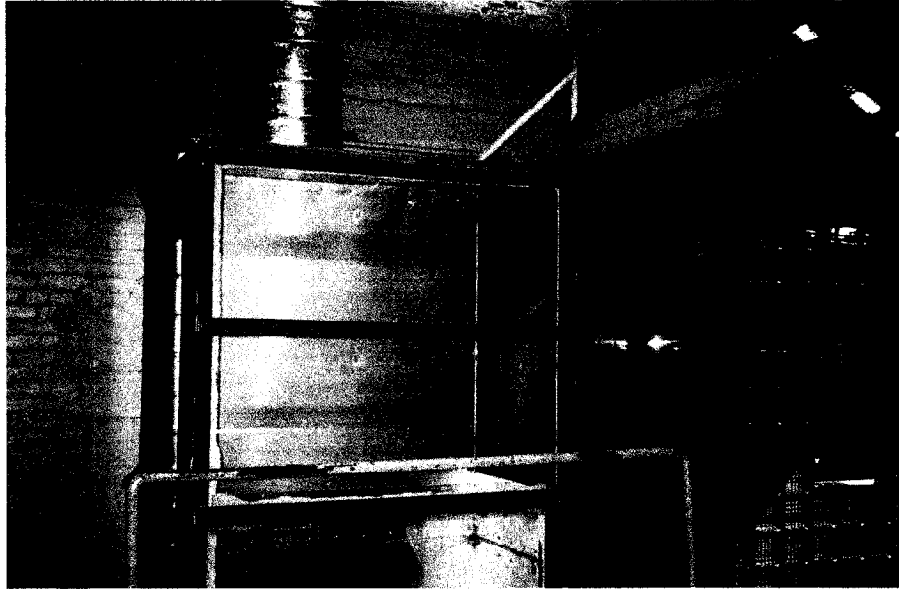


Fig. A.1 Top of the Experimental Unit before modification

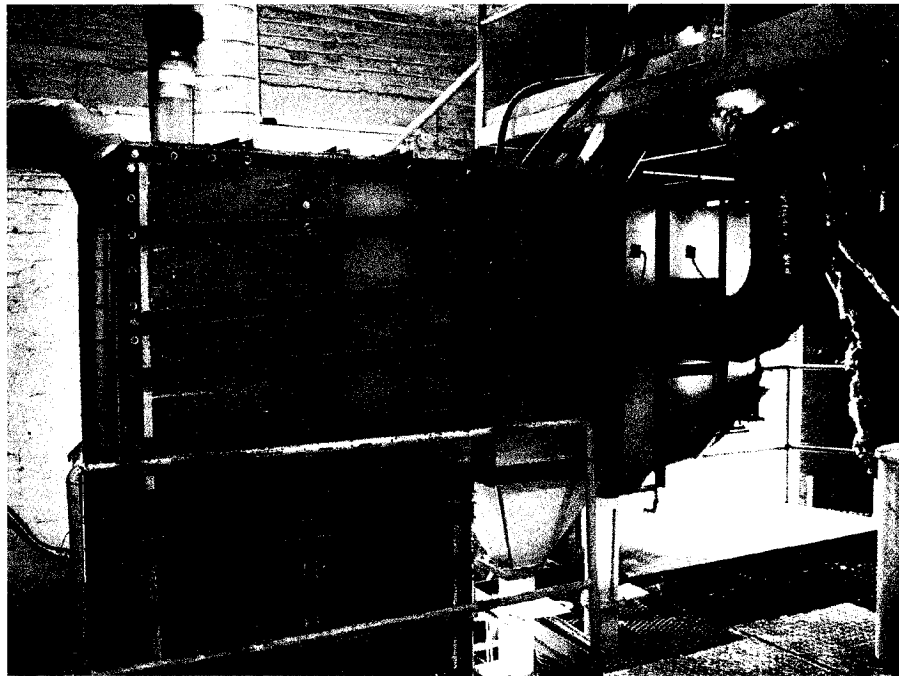


Fig. A.2 Top of the Experimental Unit after modification



Fig. A.3 Differential pressure drop measuring port

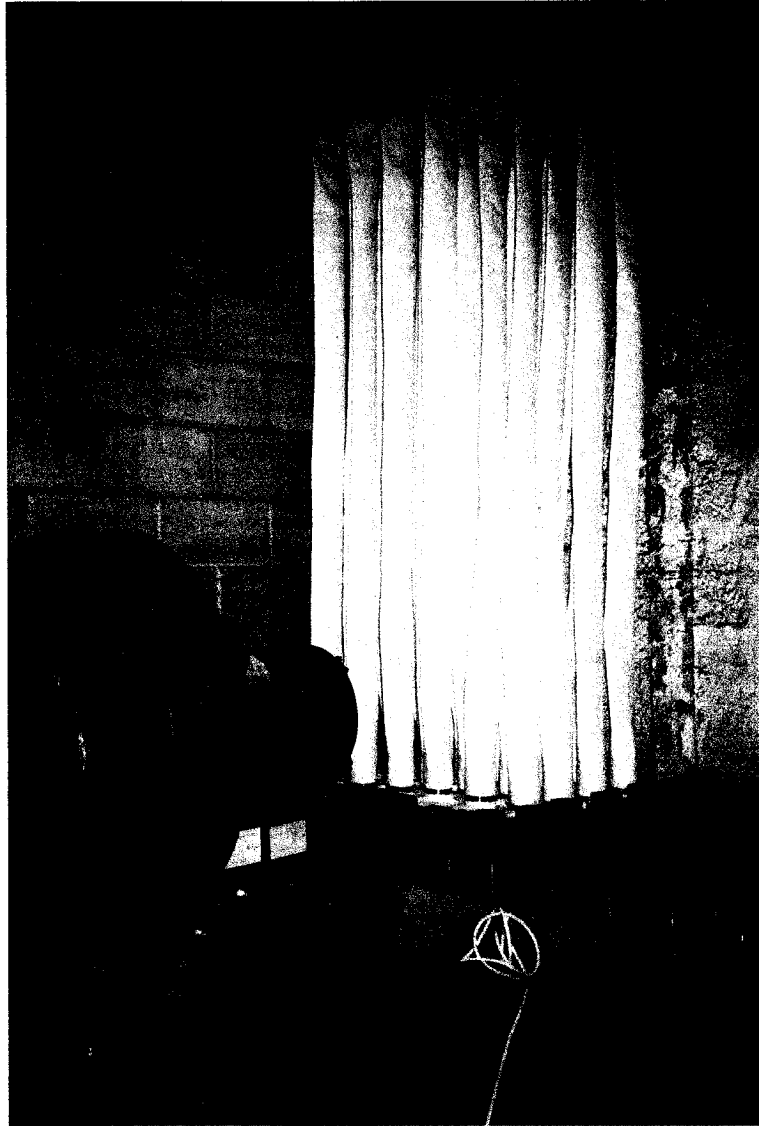


Fig. A.4 Construction of Baghouse

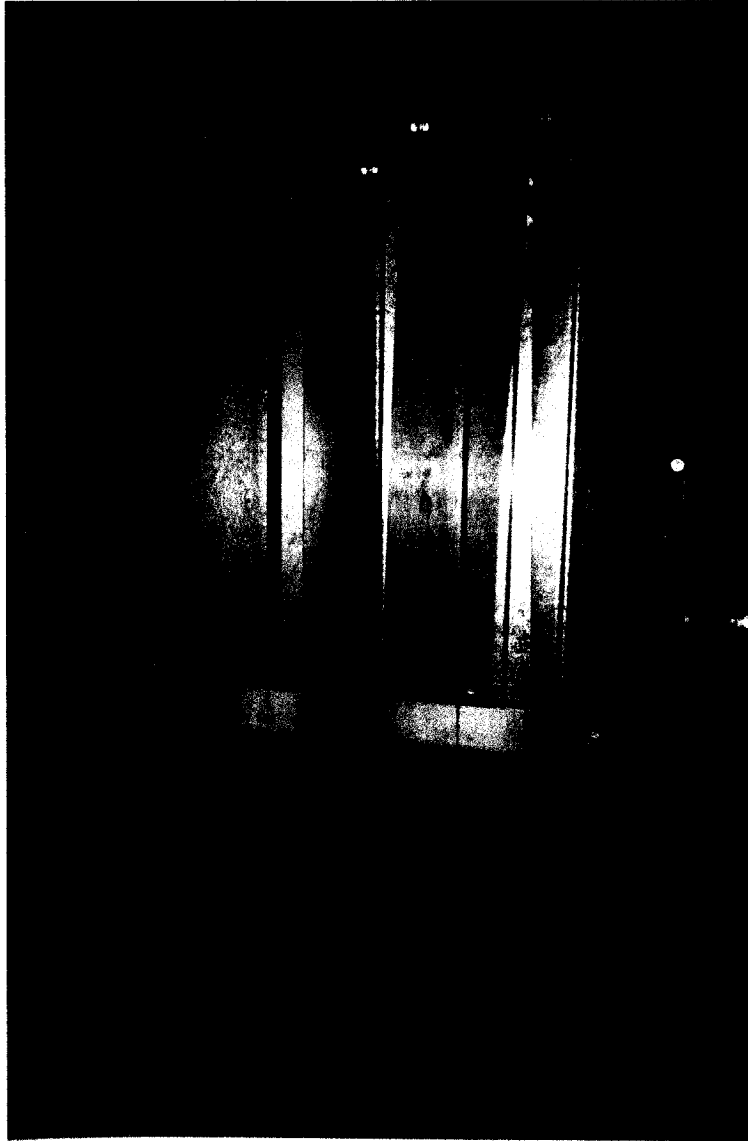


Fig. A.5 Construction of Inertial Separator

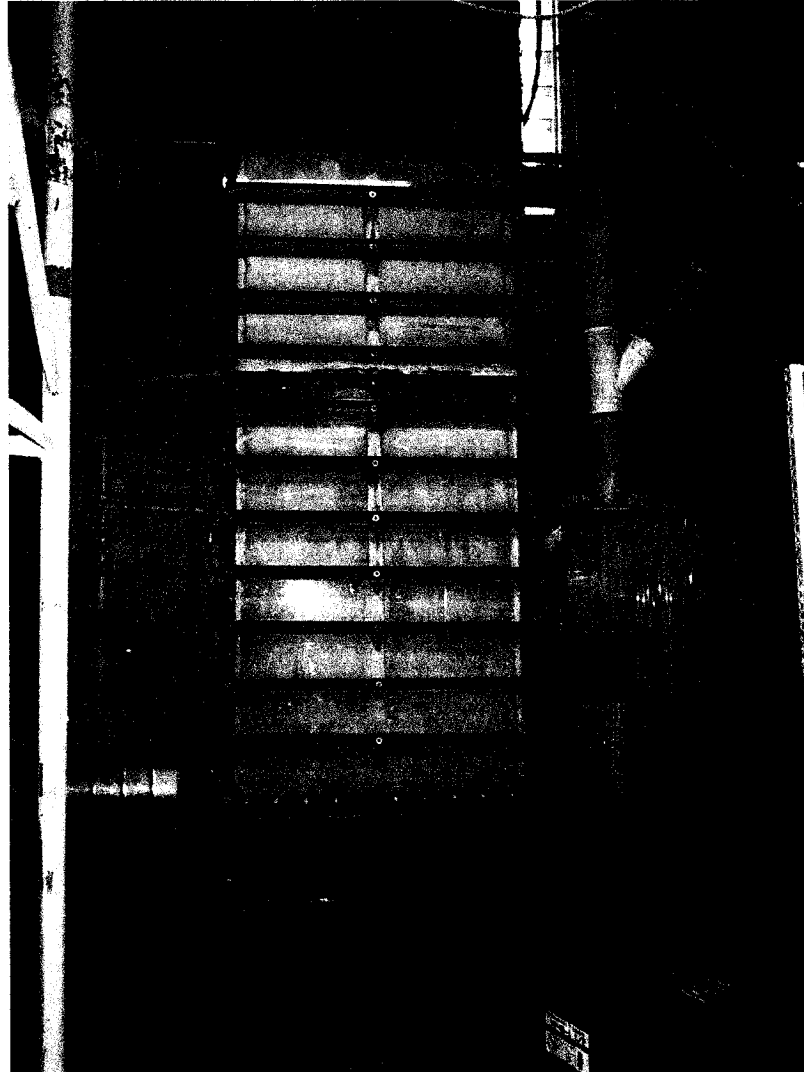


Fig. A.6 Lower part of the Experimental Unit under operation

Appendix B

Properties of Bed Material Used in the Experiments

Size distribution

If a powder contains a range of sizes which can be divided into narrow size fractions with mass fraction x_i of size $d_{sv,i}$, it can be shown that the surface/volume mean size is (Abrahamsen and Geldart 1980)

$$d_p = \frac{1}{\sum \left(\frac{x_i}{d_{pi}} \right)} \quad (\text{B.1})$$

The mean sieve diameter, d_p , which can be found using a standard sieve analysis based on equation (B.1), is equal to the surface/volume diameter if the particles are perfectly spherical. For near spherical particles such as the quartz sand used in the experiments, the following correlation was proposed by Abrahamsen and Geldart (1980):

$$d_{sv} = 0.871 d_p \quad (\text{B.2})$$

In the experiments, two different sizes of sand and Z-light ceramic microsphere were used.

Table B.1: Size analysis of “00” grade Nova Scotia sand (by sieves)

Diameter Range (μm)	Average size $d_{p,i}$ (μm)	Sample weight (g)	Weight fraction x_i	$x_i/d_{p,i}$ (mm^{-1})
600-500	550	15	0.05137	0.0934
500-425	462.5	39	0.133562	0.288782
425-325	380	86	0.294521	0.775054
335-250	292.5	55	0.188356	0.643953
250-212	231	37	0.126712	0.548538
212-180	196	25	0.085616	0.436819
180-150	165	15	0.05137	0.311333
150-125	137.5	10	0.034247	0.249066
125-106	115.5	7	0.023973	0.207555
106-0	53	3	0.010274	0.193849
		$\Sigma = 292$		$\Sigma(x_i/d_{p,i}) = 3.75$
				$d_p = 267 \mu\text{m}$

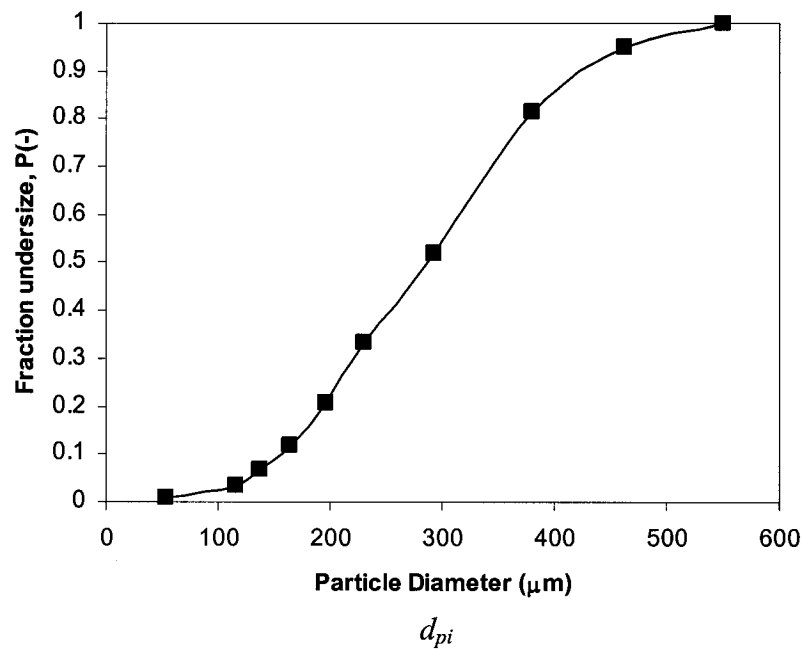
**Figure B.1.** Particle size distribution of “00” grade Nova Scotia sand

Table B.2. Size analysis of “0” grade Nova Scotia sand

Diameter Range (μm)	Average size $d_{p,i}$ (μm)	Weight fraction x_i	$x_i/d_{p,i}$ (mm^{-1})
1180-1000	1090	0.002557	0.002346
1000-710	855	0.050511	0.059077
710-600	655	0.305626	0.466605
600-500	550	0.191816	0.348756
500-212	356	0.420077	1.179992
212-180	196	0.015985	0.081556
180-150	165	0.005115	0.031
150-106	128	0.003197	0.024977
106-90	98	0.001918	0.019571
90-75	82.5	0.001279	0.015503
75-63	69	0.000639	0.009261
63-53	58	0.000639	0.011017
53-0	26.5	0.000639	0.024113
			$\sum(x_i/d_{p,i}) = 2.27$
			$d_p = 440 \mu\text{m}$

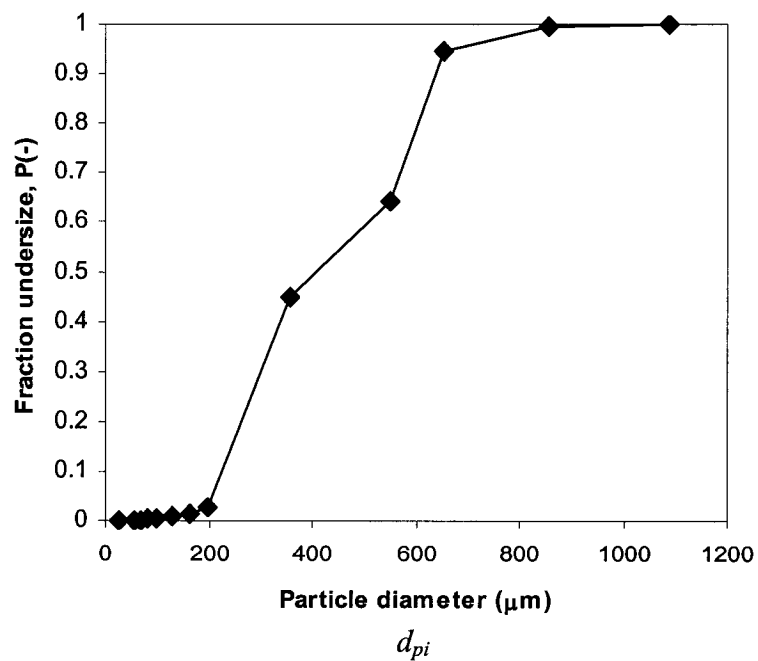
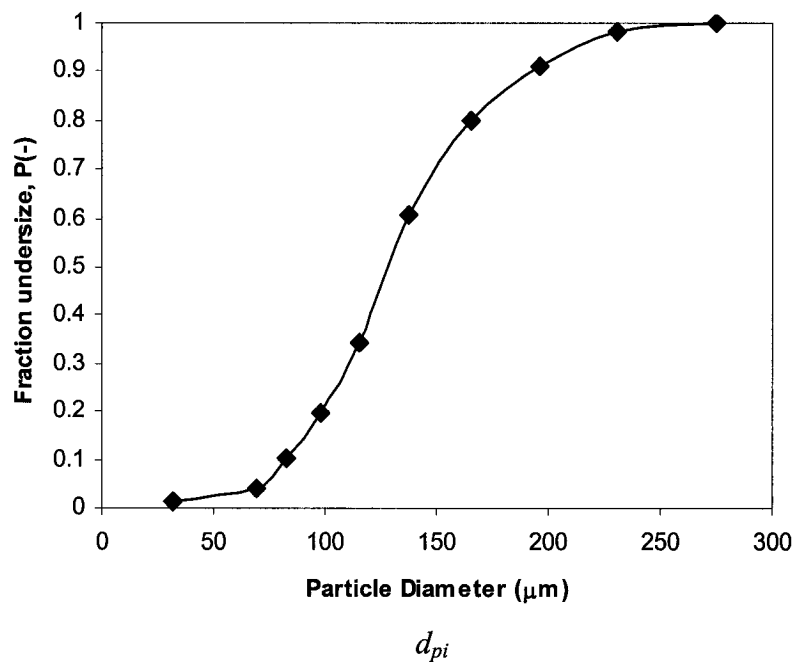
**Figure B.2.** Particle size distribution of “0” grade Nova Scotia sand

Table B.3. Size analysis of Z-light Ceramic Microsphere

Diameter Range (μm)	Average size $d_{p,i}$ (μm)	Sample weight (g)	Weight fraction x_i	$x_i/d_{p,i}$ (mm^{-1})
300-240	275	5	0.019011	0.069132
250-212	231	18	0.068441	0.296282
212-180	196	30	0.114068	0.581982
180-150	165	50	0.190114	1.152206
150-125	137.5	70	0.26616	1.935707
125-106	115.5	38	0.144487	1.250967
106-90	98	25	0.095057	0.96997
90-75	82.5	16	0.060837	0.737412
75-63	69	8	0.030418	0.440844
63-0	31.5	3	0.011407	0.362122
		$\Sigma = 263$		$\Sigma (x_i/d_{p,i}) = 7.8$
				$d_p = 128 \mu\text{m}$

**Figure B.3.** Particle size distribution of Z-light Ceramic Microsphere

Density of bed material

The density of bed material was estimated by forming a test described as follows:

- i) A graduated cylinder was filled with water to a known volume, V_1
- ii) A second graduated cylinder was placed with a measured mass of bed material, m_b
- iii) The second graduated cylinder was then filled with water from the first graduated cylinder and the new volume, V_2 , was measured
- iv) The density of the bed material was then calculated from the following relation:

$$\rho_p = \frac{m_b}{V_2 - V_1} \quad (\text{B.3})$$

where

m_b =mass of the bed material, kg

V_1 =volume of water, m^3

V_2 =volume of bed material and water, m^3

The procedure was repeated for three samples of bed materials and the result values were averaged to give a measured solid density.

Table B.4. summarizes the values of some important parameters related with the particles used in the experiments.

Table B.4: Properties particles used in the experiments

	Unit	Silica Sand ("00" grade)	Silica Sand ("0" grade)	Z-light microsphere
Geldart's classification		B	B	A
Mean sieve diameter	μm	266	440	128
Mean surface/volume diameter	μm	232	383	128
Particle density	kg/m^3	2564	2512	700
Bulk density	kg/m^3	1320	1299	390

Appendix C

Calibration of Instruments used

Calibration of flow meters

Flow rates of air in the pilot plant were measured by both venturi meter and pitot tube arrangements. The venturi meter was installed in the supply duct to the riser while the pitot tube in the discharge line to the baghouse. . The venturi meter was calibrated with the measurements from the pitot tube.

Measurement by pitot tube

The pitot tube was installed in the discharge line of the pilot plant where $L/D=11.25$. The duct diameter was 0.4 m.

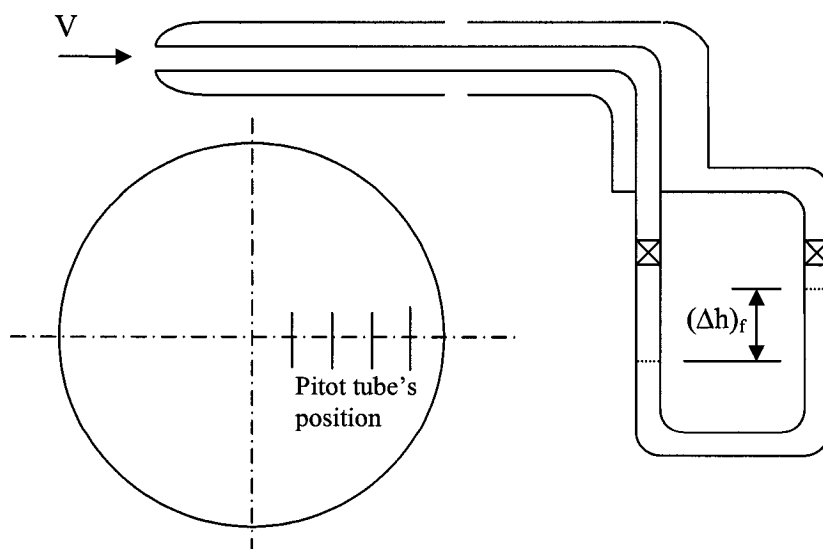


Figure C.1. Schematic diagram of pitot tube used in the experiments

The superficial velocity of air in the riser was calculated by the following way:

$$(U_g)_{pitot} = \frac{V_d * A_d}{A_{riser}} \quad (C.1)$$

where V_d was the average velocity of air in the discharge duct which was calculated by

$$V_d = \frac{\sum_{i=0}^{i=1} (V_d)_i * (A_d)_i}{A_d} \quad (C.2)$$

In the Eqn (C.2), $(V_d)_i$ was the local air velocity at the i^{th} position in the duct, which can be calculated by the following way

$$(V_d)_i = \sqrt{2g(\Delta h_i)_{air}} \quad (C.3)$$

$$\text{where } (\Delta h_i)_{air} = \frac{\rho_f (\Delta h_i)_f}{\rho_{air}} \quad (C.4)$$

$$\text{and } \rho_{air} = \frac{P_{abs}}{RT_{abs}} \quad (C.5)$$

and A_d , the cross-sectional area of the discharge duct was estimated as

$$A_d = \sum_{i=0}^{i=1} (A_d)_i \quad (C.6)$$

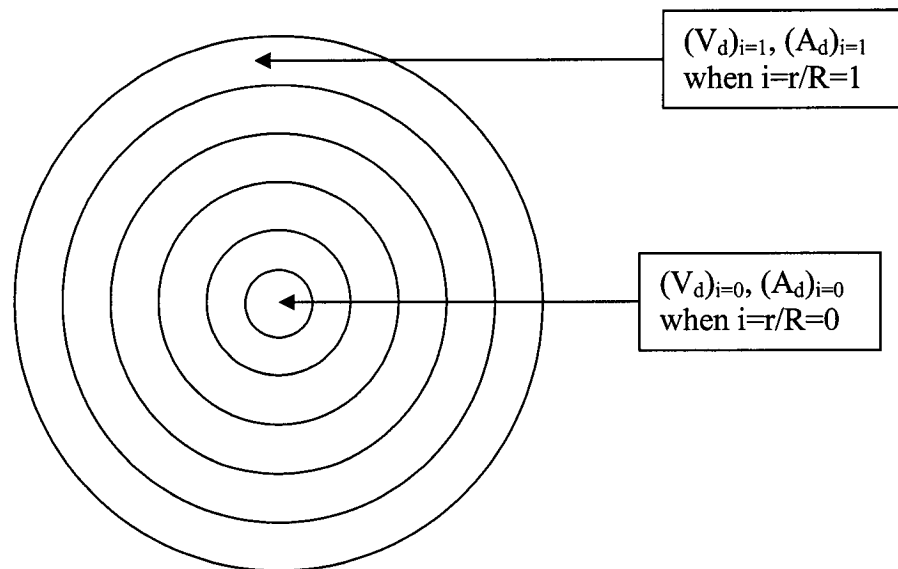


Figure C.2. Segmented cross-section of the discharge duct

Nomenclature:

$(U_g)_{pitot}$ = Superficial gas velocity in the riser estimated by pitot tube, m/s

V_d = Average velocity of air in the discharge line, m/s

$(V_d)_i$ = Local air velocity of air at i^{th} position, m/s

A_{riser} = Cross-sectional area of the riser, m^2

A_d = Cross-sectional area of the discharge duct, m^2

$(A_d)_i$ = Local cross-sectional area at the i^{th} position (Fig. C.2)

$(\Delta h)_f$ = Differential height of manometric fluid, m

$(\Delta h)_{air}$ = Differential height of air, m

Measurement by venturi meter

A venturi meter was installed in the supply duct to get online measurement of flowrate to the riser. Figure C.3 represents a typical venturi meter.

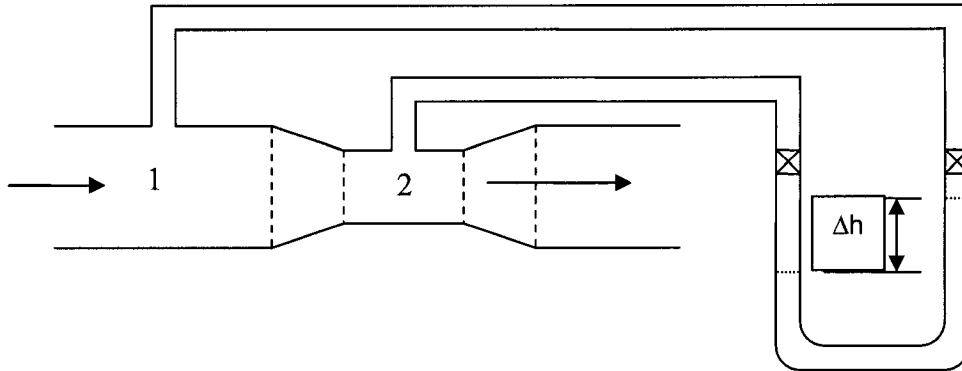


Figure C.3. Schematic diagram of the venturi meter installed in the supply duct

By using Bernoulli's equation, the superficial velocity of air inside the riser can be estimated as

$$(U_g)_{theoretical,venturi} = \frac{A_2}{A_{riser}} \sqrt{\frac{2\rho_f g(\Delta h)_f}{\rho_{air} \left[1 - \left(\frac{d_2}{d_1} \right)^4 \right]}} \quad (C.7)$$

Coefficient of discharge for venturi meter can be estimated as

$$C_d = \frac{(U_g)_{pitot}}{(U_g)_{theoretical,venturi}} \quad (C.8)$$

Therefore, actual superficial velocity of air to the riser can be estimated as:

$$(U_g)_{actual} = C_d (U_g)_{theoretical, venturi} \quad (C.9)$$

Equating E^{qn} (C.1) and (C.7), the value of C_d is estimated from E^{qn}. (C.9)

$(U_g)_{pitot}$ (m/s)	Corresponding $(\Delta h)_f$ in the venture meter (in)	$(U_g)_{theoretical, venture}$ (m/s)	Coefficient of discharge C_d
0.7812	.05	0.8432	0.9262
1.1242	0.1	1.1925	0.9425
2.2171	0.4	2.3850	0.9295
2.9559	0.7	3.1551	0.9368
4.0564	1.3	4.2997	0.9434
4.2542	1.45	4.5409	0.9368
4.7214	1.8	5.0594	0.9332
5.0428	2.1	5.4648	0.9228
			Average $C_d = .9336$

Equation (C.7) can be simplified by incorporating values of C_d , A_2 , d_2 , d_1 , A_{riesr} , ρ_f and g as

$$(U_g)_{actual} = 23.08 \sqrt{\frac{(\Delta h)_f}{\rho_g}} \quad (C.10)$$

The flowrate to the loop seal is estimated by standard volume gas flow meter, which is made by Dwyer Instruments Inc. and its capacity is 0-1000SCFH.

Solid Flux Measuring Probe

A non-isokinetic probe was fabricated to measure the upward and down solids flux in the riser. The probe is calibrated in a 15-cm diameter riser column. We have conducted a number of tests on the probe.

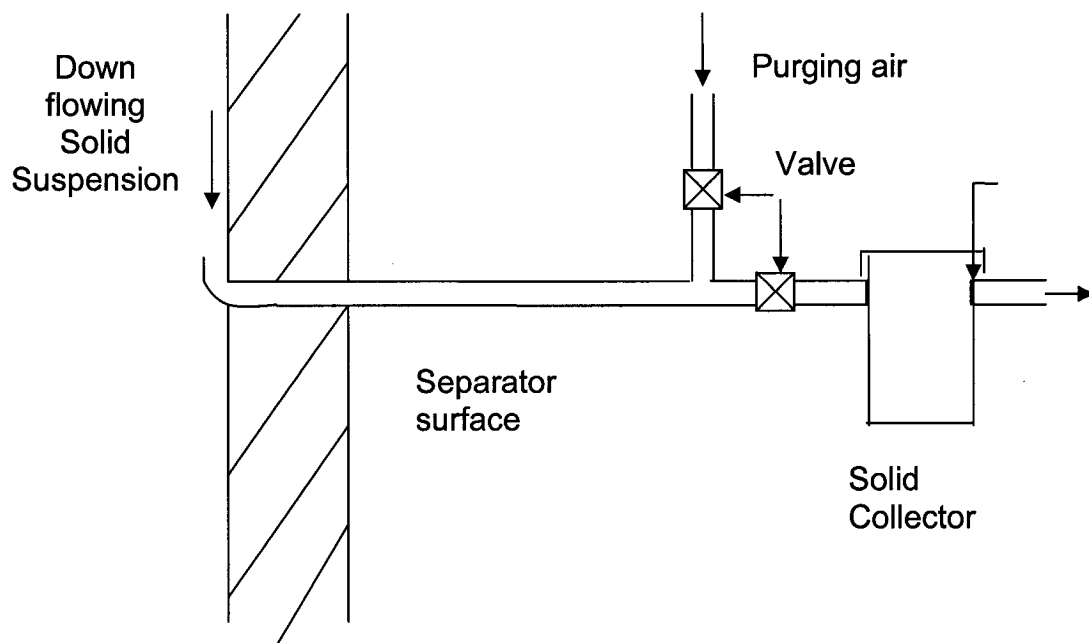


Figure C.4. Solids flux measuring probe

Net solids flux in the riser can be estimated by

$$G_{s,net} = \frac{\sum_{i=0}^{i=1} (G_{s,net})_i * (A_{riser})_i}{A_{riser}} \quad (C.11)$$

where
$$(G_{s,net})_i = (G_{s,upward})_i - (G_{s,downward})_i \quad (C.12)$$

$G_{s,net}$ should be equal to $G_{s,external}$ which is measured by measuring the time required for a known volume of solids to accumulate on top of the knife valve after the valve was closed.

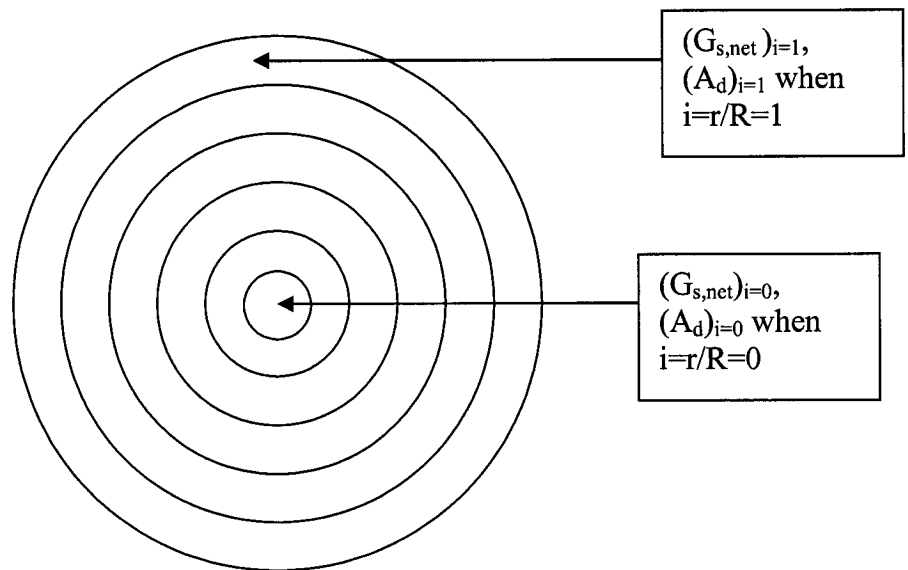


Figure C.5. Segmented cross-section of the 15 cm riser column

Fig. C.6 shows the net solid flux profile along the radial direction of the column for a test with operating variables at 3.7 m/s and 12.82 kg/m².s external solid circulation rate. This profile was integrated over the cross-sectional area of the riser to yield an integrated mean flux which was compared with the externally measured mean flux. A simple mass balance tells us that the integrated mean fluxes measured at that position should be equal to the externally measured solid mean flux.

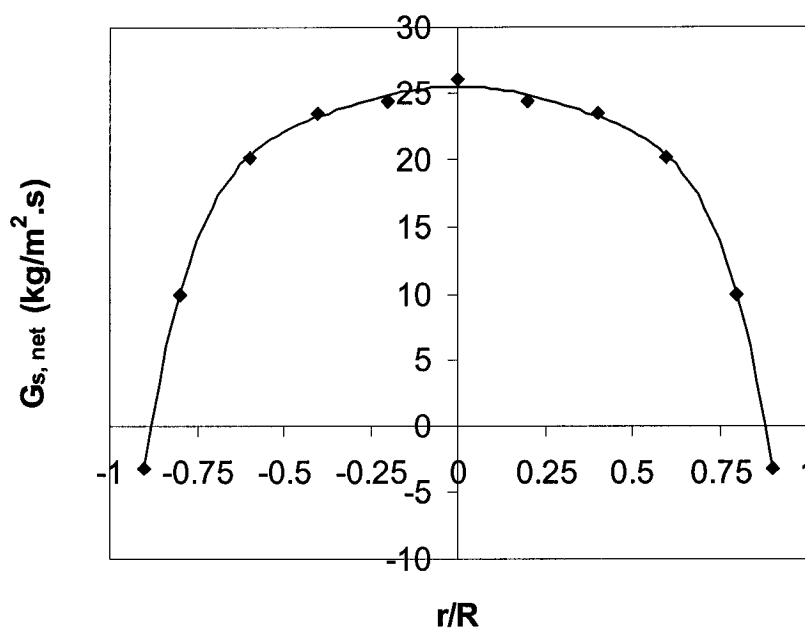


Figure C.6. Net upward solids mass fluxes with non-dimensional radial distance.

However, we found a lower mean flux than that of externally measured mean flux. The mean integrated flux was found $12.27 \text{ kg/m}^2 \cdot \text{s}$ which is 4.3% lower than that of the externally measured mean flux. The possible cause of this deviation could be difficulty in making accurate measurements very close to the riser wall where a small error is prone to have a large effect on the integrated mean flux.

Temperature measurement:

Thermocouple

OMEGA's self-adhesive T-type Teflon coated thermocouples were used for surface temperature measurement.

Specifications:

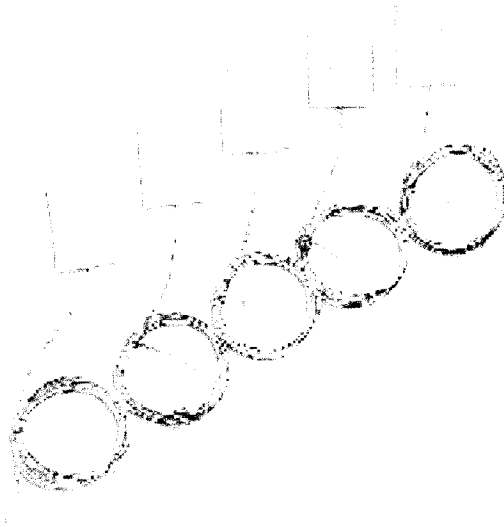
Adhesive: Silicon based cement

Maximum temperature: 175°C

Minimum temperature: -60°C

Response time: 0.3 S

Resolution: 0.1°C



These thermocouples are calibrated by OMEGA. We also calibrated them with in the range of (0° - 100°C) by boiling water and ice water at atmospheric pressure.

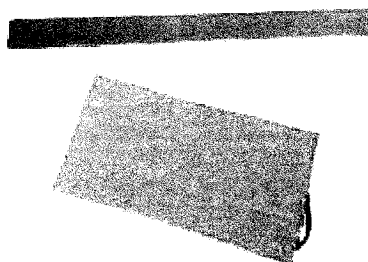
Temperature and process meter:

Programmable OMEGA's DP25-TC is used. It is selectable for J, K, T, or J DIN thermocouples.

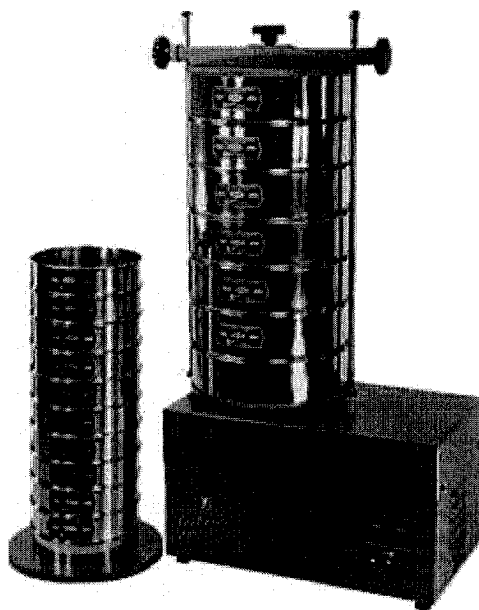


Heaters:

OMEGALUX silicon rubber fiberglass insulated flexible heaters are used in the experiments. These are 5 W/in^2 heaters which are rectangular in shape. These are having pressure sensitive adhesive where the maximum operating temperature is limited to 120°C .



Constant heat flux heating strip

Sieve shaker:

Gilson Sieve shaker for size analysis: Gilson 12" Sieve Shaker
115V/60Hz - 12"/8" Sieve Model: SS-12R

Appendix D

Experiments on wing wall

Figure D.1 shows the locations of thermocouples on the surface of the wing wall for Case 2. Experimental data were recorded from a Programmable digital OMEGA meter through a selector switch.

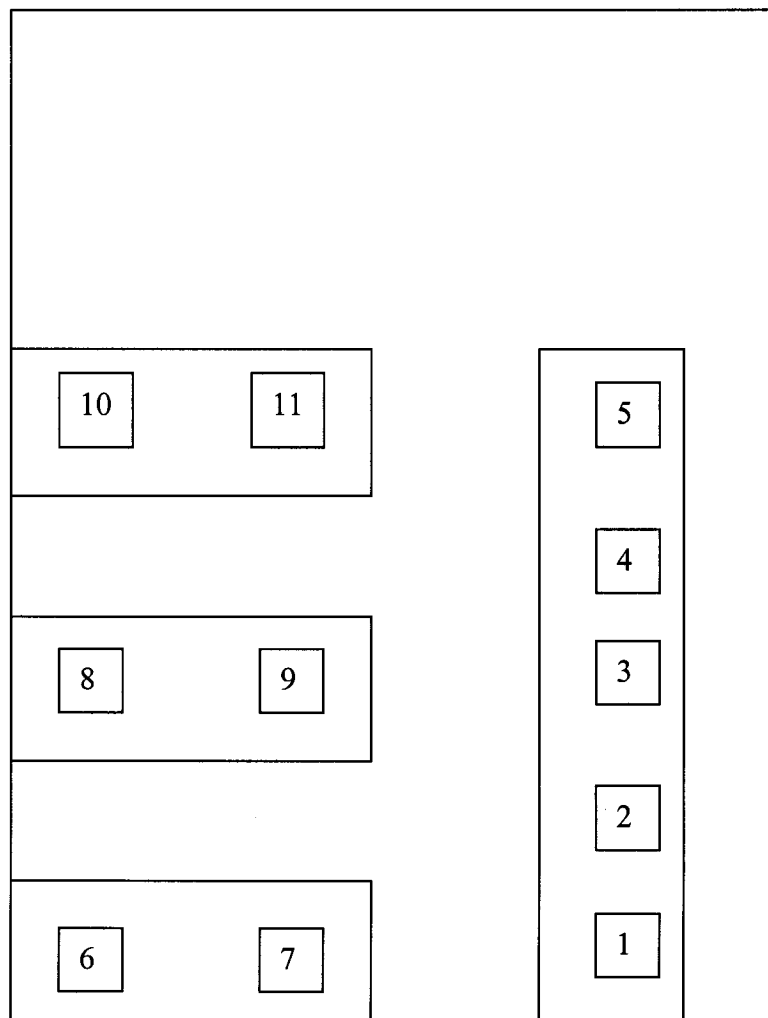


Figure D.1. Position of thermocouples on the wing wall

A number of tests were carried out in order to check the measurement systems with no load. The heat transfer measurements were carried out several times in a single run during all the experiments presented here and the mean values were used to represent the corresponding run. Equation 4.1 was used to calculate heat transfer coefficients on the noted locations.

Run #1 (Case-2)

Operating and design parameter												
Date	June01, 2001						Heat transfer surface area			0.1083 m ²		
Superficial gas velocity	4.4 m/s						Power supply			80 W		
External solid circulation rate	7.4 kg/m ² s						Voltage			35.5 V		
Bed material	"00" sand						Current			2.25 A		
T1 (°C)	T2 (°C)	T3 (°C)	T4 (°C)	T5 (°C)	T6 (°C)	T7 (°C)	T8 (°C)	T9 (°C)	T10 (°C)	T11 (°C)	Tbed (°C)	
44.5	48.7	50.3	49.9	50.6	42.8	43.6	43.1	43.8	42.6	43.4	35.3	
44.5	49	50.6	50.2	51	43.2	44.2	43.4	44	43	44	35.7	
45	49.3	50.7	50.3	51.1	43.3	44.3	43.5	44.3	43.1	44.2	35.8	
45.1	49.2	51	50.6	51.5	43.7	44.6	43.8	44.7	43.5	44.6	36.2	
45.3	50	51.3	50.9	51.7	43.9	44.9	44.1	44.9	43.7	44.8	36.4	
45.8	50.1	51.6	51.1	51.8	44	45.1	44.3	45.2	43.8	45	36.5	
h1 W/m ² K	h2 W/m ² K	h3 W/m ² K	h4 W/m ² K	h5 W/m ² K	h6 W/m ² K	h7 W/m ² K	h8 W/m ² K	h9 W/m ² K	h10 W/m ² K	h11 W/m ² K		
80.1	55.0	49.1	50.5	48.2	98.3	88.8	94.5	86.7	101.0	91.0		
83.7	55.4	49.5	50.8	48.2	98.3	86.7	95.7	88.8	101.0	88.8		
80.1	54.6	49.5	50.8	48.2	98.3	86.7	95.7	86.7	101.0	87.7		
82.8	56.7	49.8	51.2	48.2	98.3	87.7	97.0	86.7	101.0	87.7		
82.8	54.2	49.5	50.8	48.2	98.3	86.7	95.7	86.7	101.0	87.7		
79.2	54.2	48.8	50.5	48.2	98.3	85.7	94.5	84.7	101.0	86.7		
Average	81.5	55.0	49.4	50.8	48.2	98.3	87.1	95.5	86.7	101.0	88.3	

Run #2(Case-2)

Operating and design parameter	
Date	June05, 2001
Heat transfer surface area	0.1083 m ²
Superficial gas velocity	4.4 m/s
Power supply	80 W
External solid circulation rate	3.6 kg/m ² s
Voltage	35.5 V
Bed material	"00" sand
Current	2.25 A

T1 (°C)	T2 (°C)	T3 (°C)	T4 (°C)	T5 (°C)	T6 (°C)	T7 (°C)	T8 (°C)	T9 (°C)	T10 (°C)	T11 (°C)	Tbed (°C)
44	50.3	52.5	52	52.8	44.6	45.3	44.7	46.3	45	45.9	34.4
44.2	50.5	52.5	52.2	53.1	44.8	45.6	45	46.8	45.3	46.2	34.8
44.5	50.9	52.8	52.5	53.5	45.2	45.9	45.2	47.4	45.6	46.7	35.1
44.8	51.2	53	52.8	53.8	45.5	46.2	45.5	47.6	45.9	47	35.3
45.1	51.4	53.2	53.1	54.3	45.8	46.5	45.8	47.7	46.2	47.2	35.7
45.4	51.8	53.5	53.5	54.2	46.1	46.8	46.4	47.9	46.5	47.4	36.1

h1 W/m ² K	h2 W/m ² K	h3 W/m ² K	h4 W/m ² K	h5 W/m ² K	h6 W/m ² K	h7 W/m ² K	h8 W/m ² K	h9 W/m ² K	h10 W/m ² K	h11 W/m ² K
76.8	46.3	40.7	41.9	40.1	72.2	67.6	71.5	61.9	69.5	64.1
78.4	46.9	41.6	42.4	40.3	73.7	68.2	72.2	61.4	70.2	64.6
78.4	46.6	41.6	42.4	40.1	73.0	68.2	73.0	59.9	70.2	63.5
77.6	46.3	41.6	42.1	39.8	72.2	67.6	72.2	59.9	69.5	63.0
78.4	46.9	42.1	42.4	39.6	73.0	68.2	73.0	61.4	70.2	64.1
79.2	46.9	42.4	42.4	40.7	73.7	68.9	71.5	62.5	70.9	65.2
Average	78.1	46.7	41.7	40.1	73.0	68.1	72.3	61.2	70.1	64.1

Run #3(Case-2)

Operating and design parameter	
Date	June09, 2001
Heat transfer surface area	0.1083 m ²
Superficial gas velocity	4.4 m/s
Power supply	80 W
External solid circulation rate	6 kg/m ² s
Voltage	35.5 V
Bed material	"00" sand
Current	2.25 A

T1 (°C)	T2 (°C)	T3 (°C)	T4 (°C)	T5 (°C)	T6 (°C)	T7 (°C)	T8 (°C)	T9 (°C)	T10 (°C)	T11 (°C)	Tbed (°C)
45.5	50.4	52.2	51.8	52.7	46	47.1	45.7	47	46	46.5	36.7
45.9	50.9	52.7	52.2	52.9	46.2	47.6	46.1	47.4	46	46.9	37
46.1	51.1	52.8	52.4	53.4	46.5	47.7	46.1	47.7	46.5	47	37.2
46.2	51.2	53	52.5	53.6	46.7	48.2	46.5	48	46.9	47.1	37.5
46.5	51.4	53.4	53	53.7	47.2	48.3	47	48.5	47	47.5	37.9
47.1	52	53.8	53.5	54	47.6	48.6	47.5	48.6	47.1	48	38.2

h1 W/m ² K	h2 W/m ² K	h3 W/m ² K	h4 W/m ² K	h5 W/m ² K	h6 W/m ² K	h7 W/m ² K	h8 W/m ² K	h9 W/m ² K	h10 W/m ² K	h11 W/m ² K
83.7	53.8	47.5	48.8	46.1	79.2	70.9	81.9	71.5	79.2	75.2
82.8	53.0	46.9	48.5	46.3	80.1	69.5	81.0	70.9	81.9	74.4
82.8	53.0	47.2	48.5	45.5	79.2	70.2	82.8	70.2	79.2	75.2
84.7	53.8	47.5	49.1	45.8	80.1	68.9	81.9	70.2	78.4	76.8
85.7	54.6	47.5	48.8	46.6	79.2	70.9	81.0	69.5	81.0	76.8
82.8	53.4	47.2	48.2	46.6	78.4	70.9	79.2	70.9	82.8	75.2
Average	83.8	53.6	47.3	48.6	79.4	70.2	81.3	70.5	80.4	75.6

Run #4(Case-2)

Operating and design parameter	
Date	June 12, 2001
Heat transfer surface area	0.1083 m ²
Superficial gas velocity	3.9 m/s
Power supply	77.7 W
External solid circulation rate	6 kg/m ² s
Voltage	35 V
Bed material	"00" sand
Current	2.22 A

T1 (°C)	T2 (°C)	T3 (°C)	T4 (°C)	T5 (°C)	T6 (°C)	T7 (°C)	T8 (°C)	T9 (°C)	T10 (°C)	T11 (°C)	Tbed (°C)
42.3	47.8	47.6	47	47.3	41.3	42.3	41.5	42.9	41.6	41.7	32.2
42.7	48	48.1	47.5	47.5	41.8	42.5	41.7	43.1	41.8	42.2	32.5
43.2	48.7	48.6	48.9	48	42	43	42.3	43.7	42.3	42.5	32.9
43.7	48.6	48.9	48	49.1	42.4	43.5	42.2	44	42.5	42.9	33.2
43.9	49.2	49	48.4	48.9	43	43.6	43	44.2	43.2	43.1	33.7
44	49.4	49.5	49.1	49	43.3	44	43.1	44.7	43.1	43.6	34

h1 W/m ² K	h2 W/m ² K	h3 W/m ² K	h4 W/m ² K	h5 W/m ² K	h6 W/m ² K	h7 W/m ² K	h8 W/m ² K	h9 W/m ² K	h10 W/m ² K	h11 W/m ² K
71.0	46.0	46.6	48.4	47.5	78.8	71.0	77.1	67.0	76.3	75.5
70.3	46.3	46.0	47.8	47.8	77.1	71.7	77.9	67.6	77.1	73.9
69.6	45.4	45.7	44.8	47.5	78.8	71.0	76.3	66.4	76.3	74.7
68.3	46.6	45.7	48.4	45.1	77.9	69.6	79.7	66.4	77.1	73.9
70.3	46.3	46.9	48.8	47.2	77.1	72.4	77.1	68.3	75.5	76.3
71.7	46.6	46.3	47.5	47.8	77.1	71.7	78.8	67.0	78.8	74.7
Average	70.2	46.2	46.2	47.1	77.8	71.2	77.8	67.1	76.8	74.8

Wing wall places at the top

Run #1(Case-1)

Operating and design parameter	
Date	June25, 2001
Superficial gas velocity	3.9 m/s
External solid circulation rate	6 kg/m ² s
Bed material	“00” sand
	Heat transfer surface area
	0.1083 m ²
	Power supply
	81 W
	Voltage
	34.5 V
	Current
	2.35 A

T1 (°C)	T2 (°C)	T3 (°C)	T4 (°C)	T5 (°C)	T6 (°C)	T7 (°C)	T8 (°C)	T9 (°C)	T10 (°C)	T11 (°C)	Tbed (°C)
43.2	43.7	43.2	43.3	42	40.5	41.1	40.3	41.1	40.4	40.4	33.4
43.3	43.6	43.8	43.7	42.4	40.6	41.2	40.7	41.4	40.5	40.8	33.6
43.9	44	44.5	44	42.7	41.2	41.6	41	41.9	41	41	34
44.3	44.4	44.6	44.7	43	41.7	42	41.7	42.4	41.4	41.6	34.5
44.8	45.1	45	44.9	43.5	42	42.4	41.9	42.7	41.7	42.1	34.8
45.1	45.3	45.4	45.3	43.9	42.4	42.6	42.1	43	42.2	42.4	35.2

h1 W/m ² K	h2 W/m ² K	h3 W/m ² K	h4 W/m ² K	h5 W/m ² K	h6 W/m ² K	h7 W/m ² K	h8 W/m ² K	h9 W/m ² K	h10 W/m ² K	h11 W/m ² K
76.3	72.6	76.3	75.6	87.0	105.4	97.1	108.4	97.1	106.9	106.9
77.1	74.8	73.3	74.1	85.0	106.9	98.4	105.4	95.9	108.4	103.9
75.6	74.8	71.2	74.8	86.0	103.9	98.4	106.9	94.7	106.9	106.9
76.3	75.6	74.1	73.3	88.0	103.9	99.7	103.9	94.7	108.4	105.4
74.8	72.6	73.3	74.1	86.0	103.9	98.4	105.4	94.7	108.4	102.5
75.6	74.1	73.3	74.1	86.0	103.9	101.1	108.4	95.9	106.9	103.9
Average	75.9	74.1	73.6	86.3	104.6	98.9	106.4	95.5	107.6	104.9

Run #2(Case-1)

Operating and design parameter	
Date	June 29, 2001
Heat transfer surface area	0.1083 m ²
Superficial gas velocity	3.9 m/s
Power supply	80 W
External solid circulation rate	2 kg/m ² s
Voltage	35.5 V
Bed material	"00" sand
Current	2.25 A

T1 (°C)	T2 (°C)	T3 (°C)	T4 (°C)	T5 (°C)	T6 (°C)	T7 (°C)	T8 (°C)	T9 (°C)	T10 (°C)	T11 (°C)	Tbed (°C)
45.5	48.7	48.4	48.6	48.6	45.3	45.7	45.5	46.2	46.4	46.6	35.2
46	49.1	49	49	49.1	45.8	46.3	46	46.7	46.9	47.1	35.6
46.3	49.4	49.3	49.3	49.4	46.1	46.6	46.4	47	47.2	47.5	35.8
46.6	49.7	49.7	49.8	50	46.7	47	46.8	47.5	47.7	47.9	36.2
46.9	50	50.4	50.4	50.6	47	47.7	47.1	48.1	48.3	48.4	36.7
47.2	50.4	50.5	50.8	50.9	47.4	48	47.7	48.4	48.4	48.8	37

h1 W/m ² K	h2 W/m ² K	h3 W/m ² K	h4 W/m ² K	h5 W/m ² K	h6 W/m ² K	h7 W/m ² K	h8 W/m ² K	h9 W/m ² K	h10 W/m ² K	h11 W/m ² K
71.5	54.6	55.8	55.0	55.0	73.0	70.2	71.5	67.0	65.8	64.6
70.9	54.6	55.0	55.0	54.6	72.2	68.9	70.9	66.4	65.2	64.1
70.2	54.2	54.6	54.6	54.2	71.5	68.2	69.5	65.8	64.6	63.0
70.9	54.6	54.6	54.2	53.4	70.2	68.2	69.5	65.2	64.1	63.0
72.2	55.4	53.8	53.8	53.0	71.5	67.0	70.9	64.6	63.5	63.0
72.2	55.0	54.6	53.4	53.0	70.9	67.0	68.9	64.6	64.6	62.5
Average	71.3	54.7	54.3	53.9	71.6	68.3	70.2	65.6	64.7	63.4

Experiment on water wall

The locations of thermocouples on the water wall is shown in Fig. D2.

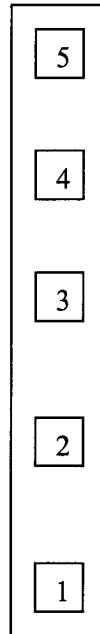


Figure D.2. Locations of thermocouples

Run #1

Operating and design parameter			
Date	July 10, 2001	Heat transfer surface area	0.031m ²
Superficial gas velocity	3.9 m/s	Power supply	20.2 W
External solid circulation rate	6.5 kg/m ² s	Voltage	35.5 V
Bed material	“00” sand	Current	0.57 A

T1 (°C)	T2 (°C)	T3 (°C)	T4 (°C)	T5 (°C)	Tbed (°C)
46.1	46	46	45.1	43.6	36.7
46.5	46.4	46.5	45.5	44.1	37
46.8	46.7	46.6	45.8	44.3	37.2
47.2	47.1	47	46.2	44.8	37.5
47.6	47.5	47.5	46.7	45.1	37.9
48	47.9	47.6	46.9	45.3	38.2

	h1	h2	h3	h4	h5
	W/m²K	W/m²K	W/m²K	W/m²K	W/m²K
	69.5	70.3	70.3	77.8	94.7
	68.8	69.5	68.8	76.9	92.0
	68.1	68.8	69.5	76.0	92.0
	67.4	68.1	68.8	75.1	89.5
	67.4	68.1	68.1	74.3	90.8
Average	66.7	67.4	69.5	75.1	92.0

Run #2

Operating and design parameter			
Date	July 14, 2001	Heat transfer surface area	0.031m ²
Superficial gas velocity	3.9 m/s	Power supply	22 W
External solid circulation rate	3.5 kg/m ² s	Voltage	36 V
Bed material	"00" sand	Current	0.61 A

T1	T2	T3	T4	T5	Tbed
(°C)	(°C)	(°C)	(°C)	(°C)	(°C)
46.7	46.5	46	45.4	44	35
47	46.8	46.4	45.7	44.3	35.2
47.4	47.2	46.8	46.1	44.7	35.5
47.9	47.7	47.2	46.6	45.2	35.9
48.2	48	47.6	47	45.6	36.2
48.6	48.2	47.9	47.1	45.9	36.5

	h1	h2	h3	h4	h5
	W/m²K	W/m²K	W/m²K	W/m²K	W/m²K
	60.6	61.7	64.5	68.2	78.8
	60.1	61.1	63.3	67.5	77.9
	59.6	60.6	62.8	66.9	77.1
	59.1	60.1	62.8	66.3	76.3
	59.1	60.1	62.2	65.7	75.4
Average	58.6	60.6	62.2	66.9	75.4

Run #3

Operating and design parameter			
Date	July 17, 2001	Heat transfer surface area	0.031m ²
Superficial gas velocity	3.62 m/s	Power supply	20.2 W
External solid circulation rate	2.5 kg/m ² s	Voltage	35.5 V
Bed material	“00” sand	Current	0.57A

T1	T2	T3	T4	T5	Tbed
(°C)	(°C)	(°C)	(°C)	(°C)	(°C)
48	47.5	47.5	47	45.5	36.6
48.1	47.9	47.9	47.4	45.9	37
48.4	48.2	48.2	47.5	46.2	37.2
48.9	48.6	48.6	48	46.6	37.4
49.5	49	49.1	48.3	47.1	38
49.6	49.4	49.2	48.7	47.4	38.1

	h1	h2	h3	h4	h5
	W/m²K	W/m²K	W/m²K	W/m²K	W/m²K
	57.3	59.9	59.9	62.8	73.4
	58.9	59.9	59.9	62.8	73.4
	58.3	59.4	59.4	63.4	72.6
	56.8	58.3	58.3	61.6	71.0
	56.8	59.4	58.9	63.4	71.8
Average	56.8	57.8	58.9	61.6	70.3

Appendix E

Experiments on the stand pipe:

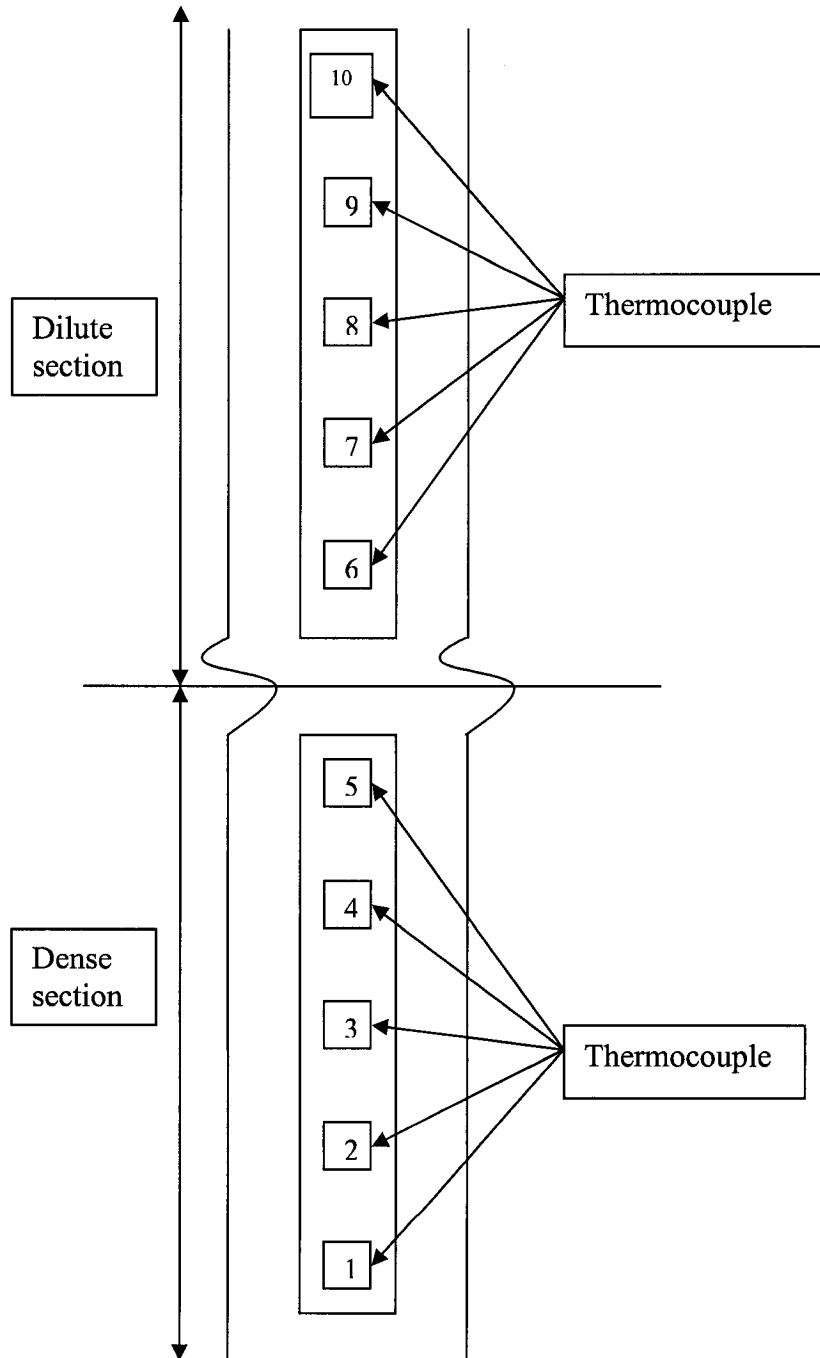


Figure E.1. Locations of thermocouples on the wall of standpipe

Run #1

Operating and design parameter	
Date	May 03, 2001
External solid circulation rate	18.8 kg/m ² s
Bed material	Ceramic
	Microsphere
	Heat transfer surface area
	0.0619 m ²
	Power supply
	45 W
	Types of particle
	A
	Conductivity of wood
	0.06 W/mK

No of data	T1 (°C)	T2 (°C)	T3 (°C)	T4 (°C)	T5 (°C)	T6 (°C)	T7 (°C)	T8 (°C)	T9 (°C)	T10 (°C)	Tbed (°C)	Tout (°C)
1	31	29.5	29	28.6	28.3	32.3	31.8	31.4	31	29.7	23.5	
2	31.1	29.8	29.2	28.8	28.5	32.6	32	31.7	31.2	30	23.7	
3	31.3	29.8	29.3	28.8	28.6	32.8	32	31.7	31.3	30	23.8	35
4	31.5	30	29.4	29.1	28.8	33	32.3	32	31.5	30.2	24	
5	31.8	30.3	29.7	29.3	29	33.2	32.5	32.2	31.6	30.4	24.2	
Average	31.3	29.9	29.3	28.9	28.6	32.8	32.1	31.8	31.3	30.1	23.8	35

	h1 W/m ² K	h2 W/m ² K	h3 W/m ² K	h4 W/m ² K	h5 W/m ² K	h6 W/m ² K	h7 W/m ² K	h8 W/m ² K	h9 W/m ² K	h10 W/m ² K
	89.7	112.1	122.3	131.9	140.2	76.5	81.1	85.2	89.7	108.5
	90.9	110.3	122.3	131.9	140.2	75.6	81.1	84.1	89.7	106.8
	89.7	112.1	122.3	134.6	140.2	74.8	82.0	85.2	89.7	108.5
	89.7	112.1	124.6	131.9	140.2	74.8	81.1	84.1	89.7	108.5
	88.5	110.3	122.3	131.9	140.2	74.8	81.1	84.1	90.9	108.5
Average	89.7	111.4	122.8	132.5	140.2	75.3	81.3	84.5	89.9	108.2

Run #2

Operating and design parameter	
Date	May 06, 2001
External solid circulation rate	13.9 kg/m ² s
Bed material	Ceramic Microsphere
	Heat transfer surface area
	Power supply
	Types of particle
	Conductivity of wood
	0.0619 m ²
	40 W
	A
	0.06 W/mK

No of data	T1 (°C)	T2 (°C)	T3 (°C)	T4 (°C)	T5 (°C)	T6 (°C)	T7 (°C)	T8 (°C)	T9 (°C)	T10 (°C)	Tbed (°C)	Tout (°C)
1	32.1	31.6	31	31.2	30	34.4	34.3	33.9	33.5	31.6	25.2	
2	32.2	31.7	31.2	31.2	30	34.5	34.5	34	33.7	31.7	25.3	
3	32.5	32	31.4	31.4	30.1	34.7	34.7	34	33.9	31.8	25.5	34
4	32.5	32	31.5	31.6	30.3	34.7	34.8	34.2	34	32	25.6	
5	32.7	32.2	31.7	31.7	30.5	35	35	34.5	34.2	32.2	25.8	
Average	32.4	31.9	31.4	31.4	30.2	34.7	34.7	34.1	33.9	31.9	25.5	34

	h1 W/m ² K	h2 W/m ² K	h3 W/m ² K	h4 W/m ² K	h5 W/m ² K	h6 W/m ² K	h7 W/m ² K	h8 W/m ² K	h9 W/m ² K	h10 W/m ² K
	87.7	94.5	104.3	100.8	126.0	65.8	66.5	69.5	72.9	94.5
	87.7	94.5	102.5	102.5	128.7	65.8	65.8	69.5	72.0	94.5
	86.4	93.1	102.5	102.5	131.5	65.8	65.8	71.2	72.0	96.0
	87.7	94.5	102.5	100.8	128.7	66.5	65.8	70.4	72.0	94.5
	87.7	94.5	102.5	102.5	128.7	65.8	65.8	69.5	72.0	94.5
Average	87.4	94.2	102.9	101.9	128.8	65.9	65.9	70.0	72.2	94.8

Run #3

Operating and design parameter	
Date	May 10, 2001
External solid circulation rate	11.14 kg/m ² s
Bed material	Ceramic
	Microsphere
	Heat transfer surface area
	0.0619 m ²
	Power supply
	30 W
	Types of particle
	A
	Conductivity of wood
	0.06 W/mK

Data of temperature at different point on the surfaces.

No of data	T1 (°C)	T2 (°C)	T3 (°C)	T4 (°C)	T5 (°C)	T6 (°C)	T7 (°C)	T8 (°C)	T9 (°C)	T10 (°C)	Tbed (°C)	Tout (°C)
1	30.2	29.6	29.4	29.3	28	33.2	33.5	32.4	31.3	30.1	24.7	
2	30.3	29.7	29.7	29.4	28.3	33.5	33.8	32.7	31.4	30.2	24.8	
3	30.3	29.9	29.7	29.4	28.3	33.5	33.9	32.9	31.5	30.4	25	33
4	30.6	30.2	29.9	29.7	28.4	33.6	34.2	33	31.6	30.7	25.2	
5	30.8	30.3	30.2	29.9	28.7	33.9	34.3	33.2	31.9	30.8	25.5	
Average	30.4	29.9	29.7	29.5	28.4	33.6	33.9	32.9	31.5	30.4	25.0	33.0

	h1 W/m ² K	h2 W/m ² K	h3 W/m ² K	h4 W/m ² K	h5 W/m ² K	h6 W/m ² K	h7 W/m ² K	h8 W/m ² K	h9 W/m ² K	h10 W/m ² K
	83.1	91.4	95	99.1	133.1	52.2	50	56.8	68.5	83.2
	83.0	90.6	95.3	99.2	133.4	52.1	50.1	56.8	68.5	83.1
	82.9	91.3	94.8	99	133.2	52.4	50.3	56.8	68.5	83.2
	83.2	91.2	95.1	99.2	133.1	52.6	50.1	56.8	68.5	82.4
	82.8	90.5	95.2	99.3	133.3	52.6	50.1	56.8	68.5	83.2
Average	83.0	91.0	95.4	99.2	133.2	52.4	50.1	56.8	68.5	83.1

Reproduced data for the same condition and experiment conducted on June 12, 2001 for type A particle and $G_s=11 \text{ kg/m}^2 \cdot \text{s}$

No of data	T1 ($^{\circ}\text{C}$)	T2 ($^{\circ}\text{C}$)	T3 ($^{\circ}\text{C}$)	T4 ($^{\circ}\text{C}$)	T5 ($^{\circ}\text{C}$)	T6 ($^{\circ}\text{C}$)	T7 ($^{\circ}\text{C}$)	T8 ($^{\circ}\text{C}$)	T9 ($^{\circ}\text{C}$)	T10 ($^{\circ}\text{C}$)	Tbed ($^{\circ}\text{C}$)	Tout ($^{\circ}\text{C}$)
1	32.4	31.7	31.7	31.4	30.4	36	36.1	35.3	33.4	32.4	27	
2	32.7	31.9	32	31.7	30.6	36.1	36.4	35.4	33.7	32.6	27.2	
3	33	32.1	32.2	31.9	30.8	36.4	36.5	35.8	33.9	32.8	27.4	35
4	33	32.4	32.3	32.2	30.9	36.5	36.4	35.8	34	33	27.5	
5	33.2	32.8	32.6	32.3	31.1	36.7	36.7	36	34.2	33.2	27.7	
Average	32.9	32.2	32.2	31.9	30.8	36.3	36.4	35.7	33.8	32.8	27.4	35.0

	h1 $\text{W/m}^2\text{K}$	h2 $\text{W/m}^2\text{K}$	h3 $\text{W/m}^2\text{K}$	h4 $\text{W/m}^2\text{K}$	h5 $\text{W/m}^2\text{K}$	h6 $\text{W/m}^2\text{K}$	h7 $\text{W/m}^2\text{K}$	h8 $\text{W/m}^2\text{K}$	h9 $\text{W/m}^2\text{K}$	h10 $\text{W/m}^2\text{K}$
	82.9	95.3	95.3	101.8	131.7	49.8	49.2	54.0	70.0	82.9
	81.4	95.3	93.3	99.5	131.6	50.3	48.7	54.6	68.9	82.9
	80.0	95.3	93.3	99.5	131.7	49.8	49.2	53.3	68.9	82.9
	81.4	91.4	93.3	95.3	131.8	49.8	50.3	54.0	68.9	81.4
	81.4	87.8	91.4	97.4	131.7	49.8	49.8	54.0	68.9	81.4
Average	81.4	93.0	93.3	98.7	131.7	49.9	49.4	54.0	69.1	82.3

Operating and design parameter	
Date	May 15, 2001
External solid circulation rate	18 kg/m ² s
Bed material	“00” Sand
	Heat transfer surface area
	Power supply
	Types of particle
	Conductivity of wood

0.0619 m²
30 W
B
0.06 W/mK

Data of temperature at different point on the surfaces.

No of data	T1 (°C)	T2 (°C)	T3 (°C)	T4 (°C)	T5 (°C)	T6 (°C)	T7 (°C)	T8 (°C)	T9 (°C)	T10 (°C)	Tbed (°C)	Tout (°C)
1	31.3	30.4	30.1	29.4	28.4	39.5	39.1	38.6	39.2	35.6	25.2	
2	31.5	30.6	30.3	29.6	28.5	39.7	39.4	38.8	39.4	35.7	25.3	
3	31.8	30.7	30.5	29.7	28.8	39.9	39.6	38.9	39.6	36	25.5	33
4	32	31	30.6	30	28.9	40	39.7	39	39.7	36	25.6	
5	32.4	31.2	30.7	30.2	29	40.2	40	39.3	40	36.2	25.8	
Average	31.8	30.8	30.4	29.8	28.7	39.9	39.6	38.9	39.6	35.9	25.5	33.0

	h1 W/m ² K	h2 W/m ² K	h3 W/m ² K	h4 W/m ² K	h5 W/m ² K	h6 W/m ² K	h7 W/m ² K	h8 W/m ² K	h9 W/m ² K	h10 W/m ² K
	73.5	86.2	91.5	106.8	140.1	31.4	32.3	33.5	32.0	43.1
	72.3	84.6	89.7	104.3	140.1	31.1	31.8	33.2	31.8	43.1
	71.2	86.2	89.7	106.8	135.9	31.1	31.8	33.5	31.8	42.7
	70.1	83.0	89.7	101.9	135.9	31.1	31.8	33.5	31.8	43.1
	67.9	83.0	91.5	101.9	140.1	31.1	31.6	33.2	31.6	43.1
Average	71.0	84.6	90.4	104.3	138.4	31.2	31.8	33.4	31.8	43.0

Operating and design parameter	
Date	May 18, 2001
External solid circulation rate	13.5 kg/m ² s
Bed material	“00” Sand
	Heat transfer surface area
	0.0619 m ²
	Power supply
	45 W
	Types of particle
	B
	Conductivity of wood
	0.06 W/mK

Data of temperature at different point on the surfaces.

No of data	T1 (°C)	T2 (°C)	T3 (°C)	T4 (°C)	T5 (°C)	T6 (°C)	T7 (°C)	T8 (°C)	T9 (°C)	T10 (°C)	Tbed (°C)	Toutside (°C)
1	34.6	33.2	33	32.5	28.6	46.6	46.6	45.6	46.8	40.5	23.8	
2	34.9	33.4	33.3	32.7	28.7	47	46.9	45.7	47	40.7	24	
3	35.3	33.8	33.6	33	29	47.1	47	46	47.3	41	24.3	35
4	35.5	34	33.7	33.2	29.4	47.5	47.4	46.3	47.6	41.2	24.5	
5	35.7	34	34	33.3	29.5	47.6	47.5	46.4	47.7	41.3	24.6	
Average	35.2	33.7	33.5	32.9	29.0	47.2	47.1	46.0	47.3	40.9	24.2	35.0

	h1 W/m ² K	h2 W/m ² K	h3 W/m ² K	h4 W/m ² K	h5 W/m ² K	h6 W/m ² K	h7 W/m ² K	h8 W/m ² K	h9 W/m ² K	h10 W/m ² K
	62.5	71.8	73.4	77.6	140.7	29.6	29.6	31.0	29.4	40.2
	61.9	71.8	72.6	77.4	143.7	29.4	29.5	31.1	29.4	40.4
	61.4	71.1	72.6	77.6	143.7	29.6	29.7	31.1	29.4	40.4
	61.4	71.1	73.4	77.7	137.8	29.4	29.5	31.0	29.2	40.6
	60.8	71.8	71.8	77.6	137.8	29.4	29.5	31.0	29.2	40.4
Average	61.6	71.5	72.8	77.6	140.7	29.5	29.6	31.0	29.3	40.4

Operating and design parameter	
Date	May 22, 2001
External solid circulation rate	11.5 kg/m ² s
Bed material	“00” Sand
	Heat transfer surface area
	Power supply
	Types of particle
	Conductivity of wood
	0.0619 m ²
	30 W
	B
	0.06 W/mK

Data of temperature at different point on the surfaces.

No of data	T1 (°C)	T2 (°C)	T3 (°C)	T4 (°C)	T5 (°C)	T6 (°C)	T7 (°C)	T8 (°C)	T9 (°C)	T10 (°C)	Tbed (°C)	Toutside (°C)
1	33.6	32.9	32.5	32.1	29.6	44.8	44.2	44.6	45.7	38.5	25.8	
2	33.8	33	32.8	32.4	29.9	45	44.4	44.9	45.9	38.7	26	
3	34.2	33.5	33	32.7	30.1	45.4	44.8	45.2	46.3	39	26.3	34
4	34.5	33.8	33.4	33	30.5	45.8	45.1	45.6	46.6	39.4	26.6	
5	34.6	33.9	33.5	33	30.7	45.9	45.2	45.7	46.8	39.5	26.7	
Average	34.1	33.4	33.0	32.6	30.2	45.4	44.7	45.2	46.3	39.0	26.3	34.0

	h1 W/m ² K	h2 W/m ² K	h3 W/m ² K	h4 W/m ² K	h5 W/m ² K	h6 W/m ² K	h7 W/m ² K	h8 W/m ² K	h9 W/m ² K	h10 W/m ² K
	57.4	63.0	66.8	71.0	117.7	23.5	24.3	23.8	22.5	35.2
	57.4	63.9	65.8	69.9	114.7	23.5	24.3	23.7	22.5	35.2
	56.6	62.1	66.8	69.9	117.7	23.4	24.2	23.7	22.4	35.2
	56.6	62.1	65.8	69.9	114.7	23.3	24.2	23.5	22.4	35.0
	56.6	62.1	65.8	71.0	111.9	23.3	24.2	23.5	22.3	35.0
Average	56.9	62.7	66.2	70.4	115.4	23.4	24.2	23.6	22.4	35.1

Operating and design parameter	
Date	May 25, 2001
External solid circulation rate	27 kg/m ² s
Bed material	“00” Sand
	Heat transfer surface area
	Power supply
	Types of particle
	Conductivity of wood
	0.0619 m ²
	50 W
	B
	0.06 W/mK

Data of temperature at different points on the surface.

No of data	T1 (°C)	T2 (°C)	T3 (°C)	T4 (°C)	T5 (°C)	T6 (°C)	T7 (°C)	T8 (°C)	T9 (°C)	T10 (°C)	Tbed (°C)	Toutside (°C)
1	34.7	33.4	33.1	32	30.7	47	46.1	44.6	44	41.5	25.7	
2	35	33.7	33.3	32.4	31	47.3	46.3	44.7	44.3	41.7	25.9	
3	35.3	33.9	33.6	32.5	31.2	47.4	46.5	45	44.5	42	26.1	38
4	35.4	34	33.7	32.6	31.4	47.7	46.7	45.3	44.6	42.1	26.3	
5	35.7	34.4	34	33	31.7	47.9	47	45.4	44.8	42.4	26.5	
Average	35.2	33.9	33.5	32.5	31.2	47.5	46.5	45.0	44.4	41.9	26.1	38.0

	h1 W/m ² K	h2 W/m ² K	h3 W/m ² K	h4 W/m ² K	h5 W/m ² K	h6 W/m ² K	h7 W/m ² K	h8 W/m ² K	h9 W/m ² K	h10 W/m ² K
	83.4	97.4	101.4	119.1	150.0	35.2	36.8	39.7	41.0	47.5
	82.4	96.2	101.4	115.4	147.1	35.1	36.9	39.9	40.8	47.5
	81.5	96.2	100.0	117.2	147.1	35.2	36.8	39.7	40.8	47.2
	82.4	97.4	101.4	119.1	147.1	35.1	36.7	39.5	41.0	47.5
	81.5	95.0	100.0	115.4	144.3	35.1	36.6	39.7	41.0	47.2
Average	82.3	96.4	100.8	117.2	147.1	35.1	36.7	39.7	40.9	47.4

Operating and design parameter	
Date	May 27, 2001
External solid circulation rate	47 kg/m ² s
Bed material	"00" Sand
	Heat transfer surface area
	Power supply
	Types of particle
	Conductivity of wood
	0.0619 m ²
	60 W
	B
	0.06 W/mK

Data of temperature at different point on the surfaces.

No of data	T1 (°C)	T2 (°C)	T3 (°C)	T4 (°C)	T5 (°C)	T6 (°C)	T7 (°C)	T8 (°C)	T9 (°C)	T10 (°C)	Tbed (°C)	Toutside (°C)
1	33.6	32.6	32.1	31.8	31	46	42.6	42.1	41.6	37	25.2	
2	33.8	32.8	32.3	31.9	31	46.1	42.7	42.3	41.7	37.2	25.3	
3	34	33	32.4	32	31.2	46.2	43	42.5	42	37.5	25.5	39
4	34.2	33.2	32.6	32.1	31.3	46.4	43	42.6	42	37.6	25.6	
5	34.5	33.5	32.8	32.3	31.6	46.7	43.3	42.9	42.3	37.9	25.8	
Average	34.0	33.0	32.4	32.0	31.2	46.3	42.9	42.5	41.9	37.4	25.5	39.0

	h1 W/m ² K	h2 W/m ² K	h3 W/m ² K	h4 W/m ² K	h5 W/m ² K	h6 W/m ² K	h7 W/m ² K	h8 W/m ² K	h9 W/m ² K	h10 W/m ² K
	107.6	122.2	131.0	137.0	155.9	43.5	52.0	53.5	55.1	76.6
	106.3	120.5	129.1	137.0	158.6	43.5	52.0	53.2	55.1	76.0
	106.3	120.5	131.0	139.1	158.6	43.7	51.7	53.2	54.8	75.3
	105.1	118.9	129.1	139.1	158.6	43.5	52.0	53.2	55.1	75.3
	103.9	117.4	129.1	139.1	155.9	43.3	51.7	52.9	54.8	74.7
Average	105.9	119.9	129.9	138.2	157.5	43.5	51.8	53.2	55.0	75.6

Reproduced data for the above condition and experiment conducted on June 12, 2001 for type B particle and $G_s=46 \text{ kg/m}^2 \cdot \text{s}$

No of data	T1 ($^{\circ}\text{C}$)	T2 ($^{\circ}\text{C}$)	T3 ($^{\circ}\text{C}$)	T4 ($^{\circ}\text{C}$)	T5 ($^{\circ}\text{C}$)	T6 ($^{\circ}\text{C}$)	T7 ($^{\circ}\text{C}$)	T8 ($^{\circ}\text{C}$)	T9 ($^{\circ}\text{C}$)	T10 ($^{\circ}\text{C}$)	Tbed ($^{\circ}\text{C}$)	Tout ($^{\circ}\text{C}$)
1	36	34.7	33.9	33.4	32.4	47.5	44.6	43.5	42.8	38.5	27.1	
2	36.3	34.8	34.3	33.7	32.9	47.8	44.9	43.8	43	38.8	27.3	
3	36.4	35.2	34.4	33.9	33	48	45.1	43.8	43.1	39	27.4	41
4	36.5	35.4	34.7	34	33.4	48.2	45.4	44	43.5	39.2	27.6	
5	36.5	35.7	34.9	34.2	33.6	48.4	45.6	44.4	43.7	39.5	27.8	
Average	36.3	35.2	34.4	33.8	33.1	48.0	45.1	43.9	43.2	39.0	27.4	41.0

	h1 $\text{W/m}^2\text{K}$	h2 $\text{W/m}^2\text{K}$	h3 $\text{W/m}^2\text{K}$	h4 $\text{W/m}^2\text{K}$	h5 $\text{W/m}^2\text{K}$	h6 $\text{W/m}^2\text{K}$	h7 $\text{W/m}^2\text{K}$	h8 $\text{W/m}^2\text{K}$	h9 $\text{W/m}^2\text{K}$	h10 $\text{W/m}^2\text{K}$
	101.5	118.9	132.9	143.4	170.5	44.3	51.6	55.1	57.5	79.3
	100.4	120.5	129.1	141.2	161.3	44.1	51.3	54.8	57.5	78.6
	100.4	115.8	129.1	139.0	161.3	43.9	51.0	55.1	57.5	77.9
	101.5	115.8	127.2	141.2	155.8	43.9	50.8	55.1	56.8	77.9
	103.8	114.4	127.2	141.2	155.8	43.9	50.8	54.4	56.8	77.2
Average	101.5	117.1	129.1	141.2	160.9	44.0	51.1	54.9	57.3	78.2

Appendix F

Experiments on the cavity type inertial separator:

Heat transfer measurements on both inner and outer wall of the cavity type inertial separators were carried out and the locations of the thermocouples are shown in Figure F.1.

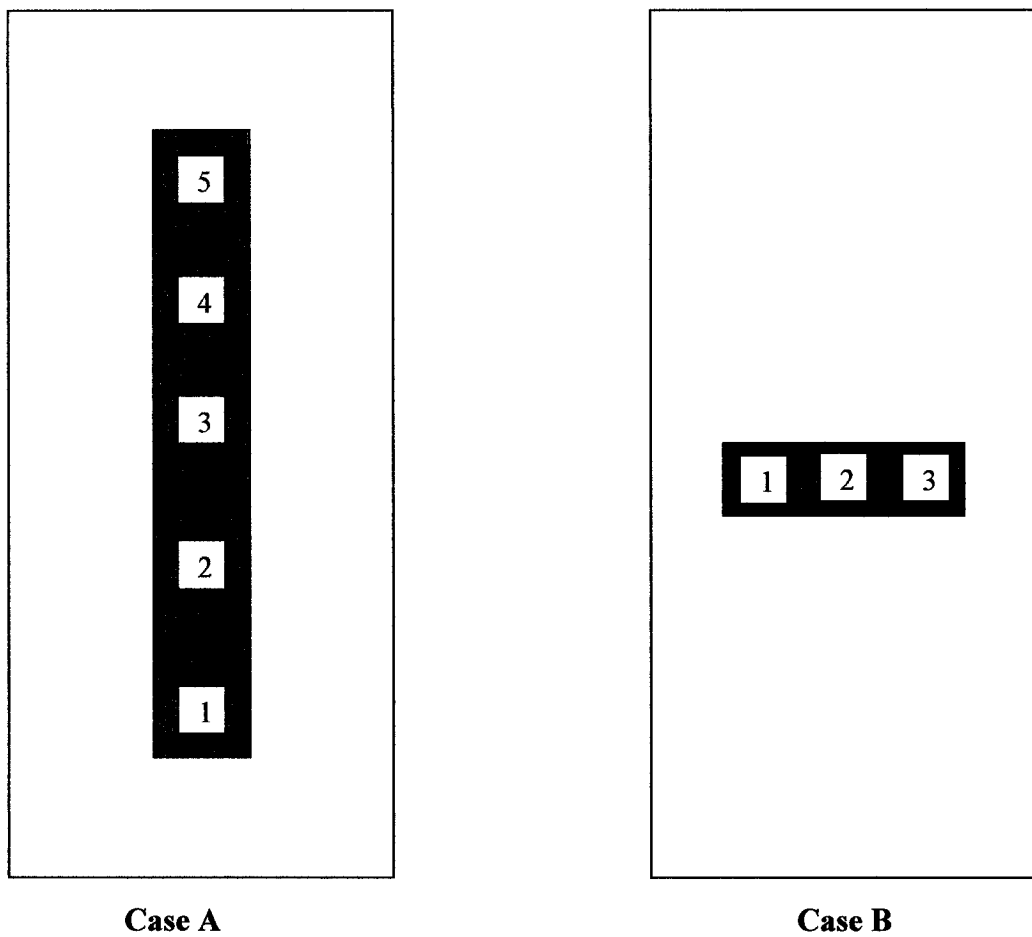


Figure E.1. Locations of thermocouples on the wall of standpipe

Run #1

Operating and design parameter		Sept 03, 2001	Heat transfer surface area
Date		Sept 03, 2001	0.0619 m ²
External solid circulation rate		2.2 kg/m ² s	40 W
Bed material		"00" sand	B
Superficial gas velocity		3.9 m/s	
			Power supply
			Types of particle

No of data	Inside furnace					Inside primary chamber						
	T1 (°C)	T2 (°C)	T3 (°C)	T4 (°C)	T5 (°C)	Tbed (°C)	T1 (°C)	T2 (°C)	T8 (°C)	T9 (°C)	T10 (°C)	Tbed (°C)
1	43.1	42.8	43.1	42.8	40.2	29.3	40.4	41	40.2	41	41	29.3
2	43.4	43.1	43.5	43.2	40.6	29.5	40.5	41.3	40.5	41.1	40.8	29.5
3	43.3	43.5	43.8	43.5	40.8	29.6	40.5	41.2	40.8	41.3	41.4	29.6
4	43.7	43.8	44.1	43.6	41.2	29.8	41	41.8	41.1	41.2	41.3	29.8
5	44.2	44.2	44.4	44	41.5	30	41.5	42	41.4	42	41.8	30
Average	43.5	43.5	43.8	43.4	40.9	29.6	40.8	41.5	40.8	41.3	41.3	29.6

Inside furnace					Inside primary chamber				
h1 W/m ² K	h2 W/m ² K	h3 W/m ² K	h4 W/m ² K	h5 W/m ² K	h1 W/m ² K	h2 W/m ² K	h3 W/m ² K	h5 W/m ² K	h5 W/m ² K
45.6	46.6	45.6	46.6	57.8	56.7	53.8	57.8	53.8	53.8
45.3	46.3	45.0	45.9	56.7	57.2	53.3	57.2	54.3	55.7
45.9	45.3	44.3	45.3	56.2	57.8	54.3	56.2	53.8	53.3
45.3	45.0	44.0	45.6	55.2	56.2	52.5	55.7	55.2	54.7
44.3	44.3	43.7	45.0	54.7	54.7	52.5	55.2	52.5	53.3
Average	45.3	45.5	44.5	56.1	56.5	53.3	56.4	53.9	54.2

Run #2

Operating and design parameter	
Date	Sept 06, 2001
External solid circulation rate	3 kg/m ² s
Bed material	"00" sand
Superficial gas velocity	3.9 m/s
	Heat transfer surface area
	Power supply
	Types of particle
	0.0619 m ²
	45 W
	B

No of data	Inside furnace					Inside primary chamber						
	T1 (°C)	T2 (°C)	T3 (°C)	T4 (°C)	T5 (°C)	Tbed (°C)	T1 (°C)	T2 (°C)	T8 (°C)	T9 (°C)	T10 (°C)	Tbed (°C)
1	45.8	47	47	48.2	43	30.1	41.4	41.2	43	43	42.7	30.1
2	46.2	47.4	47.5	48.6	43.6	30.4	41.8	42	43.6	43.5	43.2	30.4
3	46.6	47.8	47.8	48.9	43.8	30.6	41.7	42.3	43.8	43.5	43.6	30.6
4	47	48.2	48	49	44.2	30.8	42.3	42.7	43.7	43.8	43.6	30.8
5	47.3	48.5	48.4	49	44.3	31	42.5	42.8	44	44	44	31
Average	46.6	47.8	47.7	48.7	43.8	30.6	41.9	42.2	43.6	43.6	43.4	30.6

	Inside furnace					Inside primary chamber				
	h1 W/m ² K	h2 W/m ² K	h3 W/m ² K	h4 W/m ² K	h5 W/m ² K	h1 W/m ² K	h2 W/m ² K	h3 W/m ² K	h5 W/m ² K	h5 W/m ² K
	46.3	43.0	43.0	40.1	56.3	64.3	65.5	56.3	56.3	57.7
	46.0	42.7	42.5	39.9	55.0	63.7	62.6	55.0	55.5	56.8
	45.4	42.2	42.2	39.7	55.0	65.5	62.1	55.0	56.3	55.9
	44.8	41.8	42.2	39.9	54.2	63.2	61.1	56.3	55.9	56.8
	44.6	41.5	41.8	40.4	54.6	63.2	61.6	55.9	55.9	55.9
Average	45.4	42.2	42.3	40.0	55.1	64.0	62.6	55.7	56.0	56.6

Run #3

Operating and design parameter	
Date	Sept 10, 2001
External solid circulation rate	4.3 kg/m ² s
Bed material	“00” sand
Superficial gas velocity	3.9 m/s
	Heat transfer surface area
	Power supply
	Types of particle
	0.0619 m ²
	45 W
	B

No of data	Inside furnace					Inside primary chamber						
	T1 (°C)	T2 (°C)	T3 (°C)	T4 (°C)	T5 (°C)	Tbed (°C)	T1 (°C)	T2 (°C)	T8 (°C)	T9 (°C)	T10 (°C)	Tbed (°C)
1	44.6	45.1	45	46.2	41.4	29	40	40	41	40.5	40.3	29
2	45.2	45.4	45.5	46.7	41.8	29.3	40.1	40.5	41.3	40.7	40.7	29.3
3	45	45.8	46	46.6	42	29.6	40.8	40.6	41.4	40.9	41	29.6
4	45.5	46	46.2	46.9	42.3	29.7	40.7	40.9	41.8	41.1	41.3	29.7
5	45.8	46	46.7	47.2	42.5	29.9	41	41	41.9	41.5	41.6	29.9
Average	45.2	45.7	45.9	46.7	42.0	29.5	40.5	40.6	41.5	40.9	41.0	29.5

	Inside furnace					Inside primary chamber				
	h1 W/m ² K	h2 W/m ² K	h3 W/m ² K	h4 W/m ² K	h5 W/m ² K	h1 W/m ² K	h2 W/m ² K	h3 W/m ² K	h5 W/m ² K	h5 W/m ² K
	46.6	45.1	45.4	42.2	58.6	66.1	66.1	60.5	63.2	64.3
	45.7	45.1	44.8	41.8	58.1	67.3	64.9	60.5	63.7	63.7
	47.2	44.8	44.3	42.7	58.6	64.9	66.1	61.6	64.3	63.7
	46.0	44.6	44.0	42.2	57.7	66.1	64.9	60.0	63.7	62.6
	45.7	45.1	43.2	42.0	57.7	65.5	65.5	60.5	62.6	62.1
Average	46.2	45.0	44.4	42.2	58.1	65.9	65.5	60.7	63.5	63.3

Run #4

Operating and design parameter	
Date	Sept 13, 2001
External solid circulation rate	1 kg/m ² s
Bed material	“00” sand
Superficial gas velocity	3.6 m/s
	Heat transfer surface area
	Power supply
	Types of particle
	0.0619 m ²
	40 W
	B

No of data	Inside furnace					Inside primary chamber						
	T1 (°C)	T2 (°C)	T3 (°C)	T4 (°C)	T5 (°C)	Tbed (°C)	T1 (°C)	T2 (°C)	T8 (°C)	T9 (°C)	T10 (°C)	Tbed (°C)
1	45	46.2	45.9	46.5	41.9	30.1	40.9	42	42	42.4	41.6	30.1
2	44.8	46.5	45.8	46.4	42	30.3	41.1	42.1	42.6	42.3	42	30.3
3	45.6	46.8	46	46.6	42.1	30.5	41.4	42.6	42.4	42.9	42.2	30.5
4	45.3	47	46.4	47	42.6	30.6	41.4	42.8	42.5	43	42.2	30.6
5	45.5	47.3	46.8	47.3	42.7	30.8	41.6	42.7	42.7	43.5	42.6	30.8
Average	45.2	46.8	46.2	46.8	42.3	30.5	41.3	42.4	42.4	42.8	42.1	30.5

	Inside furnace					Inside primary chamber				
	h1 W/m ² K	h2 W/m ² K	h3 W/m ² K	h4 W/m ² K	h5 W/m ² K	h1 W/m ² K	h2 W/m ² K	h3 W/m ² K	h5 W/m ² K	h5 W/m ² K
	43.3	40.1	40.9	39.4	54.7	59.8	54.3	54.3	52.5	56.2
	44.5	39.9	41.7	40.1	55.2	59.8	54.7	52.5	53.8	55.2
	42.8	39.6	41.7	40.1	55.7	59.3	53.4	54.3	52.1	55.2
	43.9	39.4	40.9	39.4	53.8	59.8	52.9	54.3	52.1	55.7
	43.9	39.1	40.4	39.1	54.3	59.8	54.3	54.3	50.9	54.7
Average	43.7	39.6	41.1	39.6	54.7	59.7	53.9	53.9	52.3	55.4

Run #5

Operating and design parameter	
Date	Sept 17, 2001
External solid circulation rate	5.7 kg/m ² s
Bed material	"00" sand
Superficial gas velocity	4.4 m/s
	Heat transfer surface area
	Power supply
	Types of particle
	0.0619 m ²
	50 W
	B

No of data	Inside furnace					Inside primary chamber						
	T1 (°C)	T2 (°C)	T3 (°C)	T4 (°C)	T5 (°C)	Tbed (°C)	T1 (°C)	T2 (°C)	T8 (°C)	T9 (°C)	T10 (°C)	Tbed (°C)
1	46.1	46	46	46.6	42.4	29.2	41	41.4	41.7	41.9	42.3	29.2
2	46.1	46.1	46.4	46.9	42.8	29.4	41.1	41.7	42	42.2	42.4	29.4
3	46.7	46.5	46.8	47.4	43	29.7	41.4	41.9	42.4	42.6	42.8	29.7
4	46.9	46.7	47	47.3	43	29.8	41.7	42.2	42.6	42.8	43	29.8
5	46.7	47	47.1	47.5	43.4	30	42	42.5	42.8	43	43	30
Average	46.5	46.5	46.7	47.1	42.9	29.6	41.4	41.9	42.3	42.5	42.7	29.6

h1 W/m ² K	Inside furnace					Inside primary chamber				
	h2 W/m ² K	h3 W/m ² K	h4 W/m ² K	h5 W/m ² K	h5 W/m ² K	h1 W/m ² K	h2 W/m ² K	h3 W/m ² K	h5 W/m ² K	h5 W/m ² K
47.8	48.1	48.1	46.4	61.2	61.2	68.4	66.2	64.6	63.6	61.6
48.3	48.3	47.5	46.1	60.2	60.2	69.0	65.6	64.1	63.1	62.1
47.5	48.1	47.2	45.6	60.7	60.7	69.0	66.2	63.6	62.6	61.6
47.2	47.8	46.9	46.1	61.2	61.2	67.8	65.1	63.1	62.1	61.2
48.3	47.5	47.2	46.1	60.2	60.2	67.3	64.6	63.1	62.1	62.1
Average	47.8	47.9	47.4	46.1	60.7	68.3	65.5	63.7	62.7	61.7

Run #1

Operating and design parameter	
Date	Sept 25, 2001
External solid circulation rate	4 kg/m ² s
Bed material	"00" sand
Superficial gas velocity	3.81 m/s
	Heat transfer surface area
	Power supply
	Types of particle
	0.0619 m ²
	50 W
	B

No of data	Inner wall of Inside furnace					Outer wall of Inside furnace						
	T1 (°C)	T2 (°C)	T3 (°C)	T4 (°C)	T5 (°C)	Tbed (°C)	T1 (°C)	T2 (°C)	T8 (°C)	T9 (°C)	T10 (°C)	Tbed (°C)
1	45	45	45.8	45	42.1	29.3	38.6	38.5	37.8	37.6	37.2	29.3
2	45.2	45.1	46	45.5	42.4	29.5	38.7	38.8	38.1	37.7	37.3	29.5
3	45.4	45.5	46.3	45.3	42.3	29.6	39	39	38.1	37.9	37.6	29.6
4	45.6	45.3	46.2	45.7	42.8	29.8	39.2	39.2	38.4	39	37.7	29.8
5	45.9	45.8	46.7	45.8	43	30	39.4	39.5	38.6	39.4	38	30
Average	45.4	45.3	46.2	45.5	42.5	29.6	39.0	39.0	38.2	38.3	37.6	29.6

Inside furnace					Inside primary chamber				
h1 W/m ² K	h2 W/m ² K	h3 W/m ² K	h4 W/m ² K	h5 W/m ² K	h1 W/m ² K	h2 W/m ² K	h3 W/m ² K	h5 W/m ² K	h5 W/m ² K
51.4	51.4	48.9	51.4	63.1	86.8	87.7	95.0	97.3	102.2
51.4	51.7	48.9	50.5	62.6	87.7	86.8	93.9	98.5	103.5
51.1	50.8	48.3	51.4	63.6	85.9	85.9	95.0	97.3	100.9
51.1	52.1	49.2	50.8	62.1	85.9	85.9	93.9	87.7	102.2
50.8	51.1	48.3	51.1	62.1	85.9	85.0	93.9	85.9	100.9
Average	51.2	51.4	48.8	51.0	86.4	86.3	94.3	93.3	101.9

Run #2

Operating and design parameter	
Date	Sept 27, 2001
External solid circulation rate	4 kg/m ² s
Bed material	"00" sand
Superficial gas velocity	3.62 m/s
	Heat transfer surface area
	Power supply
	Types of particle
	0.0619 m ²
	50 W
	B

No of data	Inner wall of Inside furnace						Outer wall of Inside furnace					
	T1 (°C)	T2 (°C)	T3 (°C)	T4 (°C)	T5 (°C)	Tbed (°C)	T1 (°C)	T2 (°C)	T8 (°C)	T9 (°C)	T10 (°C)	Tbed (°C)
1	46.4	47.4	47.4	46.8	43.8	31	40.8	40.5	40.1	39.6	39	31
2	46.5	47.7	47.7	46.9	43.9	31.2	41.1	40.6	40.4	39.9	39.4	31.2
3	46.9	47.8	47.8	47.3	44.1	31.4	41.4	41	40.7	40	39.5	31.4
4	47	48	48	47.6	44.7	31.7	41.5	41.3	40.9	40.4	39.8	31.7
5	47.2	48.4	48	47.6	44.9	31.8	41.8	41.4	41.2	40.6	39.9	31.8
Average	46.8	47.9	47.8	47.2	44.3	31.4	41.3	41.0	40.7	40.1	39.5	31.4

Inside furnace						Inside primary chamber					
h1 W/m ² K	h2 W/m ² K	h3 W/m ² K	h4 W/m ² K	h5 W/m ² K	Tbed W/m ² K	h1 W/m ² K	h2 W/m ² K	h3 W/m ² K	h5 W/m ² K	h5 W/m ² K	h5 W/m ² K
52.4	49.2	49.2	51.1	63.1	63.1	82.4	85.0	88.7	93.9	100.9	100.9
52.8	48.9	48.9	51.4	63.6	63.6	81.5	85.9	87.7	92.8	98.5	98.5
52.1	49.2	49.2	50.8	63.6	63.6	80.7	84.1	86.8	93.9	99.7	99.7
52.8	49.5	49.5	50.8	62.1	62.1	82.4	84.1	87.7	92.8	99.7	99.7
52.4	48.6	49.8	51.1	61.6	61.6	80.7	84.1	85.9	91.7	99.7	99.7
Average	52.5	49.1	49.3	51.0	62.8	81.6	84.6	87.4	93.0	99.7	99.7

Run #3

Operating and design parameter	
Date	Sept 30, 2001
External solid circulation rate	4 kg/m ² s
Bed material	"00" sand
Superficial gas velocity	3.5 m/s
	Heat transfer surface area
	Power supply
	Types of particle
	0.0619 m ²
	50 W
	B

No of data	Inner wall of Inside furnace						Outer wall of Inside furnace					
	T1 (°C)	T2 (°C)	T3 (°C)	T4 (°C)	T5 (°C)	Tbed (°C)	T1 (°C)	T2 (°C)	T8 (°C)	T9 (°C)	T10 (°C)	Tbed (°C)
1	45.2	46.5	47.2	46.7	42.8	29.7	39.7	39.2	38.6	38.4	38	29.7
2	45.7	46.8	47.6	47	42.9	29.9	39.8	39.5	38.8	38.7	38.3	29.9
3	45.9	47	47.5	47.2	43.4	30.1	40	39.8	39	38.8	38.3	30.1
4	46	47.1	47.8	47.4	43.5	30.2	40.2	40	39	39	38.6	30.2
5	46.2	47.4	48	47.5	43.7	30.4	40.2	40	39.4	39	38.7	30.4
Average	45.8	47.0	47.6	47.2	43.3	30.1	40.0	39.7	39.0	38.8	38.4	30.1

Inside furnace						Inside primary chamber					
h1 W/m ² K	h2 W/m ² K	h3 W/m ² K	h4 W/m ² K	h5 W/m ² K	Tbed W/m ² K	h1 W/m ² K	h2 W/m ² K	h3 W/m ² K	h5 W/m ² K	Tbed W/m ² K	
52.1	48.1	46.1	47.5	61.6	80.7	85.0	90.7	92.8	97.3	97.3	
51.1	47.8	45.6	47.2	62.1	81.5	84.1	90.7	91.7	96.1	96.1	
51.1	47.8	46.4	47.2	60.7	81.5	83.2	90.7	92.8	98.5	98.5	
51.1	47.8	45.9	46.9	60.7	80.7	82.4	91.7	91.7	96.1	96.1	
51.1	47.5	45.9	47.2	60.7	82.4	84.1	89.7	93.9	97.3	97.3	
Average	51.3	47.8	46.0	47.2	61.2	81.4	83.8	90.7	92.6	97.0	